AEROSOL COLLECTION

IN

FIXED AND FLUIDIZED BEDS

by

Yani Doğanoğlu

Thesis submitted to the Faculty of Graduate Studies and Research

in partial fulfilment of the requirements for the

degree of Doctor of Philosophy

Chemical Engineering Department
McGill University
Montreal, Canada

August 1975

TO FULA AND TOMMY

ABSTRACT

Collection of solid and liquid aerosols in the size range 0.7 to 2.5 μm has been examined in 0.15 m diameter fixed and fluidized beds of spherical collector particles. Extensive experimental results have been obtained for collectors of 110, 550 and 600 μm diameter. Electrically neutral, closely sized aerosols were formed using a spinning disk generator, modified to give stable concentration over long periods of time. Aerosol number concentrations and size were monitored by means of light-scattering counters.

For fixed beds, dilute aerosols were used so that bed loading effects were eliminated. By varying bed height, it was possible to determine collection efficiencies without interference from entry and exit effects. It was shown that the predominant collection mechanisms under these conditions are gravitational settling and inertial deposition. The results were analyzed statistically and design correlations for single particle collection efficiencies are presented.

For fluidized beds, it was shown that high removal efficiencies can be obtained with shallow beds and superficial gas velocities up to 3 m/s, provided adequate distribution of the challenging aerosol is achieved. To interpret the results, a model for aerosol collection was developed, based on the modified two phase theory of fluidization. It was shown that the transfer between bubble and particulate phases is sufficiently rapid, in beds shallower than 0.08 m, that collection is determined solely by processes occurring in the dense phase. Expressions for the collection efficiency of individual bed particles were developed from first principles.

Analysis of the results showed that the predominant collection mechanism is inertial, enhanced by the fluctuating particle motion induced by bubbles. As a result, higher particle collection efficiencies are obtained in fluidized beds than in fixed beds, so that total aerosol penetration in a fluidized bed decreases with increasing superficial gas velocity. The industrial advantages of this technique, offering a continuously renewable filter operable at high temperatures and/or pressure, are discussed.

ABREGE

La collection d'aérosols solides et liquides, dont la grosseur varie entre 0.7 et 2.5 µm, a été examinée à l'aide de lits fixes et fluidisés contenant des particules collectrices (collecteurs) sphériques. De nombreux résultats experimentaux ont été obtenus pour des collecteurs ayant des diamètres de 110, 550 et 600 µm. Des aérosols de grosseur à peu près mé à l'aide d'un générateur à disque tournant modifié pour produire une concentration stable pour un long laps de temps. La concentration (en quantité) et la grosseur des aérosols ont été controlées avec des compteurs à lumière déviée.

Dans le cas des lits fixes, des aérosols dilués ont été employés afin que les effets de charge du lit soient éliminés. En variant la hauteur du lit, il a été possible de déterminer les efficacités de collection sans subir l'interférence des effets d'entrée et de sortie. Il est démontré que les mécanismes de collection prédominants sous ces conditions sont la sédimentation gravitationnelle et le dépôt inertiel. Les résultats ont été analysés statistiquement et des expressions de "design" pour calculer les efficacités de collection d'une particule sont ici présentées.

Pour les lits fluidisés, il est montré que de grandes efficacités de recouvrement peuvent être obtenues avec des lits peu profonds et des vitesses de gaz superficielles allant jusqu'à 3 m/s, en autant qu'une distribution adéquate de l'aérosol est accomplie. Dans le but d'interpréter les résultats, un modèle pour la collection d'aérosols a été développé, modèle basé sur la "théorie modifiée des deux phases" en

fluidisation. Il est montré que le transfert entre la phase des bulles et celle des particules est suffisamment rapide dans des lits moins profonds que 0.08 m et que la collection est déterminée seulement par des procédés ayant lieu dans la phase dense. Des expressions pour l'efficacité des particules individuelles (collecteurs) sont développées ici.

L'analyse des résultats montre que le mécanisme de collection prédominant est inertiel et est causé par le mouvement fluctuant des particules sous l'effet des bulles. Subséquemment, de meilleures efficacités de collection sont obtenues dans des lits fluidisés que dans des lits fixes, et ainsi le pénétration totale des aérosols dans un lit fluidisé décroit avec une vélocité de gaz superficielle croissante. Les avantages industriels de cette technique, offrant un filtre continuellement renouvelable et capable de fonctioner à hautes températures et/ou pressions, sont aussi discutés.

ACKNOWLEDGEMENTS

The author would like to express his thanks and appreciation to the following people who assisted in the project:

Dr. R. Clift, a dedicated man of science, for his continuing help, advice and encouragement which are the prime source of any value this work may contain;

Professor G.A. Ratcliff, in whose department the work was initiated;

Professor W.J.M. Douglas, in whose department the work was completed;

Dr. J.R. Grace, who supervised the work during the academic year of 1973/74, for his encouragement and numerous helpful comments;

the staff of the Chemical Engineering Department and particularly Mr. A. Krish and Mr. B. Stafford, for their help in designing and constructing the equipment used;

Mr. V. Jog, who performed some of the experiments and calculations, for his enthusiasm and dedication;

Miss D.T. Do, who drew the figures and graphs;

Mrs. H. Rousseau, for her great care and meticulousness when typing the thesis;

the Pulp and Paper Research Institute of Canada for the electron-micrograph of latex particles in Appendix C;

the Epidemiology Department for their courtesy in permitting the use of the Model 202 Royco Particle Counter described in Chapter 4;

the Mechanical Engineering Department for their courtesy in permitting the use of the Tornado High Capacity air blower described in Chapter 4;

the Electrical Engineering Department for their courtesy in permitting the use of numerous electrical pieces of equipment;

his fellow graduate students, who helped by creating an atmosphere suitable to academic research, for their friendship and moral support; and

finally, and by no means least, his wife Fula, who faced with him the numerous problems he encountered during his studies, for her love.

TABLE OF CONTENTS

LIST OF FIGURES

LIST OF TABLES

LIST OF APPENDICES

CHAPTER 1. INTRODUCTION

1.1 The Need for Removal of Airborne Particulates

In recent years, the general need to limit pollution of the environment has become a matter of increasing concern to all members of society. A range of new laws and emission standards have been introduced, in an effort to reduce the amount of pollutants discharged to the environment. Air pollution in general, and in particular airborne dusts and fumes which are a by-product of almost all process industries, constitute an important aspect of pollution. The need for the control and recovery of these particulates, regardless of their source, may be classified under the following headings:

(i) Health Hazard - Inhalation of excessive dust, irrespective of its chemical composition, produces a serious pulmonary disease under the general term of pneumonoconiosis, silicosis and asbestosis being its most dangerous forms. In recent months the news media have reported large scale confrontations in industry resulting from the poor health record of personnel working in asbestos mines. Another manifestation of the breathing of certain dusts is metal-fume fever, which though transient and non-cumulative is an unpleasant malady. Many dusts are irritant and cause dermatitis and other skin diseases.

(ii) Explosion Risk - Dusts such as cereals, coal, cork, flour, leather, malt, plastics, starch, sugar and wood are capable of producing explosive mixtures with air. The explosion

risk increases with decreasing particle diameter due to the larger surface available for combustion, and necessitates the introduction of expensive measures such as explosion vents, isolation of equipment and fire extinguishing systems.

(iii) Commercial Value - Economic reasons for the development of particulate recovery equipment are born from the commercial value of dust and fume resulting from manufacturing processes such as smelting, refining, crushing, grinding, screening, drying, etc.

Thus, it is seen that the need for removal of dusts and fumes is a recognized necessity in industry. However, the control technology for fine particulates is at a relatively early stage of development. Removal of airborne particulates becomes more costly and difficult for fine particles of the order of one micron. In this size range, particles are too small for inertial effects to be effective and yet too large for Brownian diffusion to be rapid. There appear to be three basic types of equipment used in industry for micron range particulate removal. These are electrostatic precipitators, fabric filters, and wet scrubbers and are reviewed in general terms in the next section.

1.2 Conventional Commercial Equipment for Particulate Removal

1.2.1 Electrostatic precipitators

In the application of electrostatic forces to precipitators the particulate matter comprising the aerosol is charged by passing through a highly ionized region. The material is thus removed from the gas stream

by electrostatic forces in an intense electric field (around 10^5 volts/m). Collected dust is removed from the system by washing or flushing the collection electrodes (wet electrostatic precipitation) or by impacting or rapping (dry electrostatic precipitation). The efficiency of an electrostatic precipitator may be semi-quantitatively determined by the Deutch-Anderson equation[01]

$$(-\ln f) = \frac{U_M A}{G} \qquad (1.1)$$

where f is the fractional penetration of aerosol, defined as the fraction not collected, A is the collecting surface area, G is the volumetric flow rate of the gas and U_M is the migration velocity of the particles under the effect of the electric field intensity, F_E(volts/m), and is estimated as

$$U_M = \frac{q'_A F_E}{3\pi d_A \mu_f} \qquad (1.2)$$

The charge on the particle, q'_A, is a function of aerosol diameter, d_A. The disadvantages of electrostatic precipitators are high capital and maintenance costs. Power requirements increase with particulate mass loading, and efficiency decreases exponentially with increasing gas velocity and decreasing collection area. Power requirements are also related to dust resistivity. Thus detailed designs of precipitators are usually specific to a particular industry. Oglesby et al.[01] discuss the application of electrostatic precipitators for the Gypsum, Phosphoric Acid, Carbon Black, Cement and Elemental Phosphorous industries. Typically,

power requirements are of the order of (0.1 - 1) kilowatts per m^3/s .

1.2.2 Fibrous filters

Fibrous filters are generally more effective than precipitators for removing particles in the micron and sub-micron ranges. Usually fibrous filters operate in the region of non-stationary filtration (see Section 2.2.2), where a significant amount of the challenging aerosol is collected by the particles already deposited on the filter. Unfortunately, most existing filtering media have rather limited resistance to corrosion, low mechanical strength and are usually restricted to low operating temperatures. Their invariably batch operation and the difficulty or impossibility of regenerating spent filters makes them relatively expensive to operate. Fibrous filters are usually replaced or regenerated when the pressure drop across the filter, which increases with increasing filter loading, becomes uneconomical to maintain.

1.2.3 Wet scrubbing devices

Wet scrubbing devices operate on the principle of bringing in contact the effluent stream with a liquid phase. There is a wide range of designs, sizes and performance characteristics available in industry. High efficiencies of micron range particles may be achieved with wet scrubbing devices but their unusually high power requirement, especially for removal of submicron particulates, constitutes their biggest disadvantage. They share with fibrous filters the disadvantage that they cannot readily be applied to hot gases, in this case because the resultant humidification causes a heavy condensation plume when the gas is finally discharged to atmosphere.

Thus, the development of efficient and low cost devices for particulate removal is a pressing demand in industry.

1.3 The Fluidized Bed as a Continuous Filter

Assuming a shallow fluidized bed can operate efficiently at high superficial gas velocities, its potentialities as a filtering device are overwhelming. Firstly, a fluidized bed can be operated continuously with no need for periodic shut down. "Spent" collector particles can be removed and fresh or regenerated particles can be added to the bed continuously. Secondly, a fluidized bed is not subject to an upper temperature limit, as the material of the collecting medium may be chosen at will to suit the operating conditions of the filtration process. Thirdly, the process of removal may be combined with a chemical reaction, i.e. the simultaneous removal of a pollutant gas in the challenging aerosol. Fourthly, heat recovery from hot effluent streams may be achieved simultaneously by the simple introduction of cooling coils in the bed.* Fifthly, the pressure drop across a shallow fluidized bed is low and independent of superficial gas velocity. Finally, the energy requirements of the bed and collection efficiency are not a function of bed or aerosol loading; higher aerosol loadings would increase efficiency due to the enhancement of collection by particle agglomeration mechanisms. Removal of aerosols by fluidized beds, however, has been only superficially examined in the past, both industrially and academically.

---

* It is well known [D2,K6] that a fluidized bed is also an excellent heat exchanger.

It appears that the potentiality of a fluidized bed in removing particulates has been noticed at least twice in industry. Cook, Swany and Colpitts[C11], reporting on the recovery of fluoride compounds in a fluidized bed and filter arrangement, noted that the major part of particulate fluoride removal was achieved in the bed. Although the superficial velocity is not reported it is likely, as the process constitutes an industrial operation, to be quite high. Rubin and Margolin[R6] have recently reported (1974) on the drying of coals and removing fines in a two-stage fluidized bed. The first stage had a low moisture content and was operated at a low superficial velocity ($0.7 < U < 1.0$ m/s). The second stage was comprised of coal of high moisture content and operated at a higher superficial velocity ($1.4 < U < 1.8$ m/s). Most of the fines were removed at the higher velocity of the second stage; a typical mass efficiency of 95% is reported. This suggests, therefore, that high efficiencies of particulate removal are possible at high velocities.

Academic research on the subject, however, concentrated on beds of unrealistic size (typically 5×10^{-2} m diameter) or on very low superficial velocity ranges. Distributor designs, which comprise a most important aspect of a fluidized bed, are generally not described and researchers tend to treat the bed as a homogeneous contactor, disregarding the two phase theory of fluidization. As a result conclusions drawn in the literature are vague, misleading and often contradictory. A general, but essentially unfounded, belief seems to have grown up that a fluidized bed operating at high superficial velocities should be inefficient. As a result of this, impossible designs such as a 4 - 5 stage fluidized bed operating at 0.2 m/s have been proposed (e.g. McCarthy et al.[Mc1],

Jackson[J2], Shannon[S4]). It is apparent that for a typical industrial flow rate[A4] of 100 - 300 m^3/s the diameter of such a device, operating at 0.2 m/s, would be about 25 to 40 meters. Resultant structural costs alone would make such a device uneconomic.

Thus, it appears that, if the fluidized bed is to establish its position as a filtering device for micron range particles, it has to be operable at superficial velocities of the order of meters per second; this has not been investigated previously.

1.4 Scope of this Work

The scope of this work is to investigate the removal of aerosols in fluidized beds of realistic size, interpreting the results in a manner that will facilitate scale up or design and, concurrently, to study aerosol removal in fixed beds comparing the efficiencies of the two devices.

First of all, previous work on fixed and fluidized beds is investigated in Chapter 2. The experimental methods and conclusions of previous studies are analyzed and the shortcomings of past work on aerosol removal in fluidized beds become apparent in Section 2.3. Chapter 3 describes the possible collection mechanisms around an isolated spherical collector; these are direct interception, inertial collection, diffusional deposition, gravitational settling and collection by electrostatic attraction. Dimensionless collection parameters are defined and approximate estimates of the individual theoretical collection efficiencies of this study are presented. The equipment used for experiments is described in Chapter 4. Basically, three designs were developed for experiments with fixed beds, fluidized beds and fluidized beds at very high superficial

velocities (up to 3 m/s). Chapter 5 describes fixed bed experiments where the collection efficiency of a collector particle is formulated in a way which eliminates end effects of the bed. The results are analyzed statistically, the dominant collection mechanisms are determined and design equations describing aerosol removal in fixed beds are presented. Extensive experiments on collection of aerosols by fluidized beds are described in Chapter 6. These cover a wide range of velocities, collector particle and aerosol diameter, and bed height. The dominant collection mechanism is shown to be inertial collection and experiments on the removal of solid aerosols are reported. The significance of the distributor in aerosol collection is demonstrated. Based on the modified two phase theory of fluidization, equations describing aerosol removal in fluidized beds are derived in Chapter 7 and compared to experimental results. The noted increase in inertial collection due to the vigorous mixing of the dense phase by bubbles is formulated in the form of a dimensionless velocity number. In Chapter 8 the promising implications of this work for industrial design are discussed, and extensions of the work for future studies are suggested.

CHAPTER 2. PREVIOUS WORK

2.1 Introduction

This chapter reviews previous work on aerosol removal by mechanical filtration, with particular emphasis on filtration in fixed and fluidized beds composed of roughly spherical collector particles. Theoretically, two phases may be distinguished: stationary filtration, and non-stationary filtration where the collection efficiency of the filter may change with time. Although this study concentrated on stationary filtration, both of these phases will be discussed in the following sections.

Published studies of filtration of aerosols in granular beds are few in number. Researchers tend to agree, in general, on the nature and relative effect of important variables on aerosol penetration. Previous studies on fluidized beds, however, are much more restricted. As will be shown later, most studies investigated rather limited ranges with relatively crude methods of aerosol generation and measurement. As a result, experimental data in the literature is limited and conclusions drawn are vague and sometimes misleading. The pioneering work of Meissner and Mickley[M4] (1949), hinting at the possibility of increased collection efficiency at high superficial gas velocities, was largely ignored by most of the subsequent studies. A general belief seems to have developed that the penetration of aerosols should be quite high at large multiples of minimum fluidization velocities because of gas bypassing in the bubble phase. Except recently (1974)[T1], there was no attempt to formulate the phenomenon of aerosol removal in fluidized

beds in terms of the classical theory of fluidization. The possibility of enhancement of collection mechanisms, caused by the rapid mixing induced by bubbles, in a fluidized bed, has not been referred to, investigated or mentioned in the literature.

Meisen and Mathur[M3] have investigated recently (1974) the application of spouted beds to aerosol removal; their work is reviewed in Section 2.4.

2.2 Particle Collection in a Fixed Bed

2.2.1 Steady state filtration

2.2.1.1 Introduction

In steady state filtration the deposition of particles takes place in a pure filter and the structural changes caused by the deposition of individual particles are assumed to be too small to influence the efficiency of the filter. In stationary filtration it is usually assumed that the collision efficiency of particles with the collector particles is 100%, so that a particle which touches a collector remains in contact and is not dislodged in the following process of filtration.[D6] The two most important parameters that have been investigated are the superficial gas velocity through the bed and the diameter of the aerosol particles. From the equations presented in Chapter 3, for the collection mechanisms around isolated spherical collectors, the effect of superficial gas velocity and aerosol diameter on penetration, defined as the fraction of the challenging aerosol not collected by the filter, would be expected to be of the form shown in Figures 2.1 and 2.2.

FIGURE 2.1 Schematic representation of the effect of superficial gas velocity on penetration

FIGURE 2.2 Schematic representation of the effect of aerosol diameter on penetration

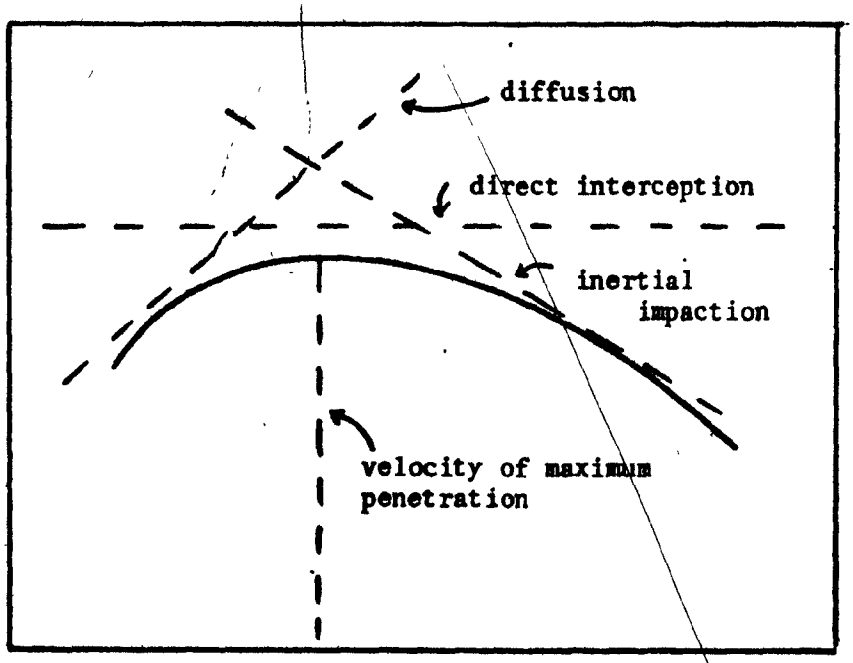

Figure 2.1

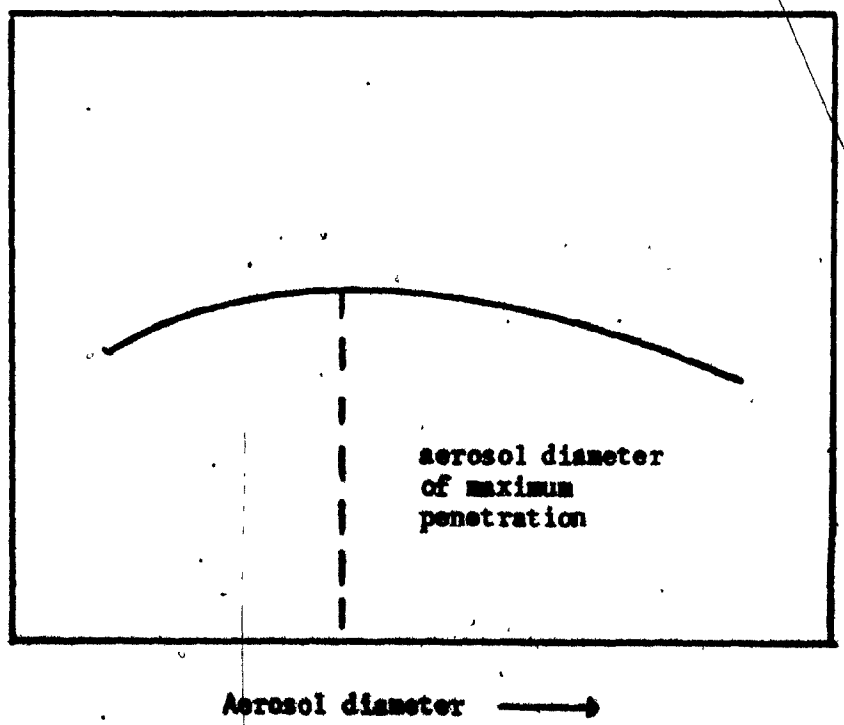

Figure 2.2

2.2.1.2 Superficial gas velocity and penetration

As the velocity through the filter increases, diffusion becomes less important, penetration reaches a maximum and then starts decreasing with growth of inertial effects. This was demonstrated by the results of Ramskill and Anderson[R2] (Figure 2.3) who conducted tests on sheets of filter materials and measured penetrations of aerosols of sulphuric acid or dioctyl.phthalate of 0.2 - 0.8 μm diameter at gas velocities of up to 2.85 m/s. They used a light scattering method and attempted an assessment of the inertial effect. Gillespie[G4] subsequently re-examined their data, and introduced a slippage coefficient in order to fit his theory. He claimed that particles do not necessarily adhere on impact with fibres and that the proportion so doing depends on the size, velocity and type of aerosol particle. Dorman[D12] correlated the relative importance of inertia, diffusion and interception in some of Ramskill and Anderson's experiments where the aerosol was dioctyl phthalate of 0.3 μm diameter. He assumed that

$$\begin{aligned} &\text{Rate of diffusional collection} \quad \propto \quad U^{-\frac{1}{2}} \\ &\text{Rate of inertial collection} \quad \propto \quad U^{2} \\ &\text{Rate of collection by interception} = \alpha_R N_R + f(U) \end{aligned} \tag{2.1}$$

$$\log(f') = 2.0 - (\alpha_I U^2 + \alpha_D U^{-\frac{1}{2}} + \alpha_R N_R) \tag{2.2}$$

where α_I, α_D and α_R are constants, and N_R is the ratio of aerosol to collector particle diameters.

FIGURE 2.3 Experimental results of Ramskill and Anderson[R2]: effect of superficial gas velocity on penetration

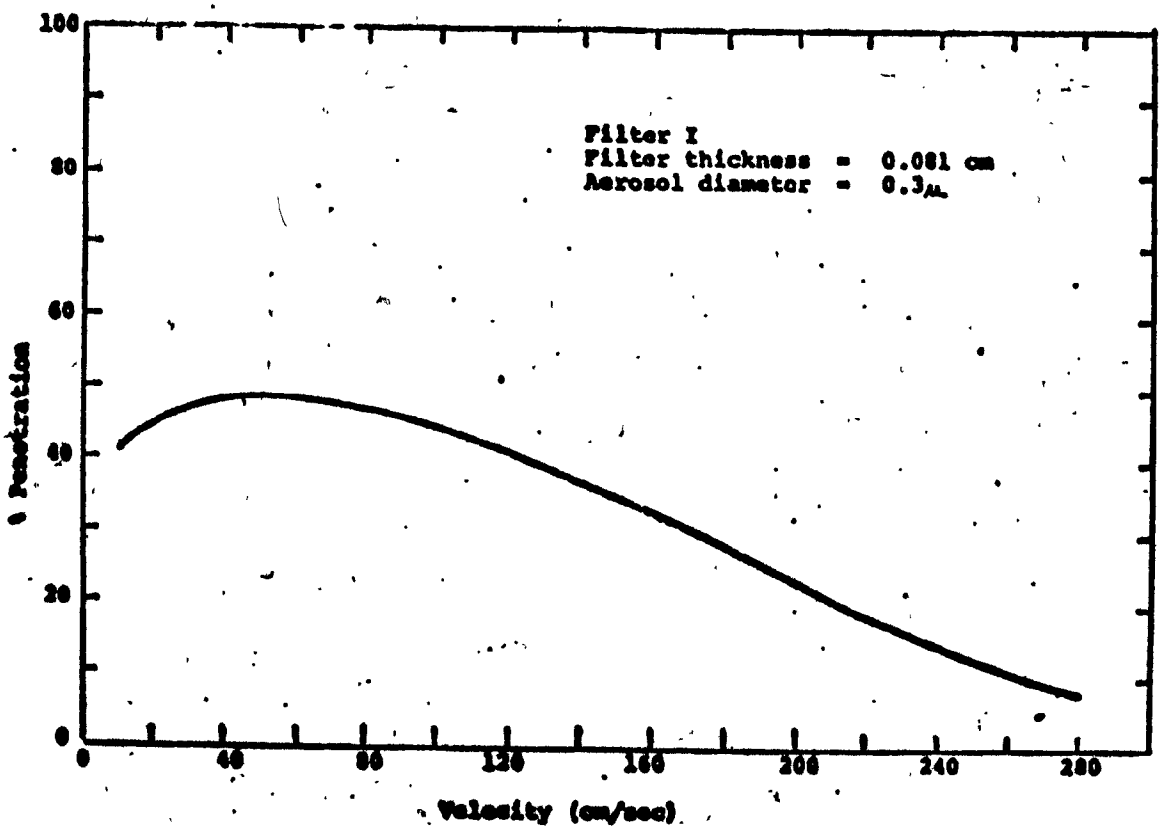
Filter I
Filter thickness = 0.081 cm
Aerosol diameter = 0.3μ
% Penetration
Velocity (cm/sec)
100
80
60
40
20
0
0
40
80
120
160
200
240
280

Dorman then differentiated Equation (2.2) and , from the condition that $\frac{d(f')}{dU} = 0$ at U_p, the velocity of maximum penetration, obtained

$$\alpha_D = 4\alpha_I U_p^{2.5} \tag{2.3}$$

Equation (2.2) was then re-written as

$$2-\log(f') = \alpha_I(U^2 + 4U_p^{2.5}U^{-0.5}) + \alpha_R N_R \tag{2.4}$$

By plotting $(2-\log(f'))$ against $(U^2 + 4U_p^{2.5}U^{-0.5})$ a straight line was obtained, the intercept on the ordinate giving α_R, whilst α_I and α_D were calculated from the gradient.

Thomas and Yoder[T2,T3] measured penetration of dioctyl phthalate aerosols through sand beds where the diameters of the collector particles were $(1.6 - 3.6)*10^{-4}$m and aerosol diameter varied from 0.2 - 2.0 μm. They demonstrated experimentally the effect of gravity settling by doing experiments with their fixed bed at different orientations with respect to gravity. Thomas and Yoder confirmed experimentally the existence of a velocity of maximum penetration for a given aerosol diameter. Some of their results are presented in Figure 2.4.

Removal of aerosol particles in fixed beds was investigated systematically by Paretsky[P1] who analysed the effect of velocity on penetration of 1.1 μm diameter polystyrene latex microspheres in a sand bed of $(1.4 - 2.0)*10^{-3}$m diameter collector particles. "Upshot" and "downshot" flows were used with superficial gas velocities from $3.0*10^{-2}$ to 10^{-1}m/s and the aerosol concentration was monitored by a Model

FIGURE 2.4 Data of Thomas and Yoder[T2]: effect of aerosol diameter on penetration

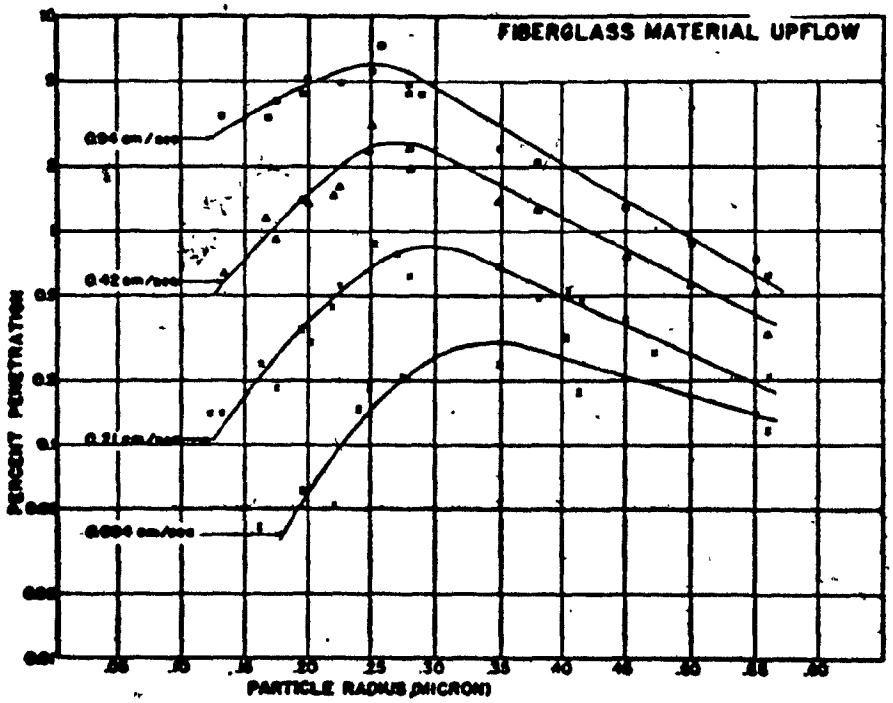

Penetration of homogeneous DOP aerosols through a Fiberglas FG-50 filter mat.

JM-3000-AL Sinclair-Phoenix photometer. Initially Paretsky tried to duplicate the experiments of Thomas and Yoder (discussed earlier) but found that they used an unsuitable inlet and exit section resulting in sizable inlet and exit losses of aerosol. Paretsky's research was examined in detail by the author and found to suffer from certain experimental inaccuracies. These are: a) The latex suspension was not placed in an ultrasonic cleaning bath prior to generation, as recommended by the manufacturers[M1], and this caused a sizable formation of doublets and triplets to be present in the resulting aerosol. Formation of doublets and triplets was confirmed by Paretsky himself, who analyzed the particles under an optical microscope, but no steps were taken in order to correct it.* b) Possible anomalous collection at the inlet and exit of the fixed bed was not accounted for, as was done in this study, but was assumed to be negligible. Anomalous collection at the ends of screen supported fixed beds has been observed by Knettig and Beeckmans[K3] who report, for fixed beds, an 11% collection at zero extrapolated bed height for 1.6 μm dioctyl phthalate aerosols at a superficial gas velocity of $8.2*10^{-2}$m/s. This effect may be expected as a result of the higher local velocities in the immediate vicinity of the support grid. It is most important in the range where inertial collection dominates, as in Paretsky's experiments. c) Paretsky found that the latex aerosol produced contained "water droplets"; this, possibly, was either because enough air was not provided for drying or because the water used for atomizing was not sufficiently pure.* Paretsky tried to correct the effect by using a second generator, which contained only distilled water, to provide an apparent "zero" concentration.

---

* See Appendix C.

d) No mention is made of coincidence losses (described in Section 4.2.2) in the particle counter which are not negligible. Correction of these losses can be made, as in the present work, with consequent improvement in experimental accuracy.

Paretsky examined the effect of superficial gas velocity and measured a velocity of maximum penetration around (8.0 - 11.0) 10^{-2} m/s (see Figure 2.5) for 1.1 μm aerosol particles. His curves for upshot and downshot flow gave different penetrations and he attributed the difference to gravity settling. Experimental results were correlated in the form of semi-empirical equations after an unsuccessful application of the cell model, discussed in Section 3.3.

2.2.1.3 Aerosol diameter and penetration

Theoretically and experimentally it has been established that as the aerosol diameter decreases, penetration increases[F5] . The trend continues down to a 0.3 μm aerosol diameter where diffusion becomes the predominant mechanism of aerosol collection and penetration decreases with decrease in aerosol size.[D6]

The earliest published results appear to be those of Freundlich[F2] who found a maximum penetration in the diameter range 0.2 to 0.4 μm. No peak penetrating size was found by LaMer[L1] in experiments with liquid monodisperse aerosols, with particles as small as 0.04 μm, produced by the Sinclair-LaMer generator and Stern et al.[S9], in similar experiments, found that penetration increased as the aerosol size was reduced down to 0.3 μm. Chen[C3] , in experiments with monodisperse aerosols of 0.15 μm diameter and glass collector fibres of 2.5 - 3.0 μm

FIGURE 2.5 Experimental results of Paretsky: effect of gravitational settling on penetration

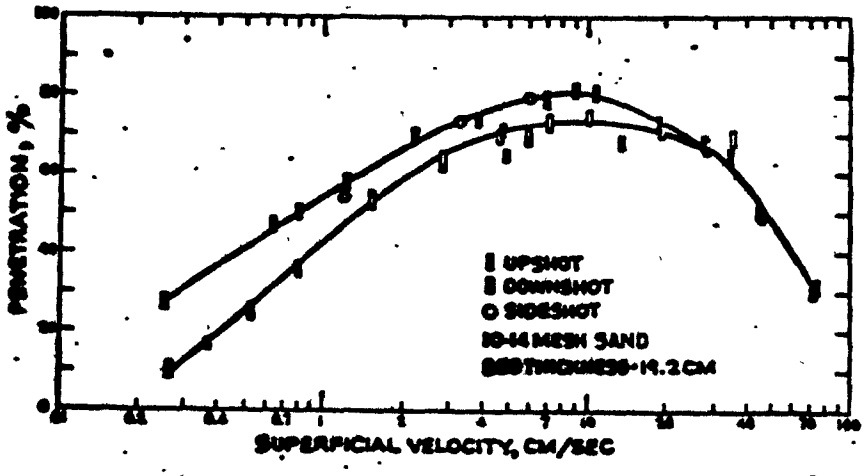

Penetration of a 1.1 micron-diameter aerosol as a function of superficial velocity.

diameter, reports that a peak penetrating size exists only if the superficial gas velocity is below .04 m/s. Chen also gives an experimentally determined "iso-efficiency point", a velocity where the collection efficiency is the same for all sizes of particles. Thomas and Yoder[T2,T3] present experiments in granular beds which illustrate that the size corresponding to maximum penetration increases with a decrease in velocity; some of their results are shown in Figure 2.4.

2.2.2 Unsteady state filtration

The process of filtration is, in reality, rather more complicated than the model assumed by stationary filtration. In stationary filtration it is assumed that the particle which touches the fibre is captured and never released. In reality, however, the captured particle may be released in the course of filtration and pass through the filter. It appears then that the behaviour of aerosol particles after capture is a function of the adhesive forces holding the particle to the collector. The magnitude of these adhesive forces depends on factors such as shape and size of aerosol particle and collector, their contact surface, chemical composition, electrical charges, etc. The subject has been investigated by many authors[G4,G5,L10,G1,F6,B6]; and Corn[D6] gives an excellent review. Reported studies, however, apply to specific situations and, as yet, there is no theory or study which allows a priori prediction of re-entrainment in general quantitative terms.

Moreover, the assumption that deposition is taking place in an idealized filter whose geometrical configuration is known and steady

with respect to time is not strictly true. In reality, the aerosol particles cause structural changes in the filter and as a result both penetration of aerosol and pressure drop across the filter may change with time. This effect is well known in liquid phase filtration[P3] and is incorporated in standard design and operating procedures.

Leers[L12] reports that the distribution of captured aerosol particles on the surface of the collector is selective; the particles tend to deposit on one another forming so-called "trees" (see Figure 2.6). The formation of these trees results in an increased efficiency with relatively small change in pressure drop. Radushkevich[R1], on theoretical grounds, suggested an equation of the form

$$(f')_t = (f')_{t=0} e^{-ct} \qquad (2.5)$$

LaMer[L2] et al.[L2] confirmed the form of the equation experimentally.

In granular beds, Englebrecht[E1] describes Lurgi's "gravel bed filter" which, of course, operates in the region of non-stationary filtration. Fairs and Godfrey[F1] describe a panel filter used in a contact acid plant burning sulphur. Pressure drop across the filter varied from 2.0×10^{-3}m to 1.5×10^{-1}m of water with respect to time; this period of time is not specified but is probably in the order of weeks. A panel bed filter design has been patented by Squires[S6] who claims his design is superior to the Lurgi bed.

Paretsky[P1] experimented with fixed beds and measured the increased efficiency of the bed in collecting latex microspheres (1.1 μm diameter) when different amounts of fly ash were deposited on the bed.

FIGURE 2.6 Formation of trees in non stationary filtration

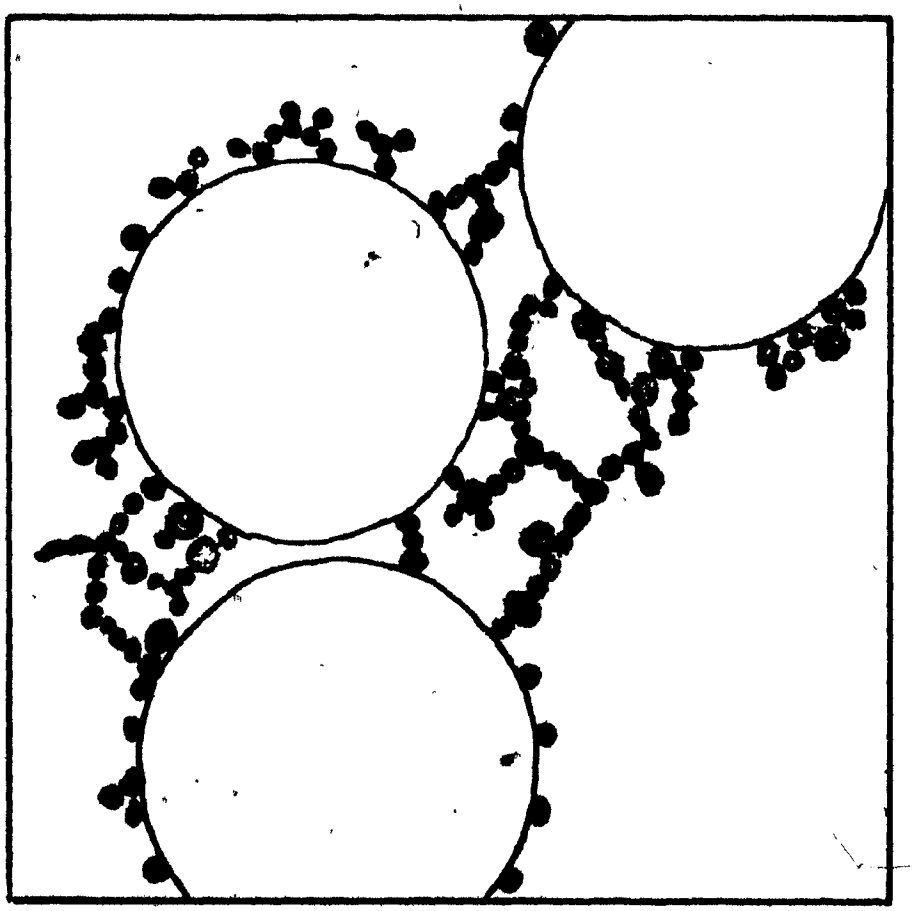

The fly ash was added to simulate the effect of bed loading on performance and different methods of deposition were tried. The fly ash was periodically removed by "puffback"*, more fly ash added and the latex aerosol particles were used again to measure the new penetration across the bed. Paretsky's experimental results are presented in Figure 2.7 and from the graph we see the marked effect of bed loading on the penetration of the challenging latex aerosol. Paretsky's data, however, are confined to the binary system latex-fly ash and no mention is made of the deposition of fly ash on fly ash. No theoretical interpretation of unsteady state filtration is presented in Paretsky's thesis.

The process of unsteady state filtration has been investigated, with relation to industrial applications, by Kalen and Zenz[K1], Hazlett[H5,H6] Schurr et al.[S1] and Blasewitz and Judson[B5].

Blasewitz and Judson[B5] investigated the removal of radioactive aerosols by glass fibres and demonstrated experimentally that penetration decreased as the bed loading increased. Hazlett[H5] studied the coalescence of water droplets in a fibrous bed and in a subsequent study[H6] investigated the effect of adding a surfactant in the water. Schurr et al.[S1] (DuPont Company) report on the application of deep bed sand filters to control the release of stack particulate activity from the chemical processing areas of the Savannah River Plant. The special

---

*A "puffback" is a sudden surge of air in the opposite direction from filtration, which fluidizes the bed momentarily, and removes the layers of filtration material which are "saturated" with filtered particulates.

FIGURE 2.7 Experimental results of Paretsky: example of non-stationary filtration

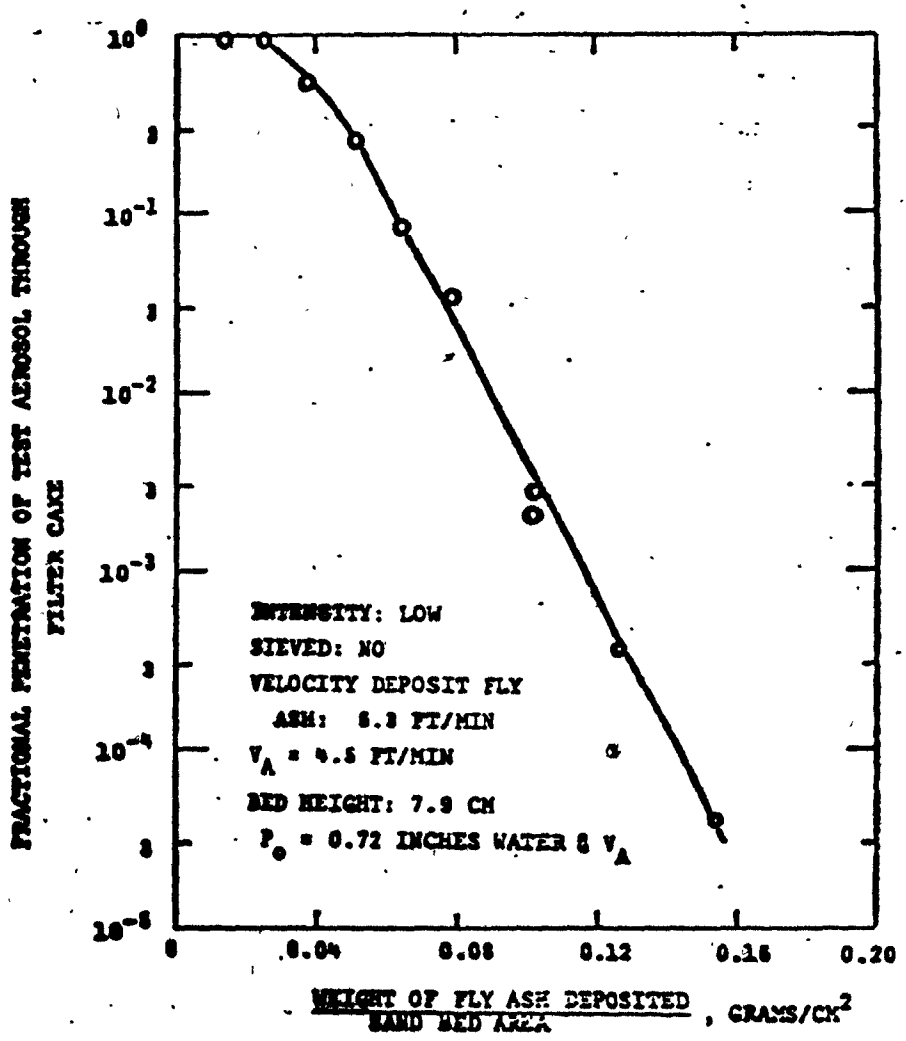

Figure 46. Effect of amount of fly ash deposited on fractional penetration of test aerosol through fly ash filter cake deposited on horizontal sand bed.

feature of these beds is their enormous size, having a cross sectional area of 2,200 m^2 and a bed depth of 2.4 meters. Collection efficiencies greater than 99.9% are reported for an unspecified range of particulate diameter. Kalen and Zenz[K1] (Ducon Company) studied filtration in a granular bed of the effluent stream from a FCC regenerator. They followed the same approach as Squires by using a "puffback" technique to momentarily fluidize the bed and break the agglomerates when the pressure drop across the bed reached a predetermined size. More than 95% collection is reported for a particulate size range of (2 - 20) μm and bed depth of 6.4×10^{-2}m.

Summarizing, it appears that in unsteady state filtration, bed loading plays a beneficial part in enhancing aerosol collection. Increased loading, however, leads to higher pressure drops across the bed necessitating the periodic removal of collected particulates by various methods. The quasi-batch operation of fixed beds is unavoidable and is in fact their big disadvantage. This has led some researchers to investigate the possible use of fluidized beds for collection of airborne particulates. This area is discussed in the next section.

2.3 Particulate Collection in a Fluidized Bed

2.3.1 Effect of fluidized bed parameters

2.3.1.1 Superficial gas velocity and minimum fluidization velocity

In a pioneering study Meissner and Mickley[M4] (1949) removed sulphuric acid mists 2 to 14 μm in diameter by passing them through beds of solids fluidized in a 5.1×10^{-2}m diameter tube. They used alumina granules, glass microspheres and silica gel as collector particles (Table 2.1).

and performed experiments varying the superficial gas velocity through the bed from 0.30 - 0.82 m/s. The aerosol was generated by rapid cooling of sulphuric acid vapour and the concentration of the aerosol was measured by a light intensity method. Substantial decrease in penetration of the incoming aerosol with increasing superficial gas velocity is reported. In one run with silica gel particles the penetration decreased from 30% to 7% when the velocity changed from 0.36 to 0.84 m/s. This, as will be seen later, is in direct conflict with results of subsequent studies but agrees partially with the results of this study. Inspection of some of the experimental results of Meissner and Mickley (Figure 2.8) shows this reduction in penetration to be quite consistent with different types of bed materials.

Unfortunately, minimum fluidization velocities are not reported in their study. If it is assumed that the minimum fluidization velocity can be calculated from Leva's equation[D2], which may be expressed as

$$U_{mf} = 1.1\times10^{-3} \frac{g^{0.94}(\rho_p-\rho_f)^{0.94} \; d_p^{1.82}}{\rho_f^{0.06}\mu_f^{0.88}} \qquad (2.6)$$

then from Table 2.1 one draws the conclusion that Meissner and Mickley were operating at multiples of U_{mf} much larger than subsequent studies. Unfortunately, in their study, the effluent aerosol was sampled after two cyclones provided to collect the bed particles, so that the significance of their measured total collection efficiencies is impossible to assess.

FIGURE 2.8 Experimental results of Meissner and Mickley: penetration versus superficial velocity in a fluidized bed

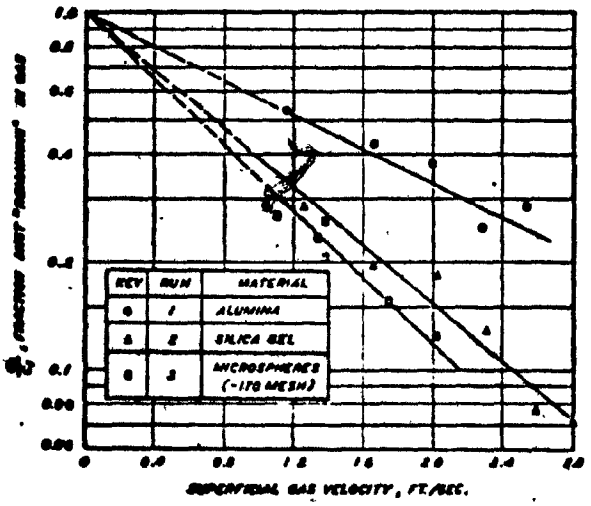

Figure 2. Effect of Type of Solid on Acid Mist Removal

Constant initial bed weight, 32 lb./sq. ft.; initial mist concentration, 70 lb./1,000,000 cu. ft

Bed Material	$\rho_p x10^{-3}$ kg/m^3	Size range μm	$U_{mf} x10^{-2}$ m/s	$Ux10^{-2}$ m/s
Alumina	$2.5x10^3$ D-9	150-75	0.7-2.4	0.35-0.78
Silica Gel	$1.8x10^3$	90-44	0.2-0.7	0.37-0.85
Microspheres	$2.5x10^3$	90-44	0.3-0.9	0.32-0.62

TABLE 2.1 Experimental Details of Meissner and Mickley[M4]

Anderson and Silverman[A3] (1957) collected Gentian violet aerosol particles, 0.54 - 1.0 μm in diameter, in shallow fluidized beds of granules carrying an electrostatic charge induced by charged wires in the bed. Atmospheric dusts were removed to an extent of 97% to 98% in $2.5x10^{-2}$m beds of 200 μm polystyrene beads at $1.5x10^{-2}$ m/s superficial gas velocity. They concluded that the penetration of the challenging aerosol increased with increasing velocity above minimum fluidization.

Scott and Guthrie[S2] (1959) investigated the removal of droplets of dioctyl phthalate, 0.87 μm in diameter, by a $5.1x10^{-2}$m diameter fluidized bed composed of 75 - 105 μm diameter silica gel collector particles. The aerosol was generated in a LaMer-Sinclair aerosol generator and a chemical method, based on the reaction between organic esters and hydroxylamine in alkaline solutions to form a hydroxamic acid, was used to measure concentrations of aerosol. A wire mesh screen of 75 μm opening was used as a distributor, the superficial gas velocity

was varied from 2×10^{-2} to 1.5×10^{-1} m/s and an inverse dependence of penetration on velocity is reported as follows

$$f' \propto \frac{1}{U^{0.78}} \qquad (2.7)$$

Scott and Guthrie, from the dependence of penetration on superficial gas velocity, conclude that the dominant collection mechanism in their work must be diffusion. As it is well known in the two-phase theory of fluidization that the relative velocity between particles and fluid in a fluidized bed is not the superficial gas velocity but the minimum fluidization velocity (U_{mf}) their logic is completely at fault. A gross experimental error exists in their work and therefore their results should be regarded with reservation. They report a drop in penetration from 86% to 72% (i.e. 14%) on increasing the superficial gas velocity from 3×10^{-2} to 14.2×10^{-2} m/s and a collection of 15 - 20% of the challenging aerosol by the inlet section and screen. Collection by inlet section and screen was not analysed as a function of velocity, nor was it removed from the overall penetration to give the effective penetration of the bed itself. Scott and Guthrie justified this by stating[S2]: "As these are integral parts of the fluidized bed no attempt was made to correct efficiencies by this amount." The possibility of different collection on different distributor designs was therefore ignored. In addition, an inlet section and a 75 μm screen (200 mesh) which collects 15 - 20% of 0.87 μm aerosol particles seems extremely high to the author, based on the experience of the work described in later chapters.

Black and Boubel[B4] (1969) investigated the effectiveness of a 5.1×10^{-2} diameter fluidized bed in removing ammonium chloride aerosol at superficial gas velocities of 4.4×10^{-2} to 12.7×10^{-2} meters per second. Glass shot was used as the fluidized medium and the diameter of their collector particles, although not stated explicitly, can be inferred from a photograph to be around 25 μm; the type of distributor used is not reported nor is the value of U_{mf}. The diameter of the challenging aerosol is given as 0.52 μm with respect to count and as 4.3 μm with respect to mass. The large geometric standard deviation, given as 2.32, confirms the fact that they used a heterodisperse aerosol. The aerosol was produced by sublimation of ammonium chloride particles with an effort to achieve monodispersity by allowing the larger particles to settle out in a stirred settling chamber. The concentration of the particles was measured by a Sinclair-Phoenix photometer and their size was analyzed by an optical microscope. Black and Boubel claim 50 - 90% collection efficiencies and report the superficial gas velocity to play a very weak part in aerosol penetration with the following equation

$$(f)' \propto \frac{1}{U^{0.1}} \qquad (2.8)$$

Jugel et al.[J4] (1970) report experiments in removing aerosol particles (0 - 60) μm in diameter, with collection efficiencies up to 95%. Diameter and substance of collector particles, type of distributor, methods of generation and measurement of the aerosol and diameter of fluidized bed are not reported. Very little can be inferred from their results except the fact that they were able to remove solid aerosols by covering the collector particles with a wetting agent called "Ostendol".

Boubel and Junge[B8] (1971) used rotating cylindrical and conical fluidized beds of very small diameter ($4x10^{-2}$m) and tried to investigate the effect of radial acceleration on the filtration of sodium chloride aerosol particles of, reportedly, "submicron" size. The collector particles were glass spheres with a mean diameter of 15 microns and, as the bed was rotated at great speed, experiments at high velocities could be performed. The method of generating the aerosol is not stated and concentrations of the challenging and penetrating aerosol were determined by collecting the particles on a filter and subsequently weighing it. Superficial gas velocities varied from 3.0 to 11.1 m/s and efficiency decreased from 50% to 20% in the range of velocities that were investigated. Boubel and Young conclude that

$$f' \propto \frac{1}{U^{0.903}} \qquad (2.9)$$

which is not significantly different from the results of Scott and Guthrie (Equation 2.7). The study of Boubel and Junge seems to offer very little potential for a practical application as it is much more preferable to use larger or denser collector particles, thus increasing the minimum fluidization velocity, than to spin a fluidized bed at great speed and cost in order to increase the operating superficial gas velocity through the bed. McCarthy et al.[Mc1] investigated the removal of dioctyl phthalate aerosol by $2.5x10^{-2}$m deep fluidized beds of 135 micron diameter alumina granules in a multistage arrangement of a 0.15 m diameter column. The aerosol was produced in a Whitby-type aerosol generator and concentrations of the challenging and penetrating aerosol

were determined with a condensation nuclei chamber. Penetrations were below 0.1% for each of several sizes of the aerosol when the gas velocity was just below that for minimum fluidization. For flows of 2.5 times the minimum fluidization velocity per cent penetrations increased substantially (see Table 2.2).

d_A,μm	f'
1.4	30%
1.0	45%
0.67	58%
0.37	43%
0.28	42%
0.13	37%
0.06	19%

TABLE 2.2 Experimental Results of McCarthy et al.[Mc1]

The conclusion of McCarthy et al. is that as the superficial gas velocity in the bed is increased above minimum fluidization penetration must increase because of gas bypassing in the bubble phase. In their work, a simple Kunii and Levenspiel[K6] model is applied where the bed is viewed as consisting of two regions, a bubble and an emulsion phase with gas interchange between the phases. Their model implicitly assumes that the limiting step is the gas interchange between the two phases (see Chapter 7), which, if true, would result in equal penetrations for each aerosol size; something which as seen from their experimental results is obviously not true. Unfortunately, theoretical predictions and experimental results are compared in this paper only after the aerosol has passed through at least two fluidized beds where, at this point, the gas

in the two phases is mixed at least twice and penetrations are in the low region of 0 - 10%. It is important to note the restricted range of velocities investigated, 1.7×10^{-2} to 3.9×10^{-2} m/s ($U_{mf} = 1.35 \times 10^{-2}$ m/s); as has been proved experimentally by the author, the sharp increase in penetration just after minimum fluidization is a special case when viewed in terms of the wider spectrum of velocities that should be investigated before any general conclusions are drawn. Also, inertial effects are neglected in their study, and Meisen and Mathur[M3] and Paretsky (1972) have shown that this assumption is incorrect even for aerosol diameters as low as 1.1 μm in diameter.

Jackson[J2] (1974) presents a review for collection of submicron particulates in fluidized beds and suggests multistage arrangements for reducing the penetration through the bed.

Knettig and Beeckmans[K3] made a study on the capture of aerosol particles in a 12.7×10^{-2} m diameter fluidized bed supported on a grid of 0.56% free area. The collector particles were glass spheres of mean size 425 μm and experiments were performed with methylene blue-uranine solid aerosol particles of 0.8, 1.6 and 2.9 μm diameter. The aerosol was produced with a spinning disk generator and quantitatively analyzed by fluorometry. Knettig and Beeckmans experimented with three different superficial gas velocities and were unable to draw any conclusions as to the effect of superficial gas velocity on fluidization. This particular work will be discussed in detail in Chapter 7.

Tardos, Gutfinger and Abuaf[T1] present numerical solutions for "Deposition of dust particles in a fluidized bed filter". As, however, the superficial gas velocities in all their calculations are taken as the minimum fluidization velocity it is not exactly clear whether

they simulated a fixed or a fluidized bed. They also claim, as a result of their calculations, that particles of 2 to 3 microns should be removed by diffusional deposition, a statement proved utterly wrong both experimentally and theoretically. A further inaccuracy in their work is that they used correlations presented by Stechina and Fuchs[S8] for cylinders ("Studies in fibrous aerosol filters") in their calculation of diffusion efficiencies for spherical collector particles. Aerosol collection in a vertical pneumatic transport line has been investigated by Behie, Beeckmans, Knettig and Bulani[B1], who combined electrostatic and inertial effects in removing 2.4 μm magnesium sulphate particles by glass beads of 310 and 514 microns diameter coated with a non-volatile oil. Experiments were performed varying the velocity up to 9.75 m/s and single collector efficiencies of up to 98% are reported. In a similar paper Knettig and Beeckmans[K4] present essentially the same experimental apparatus with very similar conclusions and use the equation presented by Johnstone[J3], for the efficiency of Venturi scrubbers (see Section 3.2.1), to correlate their results.

2.3.1.2 Effect of bed depth at minimum fluidization

None of the pioneering works attempt to explain the performance of a fluidized bed removing aerosol particles in terms of the established picture of phenomena occuring in gas fluidization. In particular, they seem to regard the fluidized bed as a homogeneous contactor while it is apparent that a certain amount of the mist or dust bypassing could arise from the part of the gas which passes through the bed as bubbles.

Meissner and Mickley[M4] correlated their results as follows

$$f \propto H_{mf}^{c} \tag{2.10}$$

where c is a constant which varies from 0.16 to 0.34 according to the type of collector particle tested. Black and Boubel[B4] suggest a similar equation:

$$f \propto H_{mf}^{0.4} \tag{2.11}$$

It is interesting to note that Meissner and Mickley who worked with much larger aerosols report a lower constant; this is probably because they also worked at higher velocities and a substantial amount of their aerosol bypassed in the bubble phase.

Knettig and Beeckmans[K3] took a similar approach in regarding the fluidized bed as a homogeneous contactor. By disregarding their results with H_{mf} below 2.5×10^{-2}m they expressed their data in a form similar to Equation (2.10). Their value of c is different for each aerosol and for each velocity used and no correlation of data was attempted. Knettig and Beeckman's results are shown in Figure 2.9 where the penetration expressed as number of transfer units is plotted versus H_{mf}; as seen from their graph curves rather than straight lines will represent their results more accurately.

McCarthy et al.[Mc1] did all their experiments with $H_{mf} = 2.5 \times 10^{-2}$m and, while recognizing the presence of bubbles, no investigation of the effect of bed height on bubble size and penetration was attempted.

FIGURE 2.9 Experimental results of Knettig and Beeckmans: penetration versus superficial velocity in a fluidized bed

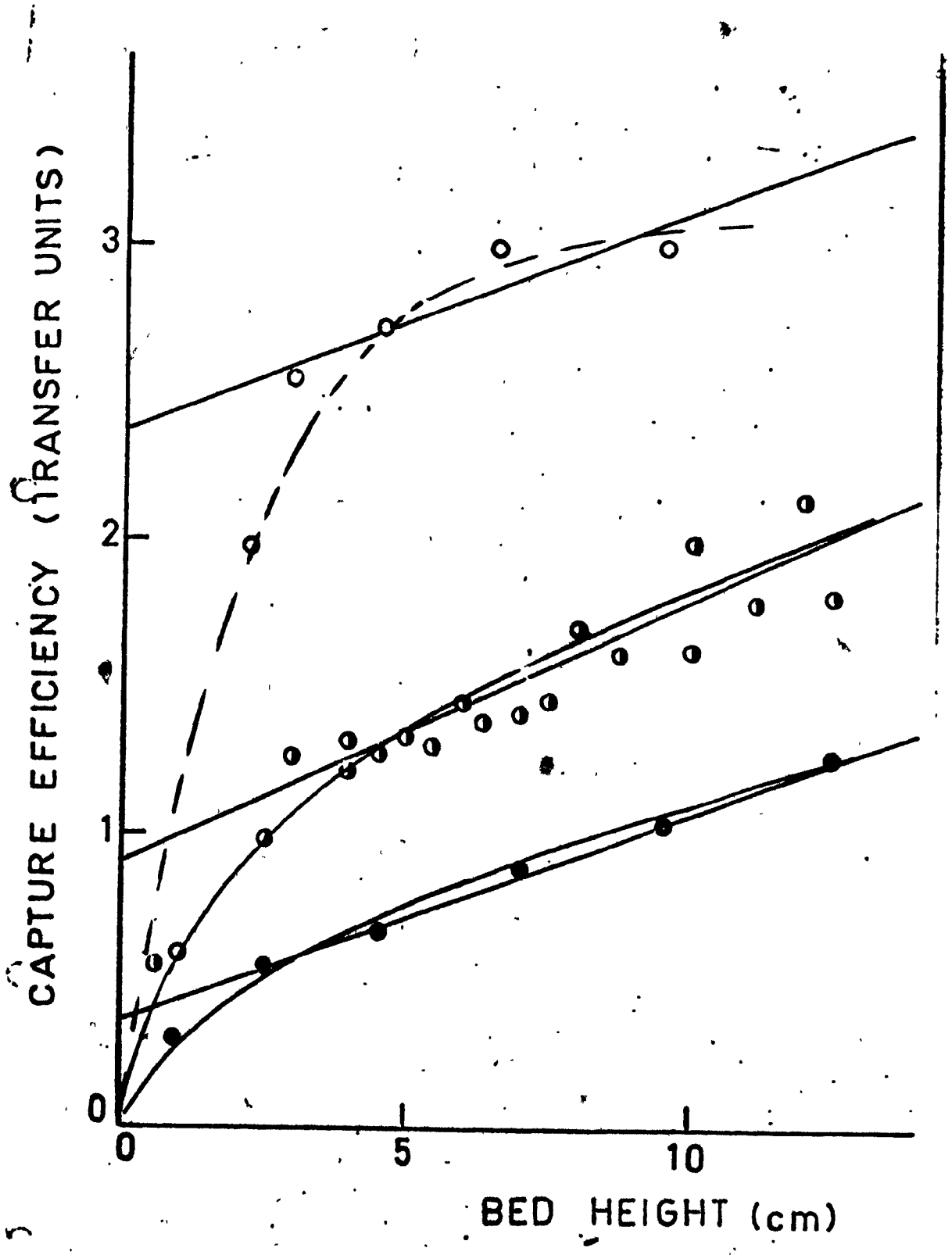
CAPTURE EFFICIENCY (TRANSFER UNITS)
3
2
1
0
0
5
10
BED HEIGHT (cm)

Tardos, et al.[T1] by basing their calculations on U_{mf} simulated what was effectively a fixed bed. Their work is purely theoretical, and bears so little relationship to reality that it need be considered no further.

Jackson[J2] in his review paper recognizes the effect of gas bypassing in the bubble phase. We are not aware of any other studies in the literature that attempt to explain the effect of bed height on aerosol removal in a fluidized bed.

2.3.1.3 Effect of distributor and bed diameter

With the exception of Knettig and Beeckmans[K3], who claim that the grid region of the bed was primarily responsible for the observed capture efficiency, and therefore implicitly recognize the effect of the distributor, there is no other mention in the literature as to the importance of this design variable. As Figure 2.9 will show, the approach of Knettig and Beeckmans who neglected experimental points below an arbitrary bed height is purely artificial and offers no explanation of the distributor effect.

The majority of the previous studies (see Section 2.3.1.1) used beds of very small diameter and it is well known that gas fluidized beds of such small diameter behave very differently from full scale beds. More specifically, beds of a small diameter tend to operate in the slugging regime at high superficial gas velocities.

2.3.1.4 Bed loading

Although at first sight it may seem that bed loading should affect the aerosol penetration, this appears not to be the case. Meissner and Mickley[M4] report that, within the precision of their measurements, the aerosol removal was independent of bed age. Alumina and silica gel collector particles could collect up to 7% by weight of sulphuric acid aerosol before the bed was too sticky to fluidize. Black and Boubel[B4] state that no effect of bed age was detected in their experiments.

2.3.2 Effect of aerosol parameters

The physical parameters describing the aerosol are diameter, d_A, physical state, i.e. solid or liquid, density, ρ_A, monodispersity, electrical charges and aerosol concentration. Except for very small aerosols[F5] ($d_A < 0.4$ μm) the penetration decreases with increasing aerosol size (see Section 2.2). In fluidized beds, McCarthy et al.[Mc1] (see Section 2.3.1.1) report a peak penetrating size around 0.67 μm for liquid dioctyl phthalate aerosols. Meissner and Mickley[M4] working with aerosols 2 to 6 μm diameter claim penetration to decrease with superficial gas velocity while Scott and Guthrie[S2] and Black and Boubel[B4] who were working with aerosols of 0.87 μm and 0.52 μm, respectively, claim the opposite. It is not, however, clear whether the decrease in penetration with respect to velocity is because of larger aerosol diameters or higher operating velocities through the bed. The density of the aerosol, ρ_A, affects the Stokes number and the gravity settling parameter (see Chapter 3). However, there is insufficient information in the literature to determine the effect of this variable on penetration.

Although in a recent paper Willeke et al.[W1] claim that the fluidized bed is an efficient device for deagglomerating and dispersing dust it appears that solid aerosols may be collected effectively provided the surface of the collector particles is coated with a non-volatile liquid. Jugel et al.[J4] report removal of quartz sand particles by collectors covered with a wetting agent called "Ostendol". Pilney and Erickson[P4] introduced oil into the pores of their collector particles (aluminum silicate) and discovered that the removal efficiency increased from 85% to 95% for solid, 8 μm fly ash aerosols. Knettig and Beeckmans[K3,K4], when studying the removal of solid methylene blue-uranine aerosols, covered the surface of their collector particles with dioctyl phthalate in order "to eliminate reentrainment".

In principle, the monodispersity of aerosols should not affect the efficiency of individual particles. However, any gravimetric measurement of heterodisperse challenging and penetrating aerosols will be biased to give most significance to the largest size of particles present. Furthermore, the implicit assumption made in almost all previous studies that the size distribution of the penetrating aerosol is equal to the size distribution of the challenging aerosol is obviously not true and is approximated only in the case of very monodisperse aerosols, with low geometric standard deviation typically less than 1.2. Therefore, the most accurate method, in this type of study, is actually counting and sizing the aerosol particles present. With the exception of McCarthy et al.[Mc1] who used a condensation nucleation counter most previous studies lack this experimental advantage.

Electrical charges and induced electrostatic forces probably contribute to collection efficiencies in a fluidized bed. Black and Boubel[B4] came to the conclusion that induced electrostatic attraction between aerosol and collector particles were about as important as diffusional deposition for 0.52 μm aerosol particles; both collection mechanisms, however, were calculated to be quite low[B4]. Anderson and Silverman[A3] with experiments on electrostatic charging in fluidized beds report uncharged beds to show lower efficiencies. It has been suggested by Pilney and Erickson[P4] that fly ash collection might be improved by use of a corona discharge upstream from a fluidized bed.

The rate of removal of aerosol particles may be considered to be proportional to the concentration. A pseudo-first order reaction is therefore postulated and there is experimental evidence in the literature to support this. Meissner and Mickley[M4] (0.6 to 2.7 mg/m^3), Scott and Guthrie[S2] (24.7 to 32.4 mg/m^3) and Black and Boubel[B4] (0.03 to 8.3 mg/m^3) report the collection efficiency in a fluidized bed to be independent of aerosol concentration. In principle, at high aerosol concentrations, the collection mechanisms could be supported by agglomeration of aerosols. However, this mechanism becomes important only at very high concentrations, typically greater than 10^{12} particles/m^3 [F5].

2.4 Particle Collection in a Spouted Bed

Meisen and Mathur[M3] reported a theoretical and experimental study of (1-3) μm aerosols in a 0.15 m diameter spouted bed of 1,700 μm collector particles. Collection in the spout and in the annular zone were treated separately but allowance was made for interphase transfer.

For the spout the correlation given by Behie et al.[B1] was used. For the annulus the uncorrected form of Equation (3.12) was used. Once spouting was established, it was found that penetration decreased with increasing gas velocity. Meisen and Mathur concluded clearly that the predominant collection mechanism in the spout was inertial. However, the relatively high pressure drop associated with a spouted bed of the depth necessary to obtain adequate collection limits the industrial attractiveness of such a device.

CHAPTER 3. COLLECTION MECHANISMS IN A DENSE PARTICULATE MEDIUM

3.1 Introduction

The three factors that are important in a filtration process are the dispersed particles, the dispersion medium and the collecting medium. The aerosol particles are characterized by diameter, d_A, shape, density, ρ_A, electric charge, q'_A, and concentration, which can be expressed on a number, weight or volume basis. The gas flow is characterized by velocity, U, density, ρ_f, absolute temperature, T, pressure, P, viscosity, μ_f, and humidity. The collecting medium is characterized by its geometrical dimensions - the filtration surface, A_B, thickness, H, the geometrical shape and size of collector particles, the void fraction of the filter, ϵ, and the specific surface and electric charge, q'_p, of the collector particles. The basic parameters that describe the process of filtration are the per cent penetration, f', and the resistance to flow or pressure drop, ΔP, of the filter. The per cent penetration is defined as the percentage of aerosol not collected by the filter (i.e. 100f, where f is the fractional penetration).

In our analysis we confine ourselves to spherical aerosol and collector particles. The dispersion medium is air at atmospheric temperature and pressure. As the system under study was almost isothermal and as the pressure differentials across the bed were of the order of cms of water, the effect of any temperature and pressure variations on penetration are assumed to be negligible.

The remaining collection mechanisms causing deposition in the present work are inertial collection, direct interception, diffusion

deposition, gravitational and electrostatic deposition. These mechanisms and their relative importance are discussed in the following section.

In our approach to aerosol deposition on fixed and fluidized beds we have used one of the most widely used approaches, namely "the method of isolated collector particles". This method was developed by Langmuir[L6,L8] during the Second World War and basically starts by calculating the velocity field around an isolated collector; this is used for the calculation of the deposition efficiency on the particle due to various mechanisms of aerosol deposition.

The deposition efficiency of a collector particle is defined as

$$E_T = \frac{\text{particles of aerosol collected}}{\text{particles in approach volume}} \qquad (3.1)$$

The influence of the neighbouring particles, which may be called "the interference effect"[C3], is expressed by the introduction of empirical or semi-empirical corrections and the final stage of the calculation passes from the efficiency of an isolated collector particle to the evaluation of the efficiency of a particle in a filter. In subsequent chapters, this approach is used to evaluate the efficiencies of fixed and fluidized beds, including in the latter case, the hydrodynamic behaviour of a fluidized bed.

3.2 Aerosol Collection Mechanisms around an Isolated Spherical Particle

3.2.1 Inertial collection

The presence of the collector causes curvature of the gas streamlines in its neighbourhood. Because of their inertia, the aerosol particles accelerate less than the gas and so their trajectories do not follow the streamlines; they are projected against the collector and may deposit there (see Figure 3.1). From the general definition of the deposition efficiency of a collector particle it follows that

$$E_I = \frac{(2y_{CR})^2}{(d_p)^2} \qquad (3.2)$$

The critical trajectory of the aerosol particle, y_{CR}, is defined as the distance from the x-axis (Figure 3.1) beyond which it is, theoretically, impossible to remove the particle by inertial collection. The critical trajectory of the aerosol particle is determined by the mass, resistance to flow and by its velocity of approach to the collector. Stairmand[S7] presents theoretical predictions of inertial collection efficiency in terms of the dimensionless group $(d_A g/U_R U_T)$ for isolated spherical and cylindrical collector particles.

In analyzing deposition by inertial impaction the particles are considered to be point masses in the calculation of the collection efficiency. However, their size is accounted for in evaluation of the fluid's resistance to the particles' motion.

Three factors determine the inertial collection efficiency. The first is the velocity distribution of the gas flowing around the collector, which varies with the Reynolds number of the gas with respect

FIGURE 3.1 Schematic representation of inertial deposition

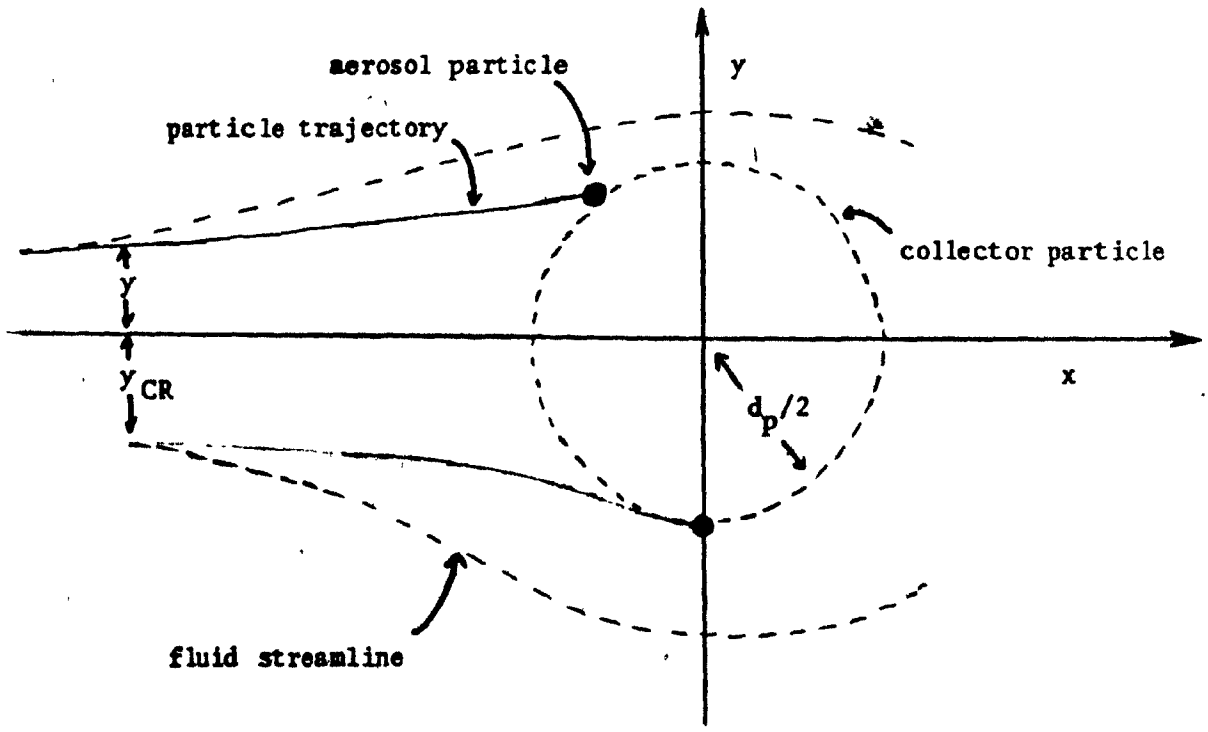
aerosol particle
y
particle trajectory
collector particle
y
x
y_{CR}
$d_p/2$
fluid streamline

to the collector. The second factor is the trajectory of the particle. This depends on the mass of the particle, the air resistance, the size and shape of the collector, and the rate of flow of the gas stream. The third factor is the adhesion of the particle to the collector - usually assumed to be 100%.

The first factor is described by the Reynolds number of the collector particle defined as

$$Re_p = \frac{d_p U_{pf}}{\mu_f} \tag{3.3}$$

and the second factor is described by the Stokes number defined as

$$St = \frac{d_A^2 U_{pA}}{9 \mu_f d_p} \tag{3.4}$$

At high values of Reynolds number (potential flow régime) the perturbing effect of the collector particle is limited to a relatively small region close to the collector. Except near the collector surface the flow pattern corresponds to that of an ideal gas. Potential flow is an idealization which is never approximated truly. While potential flow is a reasonable approximation for the forward half of an isolated collector it is less good for packed beds where the collector will be affected by the wakes of neighbouring particles. In the creeping flow régime ($Re_p < 0.1$)[83] , where the viscous terms in the equation of fluid motion dominate, the disturbance created by the collector is felt at much larger distances. The effect of the sudden spreading of the streamlines at high Reynolds numbers is to enhance the influence of particle

inertia and therefore cause a higher collection efficiency. If this mechanism is studied independently and if it is assumed that the aerosol particles obey Stokes Law then the equations of motion for the particles can be derived by applying Newton's second law to the aerosol particle.

The equations in dimensionless form and rectangular co-ordinates are (see Appendix A for the derivation of these equations)

$$St\frac{d(U_A)'_x}{d\tau} = ((U_{rel})'_x - (U_A)'_x) \tag{3.5}$$

and

$$St\frac{d(U_A)'_y}{d\tau} = ((U_{rel})'_y - (U_A)'_y) \tag{3.6}$$

The solution to the equation of motion will depend upon the velocity field assumed and several studies on inertial collection are reported.[H3,T1,A2,S3,D5,D7,D8]

For potential flow around spheres Langmuir and Blodgett[L9] suggest that the collection efficiency can be expressed in the region St $\geq$ 0.02 by the empirical formula

$$E_I = \frac{(St)^2}{(St+0.05)^2} \tag{3.7}$$

For creeping flow around spherical collector particles Langmuir and Blodgett[L9] obtained a curve which is represented by

$$E_I = \left[1.0 + \frac{0.751n(2St)}{St-1.214}^{-2}\right] \tag{3.8}$$

Most of the theoretical solutions to Equations (3.5) and (3.6) yield a "critical Stokes number" below which no inertial deposition takes place. For spherical collectors $St_{CR} = 0.083$[F5] . In reality, in cases of turbulent flow, particles may also deposit on the back of the collector and the inertial collection efficiency for $St \leqslant St_{CR}$ is not zero.

In the case of a fixed bed consisting of loosely packed collector particles ($0.42 < \varepsilon < 0.50$), Paretsky[P1] reports inertial collection efficiencies far below the critical Stokes number ($7.4 \times 10^{-5} < St < 4.4 \times 10^{-2}$) and suggests the following empirical correlations for inertial collection in fixed beds for $1{,}410\ \mu m < d_p < 2{,}000\ \mu m$.

$$E_I = 2.5\ St^{1.13} \tag{3.9}$$

for $710\ \mu m < d_p < 840\ \mu m$

$$E_I = 0.78\ St^{0.98} \tag{3.10}$$

Paretsky combines the data from the two sand sizes (Equations (3.9) and (3.10)) into one equation of the form

$$E_I = 2.0\ St^{1.13} \tag{3.11}$$

for low Stokes numbers. ($St < 4.4 \times 10^{-2}$).

Meisen and Mathur[M3] investigated aerosol removal in a spouted bed composed of cement clinker particles approximately 1700 μm diameter. For the annulus region of a spouted bed, which essentially

behaves like a fixed bed, they suggest an equation to describe the total collection efficiency of collector particles*

$$E_I = 2.6\ St + 7.5\times10^{-4} \qquad (3.12)$$

where the first term represents collection by inertial impaction. Limited experimental results obtained by Meisen and Mathur suggest, according to the authors, that Equation (3.12) may be extrapolated to a Reynolds number of at least 250 and a Stokes number of 0.007.

Knettig and Beeckmans[K4] based on the experimental results presented by Herne[H8] on isolated spherical collectors suggest a polynomial approximation for $0.0416 < St < 0.3$ of the form

$$E_I = 3.76\times10^{-3} - 0.464\ St + 9.68\ St^2 - 16.2\ St^3 \qquad (3.13)$$

It will be shown in Section 3.2.6 that the empirical Equations (3.9) to (3.12) are a simplified version of an equation proposed by Davies for isolated collector particles. The hypothesis that there exists a critical Stokes number below which no inertial impaction takes place has not been proved experimentally. According to Fuchs[F5] the theoretical proof of St_{CR} is not rigorous because it assumes that the velocities of the fluid and aerosol particles are equal not at infinity but at some finite distance from the center of the collector. It seems, therefore, that in general the efficiency due to inertial impaction at low Stokes number is not zero and is represented by an equation of the form

*Examination of the calculations on which this equation is based showed that St was based on the density of the collector rather than the aerosol. Therefore the coefficient of St in Equation (3.12) has been corrected by multiplying by ρ_A/ρ_p.

$$E_I = \alpha_I St * f(Re) \qquad (3.14)$$

3.2.2 Direct interception

The direct interception mechanism results from the finite size of the aerosol particles. The particle is intercepted as soon as it approaches the surface of the collector to a distance equal to its radius. This mechanism can be studied independently or by changing the boundary conditions when the equations of convective diffusion (Section 3.2.3) or the equations of motion of the aerosol particles are being solved (Equations 3.5, 3.6). The latter method, however, requires numerical solutions and is quite complicated even for a single isolated particle. Obviously, this approach is of little value when studying aerosol collection in a fixed or fluidized bed.

The first method studies the direct interception mechanism independently from other collection mechanisms. This has the obvious advantage that it presents analytical solutions for simple flow patterns which can then be incorporated with other collection mechanisms.

The direct interception mechanism is described by the following parameter.

$$N_R = \frac{d_A}{d_p} \qquad (3.15)$$

The efficiency of deposition due to this mechanism is a function of N_R and the Stokes number (Equation 3.4). To get the form of this relation in the following two extreme cases is relatively straightforward.

3.2.2.1 Interception efficiency for St → ∞

In this case the inertia of particles is such that their trajectories, in the vicinity of the collector particle, are rectilinear. The efficiency due to direct interception is (see Appendix B)

$$E_R = \frac{(d_p+d_A)^2 - d_p^2}{d_p^2} \qquad (3.16a)$$

which is approximated for small N_R by

$$E_R \approx 2\frac{d_A}{d_p} \equiv 2N_R \qquad (3.16b)$$

3.2.2.2 Interception efficiency for St → 0

Here the particles have no inertia and follow the streamlines of the gas. The interception collection depends on the type of flow assumed around the spherical collector particle.

The volumetric flow rate around the spherical collector is obtained by integrating, analytically, the velocity field from $r = d_p/2$ to $r = (d_p+d_A)/2$ for creeping flow around a sphere (see Appendix B)

$$E_R = (1+N_R)^2 - \frac{3}{2}(1+N_R) + \frac{1}{2(1+N_R)} \qquad (3.17)$$

which, for small N_R, is approximated by

$$E_R \approx \frac{3}{2}(N_R)^2 \qquad (3.18)$$

for potential flow around a sphere

$$E_R = (1+N_R)^2 - \frac{1}{(1+N_R)} \tag{3.19}$$

which is approximated by

$$E_R \approx 3N_R \tag{3.20}$$

Then, for potential flow around an isolated sphere the efficiency due to direct interception is

$$E_R = \alpha_R N_R, \; 2 < \alpha_R < 3 \tag{3.21}$$

In a fixed bed the effect of neighbouring particles will probably be to increase the value of α_R due to the sharper curving of the streamlines. For creeping flow around a sphere

$$E_R = \alpha_R N_R^2, \quad \alpha_R \approx 3/2 \tag{3.22}$$

3.2.3 Diffusional deposition

Because of Brownian movement (sometimes described as "The Drunkard's Walk" or "Random Walk") the trajectories of particles do not coincide with the streamlines of the gas even in the absence of inertial

effects. Particles will migrate to a collector surface purely as a result of this random diffusional motion. As the Brownian movement of the aerosol particles increases with decrease in aerosol size, diffusional collection goes up. When diffusional collection is considered the aerosol particles may be considered to be infinitesimally small.

We define a mass transfer coefficient k_A(m/s) based on the local concentration of aerosol particles, C,

$$R_D = \pi d_p^2 k_A C \tag{3.23}$$

where R_D is the rate of deposition of aerosol particles on the collector by diffusion and the efficiency due to diffusion deposition is

$$E_D = \frac{4k_A}{U} \tag{3.24}$$

The problem is to determine the mass transfer coefficient in terms of aerosol and collector particle diameter and superficial gas velocity. The analysis may be expressed in terms of the Peclet number, or its equivalent, the product of Reynolds number and Schmidt number, and the Sherwood number. These dimensionless numbers are defined as follows:

$$Pe = \frac{d_p U}{D_A} \tag{3.25}$$

$$Sc = \frac{\mu_f}{\rho_f D_A} \tag{3.26}$$

where D_A(m^2/s) is the effective diffusivity of aerosol particles.

$$Sh = \frac{k_A d_p}{D_A} \tag{3.27}$$

$$Pe = Re * Sc \tag{3.28}$$

using Davies'[D4] equation for the effective diffusivity of the aerosol particles

$$D_A = \frac{k_B T F}{3\pi\mu_f d_A} \tag{3.29}$$

where k_B is Boltzmann's constant, T is the absolute temperature, ^oK, and

$$F = 1.0 + \frac{2.632\times10^{-8}}{d_A}\left[6.32 + 2.01\exp(-8.322\times10^{6} d_A)\right] \tag{3.30}$$

where F is the Stokes-Cunningham slip correction factor. Diffusion from a flow towards the surface of a sphere has been investigated theoretically and experimentally in connection with the condensation of vapour on the surface of droplets or their evaporation. It can be shown that[F5] the rate of diffusion of aerosols towards the surface of a stationary spherical collector particle situated in an infinitely large volume of aerosol is

$$R_D = 2\pi D_A d_p C \tag{3.31}$$

from Equations (3.23) and (3.31), for a stationary sphere

$$k_A = \frac{2D_A}{d_p} \tag{3.32a}$$

or,

$$Sh = 2.0 \tag{3.32b}$$

R_D for a stationary sphere increases in flow for $Re_p > 3.0$[F4] by a factor $2.0 + 0.54\ Re_p^{1/2}Sc^{1/3}$. Table 3.1 gives D_A and the corresponding Schmidt number for dioctyl phthalate aerosol in air at 30°C. As can be seen particle diffusivities are several orders of magnitude smaller than diffusivities of gases and are closer to the values obtained for diffusivities of solutes in liquid. The Schmidt number which is around unity for gases is greater than 10^5 even for 0.1 μm diameter aerosols. For this reason, experimental data on diffusion of vapours cannot be extended to aerosols. What is required here is correlations that apply to low Reynold numbers and very high Schmidt numbers.

The theory of diffusion towards a sphere at these conditions has been investigated by various authors and their results in dimensionless parameters are of the form

$$Sh = \beta_D Re_p^{1/3} Sc^{1/3} \tag{3.33}$$

where, according to Levich[L15] $\beta_D = 1.0$, to Friedlander[F3] $\beta_D = 0.89$ and to Aksel'rud[A1] $\beta_D = 1.07$.

We are not aware of any experimental data on the diffusion of flowing aerosols on to spheres but Equation (3.33) can be verified by the data of Aksel'rud for the dissolution rate in oil of spheres of benzoic acid at $0.1 < Re_p < 2.5$ and $Sc = 2.3 \times 10^6$; these experiments give

TABLE 3.1 Effective Diffusivities and Schmidt Number for Dioctyl Phthalate Aerosol in Air at 30°C

d_A m	D_A m^2/sec	S_c
0.1	3.3×10^{-10}	4.58×10^{9}
0.2	1.26×10^{-10}	1.2×10^{10}
0.5	4.14×10^{-11}	3.65×10^{11}
1.0	1.95×10^{-11}	7.73×10^{10}
2.0	9.24×10^{-12}	1.63×10^{11}

$\beta_D = 1.1$ in an excellent agreement with theory.

For large Reynolds number, $600 < Re_p < 2600$ and $Sc = 2.3 \times 10^6$ Aksel'rud deduced the following equation which was confirmed experimentally

$$Sh = 0.8\, Re_p^{1/2} Sc^{1/3} \tag{3.34}$$

For intermediate Reynolds number, $100 < Re_p < 700$, and Schmidt numbers of the order of 10^3 Garner[G2] obtained an equation similar to (3.34) but with a value for $\beta_D = 0.95$.

For the ranges of Reynolds and Schmidt number in this research Equation (3.33) is a better candidate for describing the diffusional deposition of aerosols on spherical collector particles. Substituting for dimensionless parameters in Equation (3.33)

$$\frac{k_A d_p}{D_A} = \beta_D \frac{d_p^{1/3} U^{1/3}}{D_A^{1/3}} \tag{3.35}$$

and the local mass transfer coefficient is

$$k_A = \beta_D U^{1/3} D_A^{2/3} d_p^{-2/3} \tag{3.36}$$

the efficiency due to diffusional deposition is, from Equation (3.23),

$$E_D = \alpha_D N_D \tag{3.37}$$

$$\alpha_D = \frac{\beta_D}{4} = 0.22 - 0.27 \tag{3.38a}$$

$$N_D = U^{-2/3} D_A^{2/3} d_p^{-2/3} \qquad (3.38b)$$

3.2.4 Gravitational deposition

The gravitational collection of the aerosol particles represents the sedimentation or settling of particles due to gravity forces. Gravitational collection occurs because the gaseous boundary layer surrounding the collector surface is effectively at rest. Particles of negligible inertia will settle onto the collector while falling vertically at their sedimentation velocity, U_S.

The parameter for gravitational deposition, N_G for an isolated collector particle may be defined as[R3]

$$N_G = \frac{U_S}{U} \qquad (3.39a)$$

and, in the absence of other collection mechanisms, the gravitational collection efficiency is

$$E_G = \alpha_G N_G \qquad (3.39b)$$

if we assume that the aerosol particle is in the Stokes flow regime; then the terminal velocity can be calculated from Equation (3.40)[P3]

$$U_S = \frac{d_A^2 g(\rho_A - \rho_g)}{18\mu_g} \qquad (3.40)$$

Thomas and Yoder[T2,T3] and Paretsky[P1] report different collection efficiencies due to gravitational deposition for "upshot" and "downshot" flow.

However, as the terminal velocity of a 1 μm particle of specific gravity 1 is around 3.5×10^{-5} m/sec[D5] this mechanism of aerosol removal plays only a subsidiary part under the normal conditions of filtration[F5] and becomes important only when U_s becomes appreciably large and/or U is low.

3.2.5 Electrostatic deposition

The electrostatic properties of small particles could affect their motion and collection in an electric field. As there is some indication of electrostatic charging in fluidized beds (see Section 3.4) the mechanisms of electrostatic deposition of aerosols on a collector particle are discussed here. The equations presented were derived basically by Kraemer and Johnstone[K5] (1955) who solved the equations of motion for aerosol particles in an electric field neglecting all other forces. They calculated the collection efficiency of conducting and non-conducting aerosol particles by a conducting sphere due to electrostatic forces, for potential and viscous flows and for several interception parameters. Potential flow and negligible Brownian motion of aerosol particles were assumed.[K5]

There are five aspects of electrical forces acting in a system of particles approaching a collector. For each case a collection parameter, the ratio of the electrostatic force to the Stokes-Cunningham drag force has been defined by Kraemer and Johnstone.

For the coulombic force between a charged collector and a charged particle the descriptive parameter is

$$N_{E1} = \frac{Fq_A q_p}{3\pi^2 d_p^2 d_A \mu_f U_{rel} \epsilon_o'} \tag{3.41}$$

For the induction force between a charged spherical collector and an uncharged particle

$$N_{E2} = \frac{(\epsilon'-1)}{(\epsilon'+2)} * \frac{2}{3} * \frac{F d_A^2 q_p^2}{\mu_f U_{rel} d^5 \epsilon_o'^2} \tag{3.42}$$

The induction parameter representing forces between charged particles and uncharged spherical collectors is given by

$$N_{E3} = \frac{Fq_A^2}{3\pi^2 \mu_f d_A U_{rel} \epsilon_o' d_p^2} \tag{3.43}$$

For the case of the repulsion force exerted by unipolar charged collector particles on the aerosol particles being deposited

$$N_{E4} = \frac{Fq_A^2 D_p C}{18\, \mu_f d_A U_{rel} \epsilon_o'} \tag{3.44}$$

For the attraction between a charged aerosol particle and a grounded collector which has a charge induced by the surrounding unipolar aerosol particles

$$N_{E5} = \frac{Fq_A^2 C D_{AER}^2}{12\, \pi d_A U_{rel} d_p \epsilon_o'} \tag{3.45}$$

where D_{AER} (meters) is the diameter of the spherical aerosol cloud which influences the collector.

The induction parameter representing forces between charged particles and uncharged spherical collectors, N_{E3}, is quite small and may be neglected[K5]. The forces corresponding to N_{E4} and N_{E5} depend upon aerosol concentration and start becoming important only at high aerosol concentrations ($C > 10^{16}$ particles/m^3). Approximate solutions for the equations of motion and collection efficiency may be obtained if only one type of the electrostatic forces is considered at a time and if interception is neglected. Kraemer and Johnstone carried out these calculations for potential flow around spheres and their results are presented here in their appropriate form.

For the collection of a charged aerosol by a spherical, charged collector, considering only the coulombic attraction force

$$E_{E1} = -4N_{E1} \tag{3.46}$$

and, for the collection of uncharged aerosol particles by a charged collector, considering only the induced charge on the particle

$$E_{E2} = \left(\frac{15\pi}{8} N_{E2}\right)^{0.4} \tag{3.47}$$

It should be noted that for maximum collection of aerosol particles by collectors both the particles and the collectors should be highly charged. Electrostatic collection is enhanced by decreased relative velocity between the aerosol particles and the collector (Equations (3.41) to (3.45)). All electrostatic collection parameters

except the one describing the induction force between a charged collector and an uncharged aerosol particle decrease with increasing diameter of particle.

For the case of a neutral aerosol only Equation (3.47) could provide a contribution to aerosol collection by induced electrostatic attraction. As the aerosol, in this study, is bathed in a high concentration of bipolar air ions which are generated by a radioactive source (see Section 4.2) it can be assumed to be electrically neutral.

In general terms

$$E_E \approx E_{E2} - \alpha_E \left[\frac{(\epsilon'-1)}{(\epsilon'+2)*\epsilon'_o} * \frac{Fd^2_A q^2_p}{\mu_f U_{rel} d_p^5} \right]^{0.4} \qquad (3.48)$$

where α_E is the constant of proportionality. This equation could contribute to collection only in a fluidized bed where the collector particles pick up an average charge, q_p, as a result of fluidization (see Section 3.4).

3.2.6 Total collection efficiency of an isolated spherical particle

When depositing from flow past a sphere, aerosol particles may be subject to the simultaneous effect of all the mechanisms so far mentioned. Fuchs[F5] has shown that the individual efficiencies of a collector particle are not additive. Indiscriminate summation of partial efficiancies will approximate the correct solution only if individual efficiencies are quite low. Robinson[R4] has shown that only for $N_G << 1$ are gravitational and inertial depositions additive. According to Fuchs[F5] the total efficiency is greater than any of the partial efficiencies and smaller than their sum.

If, however, the individual collection efficiencies are very small and we are allowed to make the assumption that there is no appreciable interference between mechanisms, it is quite safe to carry out the addition.

For the total collection of an isolated spherical particle the best equation for inertial deposition plus direct interception is given by Davies[D5]

$$E_{IR} = c_1\left[N_R + (c_2+c_3N_R)St - c_4N_RSt^2\right] \tag{3.49}$$

assuming N_R, $St \gg N_RSt$, N_RSt^2 Equation (3.49), reduces to

$$E_{IR} \approx c_1N_R + c_2St \tag{3.50}$$

which has the same form as the equations obtained experimentally by Meisen and Mathur[M3] (Equation (3.12)) and Paretsky[P1] (Equations (3.9) to (3.11)) for fixed beds.

If we further assume that diffusional and gravitational settling efficiencies are small enough to be additive then, in the absence of any electrostatic effects, the total collection efficiency of an isolated spherical particle is given by

$$E_T = E_R + E_I + E_D + E_G \tag{3.51}$$

where E_D is given by Equation (3.37) and E_G by Equation (3.39b).

In the presence of an electrostatic field, considering only the induced charge on the aerosol particles by the charged spherical collector total efficiency becomes

$$E_{TE} = E_T + E_E \tag{3.52}$$

where E_E is given by Equation (3.48).

3.3 Total Collection Efficiency of a Spherical Particle in a Fixed Bed

The efficiency of an isolated spherical particle is different from its efficiency when it is surrounded by other collector particles. There are two main reasons for this effect: a) the interstitial gas velocity in the bed is higher than the superficial gas velocity; and b) the streamlines around the collector particle are different because of the interfering effect of the neighbouring particles. The presence of other particles results in an increase in the total efficiency of the collector. It is possible that this increase is different for every mechanism. The most important parameter describing the interference effect is the voidage of the fixed bed; but the effect of voidage may depend on other parameters such as the collector particle Reynolds number.

There is some disagreement among researchers as to how to take account of the interference effect. Chen [C3] states that the increase is a function of the filter porosity and probably Reynolds number. Langmuir [L6] introduced a correction constant, calculated experimentally from pressure drop; implicitly this too depends on bed voidage and Reynolds number. Chen [C3] suggests an empirical formula of the form

$$E_{BT} = E_T(1.0 + 4.5(1-\epsilon)) \tag{3.53}$$

and Davies[D5] claims that the interference effect is the same for different mechanisms and introduces an equation of the form.

$$E_{BT} = E_T(0.16 + 10.9(1-\epsilon) - 17(1-\epsilon)^2) \tag{3.54}$$

Both of these equations are for fibrous filters of high voidage.

Dorman[D12,D6] suggested an equation which assumes that the interference effect is the same for different mechanisms.

$$E_{BT} = \frac{E_T}{\epsilon} \tag{3.55}$$

Paretsky[P1] tried to explain penetration in a fixed bed in a more rigorous manner. He used Happel's[H1] "Free Surface Model" to obtain analytical expressions that would predict the capture of aerosols by each of the filtration mechanisms in granular beds. The free surface, or cell model, assumes the fixed bed is composed of many cells; each cell containing a particle surrounded by a fluid envelope. The outside surface of each cell is assumed to be frictionless and the entire disturbance caused by the particle is confined in the cell. Paretsky then included the effect of gravitational, inertial and diffusional collections in the equations of motion of the aerosol particle (Equations (3.5) and (3.6)) and solved them numerically. Unfortunately, his theoretical predictions for aerosol collection were a few orders of magnitude lower than his experimental results. The

conclusion to draw from this is that the interference effect of neighbouring particles penetrates well into the cell boundaries resulting in much higher collection efficiencies. The results of LeClair and Hamielec[L11] show that application of the cell model is inaccurate even for mass transfer processes. In its general form the interference effect may be expressed as

$$E_{BT} = f_1(\epsilon)c_R E_R + f_2(\epsilon)c_I St^2 + f_3(\epsilon)E_I + f_4(\epsilon)E_G \qquad (3.56)$$

where $f(\epsilon)_{i=1,4}$ are functions of voidage.

If we make the assumption that either (i) one of the terms is dominant in the R.H.S. of the equation; or (ii) that

$$f_1(\epsilon) \approx f_2(\epsilon) \approx f_3(\epsilon) \approx f_4(\epsilon) \qquad (3.57)$$

then, Equation (3.56) may be written as

$$E_{BT} = F(\epsilon)\, E_T \qquad (3.58)$$

As the voidage is constant in a fixed bed and as the same assumption may be made in the dense phase of a fluidized bed, we can write for our purposes,

$$E_{BT} = \alpha_B E_T \qquad (3.59)$$

This, then, is the total collection efficiency of a spherical particle in a fixed bed, or of a spherical particle in the dense phase of a

fluidized bed in the absence of any electrostatic forces.

3.4 Total Collection Efficiency of a Spherical Particle in a Fluidized Bed

When a bed of spherical collector particles is fluidized, electrostatic charges are produced because of particle to particle contact and particle to bed wall contact. Thus, the bed particles could get charged and contribute to the collection of aerosol in a fluidized bed. There is very little in the literature on electrostatic charging of fluidized beds. Several authors have commented on static generation in fluidized systems[D9,P2,L14,L16,W2] but only a few have carried out serious investigations. Cirorowski and Wlodarski[C4] report that the maximum charge was recorded just below the surface of the bed. Kisel'nikov et al.[K2] confirmed this result. Boland and Geldart[B7] made the important discovery that static electrification is generated by the motion of particles around gas bubbles, particularly in the region of the wake. (This is significant because a high amount of unconverted gas is contained in the bubbles). The same authors claim that charges generated in the nose of the bubble and in the wake are of opposite signs; their results, however, apply to two-dimensional beds and should be regarded with reservation.

Other factors affecting electrostatic charging in fluidized beds are particle size and material, and bed wall material[B7]. Relative humidity does not affect generation of charges but plays an important role on the rate of charge dissipation.[B7]

Black and Boubel[B4] report that for 0.52 μm ammonium chloride aerosol induced electrostatic attraction (see Equation (3.47)) could

be as important as Brownian diffusion. It is interesting to note that (Equation (3.47))

$$E_{E2} \propto d_A^{0.8} \tag{3.60}$$

This is because the induced dipole increases with distance of separation of charges.

Although much research is required in this area, it seems likely that at certain operating conditions the slightly disadvantageous phenomenon of electrostatic charging in fluidized beds could contribute significantly in removing airborne particulates. Figure 3.2 gives[K5] some calculated values for efficiencies resulting from induced electrostatic charges in spherical collector particles.

From Equation (3.48)

$$E_{E2} \propto q_p^{0.8} \tag{3.61}$$

As the results of Boland and Geldart indicate that the amount of electrostatic generation in a fluidized bed depends on the collector to collector friction we can assume from Equation (3.61) that

$$E_{E2} = f(d_b) \tag{3.62}$$

where d_b refers to bubble size in a fluidized bed. As[D2], with an orifice type distributor, both the number and size of the bubbles increases with velocity one would expect that the efficiency due to induced electrostatic attraction would increase with the superficial gas velocity through the bed.

FIGURE 3.2 Experimental results of Kraemer and Johnstone for collection of dioctyl phthalate aerosol particles on a spherical collector

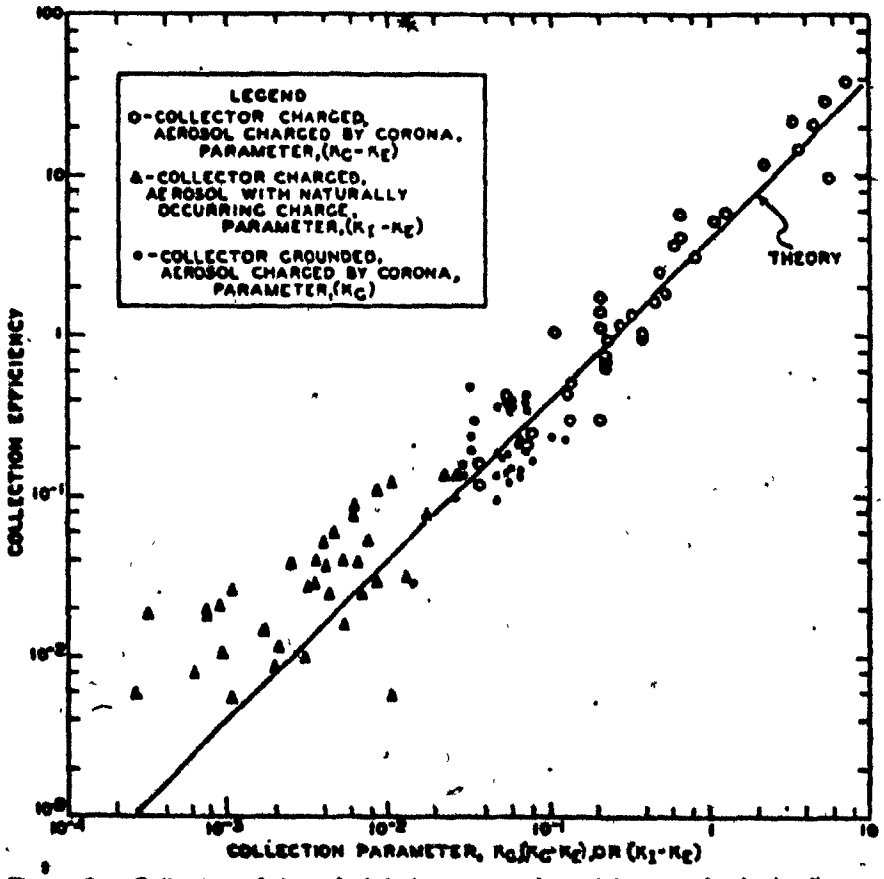

Figure 9. Collection of dioctyl phthalate aerosol particles on spherical collector

To summarize, the individual collection efficiency of a spherical collector particle in a fluidized bed where only induced electrostatic attractions are considered is given by

$$E_{FT} = E_{BT} + E_{E2} \tag{3.63}$$

and, although E_{E2} cannot be estimated quantitatively, inspection of Figure 3.2 shows that it could be an important collection parameter.

CHAPTER 4. DESCRIPTION OF EXPERIMENTAL APPARATUS

4.1 Introduction

The following chapter gives a detailed account of the equipment used in this study and describes the procedure for a typical run. Figure 4.5 shows a schematic diagram of the equipment used for fixed and fluidized bed experiments for superficial gas velocities up to 0.7 m/s. For higher velocities, up to 3 m/s, a completely different system had to be designed and built; this is shown in Figure 4.14. The aerosol was generated in a spinning disk generator and measured with a particle counter; these two items are described in the following section.

4.2 Generation and Sampling of Aerosols

4.2.1 The aerosol generator

The spinning disk generator* produces an aerosol from a solution or suspension of particle formation material. The feed is introduced, at a flow rate of 1.6×10^{-8} to $5 \times 10^{-8} m^3/s$, to the center of a $2.54 \times 10^{-2} m$ diameter stainless steel disk rotating at 1,000 revolutions per second. The liquid is atomized into two discrete droplet sizes. Primary droplets, typically 30 microns in diameter, are formed during liquid break up and used as the test aerosol. The smaller or satellite droplets which, according to Harstad et al.[H4] are about one third the diameter of the primary droplets, are removed from the flow system.

---

* manufactured by the Environmental Research Corporation, 3725 North Dunlap Street, St. Paul Minnesota (55112).

The size of the primary droplets, d_{PR}, is related to the angular disk speed, ω, disk diameter, d_{disk}, fluid surface tension, σ, and fluid density, ρ by the following expression

$$d_{PR} \propto \left(\frac{\sigma}{\rho \cdot \omega^2 d_{disk}}\right) \qquad (4.1)$$

where the constant of proportionality is equal to 4.5 according to May[M2] and $(12)^{\frac{1}{2}}$ according to the manufacturers[E1].

The generator is shown schematically in Figure 4.1. Ambient air is drawn through an absolute filter and a calibrated flowmeter into the mixing chamber by the main air blower. The air then mixes with the air flow recycled from the satellite removal system. After being heated (optional) it passes through an absolute filter and turbulence damping screen and into the air classifier. In the classifier (Figure 4.2) the liquid solution or suspension is fed onto the center of a rotating disk; the resulting bimodal spray distribution is separated into primary and satellite aerosols. A flow rate of approximately $3.8 \times 10^{-5} m^3/s$ was used to entrain the satellite droplets. This air passes into the satellite removal head, flows around and cools the electric motor and is finally exhausted into the mixing chamber. The remaining fraction of the air flows around the outside of the satellite removal head and entrains the primary droplets. These droplets which rapidly evaporate, are carried into the particle charge neutralizer where they are mixed with a high concentration of bipolar ions generated by a Krypton 85 source. Thus, residual electrical charges on the particles are neutralized and aerosol leaving the generator has a charge distribution that closely approximates the equilibrium Boltzmann distribution.

FIGURE 4.1 Schematic diagram of spinning disk aerosol generator

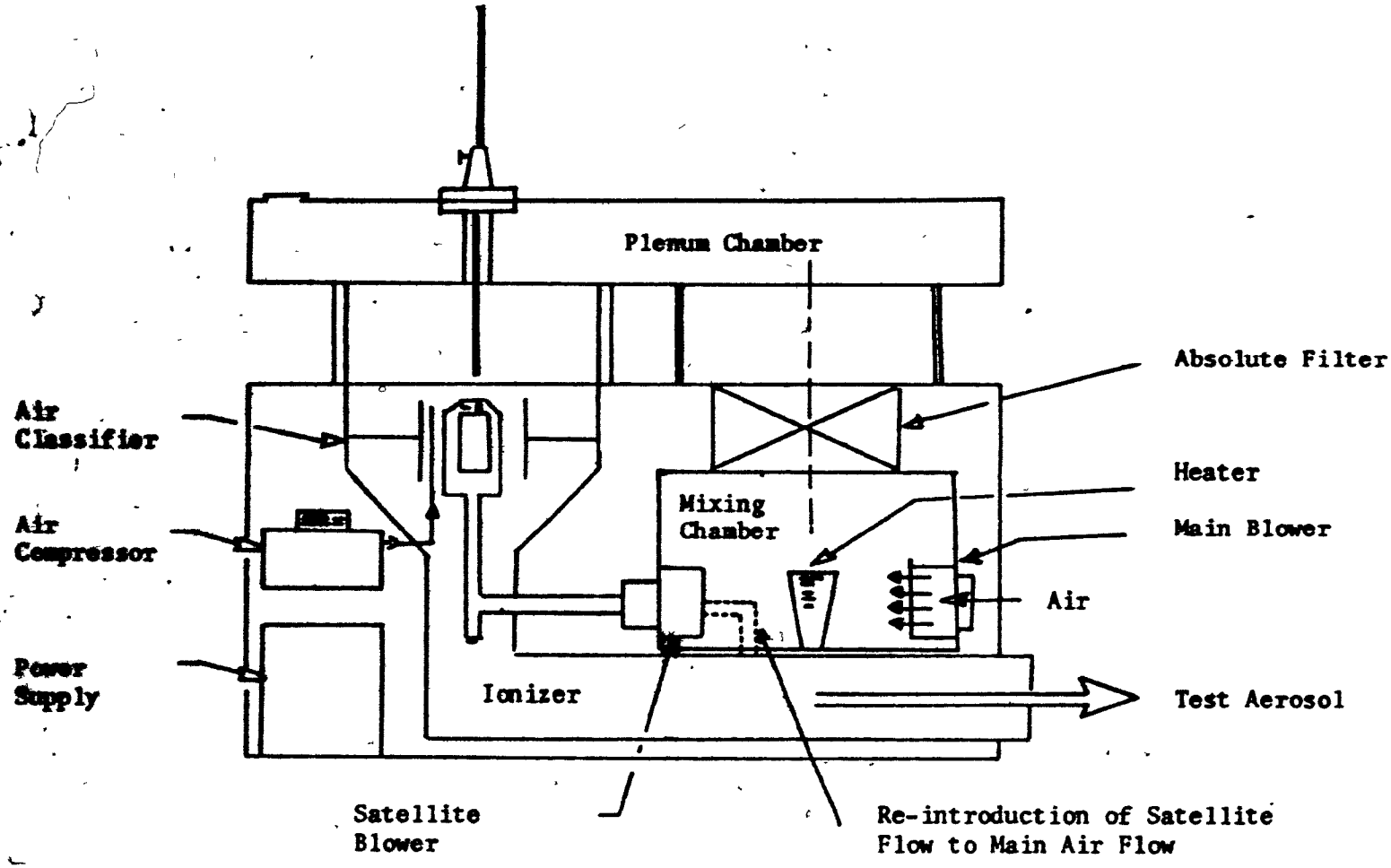
Plenum Chamber
Absolute Filter
Air Classifier
Heater
Mixing Chamber
Air Compressor
Main Blower
Air
Power Supply
Ionizer
Test Aerosol
Satellite Blower
Re-introduction of Satellite Flow to Main Air Flow

FIGURE 4.2 Air classifier section of spinning disk aerosol generator

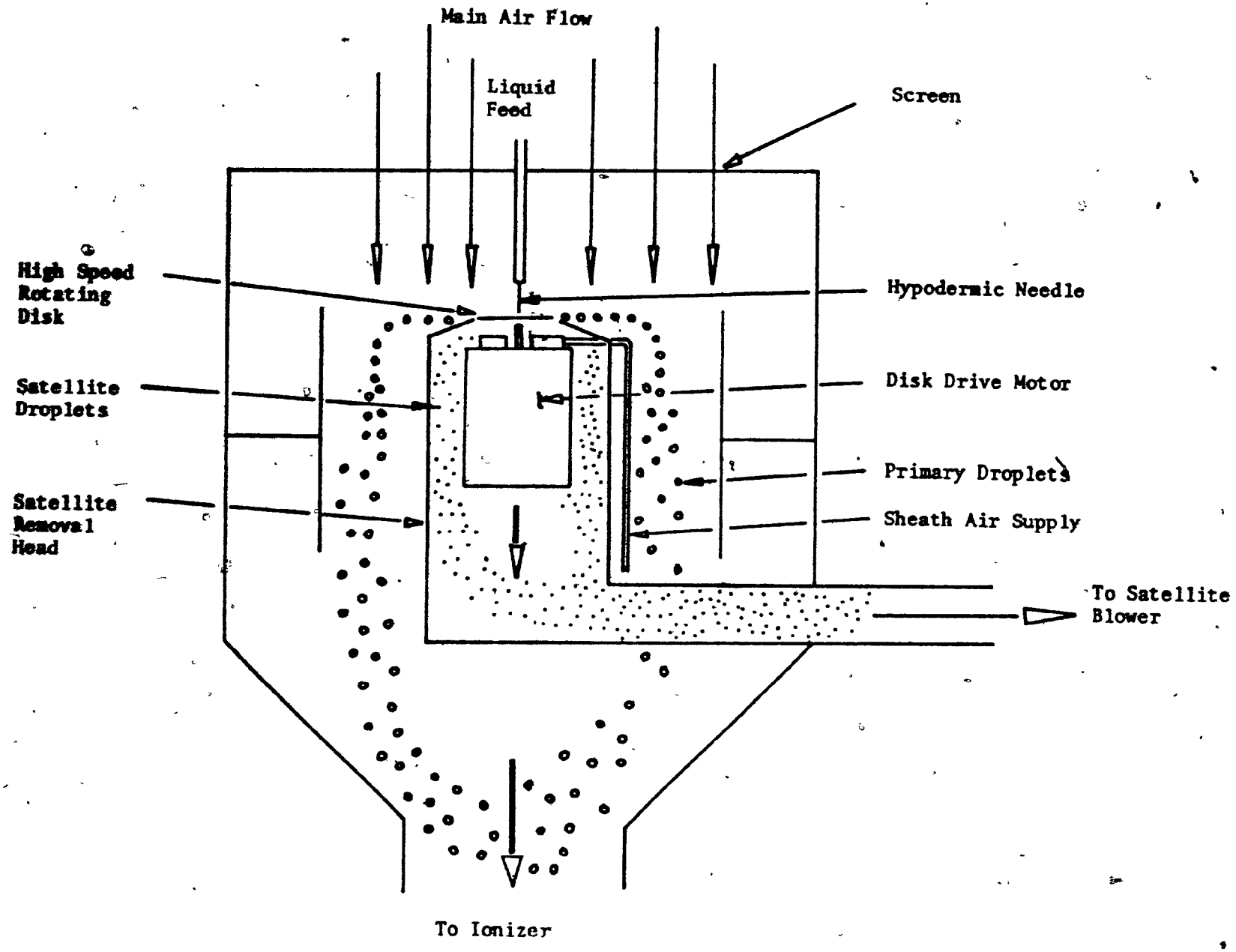
Main Air Flow
Liquid Feed
Screen
High Speed Rotating Disk
Hypodermic Needle
Satellite Droplets
Disk Drive Motor
Primary Droplets
Satellite Removal Head
Sheath Air Supply
To Satellite Blower
To Ionizer

Experimentally, it was found that small fluctuations in the satellite blower resulted in correspondingly greater fluctuations in the concentration of the aerosol. The aerosol generator was therefore modified by connecting the output of the satellite blower to the test aerosol, this arrangement is shown by a broken line in Figure 4.1. Thus, any primary droplets captured by the satellite blower were re-introduced, with the satellite droplets, back to the system, the satellite droplets being far too small to affect the monodispersity of the test aerosol around the measured peak range. This modification involved disassemblement of the generator, removal of the satellite blower from the generator and building of a separate housing for the blower.

The generator is capable of producing up to $3 \times 10^{-2} m^3/s$ of aerosol, at a positive pressure head of 0.1m of water, of neutral, monodisperse, spherical aerosol at a concentration of around 10^8 particles/m^3 and a geometric standard deviation around 1.1 - 1.2 based on number size distribution. Methylene blue aerosols (1.1 μm diameter) were produced by dissolving methylene blue in 20% distilled water/80% methyl alcohol in concentrations around 40 - 60 parts per million. Liquid aerosols were generated at various size ranges by atomizing a mixture of dioctyl phthalate (DOP) and methanol in concentrations of 40 to 350 ppm. An inherent problem in generating aerosols around 1 micron using this generator is the amount of solids residue in methyl alcohol which is ppm in normal reagent grade. This error was minimized by using alcohol of very high purity (solids residue 1 - 2 ppm, Fisher Scientific Co., Cat. No. A-412). Three methods of feeding the solution to the disk were tried:

i) through a micro-metering peristaltic pump (The Peri Pump Company Ltd., Model No.66);

ii) using the liquid container provided by the manufacturers situated at a height of 0.15 to 0.45m above the surface of the disc, feeding through a No.22 needle;

iii) using the $4.5 \times 10^{-3} m^3$ bottle containing the solution at a height of 1.2m and, with gravity feed, to a No.24 hypodermic needle.

The last method was found to be far superior to the rest, providing an aerosol constant in size and concentration for periods up to 5.4×10^4s (15 hours). Maintenance of the generator required:

i) replacing the bearings of the synchronous motor every 100 - 200 hours (Bardon-high speed bearings, Cat. No.SR4-SST5, distributed by Philip French Sales Ltd., Montreal);

ii) replacing the sponge rubber seals of the generator and polishing the stainless steel disk at suitable intervals;

iii) replacing the main air filter, satellite and main air blower every 500 - 1000 hours;

iv) disassembling and cleaning the generator at frequent intervals.

The author recommends that the manufacturers alter the design of the synchronous motor assembly by changing the disk diameter to 5.1×10^{-2}m and raising the disk speed, if that is possible. Then, from Equation (4.1) the lower practical limit of aerosol diameter would be extended substantially. Furthermore, the satellite droplets, which have a good monodispersity [H7] should not be destroyed but passed to a second, much smaller radioactive charge neutralizer. The aerosol generator would

then be able to produce two monodisperse aerosols, of different sizes, simultaneously, at a relatively small additional cost.

4.2.2 The particle counter[R-5]

The ~~Royco~~ Model 200 and 202 is an accurate and convenient instrument for determining the number concentration, particles/m^3, and size of particles of micron and submicron sizes in ambient air or in a closed system. This counter provides rapid and convenient analysis of size distributions of particles with diameter ranging from 0.3 to 10 microns in 15 selectable channels at a sample flow rate of $5.0 \times 10^{-6} m^3/s$. Each measurable range represents an increment of approximately 25% in particle diameter or 95% in particle volume. The particle counter will either count all particles in one or more size ranges (single mode operation) or it will count all particles larger than any selected size range (total mode operation). Any combination of particle size ranges may be preselected for automatic monitoring, in sequence, with a prespecified interval spent counting each range (this interval may be 18, 60, 180 or 600 seconds). The number of particles for the range being counted is indicated on a five-digit bank of decade counters and there are provisions made for connection of recorders or a printer for a record of the particle count.

The Model 202 Counter is different, having in addition an air dilution system and slightly different size ranges. The purpose of the dilution system is to dilute aerosols whose concentration results in high coincidence loss (explained later); both models were used at

77

different times* and Table 4.1 gives channel numbers and the corresponding size ranges which are of interest to this study.

Channel No.	Size Range, Microns	
	Model 200	Model 202
4	0.64 - 0.8	0.60 - 0.80
5	0.8 - 1.0	0.8 - 1.0
6	1.0 - 1.3	1.0 - 1.2
7	1.3 - 1.6	1.2 - 1.5
8	1.6 - 2.0	1.5 - 2.0
9	2.0 - 2.5	2.0 - 3.0

TABLE 4.1 Size Ranges of Model 200 and 202 Royco Particle Counter

The principle of operation is based upon the well-established phenomena of light scattering and reflection by small particles. The air sample passes through an optical system with a small volume-sensitive area ($1.98 \times 10^{-9} m^3$) where the particles deflect light from a controlled source with a photomultiplier tube positioned at 90^o to the main projection axis (Figure 4.3). The pulse train from the photomultiplier is analyzed electronically to segregate the pulses by size, and pulses corresponding to the preselected particle sizes are indicated by the decade counters. The mechanism producing this deflection is light scattering for particles approximately below one micron in diameter and

* Model 202 - use permitted by courtesy of the Department of Epidemiology, McGill University, Montreal.

FIGURE 4.3 Optical system of Model 200/202 Royco particle counter

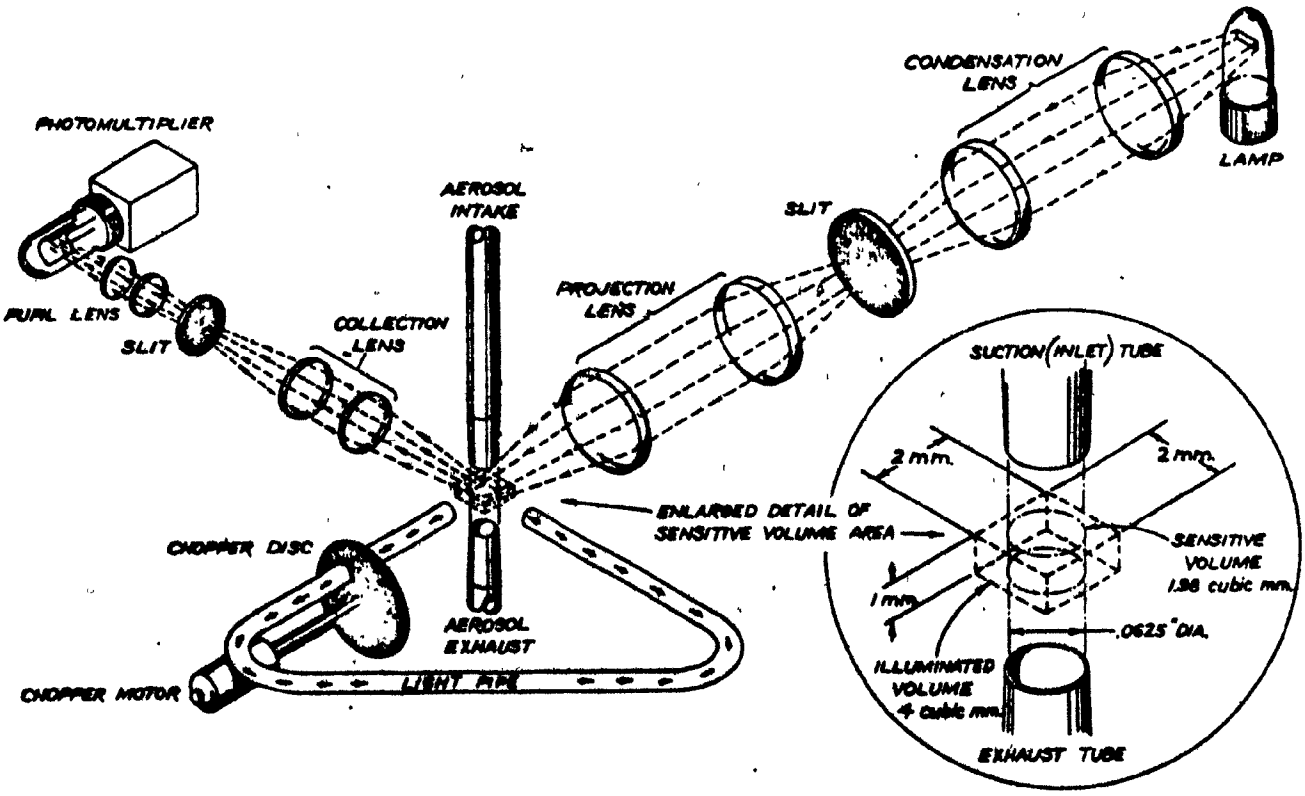
CONDENSATION LENS
LAMP
PHOTOMULTIPLIER
AEROSOL INTAKE
SLIT
PROJECTION LENS
PUPIL LENS
SLIT
COLLECTION LENS
ENLARGED DETAIL OF SENSITIVE VOLUME AREA
CHOPPER DISC
AEROSOL EXHAUST
CHOPPER MOTOR
LIGHT PIPE
SUCTION (INLET) TUBE
2 mm.
2 mm.
SENSITIVE VOLUME 1.96 cubic mm.
1 mm.
.0625" DIA.
ILLUMINATED VOLUME 4 cubic mm.
EXHAUST TUBE

reflection of light for particles above one micron in diameter. Each of these mechanisms produces light pulses which have an amplitude proportional to the projected area of the particle (i.e. to the square of the particle diameter) and which have the same constant factor relating pulse amplitude to area. Hence, there is a smooth transition between the size ranges where actual scattering takes place and where reflection predominates so that pulses with uniform amplitude increments are provided in proportion to $(d_A)^2$ for particles of any size range.

The particle counter was "prime calibrated" at periodic intervals using an aerosol of polystyrene latex particles 0.750 ± 0.0026 μm diameter* produced by a nozzle type generator built by R. Allen**. The procedure and precautions to be taken for prime calibration are described in Appendix C for the benefit of future users of this instrument. Basically, prime calibration is carried out by passing particles of known size through the counter, comparing the indicated size distribution with the known distribution and making any necessary calibration adjustments. The latex particles have a refractive index of 1.595 and a density of $1.06 \times 10^3 kg/m^3$. There is, however, negligible degradation in sizing accuracy when measuring particles with entirely different characteristics because the operation of the instrument utilizes white illumination that is scattered by particles and collected over a large spherical angle.

---

* Manufactured by Dow Chemical Company, Bio-Products Department, Midland, Michigan.
** Department of Chemical Engineering, McGill University, Montreal.

The sizing* error in the equipment depends primarily on the care taken when prime calibration is performed; in general, taking all the necessary precautions, the diameter of a particle can be determined to an accuracy of ±15%. The second possible source of error in the counter is "coincidence loss", which results from the simultaneous appearance of two particles within the sensitive volume where measurement takes place. The operation is such that if the particles are not of the same size the larger particle masks the smaller one, effectively hiding the smaller one while the larger is counted; two particles of the same size produce an additive effect which simulates a larger particle. Coincidence loss, therefore, is not the same in all channels, but is a function of the count in a particular size range related to the total count in that range plus all larger particles. It becomes important at concentrations greater than 6×10^7 particles/m^3 and can be predicted statistically. Coincidence losses in this study were corrected from a graph supplied by the manufacturers (Figure 4.4) and corrections were around 12% in the extreme cases. (See Appendix D for an example of correcting coincidence loss.) The instrument must be "field calibrated" before each run. Field calibration is a simple operation and compensates for the deterioration of the various degradable components in the counter between prime calibrations.

Maintenance of the instrument, excluding troubleshooting, involves

i) bi-monthly prime calibration;

ii) field calibration before each run;

---

*See Section 6.3.3 for further information on sizing error.

FIGURE 4.4 Correction of coincidence loss. Actual concentration (R_A) as a function of measured concentration (R_M). Axes - $x10^3$ particles counted per minute sampling at a flow rate of $5x10^{-6}$ m^3/s

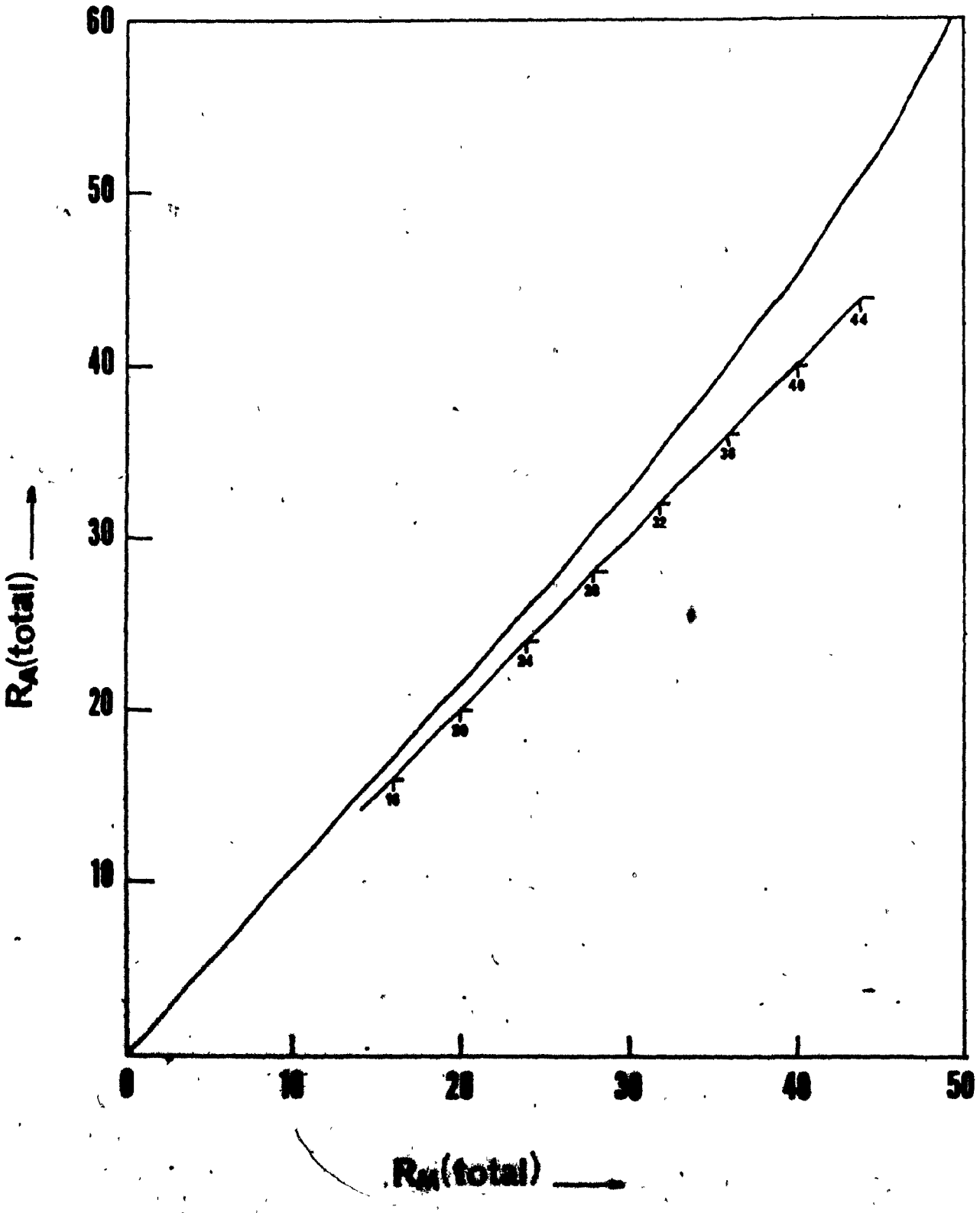
60
50
40
30
20
10
0
10
20
30
40
50
R_A(total)
R_B(total)
16
20
24
28
32
36
40
44

iii) yearly inspection of electronic chassis;

iv) monthly inspection of optical system;

v) tube replacement when necessary;

vi) maintenance of vacuum pump drawing sample air;

vii) replacement of air filters when necessary;

viii) periodic lubrication of various moving parts of the counter.

4.3 Description of Experimental Apparatus for Fixed and Fluidized Bed Experiments (U < 0.7 m/s)

The equipment used for carrying out experiments with fixed and fluidized beds with superficial gas velocity up to 0.7 m/s is shown schematically in Figure 4.5. The aerosol generator was adjusted to produce an aerosol of 5×10^7 to 10^6 particles/m^3 at a constant flow rate, usually around 0.9 to $1.4 \times 10^{-2} m^3/s$. Part of the aerosol was taken to the fluidized bed, while the remainder passed to the laboratory fumehood. In this way, by producing more aerosol than that required for experimentation and discarding the remainder, experiments could be performed at different velocities through the bed without varying conditions at the generator and thus changing the particle size or concentration of the aerosol. From the fluidized bed the aerosol passed through a filter*, to remove particles larger than 0.5 μm, to two parallel-mounted rotameters thus eliminating contamination of the rotameters by the aerosol. The larger rotameter** had a maximum range $1.8 \times 10^{-2} m^3/s$ at room temperature and atmospheric pressure and a calibrated accuracy of ±1% of full scale

*Filterite - reverse duo fine - distributed by Industrial Projects Ltd., 3300 Cavendish Boulevard, Montreal.
**Brooks-Hi-Accuracy full view flowmeter (Cat.No.1110-24), distributed by Brooks Instruments Div., Emerson Electric Canada Ltd., Markham, Ontario.

FIGURE 4.5 Schematic diagram of apparatus used for fluidized bed experiments ($0 < U < 0.7$ m/s)

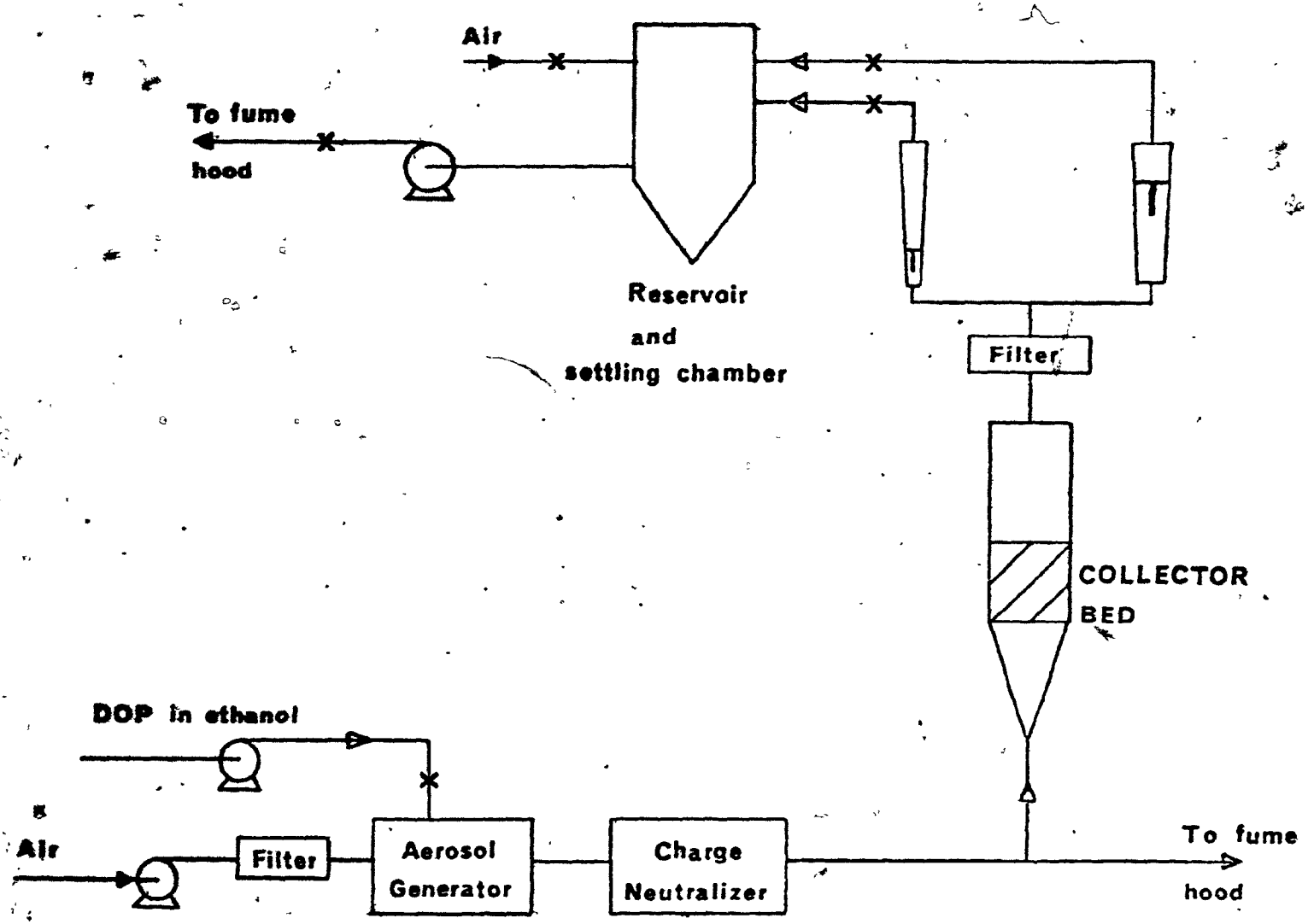
Air
To fume
hood
Reservoir
and
settling chamber
Filter
COLLECTOR
BED
DOP in ethanol
Air
Filter
Aerosol
Generator
Charge
Neutralizer
To fume
hood

reading. The smaller rotameter* could be used with flows up to 2.1×10^{-3} m^3/s with an industrial accuracy of ± 2% of full scale reading; the capacity of this instrument was chosen after the total error of the two rotameters was optimized numerically (see Appendix E). Flow through the fluidized bed and downstream system was maintained by a vacuum pump** with free air capacity $2.5 \times 10^{-2} m^3/s$. The pump was designed to operate at high vacuum and was incapable of dealing with the air mass flow rates demanded of it in this study. Therefore, it was modified by removing the existing oil filtering system and installing an inertial impaction device. This was designed and built to remove oil droplets greater than 10 - 20 microns. The pump oil discharged by the pump and collected by the impactor was trickled to a reservoir where it was cooled and subsequently returned to the pump. With this arrangement the pump could operate continuously without overheating and with negligible oil losses. As the inertial impactor worked most efficiently at high flow rates, additional air was added to the reservoir to ensure sufficient flow through the pump. In this way the aerosol generator operated slightly above atmospheric pressure (at its normal design conditions) while the fluidized bed was at a slight negative pressure. Manometers were provided to determine the pressure drop across the distributor, across the bed and to indicate the pressure at the rotameters. The measured volumetric flow through the rotameters was subsequently corrected

---

*Brooks full-view, O-ring seal, glass tube flow meter (Cat.No.1112-A).
**VacTorr High Vacuum Pump, Cat.No.D-1500, distributed by Precision Scientific Co., 3737 West Cortland Street, Chicago, Illinois.

for any deviations from atmospheric pressure with the following standard equation

$$(\text{Flow})_{RP} = (\text{Flow})_{atm} \times \sqrt{\frac{P_{RP}}{P_{atm}}} \qquad (4.2)$$

where subscript RP refers to the absolute pressure at the rotameter, n/m^2.

The bed was contained in a cylindrical glass column of 0.15m inside diameter and 0.30m long or in a plexiglass column of the same diameter and 0.41m long. The fluidized bed distributor, Figure 4.6a, consisted of a flat aluminum plate 3.2×10^{-3}m thick, drilled with 1.2×10^{-4}m diameter holes on a 9.5×10^{-3}m triangular pitch giving a free surface area of 1.5%. The fixed bed support, Figure 4.6b, consisted of an aluminum plate 9.37×10^{-3}m thick, drilled with 6.15×10^{-4}m diameter holes on a 6.35×10^{-3}m triangular pitch covered with a 74 micron opening stainless steel wire mesh; the design of the plate was flexible enough to allow its use as a distributor for experiments with high superficial gas velocities. To minimize aerosol collection on the distributor the holes were reamed out on the upstream side of the plates and the aerosol stream approached the distributor through a plexiglass conical expansion chamber of approximately 5° half angle. For the fixed bed experiments the flow through the bed was reversed and an additional 0.30m length glass column was added after the support plate in order to avoid having the top of the sampling probe too near the support plate. The pressure drop across the fluidized bed distributor and across the fixed bed support plate was measured, with an inclined micromanometer, as a function of superficial gas velocity, and the results are shown in Figures 4.7 and 4.8. The

FIGURE 4.6a Schematic representation of fluidized bed distributor A

a = 9.5×10^{-3} m
b = 1.6×10^{-3} m
c = 1.7×10^{-3} m
d = 1.2×10^{-3} m
number of orifices = 259

FIGURE 4.6b Schematic representation of fluidized bed distributor B. Also used as fixed bed support plate.

a = 6.4×10^{-3} m
b = 9.4×10^{-3} m
c = 6.2×10^{-3} m
d = 1.7×10^{-3} m
number of orifices = 557

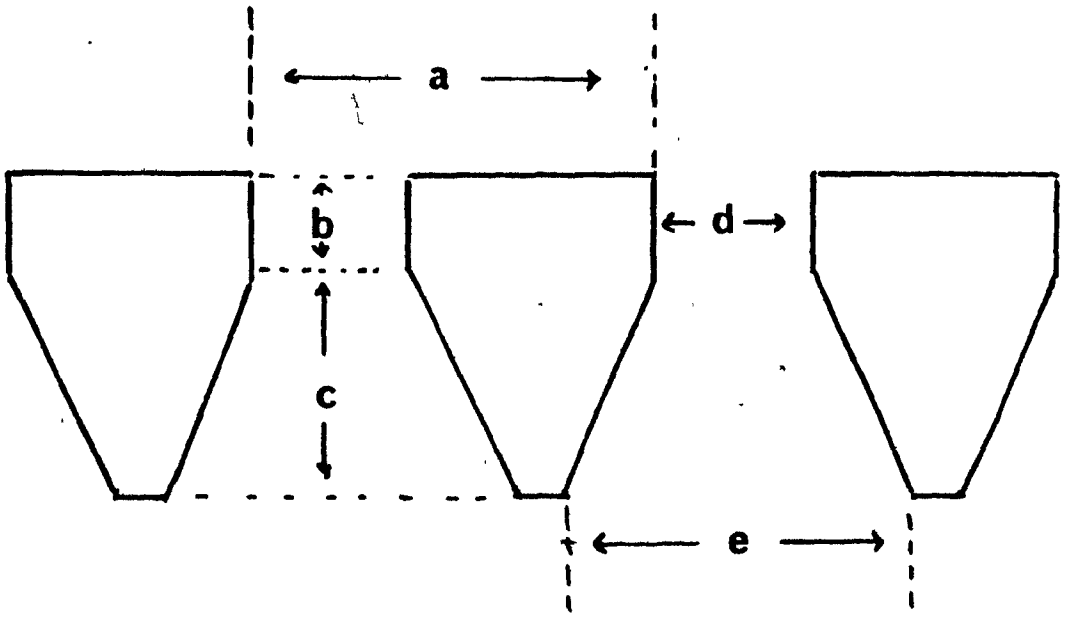

Figure 4.6a

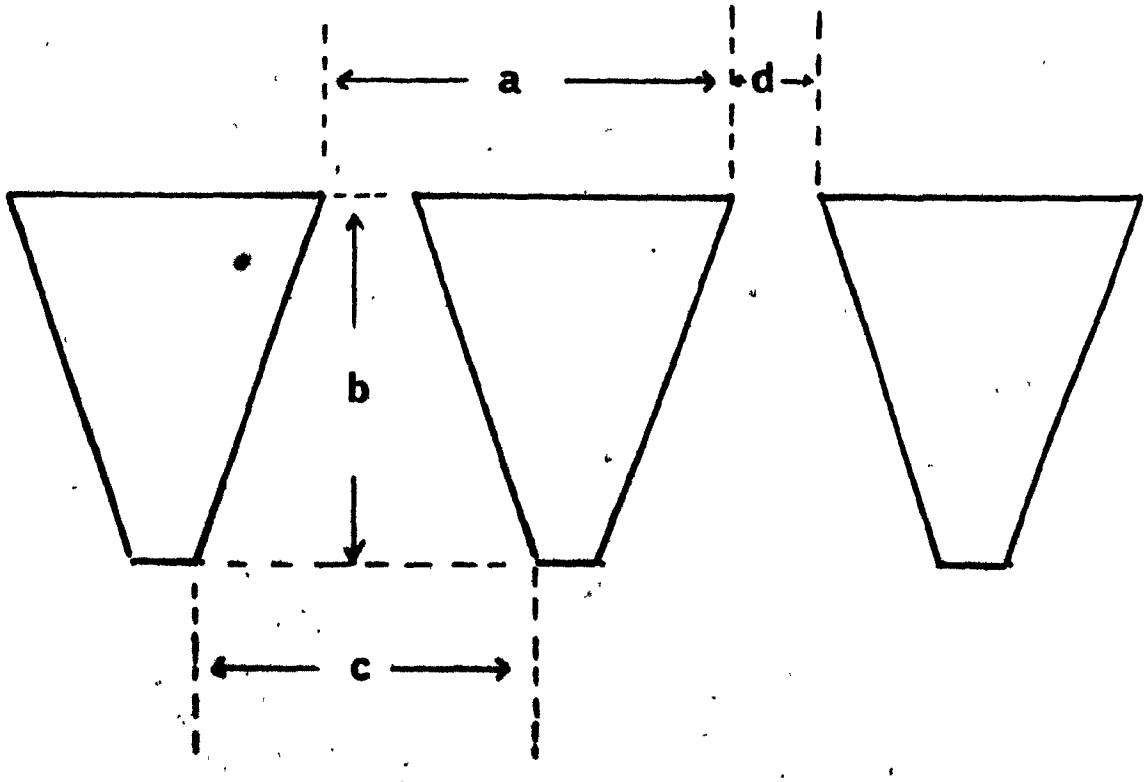

Figure 4.6b

FIGURE 4.7 Pressure drop across fluidized bed distributor A as a function of superficial gas velocity

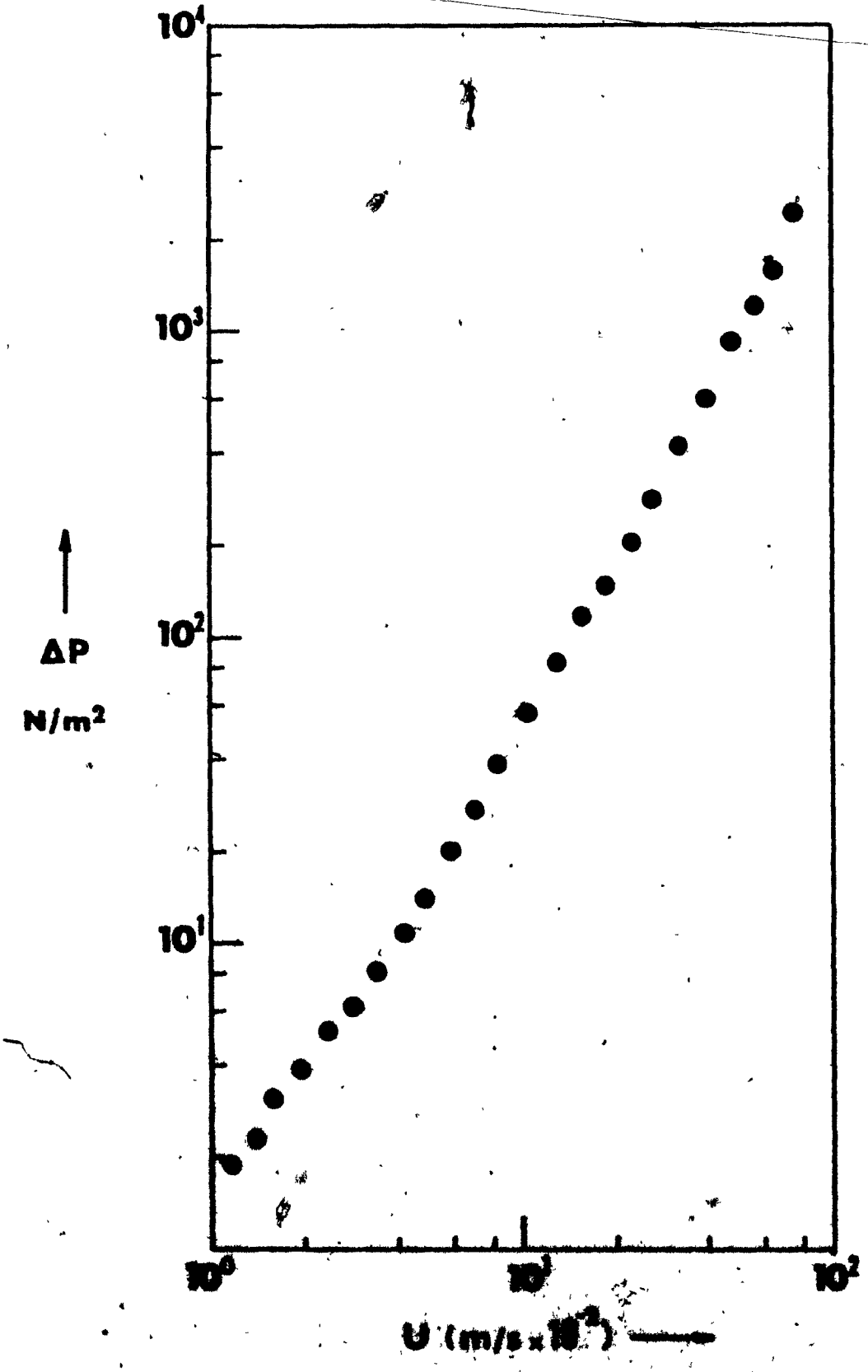
10^4
10^3
10^2
10^1
ΔP
N/m²
10^0
10^1
10^2
U (m/s x 10^{-2})

FIGURE 4.8 Pressure drop across fluidized bed distributor B as a function of superficial gas velocity

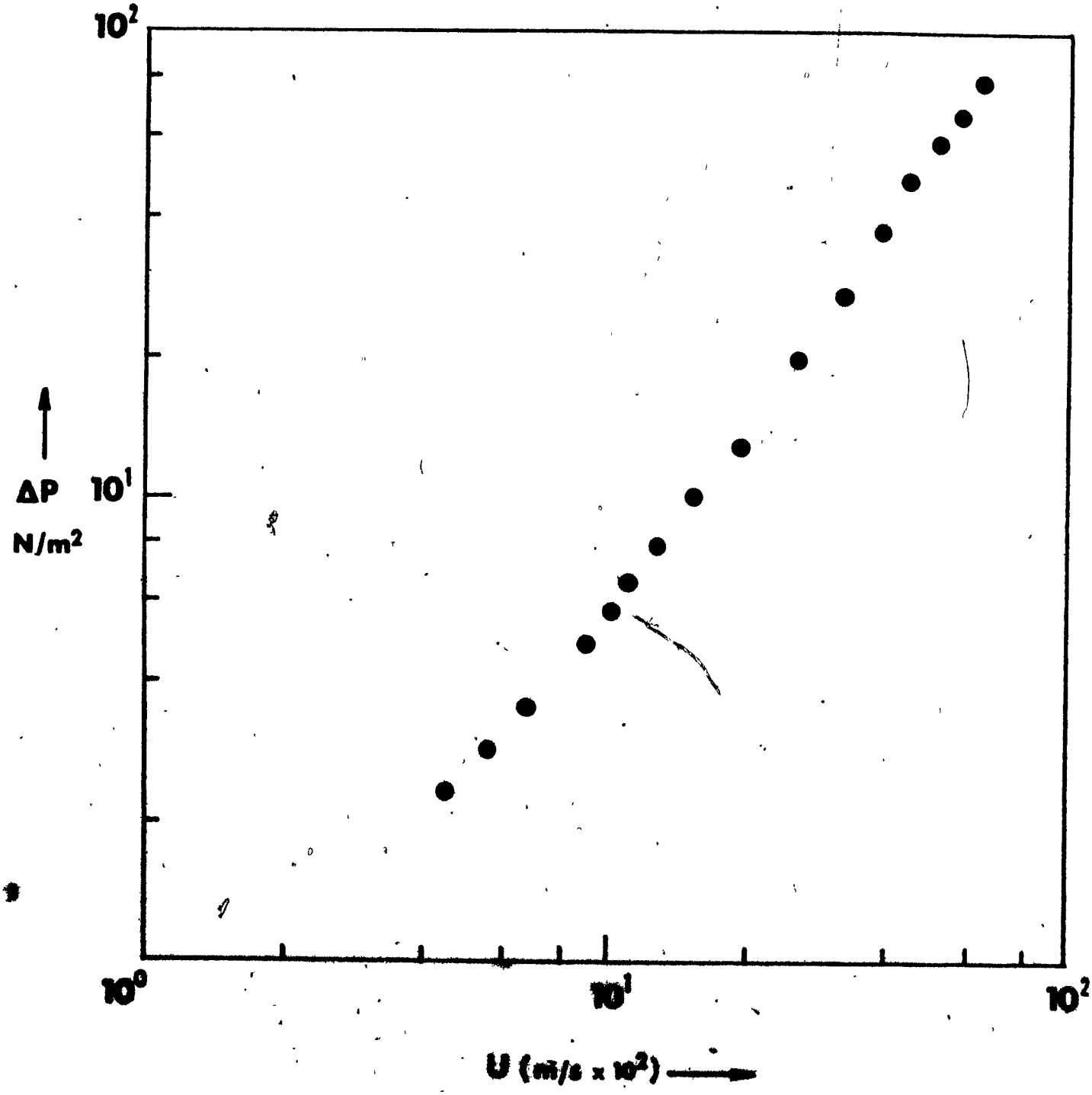
10^2
10^1
10^0
10^1
10^2
ΔP
N/m²
U (m/s x 10^2)

pressure drop across the distributor, although low compared to values recommended in the literature[K6] was higher than most of the previous studies (see Section 2.3.1). Visual inspection showed that it provided adequate distribution of gas in the bed because of the very shallow beds required for this type of study (typically around 3×10^{-2}m). The distributor plate was designed to minimize collection of the incoming aerosol by the plate. Figure 4.9 shows penetration through the distributor as a function of superficial gas velocity. As seen from the figure, penetration through the distributor plate is 86% of the incoming aerosol at the extreme case (1.5 μm diameter aerosol at a velocity of 0.77m/s). For smaller aerosols and lower velocities aerosol removal was insignificant, typically around a few per cent.

The experiments were performed with three different types of collector particles, namely, closely sized glass spheres in two sizes and high density, technical quality glass beads. The surface mean diameter of each type of collector was determined experimentally by measuring the diameter of 300 particles for each size under an optical microscope to an accuracy of ± 2 μm and was 108 μm, 596 μm, and 546 μm, respectively. The results of these measurements are shown on Tables 4.2, 4.3 and 4.4 and histograms of the size ranges are plotted on Figures 4.10, 4.11 and 4.12. The density, voidage and bulk density of the collector particles were determined experimentally and the averages of three independent measurements are given in Table 4.5. The particles forming the bed were cleaned before each run by immersing them in ethanol, placing the mixture in an ultrasonic cleaning bath for at least 20 minutes, decanting off the ethanol and then drying the glass spheres. After charging to the column the particles were fluidized by aerosol-free air to remove

FIGURE 4.9 Penetration of 1.5 μm DOP aerosol through fluidized bed distributor A ($0 < U < 0.7$ m/s)

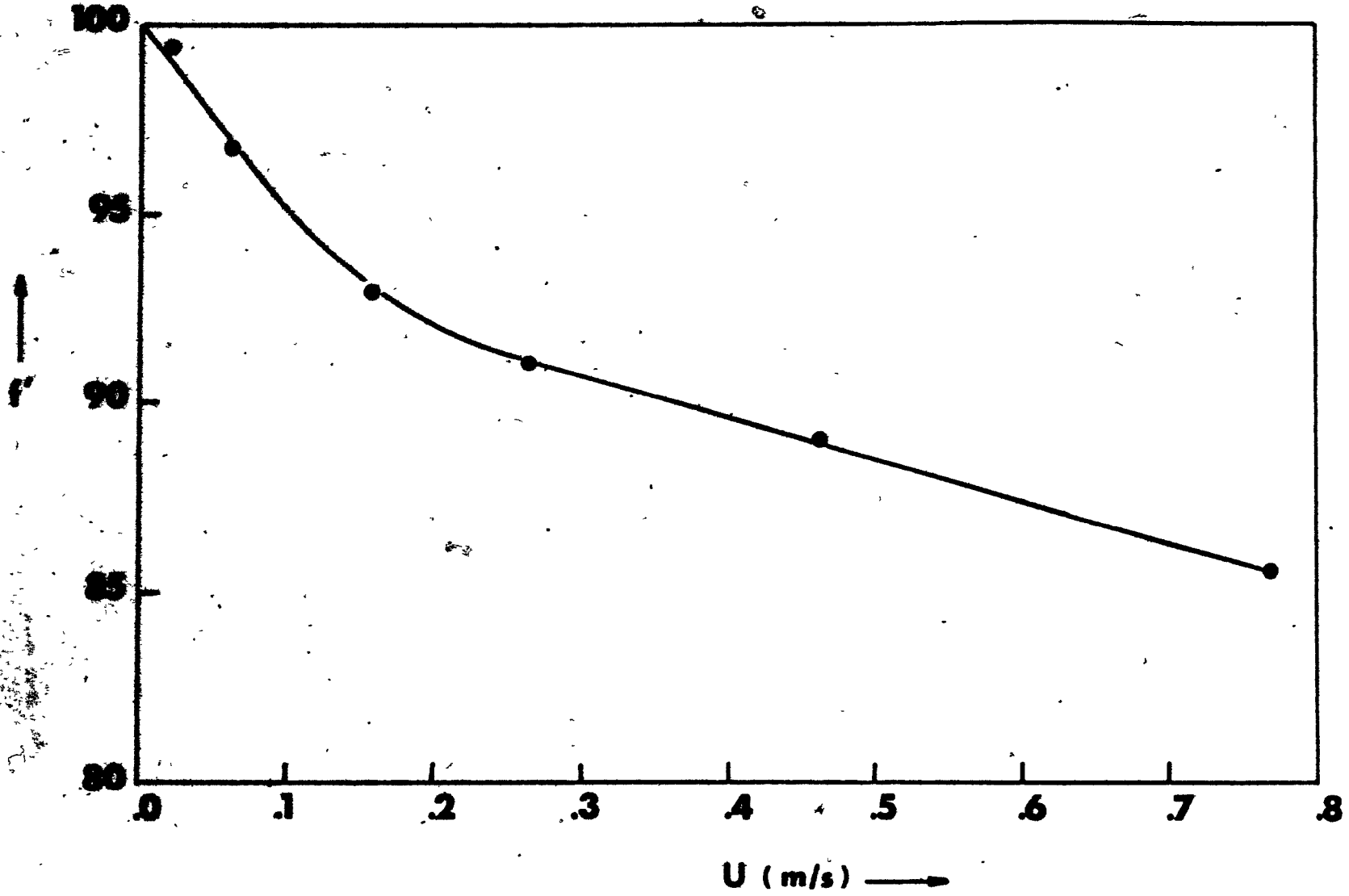
100
95
90
85
80
f'
.0
.1
.2
.3
.4
.5
.6
.7
.8
U (m/s)

Table 4.2- Analysis of 110 microns collector particles

ANALYSIS OF 300 PARTICLES

NUMBER OF PARTICLES COUNTED= 300 NUMBER OF SIZE RANGES= 10
ARITHMETIC MEAN DIAMETER= 100.18 MICRONS
GEOMETRIC MEAN DIAMETER= 107.90 VOLUMETRIC MEAN DIAMETER= 108.71 MICRONS
SURFACE TO VOLUME MEAN DIAMETER = 109.24 MICRONS
SURFACE MEAN DIAMETER= 100.45 MICRONS
GEOMETRIC STANDARD DEVIATION = 1.0729
LARGEST PARTICLE PRESENT= 131.32 MICRONS
SMALLEST PARTICLE PRESENT IS 83.82 MICRONS
EACH SIZE RANGE REPRESENTS 4.75 MICRONS

OUTPUT IN INPUT DATA, PARTICLES,MICRONS

111.3	100.2	115.8	112.5	101.6	104.9	120.6	107.4	109.2	115.6	106.2	113.3
100.9	106.9	112.5	103.4	101.3	113.8	90.9	94.5	107.9	111.8	103.1	101.1
108.9	100.7	111.8	99.6	110.9	104.1	109.2	102.4	104.1	105.2	107.4	107.9
119.7	104.2	102.9	99.1	109.0	114.8	114.6	119.1	121.9	113.0	112.8	99.3
96.3	110.7	126.7	107.4	104.6	95.5	105.9	107.7	102.4	104.9	113.8	100.8
115.6	103.9	99.6	98.3	109.5	104.4	114.3	112.5	121.2	102.1	91.9	96.8
107.7	97.8	123.2	102.1	122.4	110.6	114.8	109.2	112.3	107.2	114.3	102.4
116.8	121.9	101.1	112.5	105.7	104.9	109.5	116.1	99.1	103.6	103.6	115.6
115.3	105.9	114.8	99.6	117.6	116.8	131.3	116.1	111.3	99.6	104.4	106.7
108.2	112.5	115.8	108.2	102.1	115.1	99.1	105.2	103.9	112.8	104.1	98.3
96.8	109.7	100.8	93.2	117.6	88.9	125.5	121.9	102.3	116.1	113.3	113.8
99.3	111.0	107.7	93.5	115.6	110.7	107.7	102.4	112.3	102.1	104.4	105.9
105.6	126.5	111.0	101.9	118.9	108.2	122.2	115.1	96.5	120.6	120.4	119.4
113.8	100.3	114.6	114.3	99.1	106.7	109.0	109.2	116.1	110.0	96.5	122.2
113.3	113.8	98.3	83.8	119.4	112.8	102.4	96.5	106.7	116.8	117.8	98.3
119.4	98.3	110.7	98.0	106.7	114.6	115.8	107.2	98.6	106.9	115.1	110.0
109.2	111.3	113.3	100.6	99.1	102.9	115.8	106.2	102.4	106.7	116.3	102.9
110.7	106.4	108.5	103.9	94.2	104.6	102.6	109.7	114.8	114.8	104.1	104.1
102.1	97.8	109.7	104.1	104.1	100.3	105.4	104.1	102.9	106.7	106.7	105.4
107.9	104.6	118.1	104.1	111.8	114.3	120.6	111.8	95.8	109.2	115.8	101.1
102.9	100.3	108.7	109.2	116.3	112.5	100.3	88.9	111.3	102.1	114.8	110.5
105.4	107.7	102.1	101.6	98.3	111.3	106.2	101.3	111.8	105.4	116.8	121.9
107.9	119.4	109.2	125.0	107.4	110.0	118.6	99.3	106.2	116.1	94.5	105.4
104.2	94.8	105.7	104.6	105.9	116.3	108.2	110.0	102.1	109.2	117.8	110.2
104.7	120.6	101.1	100.3	107.4	102.1	113.0	108.7	108.7	107.4	115.6	120.6

OUTPUT OF NUMBER OF PARTICLES AND % OF TOTAL IN EACH RANGE

NUMBER OF RANGE	TOTAL PARTICLES	PERCENT OF TOTAL
1	1	0.3
2	5	1.7
3	16	5.3
4	53	17.7
5	70	23.3
6	62	20.7
7	60	20.0
8	20	6.7
9	11	3.7
10	2	0.7

Table 4.3-Analysis of 550 microns collector particles

ANALYSIS OF 600 PARTICLES

NUMBER OF PARTICLES COUNTED= 301 NUMBER OF SIZE RANGES= 10
ARITHMETIC MEAN DIAMETER= 543.89 MICRONS
GEOMETRIC MEAN DIAMETER= 541.58 VOLUMETRIC MEAN DIAMETER= 546.27 MICRONS
SURFACE TO VOLUME MEAN DIAMETER = 552.64 MICRONS
SURFACE MEAN DIAMETER= 546.10 MICRONS
GEOMETRIC STANDARD DEVIATION = 1.0951
LARGEST PARTICLE PRESENT= 652.78 MICRONS
SMALLEST PARTICLE PRESENT IS 430.53 MICRONS
EACH SIZE RANGE REPRESENTS 22.22 MICRONS

OUTPUT IN INPUT DATA, PARTICLES,MICRONS

563.9	574.8	588.8	608.3	560.1	635.8	558.8	600.7	629.9	615.9	599.4	603.2
604.8	543.6	487.7	499.1	556.3	604.5	565.1	589.3	535.9	584.2	509.3	605.8
614.7	598.9	560.1	544.8	487.7	558.8	618.5	586.7	575.3	599.4	610.9	553.7
487.7	598.9	595.6	607.1	459.7	527.0	594.4	621.0	565.1	547.4	490.2	609.6
579.3	614.7	548.6	548.6	549.9	635.0	468.6	508.0	516.9	555.0	515.6	525.8
495.9	574.1	577.8	609.6	602.0	571.5	617.2	502.9	614.7	481.3	579.1	572.8
564.4	518.2	492.8	649.0	546.1	490.2	487.7	647.7	469.9	556.3	459.7	538.5
553.7	624.8	490.2	472.4	561.3	566.4	543.6	614.7	586.7	535.3	589.3	480.1
544.1	518.5	556.3	561.3	449.6	572.8	523.2	548.6	452.1	591.8	482.6	468.6
482.6	509.3	548.6	473.7	476.2	490.5	581.7	562.6	505.5	596.9	579.1	487.7
528.3	594.4	464.8	525.8	525.8	581.7	528.3	501.6	477.5	469.6	482.6	467.4
553.7	532.1	462.3	516.9	607.1	542.3	585.5	546.1	605.8	604.5	576.6	472.4
558.8	535.9	508.0	480.1	514.3	558.8	556.3	609.6	508.0	534.7	529.6	586.7
586.9	535.9	638.8	631.2	478.8	530.9	584.2	966.4	581.7	477.5	464.8	475.0
577.8	467.4	523.2	513.1	500.4	520.7	515.6	510.5	490.2	591.8	549.5	525.8
519.6	538.9	591.8	518.5	582.9	551.2	607.1	533.4	612.1	558.8	533.4	599.4
556.5	475.8	543.6	492.8	579.1	584.2	607.1	500.4	581.7	561.3	586.7	533.4
467.4	513.1	515.6	458.5	520.7	508.0	576.6	510.5	594.4	472.4	458.5	558.8
492.8	594.4	647.7	520.7	563.9	566.4	520.7	612.1	602.0	541.0	523.2	541.0
525.8	556.3	500.4	586.7	594.4	558.8	528.3	495.3	464.8	594.4	448.3	543.6
586.7	581.7	543.6	533.4	510.5	502.9	469.9	581.7	513.1	503.4	586.7	482.6
487.7	574.8	558.8	591.8	585.5	556.3	539.7	599.4	594.4	500.4	594.4	533.9
502.9	563.9	505.5	586.7	535.9	551.2	457.2	535.9	574.0	652.8	599.4	487.7
495.3	480.1	561.3	452.1	591.8	520.7	510.5	490.2	469.9	497.8	614.7	576.6
548.6	536.5	497.8	556.3	581.7	523.2	604.5	500.4	551.2	602.0	492.6	497.8
495.3											

OUTPUT OF NUMBER OF PARTICLES AND % OF TOTAL IN EACH RANGE

NUMBER OF RANGE	TOTAL PARTICLES	PERCENT OF TOTAL
1	5	1.7
2	24	8.0
3	33	11.0
4	40	13.3
5	38	12.6
6	48	15.9
7	39	13.0
8	48	15.9
9	18	6.0
10	8	2.7

Table 4.4- Analysis of 600 microns collector particles

ANALYSIS OF 600 PARTICLES

NUMBER OF PARTICLES COUNTED= 296 NUMBER OF SIZE RANGES= 10
ARITHMETIC MEAN DIAMETER= 595.53 MICRONS
GEOMETRIC MEAN DIAMETER= 594.53 VOLUMETRIC MEAN DIAMETER= 597.30 MICRONS
SURFACE TO VOLUME MEAN DIAMETER = 599.04 MICRONS
SURFACE MEAN DIAMETER= 598.43 MICRONS
GEOMETRIC STANDARD DEVIATION = 1.0573
LARGEST PARTICLE PRESENT= 693.42 MICRONS
SMALLEST PARTICLE PRESENT IS 473.71 MICRONS
EACH SIZE RANGE REPRESENTS 21.97 MICRONS

OUTPUT IN INPUT DATA, PARTICLES,MICRONS

591.8	601.5	556.0	577.8	633.7	626.6	604.0	605.3	600.7	586.7	619.8	617.2
626.1	633.0	601.2	632.5	596.4	588.7	617.7	602.7	609.1	533.9	586.0	575.1
612.6	598.7	598.2	577.8	601.7	601.0	610.9	590.5	572.8	631.2	597.7	607.8
648.1	606.3	617.7	635.5	610.9	645.2	615.7	543.6	612.1	572.8	610.1	605.8
543.6	574.0	634.5	607.1	643.9	577.8	629.9	632.5	607.8	611.4	633.0	579.1
578.2	588.0	618.0	596.1	535.2	593.1	589.8	607.1	603.8	620.3	524.8	596.9
629.9	621.0	575.3	579.1	590.5	629.9	539.3	626.1	611.1	587.2	560.1	568.5
593.1	609.4	617.2	588.0	581.7	651.5	581.7	551.2	588.0	647.7	615.9	605.3
610.9	580.4	615.9	581.7	617.2	577.8	614.7	553.7	541.0	595.1	589.3	633.2
624.8	589.3	598.2	602.7	608.3	607.1	605.8	637.5	589.3	626.1	594.4	551.2
579.8	562.6	579.9	621.8	637.5	636.3	555.5	642.6	643.9	599.4	619.8	566.4
562.6	590.0	581.7	640.1	584.2	596.9	632.5	616.7	628.6	543.6	610.1	637.5
618.9	586.7	567.7	591.8	596.3	538.5	594.4	601.2	615.2	615.9	602.0	576.6
559.6	558.3	579.1	591.8	528.3	631.2	594.4	596.9	563.9	652.8	599.4	569.0
633.5	567.7	609.6	621.0	581.2	599.4	584.2	619.8	604.5	602.0	558.8	557.5
605.2	589.3	562.6	609.6	628.6	621.0	551.2	572.8	567.7	572.8	613.4	628.6
593.9	595.6	596.9	638.8	581.8	693.7	693.4	592.3	584.2	629.9	591.3	647.7
613.4	622.3	693.4	632.5	588.0	558.3	574.3	591.8	604.5	612.9	549.9	605.8
548.3	622.3	635.0	544.3	628.6	567.2	595.6	643.9	622.3	513.1	525.1	619.8
605.8	551.2	565.1	534.9	617.2	584.2	622.3	590.5	651.5	608.3	635.0	565.1
623.6	601.5	519.6	574.8	609.6	609.6	623.6	595.9	534.4	585.5	581.2	621.3
635.0	589.8	505.5	555.5	610.9	622.8	577.8	646.4	598.2	551.9	529.6	542.3
609.8	598.2	586.7	614.7	607.1	538.5	626.1	651.5	614.7	481.3	566.4	608.3
626.1	623.6	558.8	615.9	565.1	532.1	545.8	581.7	582.9	506.7	590.5	550.4
605.8	510.5	607.1	473.7	595.6	588.5	557.5	569.0	582.9	609.6		

OUTPUT OF NUMBER OF PARTICLES AND % OF TOTAL IN EACH RANGE

NUMBER OF RANGE	TOTAL PARTICLES	PERCENT OF TOTAL
1	2	0.7
2	5	1.7
3	9	3.0
4	29	9.7
5	48	16.1
6	78	26.2
7	82	27.5
8	39	13.1
9	4	1.3
10	2	0.7

FIGURE 4.10 Size histogram of 110 μm collector particles

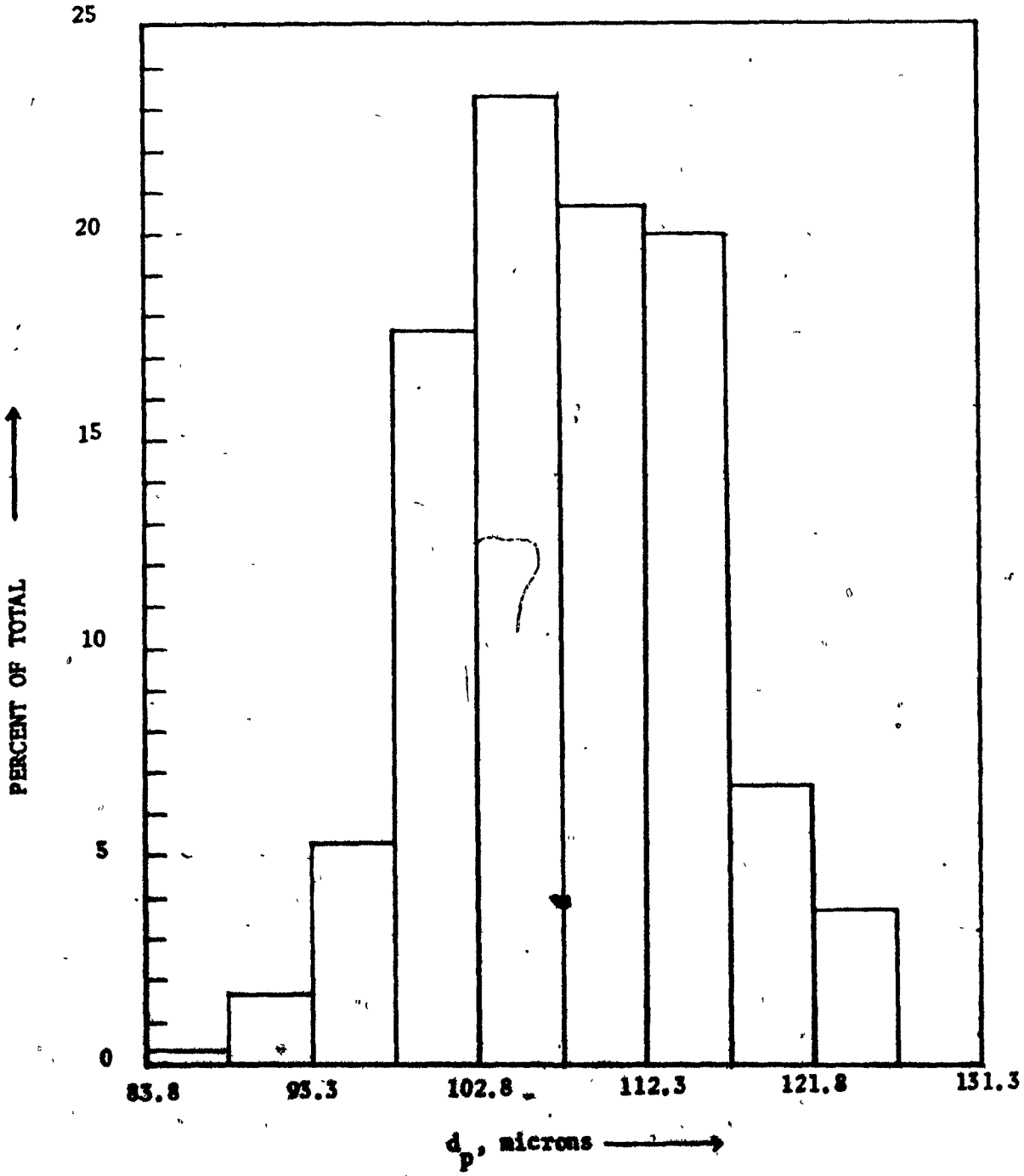
25
20
15
10
5
0
PERCENT OF TOTAL
83.8
95.3
102.8
112.3
121.8
131.3
d_p, microns

FIGURE 4.11 Size histogram of 550 μm collector particles

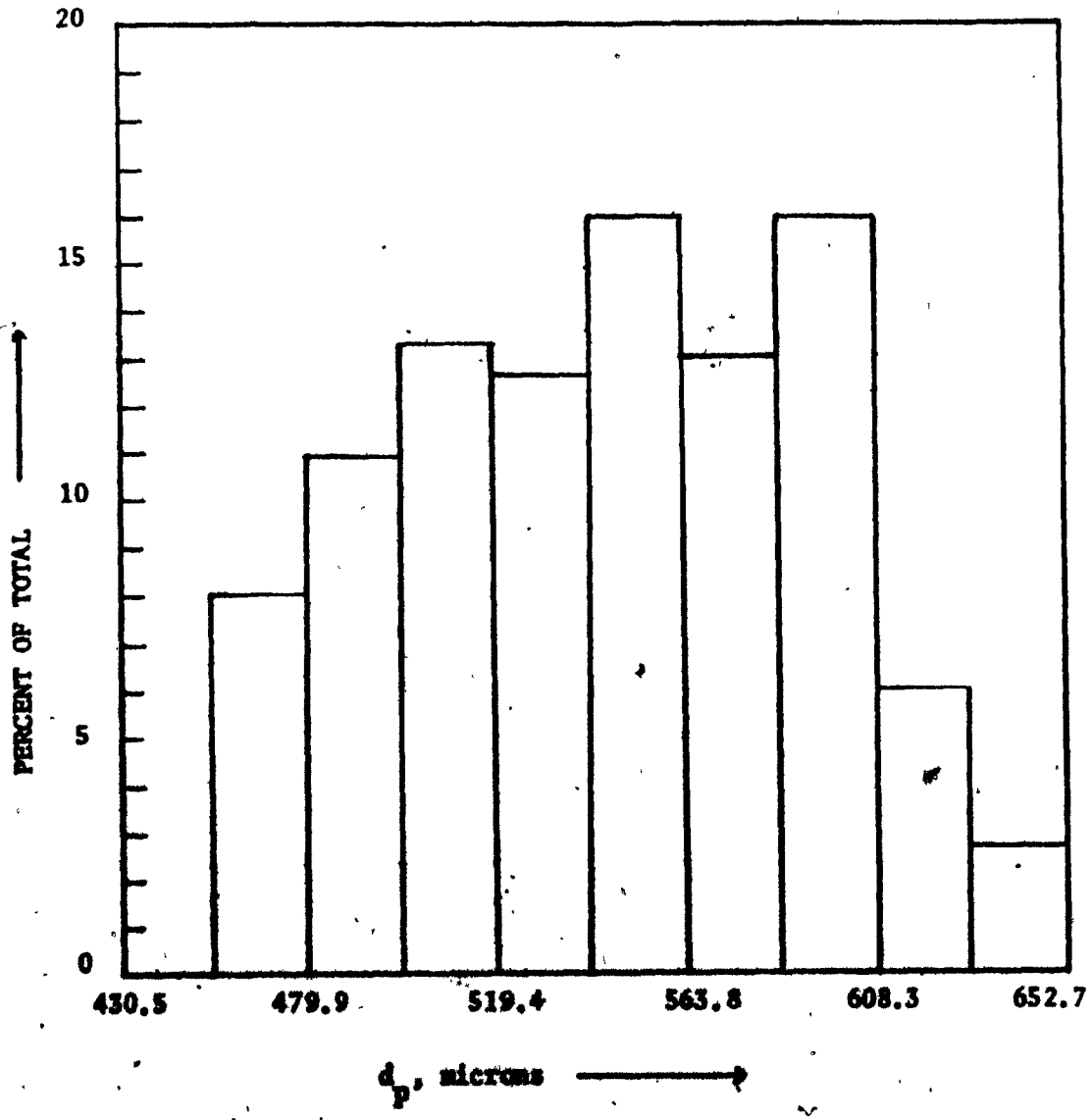
20
15
10
5
0
PERCENT OF TOTAL
430.5
479.9
519.4
563.8
608.3
652.7
d_p, microns

FIGURE 4.12 Size histogram of 600 μm collector particles

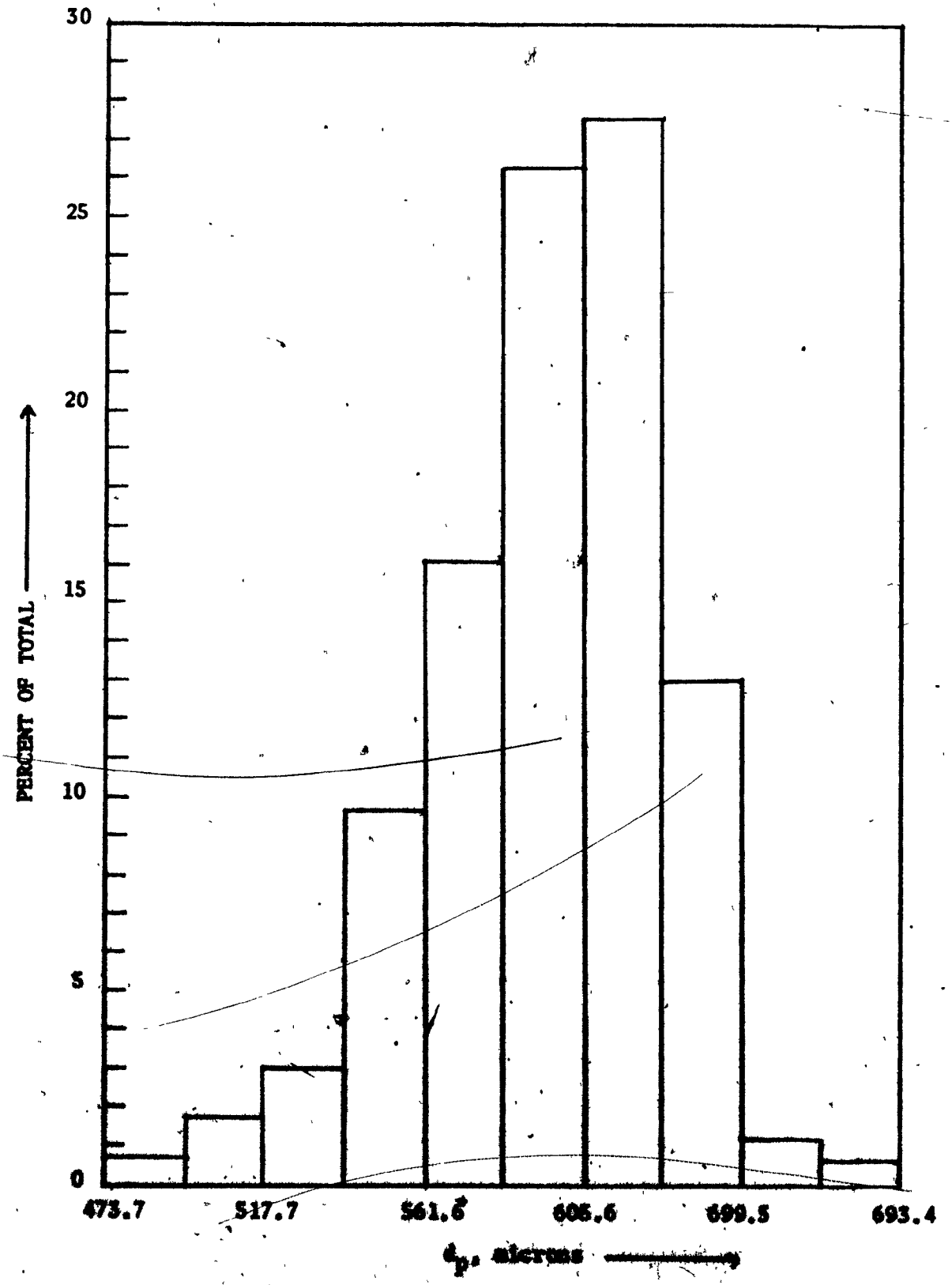
30
25
20
15
10
5
0
PERCENT OF TOTAL
473.7
517.7
561.6
605.6
649.5
693.4
d_p, microns

TABLE 4.5 Properties of Collector Particles

Average Values	d_p = 110 μm	d_p = 600 μm
particle density, kg/m^3	2.44×10^3	2.43×10^4
voidage	0.40	0.40
bulk density, kg/m^3	1.47×10^3	1.47×10^3

any remaining dust or aerosol particles. In this way the "background" concentration of particles in the gas from the bed was reduced to less than 0.05% of the aerosol concentration in an experimental run. Since the smallest particles in the bed were 80 μm in diameter, and at least 0.20m of freeboard was left above the fluidized bed, there was negligible carryover of bed particles to the filter or sample probe.

Aerosol samples were drawn off from the gas space below the distributor and above the fluidized bed at 4.8×10^{-6} to $5.2 \times 10^{-6} m^3/s$ through a 6.0×10^{-3}m inside diameter probe to the particle counter. The flow rate through the counter was measured initially to ± 2% with a calibrated orifice meter and inclined manometer and subsequently determined to ± 0.4% with a bubble meter. In order to minimize the lengths of the sample lines, which were then left unchanged throughout the experiments, the optical section of the particle counter was disassembled from the instrument and placed in a construction which fitted around the bed; the length of the freeboard sample probe was thus reduced to approximately 0.4m. This construction incorporated a pulley arrangement where the weight of the optics section was balanced with two twenty kilograms lead weights* and the optics section could be vertical and rotated around 360°. The construction, like any other major piece of equipment built, was placed on lock-roller casters to facilitate rearrangement into different configurations. A non-isokinetic sampling system was used in this study. As the aerosol was sampled downstream of the column, with and without the bed at the same experimental velocity,

*Courtesy of the Metallurgy Department, McGill University, Montreal.

any errors in sampling non-isokinetically plus any collection by the support plate, inlet section, walls of column and sampling system were automatically eliminated. If f_D, f_c, f, f_U and f_s refer to fractional penetration of the aerosol through distributor, column, bed, non-isokinetic sampler, and sampling system and C_{in} and C_c refer to concentration of aerosol at inlet and concentration of particles counted, respectively, then without the bed

$$(C_p)_o = f_D f_c f_U f_s C_{in} \tag{4.3}$$

and with the bed in place

$$(C_p)_1 = f_D f_c f_U f_s f C_{in} \tag{4.4}$$

The fraction of the aerosol collected by the bed is then

$$f = \frac{(fC_{in})}{C_{in}} = \frac{(C_c)_1}{(C)_o} \tag{4.5}$$

The distortion introduced by sampling non-isokinetically, although eliminated, is in any case small and within experimental errors, as shown by blank test experiments plotted in Figure 4.13. This is hardly surprising as we are dealing with aerosol diameters that are most difficult to remove from an air stream. The support plate used in fixed bed experiments also collected a negligible amount of the incoming aerosol, but distorted experimental readings, with the bed in place, by affecting the velocity field in its vicinity. The way this problem was solved is described in Section 4.2.

FIGURE 4.13 Effect of sampling non-isokinetically.(DOP aerosol 1.5 μm diameter). Broken line indicates isokinetic sampling point.

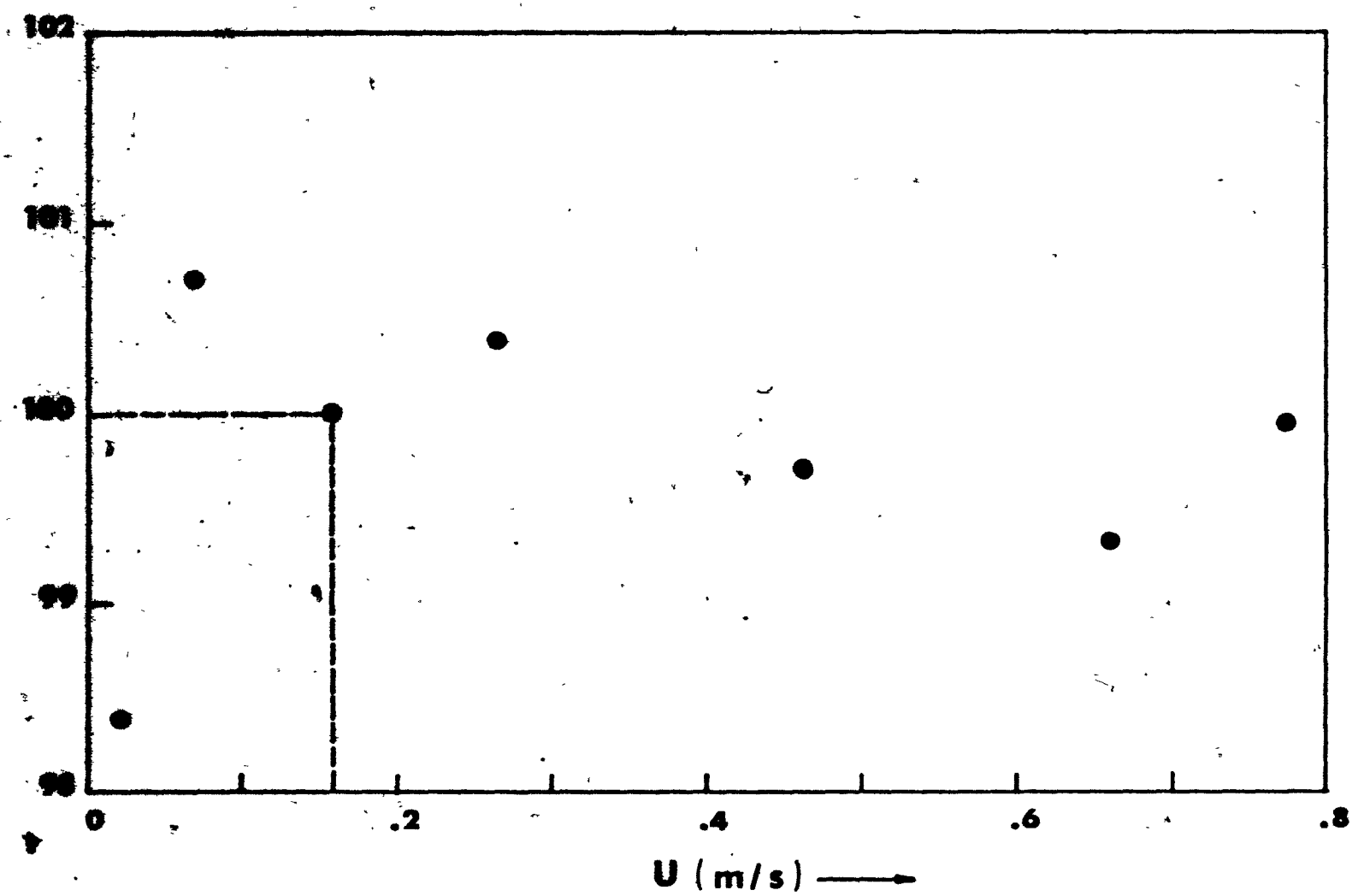
102
101
100
99
98
0
.2
.4
.6
.8
U (m/s) ⟶

During operation possible variations in the concentration and size of the aerosol particles produced by the generator were detected by drawing samples from below the support plate. Reproducibility of these "check tests" was better than 2% after allowing a one-hour "warm up" period for the generator. Reproducibility of check tests improved markedly after the aerosol generator was modified as described in Section 4.2.

4.4 Air Flow System for Fluidized Bed Experiments at High Velocities (0.6 < U < 3m/s)

As the fluidized bed apparatus, described in Section 4.3 and used for aerosol removal with velocities up to 0.7m/s, yielded encouraging results at high superficial gas velocities a second system, capable of handling up to $5 \times 10^{-2} m^3/s$, was designed and built. The system is shown schematically in Figure 4.14. The aerosol generator was adjusted to produce $2.36 \times 10^{-2} m^3/s$ of aerosol which was near its maximum capacity. This aerosol was subsequently mixed with clean air, which had been drawn through an absolute filter of the same make and manufacture as the one incorporated in the generator inlet*, in a $9.6 \times 10^{-2} m^3$ mixing tank. Part of the diluted aerosol thus produced (around $9.0 \times 10^{-2} m^3/s$) was passed through the fluidized bed and the remainder discharged to the fumehood. The fixed bed support plate described in Figure 4.6b was used as a distributor giving a 7% free surface area. The fluidized bed was contained in a 0.15m diameter, 0.61m high cylindrical glass column.

---

*Ultra Aire Filter, Cat.No.82141, manufactured by Mine Safety Appliances Co., Pittsburgh, Pennsylvania.

FIGURE 4.14 Schematic diagram of high velocity system ($0.6 < U < 3.0$ m/s)

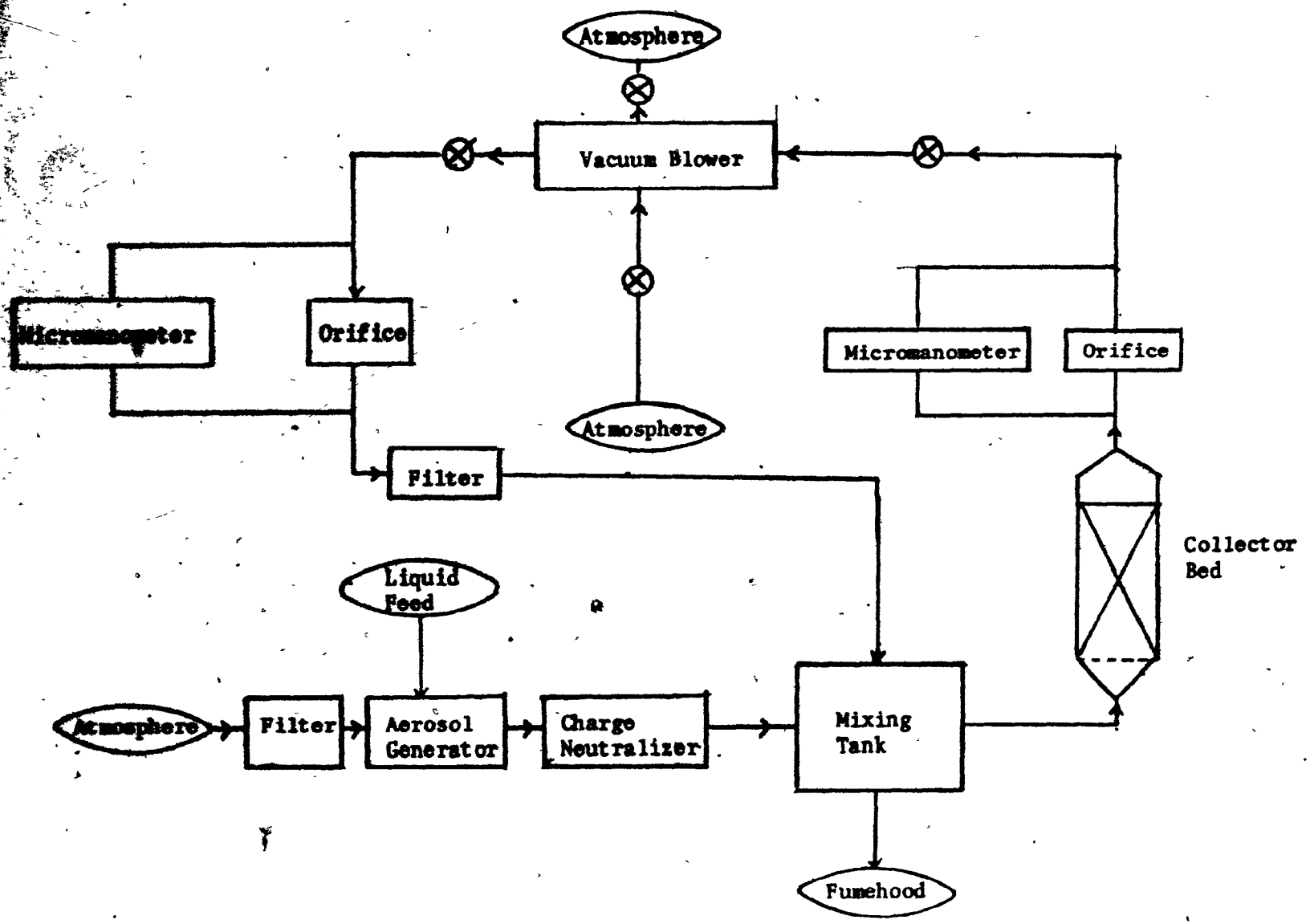
Atmosphere
Vacuum Blower
Micromanometer
Orifice
Micromanometer
Orifice
Atmosphere
Filter
Collector Bed
Liquid Feed
Atmosphere
Filter
Aerosol Generator
Charge Neutralizer
Mixing Tank
Fumehood

The sampling system was similar to the one described in Section 4.3 except that the diameter of the sampling probe was reduced to 2.1×10^{-3}m. Flow through the system was maintained with a high capacity air blower* and the exit of the blower was used to provide the clean air diluting the aerosol produced by the generator. The amount of clean air added and the total flow through the bed was measured by two 5.1×10^{-2}m diameter orifice meters,** with upstream and downstream taps connected to inclined micromanometers, calibrated by a gas metering device to an accuracy of ± 5%. The flow system was controlled by four valves as shown in Figure 4.14.

4.5 Procedure

4.5.1 Introduction

The following procedure describes an experimental run which takes approximately two days, one for preparing the apparatus and an aerosol in the desired size range and one for performing the experiments. It involves measurement of penetration vs. velocity at different bed heights in a fluidized bed and assumes no major breakdowns or unstable performance of the aerosol generator.

4.5.2 Preparation (first day)

1. Clean the collector particles as described in Section 4.3; after drying weigh the necessary amount for experiments.

---

*Tornado Centrifugal Fan, manufactured by Keith Blackman Ltd. Engineers, London, England.

**For comparison, this is equal to the diameter of fluidized beds used by some previous studies (see Section 2.3).

ii. Clean the aerosol generator (if necessary), clean surface of disk with alcohol and adjust the liquid feed needle at the center of the spinning disk and at a height 0.51 to 1.0×10^{-3} m above the disk surface.

iii. Check the oil level of the vacuum pump and add oil if necessary.

iv. Disassemble the fluidized bed, clean the cylindrical column, expansion chamber, distributor and sampling probe, wash in distilled water, dry and assemble.

v. Turn on the particle counter and generator and allow a warming up period of 1 - 2 hours.

vi. Field calibrate particle counter.

vii. Add a sufficient amount of dioctyl phthalate to a $4.5 \times 10^{-3} m^3$ bottle of methanol to produce an aerosol at the desired size range monitoring the aerosol with the particle counter. As the diameter and concentration of the test aerosol is a function of the distance of the liquid feed needle from the center and surface of the spinning disk, this trial and errors procedure is unavoidable. Once an acceptable aerosol is produced the equipment is ready for experiments.

4.5.3 Experiments (second day)

i. Start up the particle counter and generator and field calibrate counter after an initial warm up period.

ii. Turn on disc motor and liquid feed and measure the concentration and size of challenging aerosol from the gas space above the distributor at the predetermined gas flow rates through the bed. Measure

the aerosol at one, fixed, velocity below the distributor; this is the "side check test".

iii. Turn off the liquid flow, place the collector particles in the bed and fluidize for half an hour with aerosol free air. Check with the particle counter to ensure a zero or minimal "background" concentration.

iv. Turn on liquid flow and, after reaching steady state, measure the penetration of the challenging aerosol at a predetermined flow rate indicated by the rotameters; typically steady state is reached in around 5 to 10 minutes.

v. Change the flow through the bed and repeat Step iv.

vi. After the penetration of the challenging aerosol through the bed has been measured for 2 - 3 different flow rates place more collector particles in the bed and repeat Steps iii to v. At frequent intervals, typically every hour or so, verify that the generator is producing a constant aerosol by making a "side check".

At the end of a 14 - 18 hour period the penetration of the challenging aerosol will have been determined at 4 - 5 bed heights and at 2 - 3 different flow rates. During the same period of time the fluidized bed will have collected around 10^{-7} to 10^{-5} kg of dioctyl phthalate; this is a minute amount and too small to introduce an effect of bed loading although it represents 10^{11} to 10^{13} one micron diameter aerosol particles each weighing 5.0×10^{-19} kg.

CHAPTER 5. COLLECTION MECHANISMS IN A FIXED BED OF SPHERICAL COLLECTOR PARTICLES

5.1 Introduction

The various mechanisms resulting in the collection of airborne particulates by isolated spherical collectors were discussed in Section 3.2. These mechanisms were direct interception, inertial collection, diffusional deposition and gravity settling; on the assumption that these effects are additive, the total collection by an isolated collector particle was given by Equation (3.51) as

$$E_T = E_R + E_I + E_D + E_G \tag{3.51}$$

The presence of other particles results in an increase of total efficiency of the collector and Equation (3.59) was derived on the assumption that this interference effect is the same for all mechanisms (Section 3.3).

$$E_{BT} = \alpha_B E_T \tag{3.59}$$

The following chapter tests experimentally the validity of these assumptions and determines, again experimentally, the dominant collection mechanisms under the conditions in this study. Experimental collection efficiencies are compared with the theoretical predictions of Chapter 3. The semi-empirical equations for collection in a fixed bed are compared in Chapter 7 with collection efficiencies in a fluidized bed.

5.2 Preliminary Experiments

5.2.1 Collection behaviour of a fixed bed

Figure 5.1 shows some preliminary experiments which were performed with 110 μm collector particles and three aerosol sizes; 1.1 μm, 1.35 μm and 1.75 μm. The bed height was 7.4×10^{-3} m and the per cent penetration of the liquid DOP aerosol used is plotted as a function of superficial gas velocity. Inspection of the figure shows that penetration decreases with increasing aerosol diameter and gas velocity. This suggests the dominance of inertial effects at superficial velocities greater than around 0.1 m/s. At lower gas velocities, up to 4×10^{-2} m/s, penetration increases with increasing velocity and with decreasing aerosol size. This indicates that at these velocities gravitation is the predominant collection mechanism; this is discussed in more detail in Section 5.5. In both ranges, the dependence of penetration on aerosol size shows that diffusional collection cannot be significant; if it were, penetration would increase with increasing aerosol size. These same qualitative conclusions follow from all the fixed bed experiments in this work. All curves pass through a maximum penetration point around 4 to 8×10^{-2} m/s indicating the area where gravitational and inertial parameters are comparable in importance.

Unfortunately, such a simple approach cannot be used to estimate the parameters of aerosol collection because of the end effects of a fixed bed. The end effects of a fixed bed and how they may distort the values of the estimated coefficients are discussed more fully in Section 5.3. The figure presented here serves only to illustrate the general collection behaviour of a fixed bed as a function of aerosol size and velocity.

FIGURE 5.1 Preliminary experiments on penetration of DOP aerosol as a function of superficial velocity

d_p = 110 μm
H = 7.4×10^{-3} m
full circles; d_A = (1.0 - 1.2) μm
open circles, d_A = (1.2 - 1.5) μm
full squares, d_A = (1.5 - 2.0) μm

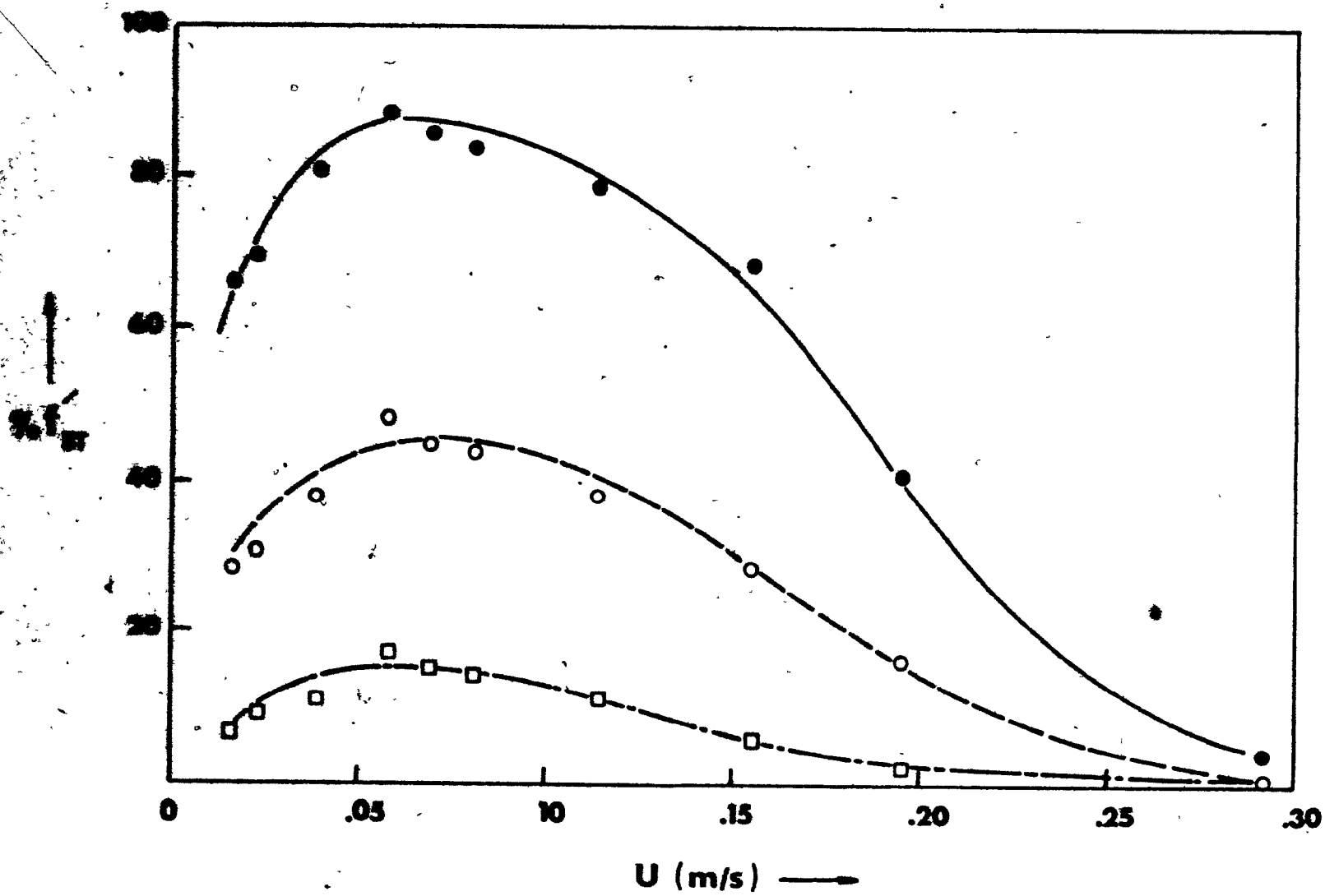
100
80
60
40
20
0
.05
10
.15
.20
.25
.30
U (m/s)

5.2.2 Collection of solid methylene blue aerosol in a fixed bed

Figure 5.2 describes an experiment which was devised to determine the feasibility of fixed bed experiments with solid methylene blue aerosol. The experiment was performed as follows:

0.6 kg of 600 μm collector particles were first cleaned by the method described in Chapter 4. They were subsequently fluidized with DOP aerosol in order to cover their surface with a thin layer of DOP and thus prevent any subsequent re-entrainment of solid aerosol particles. Penetration of 1.1 μm, 1.35 μm and 1.75 μm solid methylene blue particles through a fixed bed composed of the above collectors was then measured with respect to time. 50 one-minute readings were monitored by the particle counter after a period of 10 minutes was allowed for the system to reach "steady state". The first reading was assigned an arbitrary value of 100% and the subsequent readings were expressed as a percentage of this. The superficial gas velocity of the bed was 0.13 m/s and the experiment lasted approximately 2 hours and 40 minutes.

Figure 5.2 shows the variation in the penetration of the three aerosol sizes with respect to time plotted on semi-logarithmic axes. As seen from the figure the dependence of penetration on time is exponential. This set of experiments belongs to the area of unsteady state filtration (Section 2.2.2) where the aerosol particles cause structural changes in the filter and as a result both penetration and pressure drop across the filter may change with time. It also appears that the equation

FIGURE 5.2 Penetration of methylene blue aerosol as a function of time

M — 0.6 kg
U — 0.13 m/s
full squares, d_A — 1.1 μm
open triangles, d_A — 1.35 μm
full circles, d_A — 1.75 μm

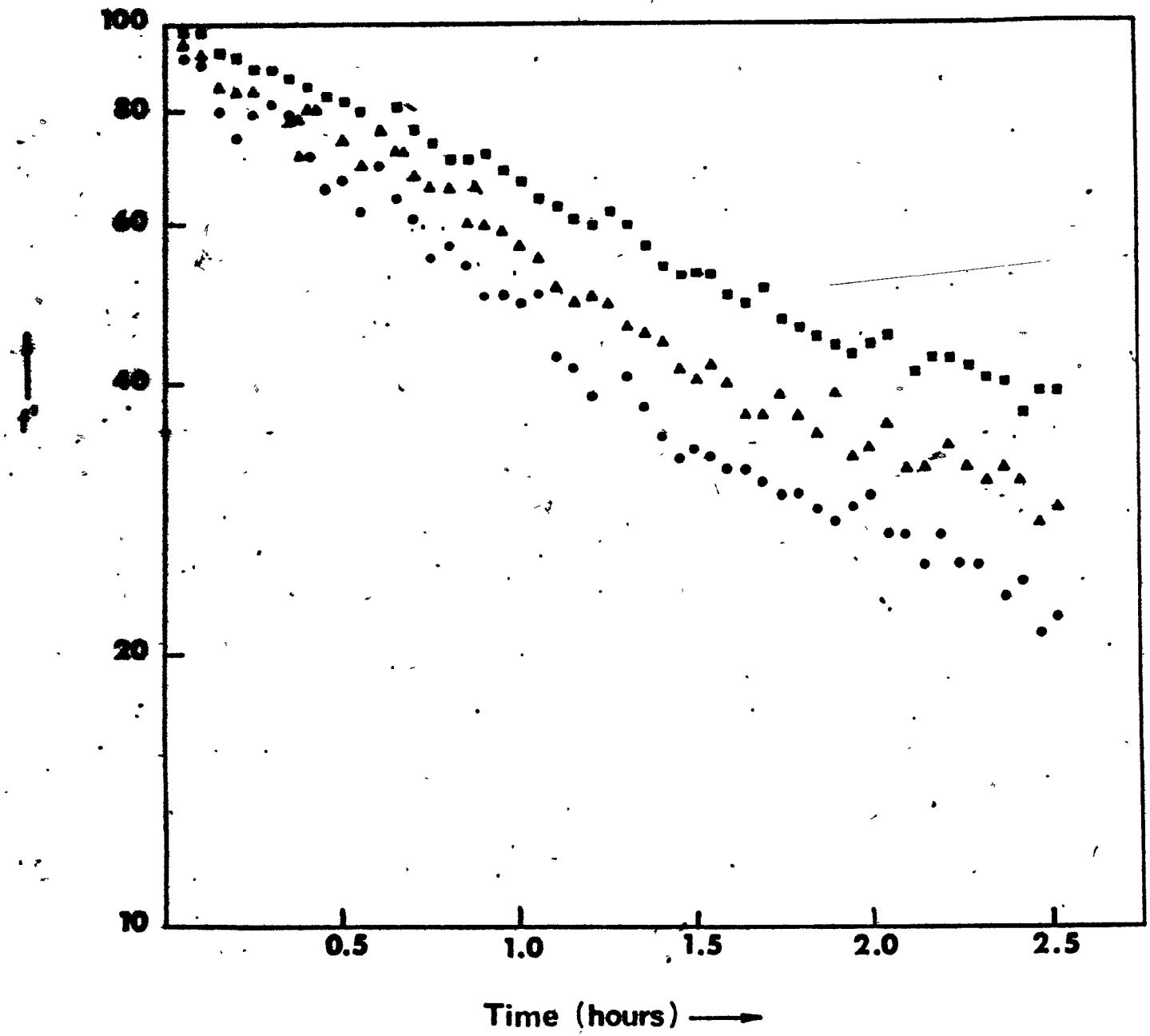
100
80
60
40
20
10
0.5
1.0
1.5
2.0
2.5
Time (hours) ⟶

suggested by Radushkevich[R1] on theoretical grounds for unsteady state filtration

$$(f')_t = (f')_{t=0} e^{-ct} \qquad (2.5)$$

is of the correct form. Leers[L12] reports that the distribution of captured aerosol particles on the surface of the collector is selective. The particles tend to deposit on one another forming so-called "trees", causing a marked increase in efficiency with relatively small change in pressure drop. It would be possible, by performing experiments of the form described above, to determine the value of c in Equation 2.5 for different values of U, d_A and d_p and thus to present useful empirical equations predicting the start-up behaviour of fixed beds operating in the unsteady state filtration régime. However, this was not the object of this study and the above experiment was done in order to determine whether fixed bed experiments with solid aerosols could be performed. As a result of this experiment it was decided that experiments with solid aerosol would not yield accurate collection parameters and all subsequent fixed bed experiments were performed with liquid DOP aerosols.

5.3 Mathematical Formulation of Aerosol Removal in a Fixed Bed

This section develops the equations defining aerosol removal in a fixed bed composed of spherical collector particles. As the performance of the fixed bed may be substantially distorted by end effects the equations defining aerosol collection are formulated in a way which eliminates possible anomalous behaviour at the bed extremes.

In Section 3.1 the total collection efficiency for one collector particle was defined, in general terms, as

$$E_T = \frac{\text{particles of aerosol collected}}{\text{particles in approach volume}} \tag{3.1}$$

The number of aerosol particles collected by one spherical collector of diameter d_p per unit time is then

$$R_T = E_{BT} \frac{\pi d_p^2}{4} * U * C \tag{5.1}$$

where U is the superficial gas velocity through the bed and C is the number concentration of aerosol particles in the approach volume. The number of spherical collector particles per unit dense phase volume is given from simple geometry as

$$N_p' = \frac{6(1-\varepsilon)}{\pi d_p^3} \tag{5.2}$$

If we define K_V as the collection parameter based on unit dense phase volume, then the number of aerosol particles collected per unit dense phase volume is given as

$$K_V C = N_p' * R_T \tag{5.3a}$$

Substituting expressions for N_p' and R_T from Equations (5.1) and (5.2) and re-arranging

$$K_V = \frac{3}{2} * \frac{(1-\varepsilon)E_{BT}U}{d_p} \tag{5.3b}$$

Similarly, if we define a collection parameter K_M based on unit bed mass

$$K_M = \frac{K_V}{\rho_p(1-\varepsilon)} \tag{5.4a}$$

$$= \frac{3E_{BT}U}{2\rho_p d_p} \tag{5.4b}$$

and the collection efficiency of a spherical particle in a fixed bed is expressed in terms of the collection parameter K_M as

$$E_{BT} = \left(\frac{2\rho_p d_p}{3U}\right) * K_M \tag{5.4c}$$

Now suppose the collector bed contains mass M of collector particles and has a cross sectional area A_B perpendicular to the direction of the gas flow. Then

$$M_A = \frac{M}{A_B} \tag{5.5a}$$

where M_A is the mass of collector particles per unit bed area.

Similarly, if $\underline{h}$ is the distance from the inlet surface of the bed and $\underline{m}$ is the mass of bed between the surface and $\underline{h}$, we can define

$$m_A = \frac{m}{A_B} \tag{5.5b}$$

where

$$0 < h < H$$

$$0 < m < M$$

$$0 < m_A < M_A$$

Referring to Figure 5.3 we consider an aerosol which approaches the bed with superficial gas velocity U m/s and aerosol concentration C_{in} particles/m^3. In the neighbourhood of the upper surface of the bed, the velocity of the aerosol stream relative to the collector particles changes from U to the interstitial gas velocity u_I where u_I is given by

$$u_I = \frac{U}{\epsilon} \tag{5.6}$$

If we now assume that during this transition an anomalous collection takes place at the top of the bed then the true concentration immediately below $m_A = 0$ is $(1-\delta_o)C_{in}$. In this context δ_o represents the anomalous collection at the upper surface of the bed. The concentration of the aerosol after passing through mass m_A per unit area is C. Taking a mass balance over a differential element dm_A gives

$$UC = U(C + dC) + K_M C dm_A \tag{5.7}$$

so that

$$\frac{dC}{dm_A} = -\frac{K_M}{U} C \tag{5.8}$$

FIGURE 5.3 Schematic representation of aerosol collection in a fixed bed with end effects

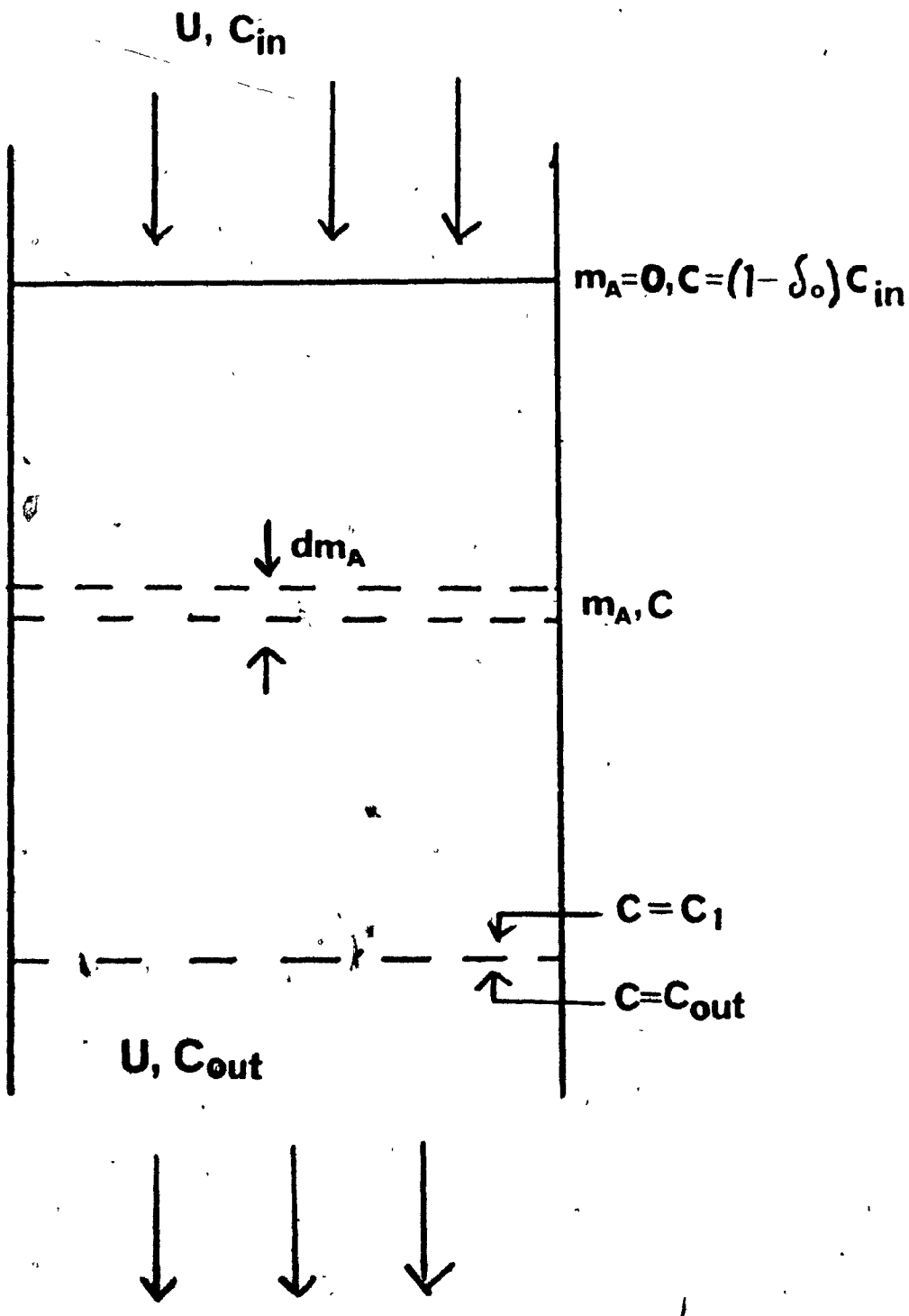
U, C_{in}
$m_A=0, C=(1-\delta_o)C_{in}$
dm_A
m_A, C
$C=C_1$
$C=C_{out}$
U, C_{out}

Solving the first order differential equation with the boundary condition that at $m_A = 0$, $C = (1-\delta_o)C_{in}$

$$C = (1-\delta_o)C_{in}EXP\left[-K_M m_A/\bar{U}\right] \tag{5.9}$$

Then immediately above the support plate at $m_A = M_A$ the concentration of the aerosol is given by $C = C_1$ where

$$C_1 = (1-\delta_o)C_{in}e^{(-M_A K_M/U)} \tag{5.10}$$

There is bound to be some collection at the support plate. However large the free surface area of the plate, the fluid will always accelerate in its vicinity. Moreover, design details like the unavoidable introduction of airtight seals between support plate and column will probably result in a non-uniform flow distribution. Furthermore, the collector particles, depending on their size and the size of the support plate openings may stick on the plate and result in anomalous collection. Simply taking a blank test without the fixed bed and subtracting the result from the collection with the bed in place will not eliminate this effect, which depends on both the bed particles and the support plate. Therefore, all previous studies in which collection efficiencies were determined from experiments with a single bed depth are liable to error resulting from anomalous collection at entry and exit from the bed.

If it is assumed then that there is an anomalous collection at the support plate represented by δ_1 so that C immediately changes from C_1 to C_{out} then

$$C_{out} = (1-\delta_1)C_1 \tag{5.11a}$$

$$= (1-\delta_o)(1-\delta_1)C_{in}\,EXP\left[-\frac{M_A K_M}{U}\right] \tag{5.11b}$$

The overall fractional penetration, f, through the bed is

$$f = \frac{C_{out}}{C_{in}} = (1-\delta_o)(1-\delta_1)EXP\left[-\frac{M_A K_M}{U}\right] \tag{5.12}$$

or

$$\ln f = \ln(1-\delta_o)(1-\delta_1) - \left[\frac{M_A K_M}{U}\right] \tag{5.13}$$

Preliminary experiments in this study confirmed that $\ln(1-\delta_o)(1-\delta_1)$ cannot be eliminated by simply carrying out blank tests without the bed. The value of this variable may be positive or negative and as the phenomenon results partially from an acceleration of the fluid its sign depends on whether gravitation or inertial effects are predominant.

Figure 5.4 demonstrates this schematically where it is assumed that blank tests are done with the support plate in place.

Inspection of Figures 5.5 to 5.23 will confirm qualitatively the argument presented above. At high velocities and large aerosol diameters semi-logarithmic plots of per cent penetration versus bed weight extrapolate to a penetration at zero bed weight of less than 100% while at low velocities and smaller aerosol diameters the reverse is true.

The correct approach therefore is to measure aerosol penetrations at different bed heights for a fixed set of conditions and if the results are plotted in the form

FIGURE 5.4 Demonstration of correct approach in performing fixed bed experiments

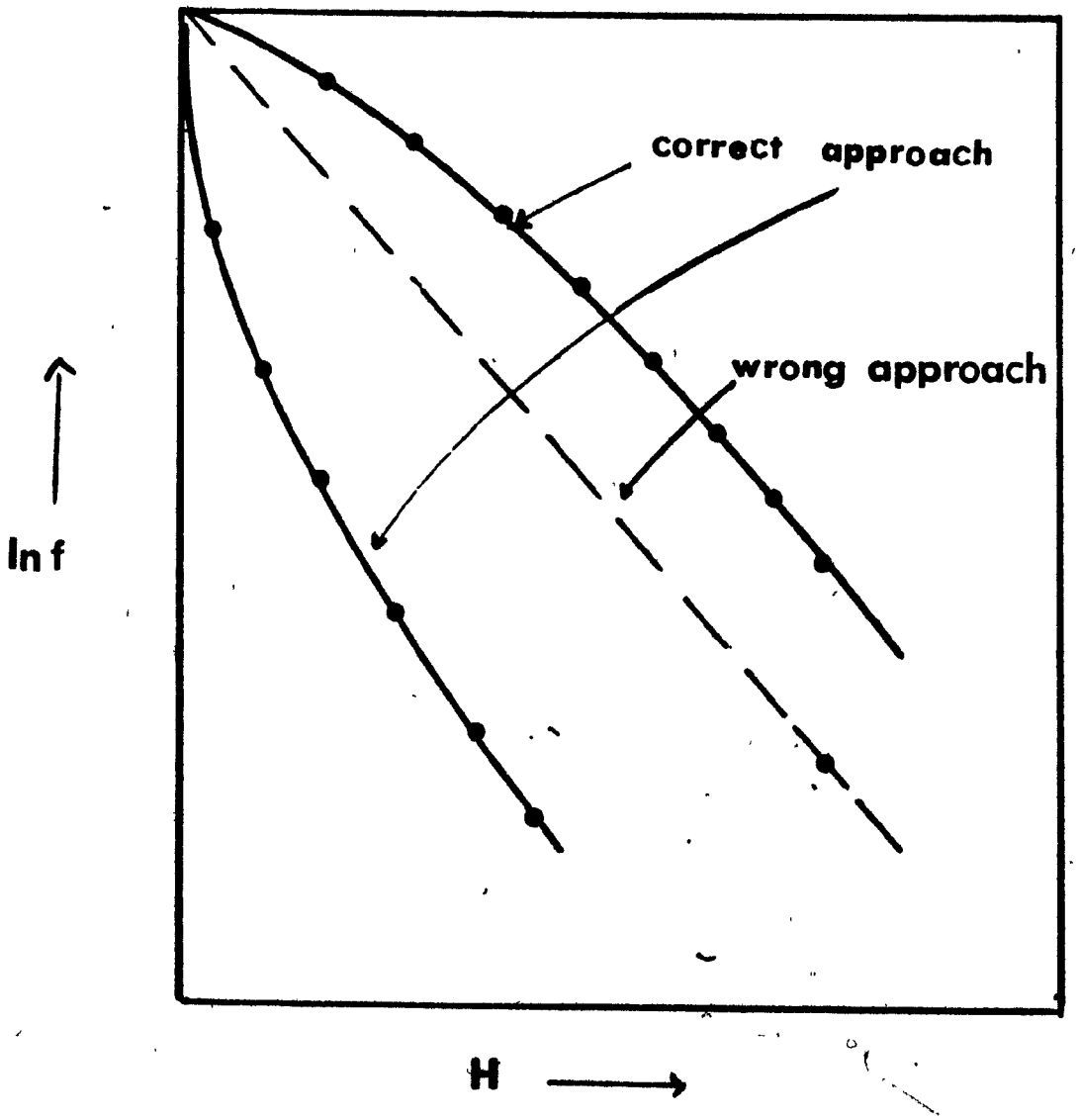
correct approach
wrong approach
ln f
H

FIGURE 5.5 Fixed bed experiments - aerosol penetration vs bed depth

d_c = 110 μm
U^p = 0.0098 m/sec
open circles, d_A = 1.35 μm
full circles, d_A = 1.75 μm

FIGURE 5.6 Fixed bed experiments - aerosol penetration vs bed depth

d_c = 110 μm
U^p = 0.0202 m/sec
open circles, d_A = 1.35 μm
full circles, d_A = 1.75 μm
open squares, d_A = 2.50 μm

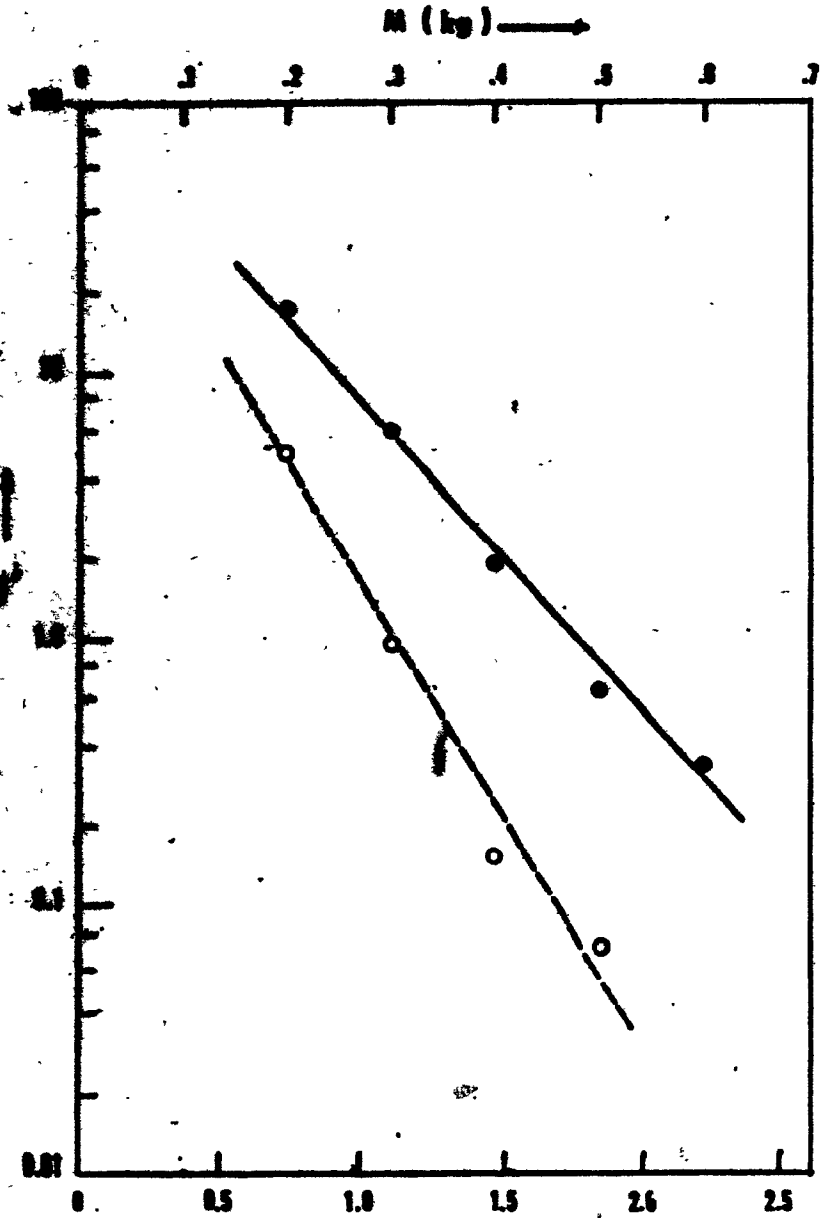
M (kg)
0
.1
.2
.3
.4
.5
.6
.7
0.5
1.0
1.5
2.0
2.5
H (m • 10²)

Fig .5.5

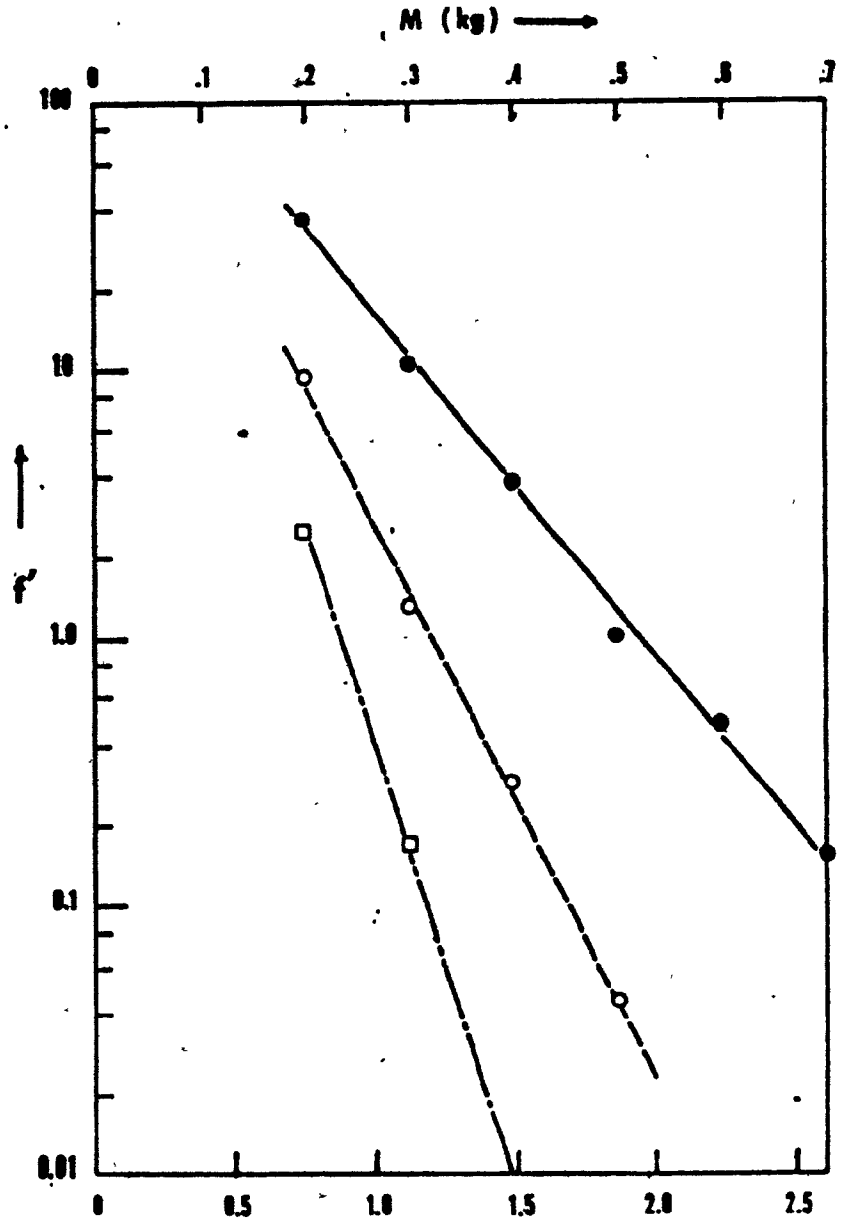
M (kg)
0
.1
.2
.3
.4
.5
.6
.7
100
10
1.0
0.1
0.01
f'
0
0.5
1.0
1.5
2.0
2.5
H (m • 10²)

Fig .5.6

FIGURE 5.7 Fixed bed experiments - aerosol penetration vs bed depth

d_p = 110 μm
U^p = 0.0269 m/sec
open circles, d_A = 1.35 μm
full circles, d_A = 1.75 μm
open squares, d_A = 2.25 μm

FIGURE 5.8 Fixed bed experiments - aerosol penetration vs bed depth

d_p = 110 μm
U^p = 0.0383 m/sec
open circles, d_A = 1.35 μm
full circles, d_A = 1.75 μm
open circles, d_A = 2.25 μm

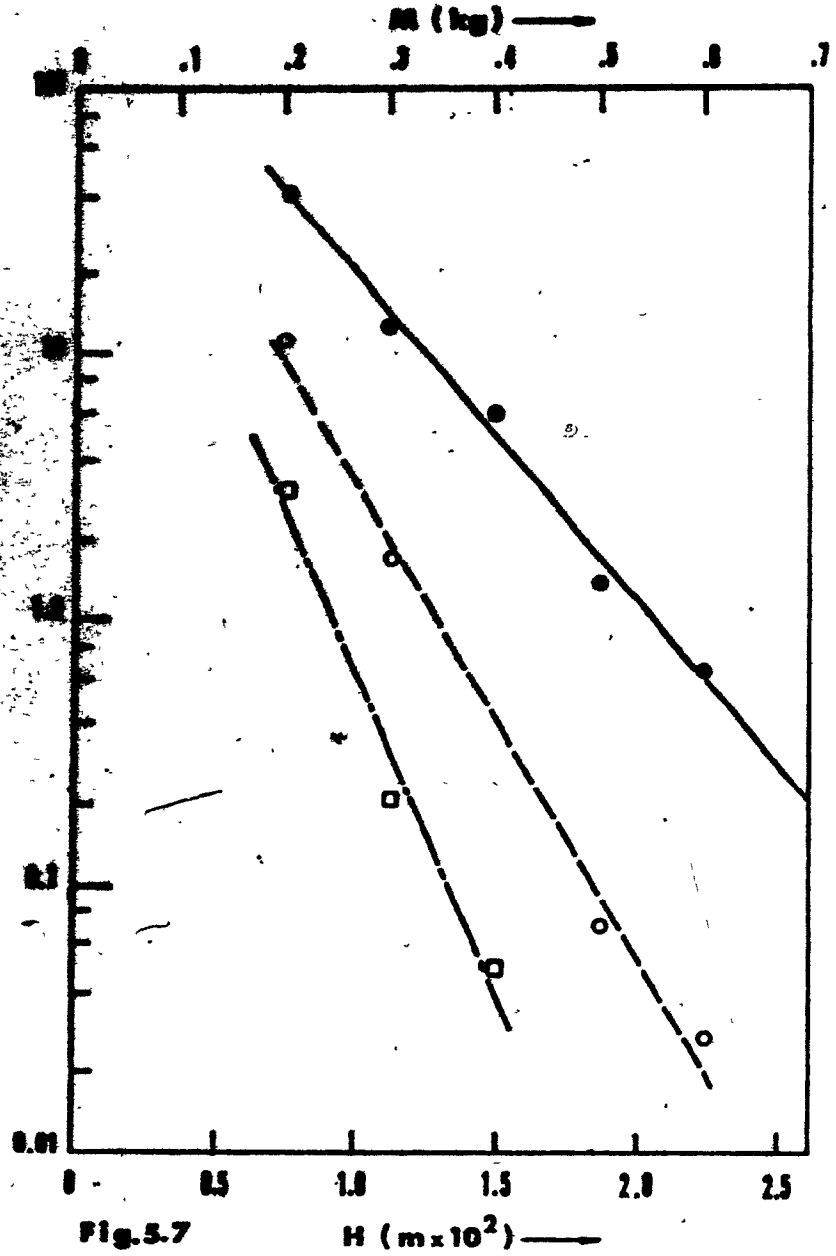
M (kg)
0
.1
.2
.3
.4
.5
.6
.7
0.01
0.1
1.0
0
0.5
1.0
1.5
2.0
2.5
H (m x 10²)

Fig.5.7

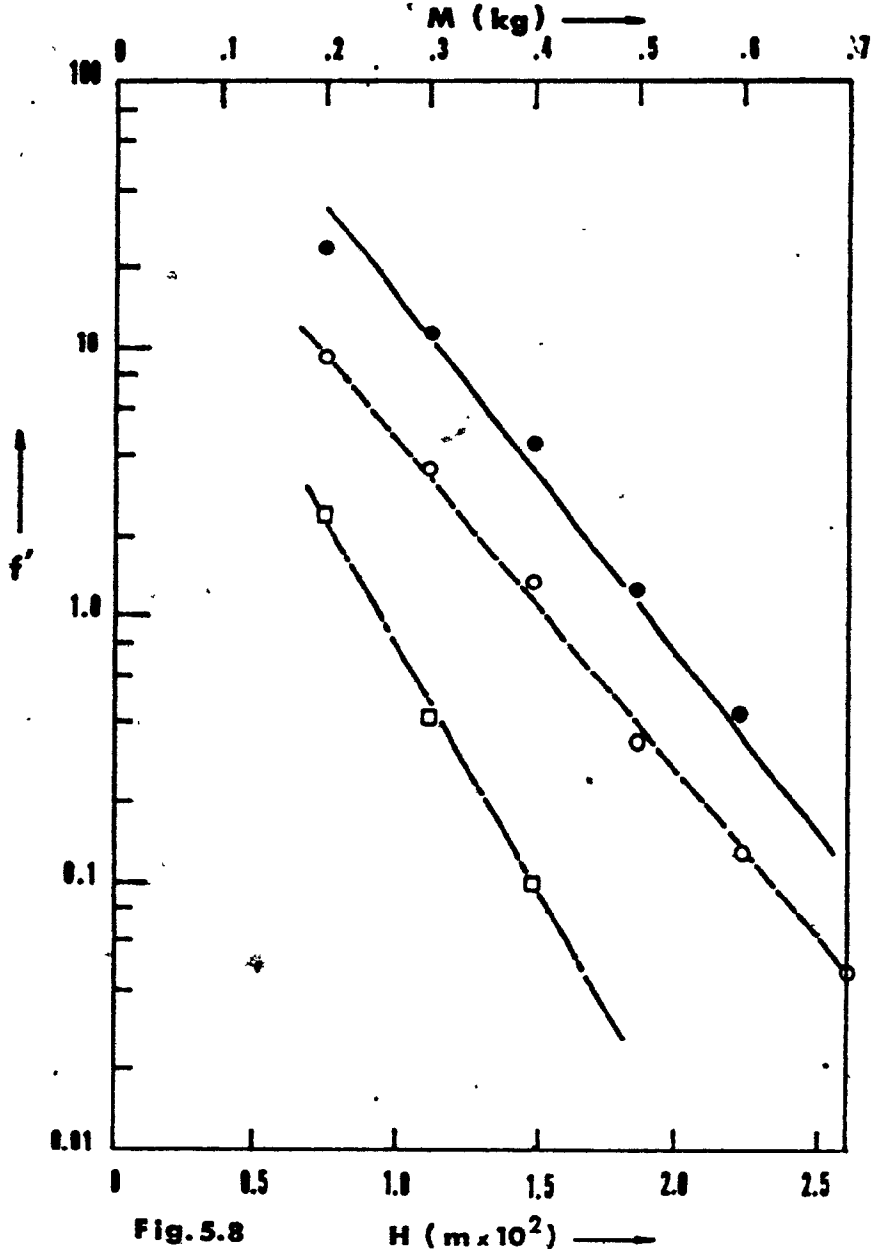
M (kg)
0
.1
.2
.3
.4
.5
.6
.7
100
10
1.0
0.1
0.01
f'
0
0.5
1.0
1.5
2.0
2.5
H (m x 10²)

Fig. 5.8

FIGURE 5.9 Fixed bed experiments - aerosol penetration vs bed depth

d_p = 110 μm
U^p = 0.0383 m/sec
open circles, d_A = 1.1 μm
full circles, d_A = 1.35 μm

FIGURE 5.10 Fixed bed experiments - aerosol penetration vs bed depth

d_p = 110 μm
U^p = 0.0492 m/sec
open circles, d_A = 1.35 μm
full circles, d_A = 1.75 μm

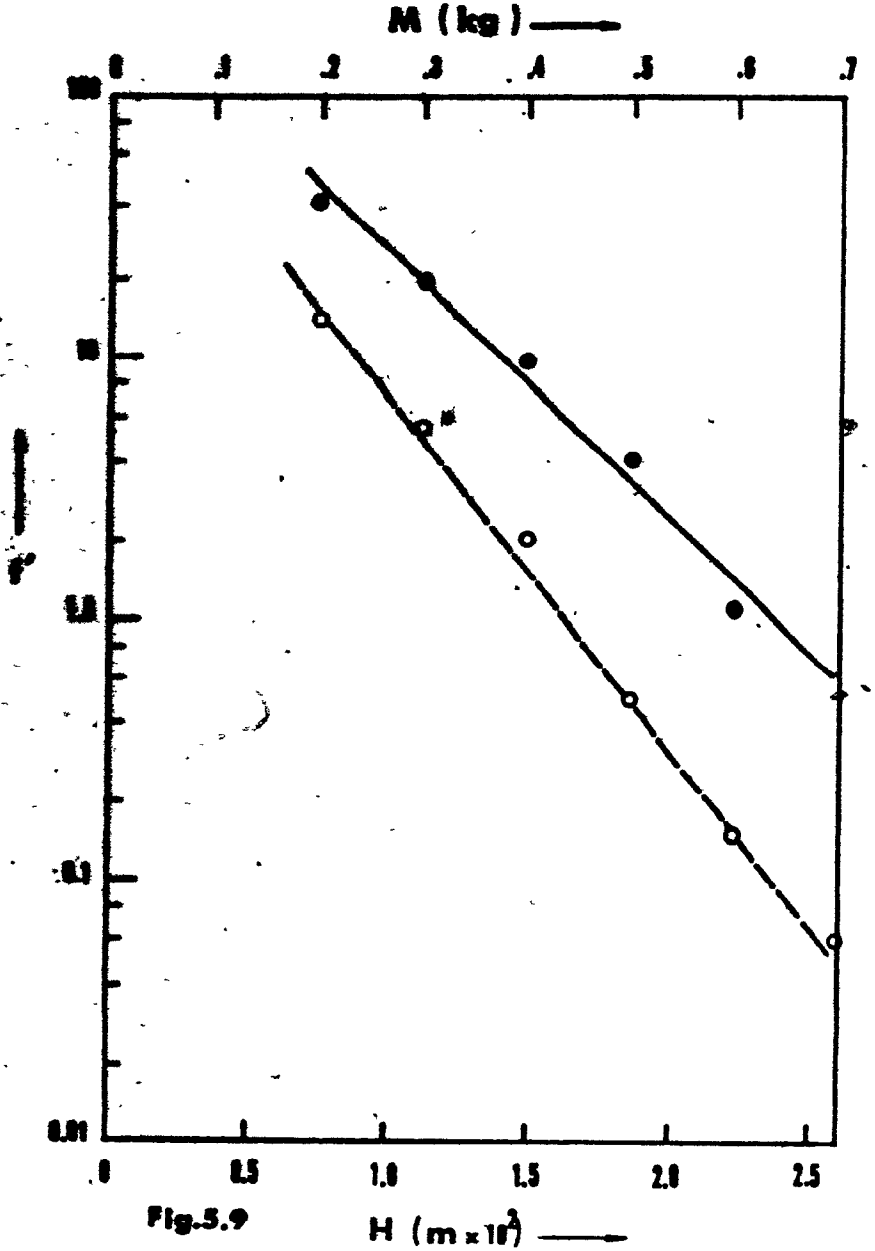

Fig.5.9

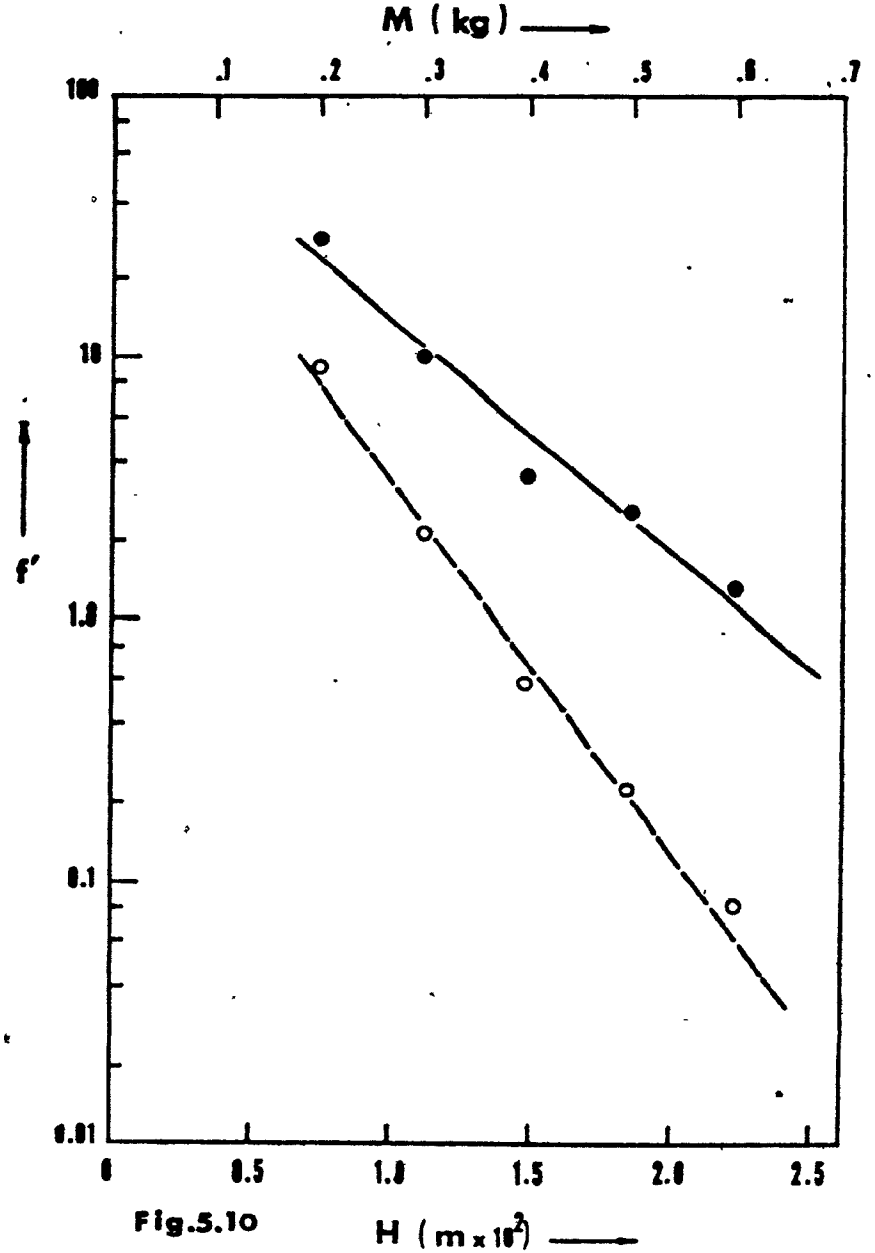

Fig.5.10

FIGURE 5.11 Fixed bed experiments - aerosol penetration vs bed depth

d_c = 110 μm
U^p = 0.0804 m/sec
open circles, d_A = 1.75 μm
full circles, d_A = 1.35 μm

FIGURE 5.12 Fixed bed experiments - aerosol penetration vs bed depth

d_c = 110 μm
U^p = 0.0869 m/sec
open circles, d_A = 1.75 μm
full circles, d_A = 1.35 μm

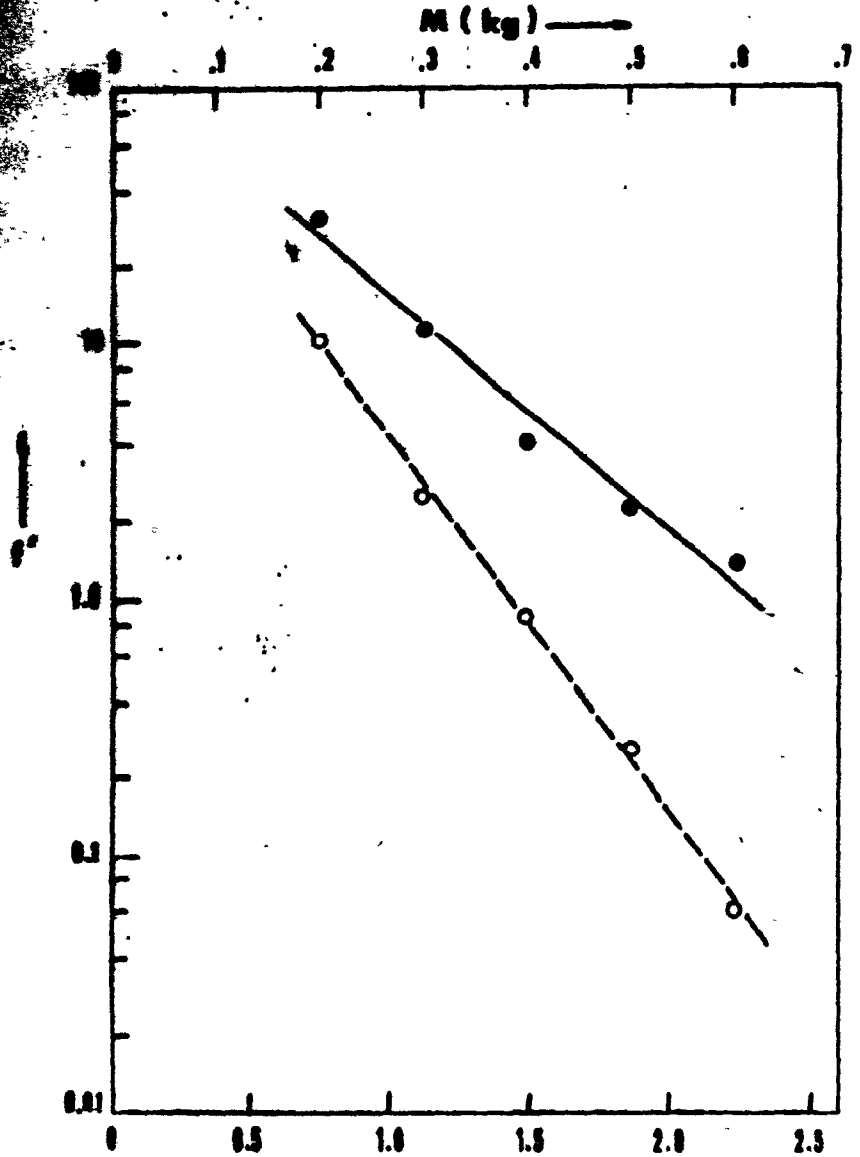

Fig.5.11

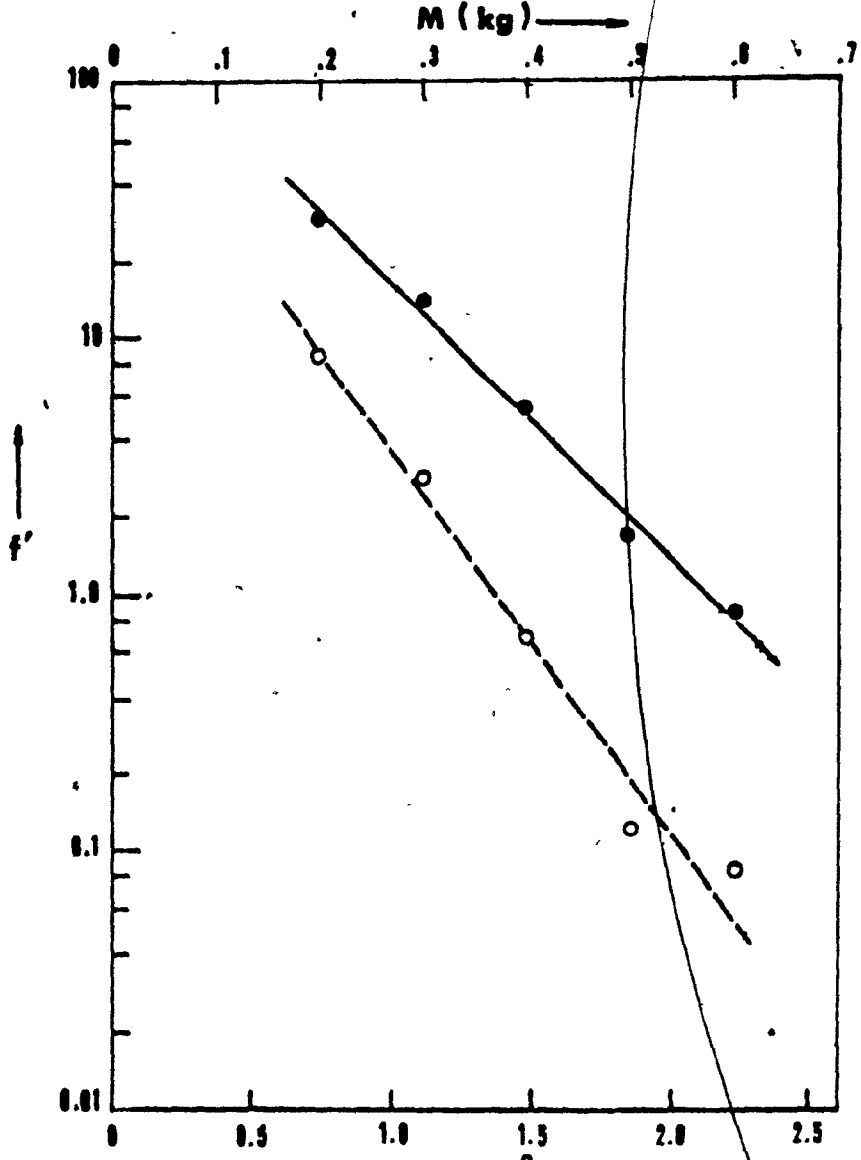

Fig.5.12

FIGURE 5.13 Fixed bed experiments - aerosol penetration vs bed depth

d_p = 110 μm
U^p = 0.1855 m/sec
open circles, d_A = 1.75 μm
full circles, d_A = 1.35 μm

FIGURE 5.14 Fixed bed experiments - aerosol penetration vs bed depth

d_p = 110 μm
U^p = 0.1237 m/sec
open circles, d_A = 1.75 μm
full circles, d_A = 1.35 μm

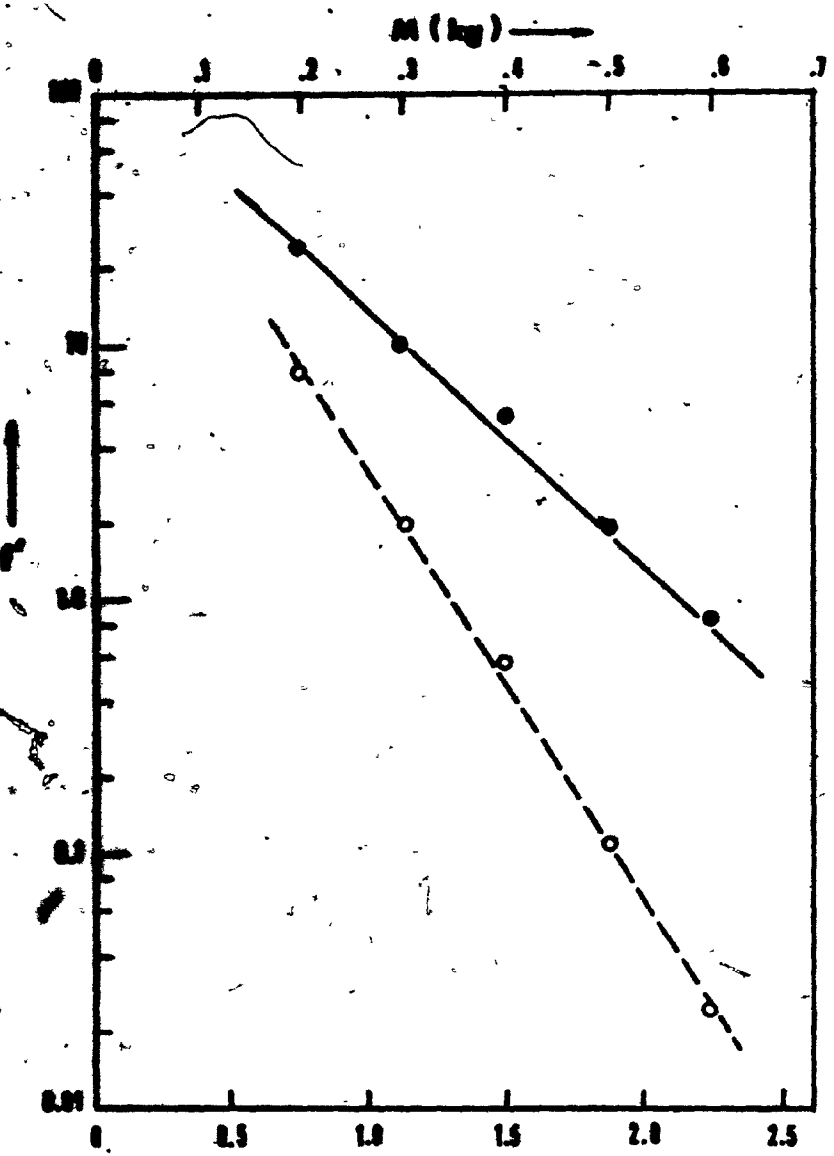

Fig.5.13

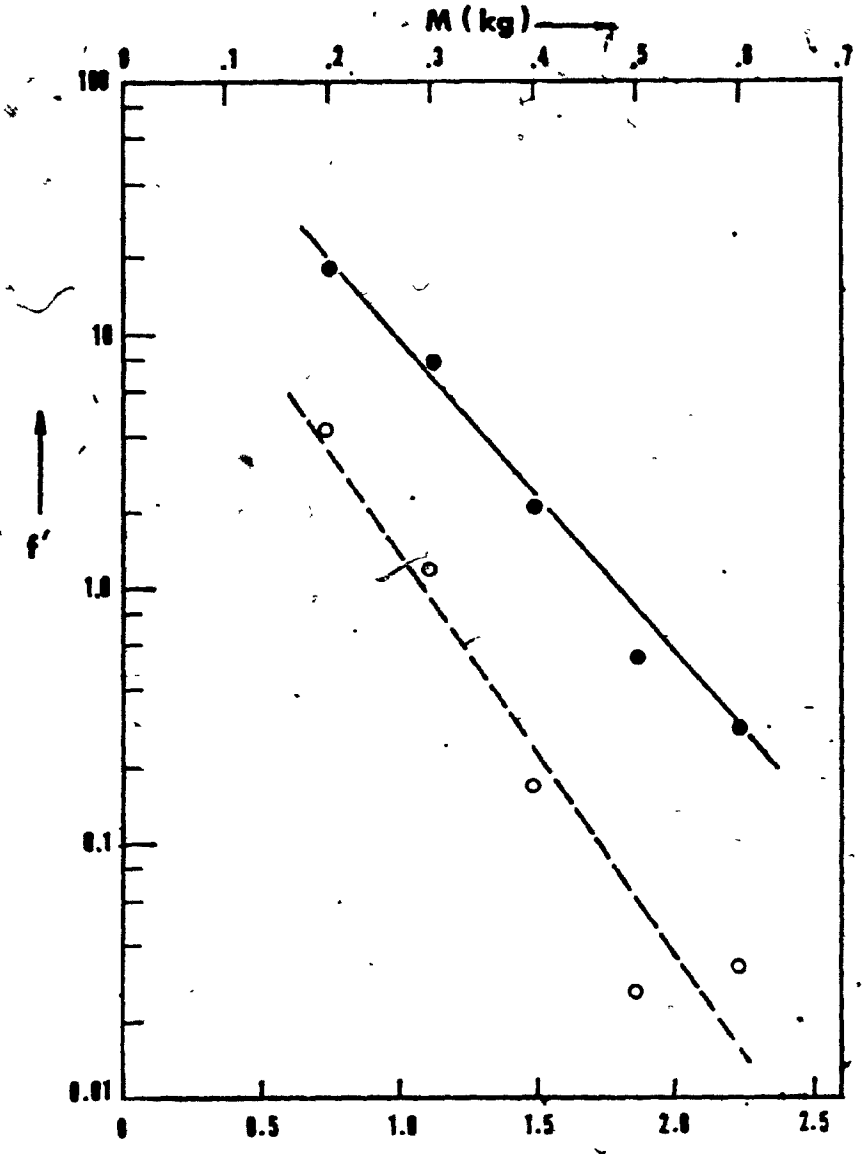

Fig.5.14

FIGURE 5.15 Fixed bed experiments - aerosol penetration vs bed depth

d_c = 110 μm
U^p = 0.1319 m/sec
open circles, d_A = 1.75 μm
full circles, d_A = 1.35 μm

FIGURE 5.16 Fixed bed experiments - aerosol penetration vs bed depth

d_c = 110 μm
U^p = 0.1953 m/sec
open circles, d_A = 1.75 μm
full circles, d_A = 1.35 μm

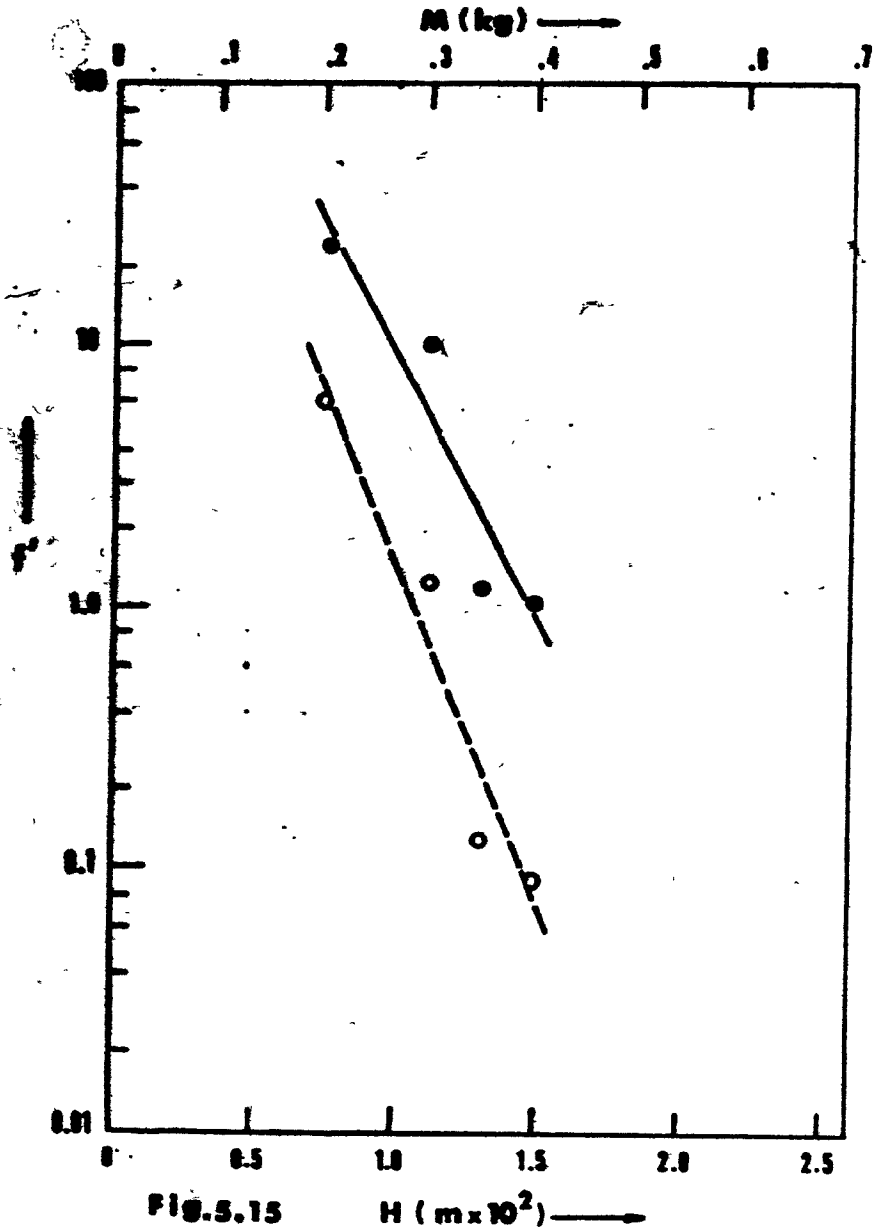

Fig.5.15

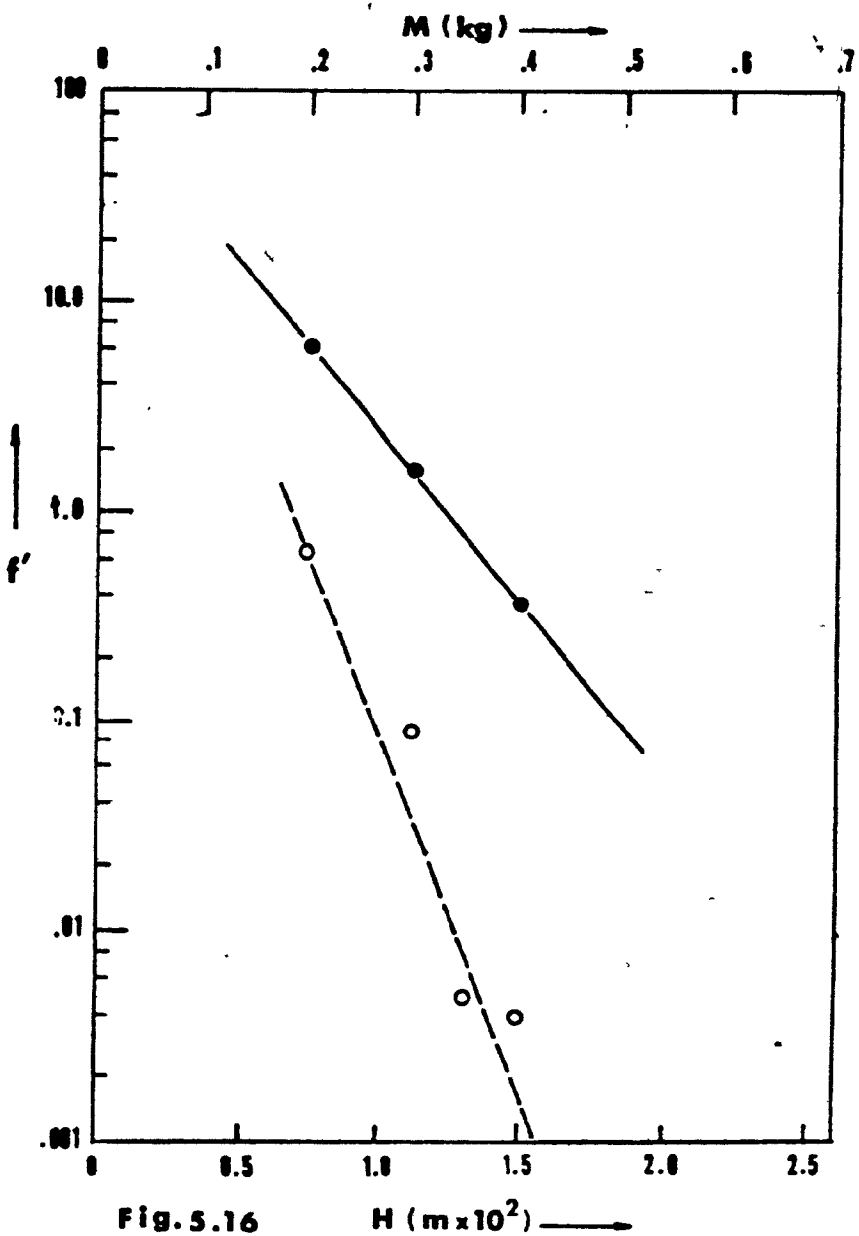

Fig. 5.16

FIGURE 5.17 Fixed bed experiments - aerosol penetration vs bed depth

d_p = 600 μm
U^p = 0.0286 m/sec
open circles, d_A = 1.75 μm
full circles, d_A = 1.35 μm

FIGURE 5.18 Fixed bed experiments - aerosol penetration vs bed depth

d_p = 600 μm
U^p = 0.0383 m/sec
open circles, d_A = 1.75 μm
full circles, d_A = 1.35 μm

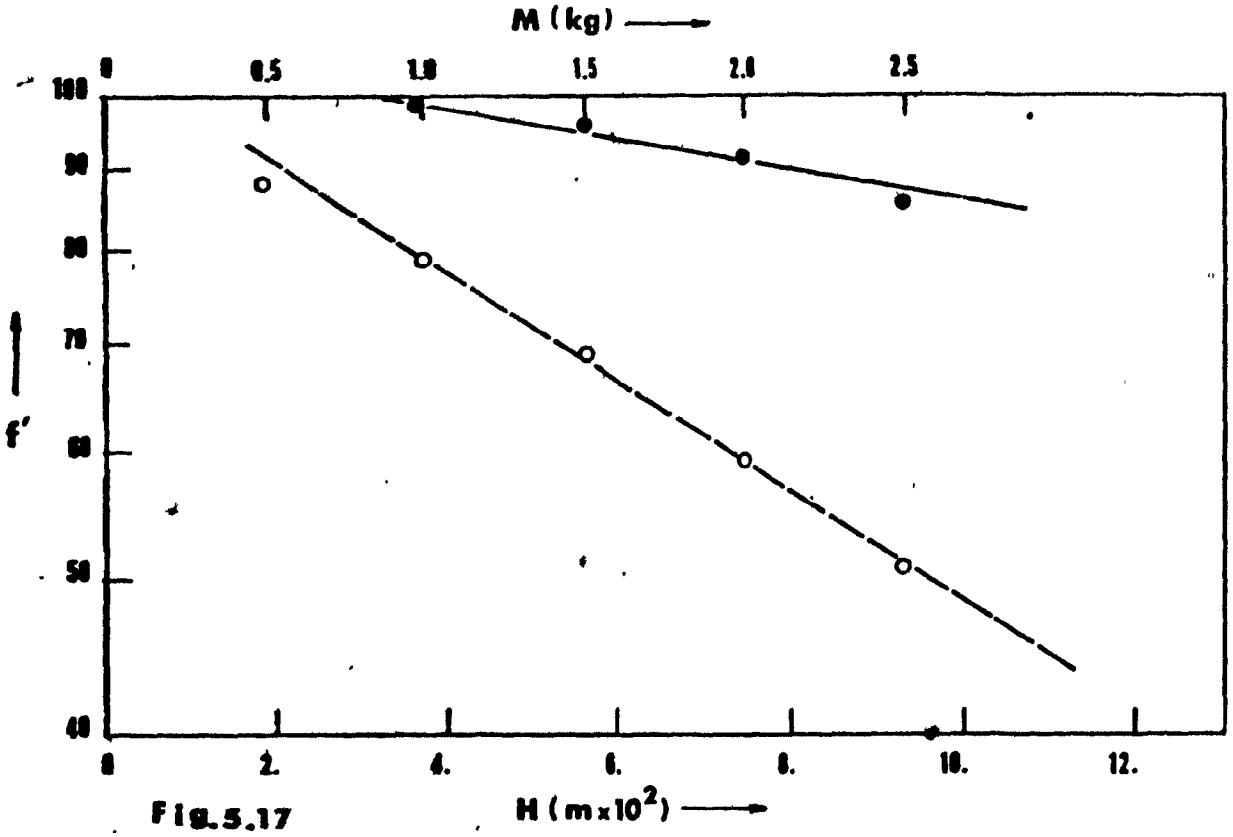

Fig.5.17

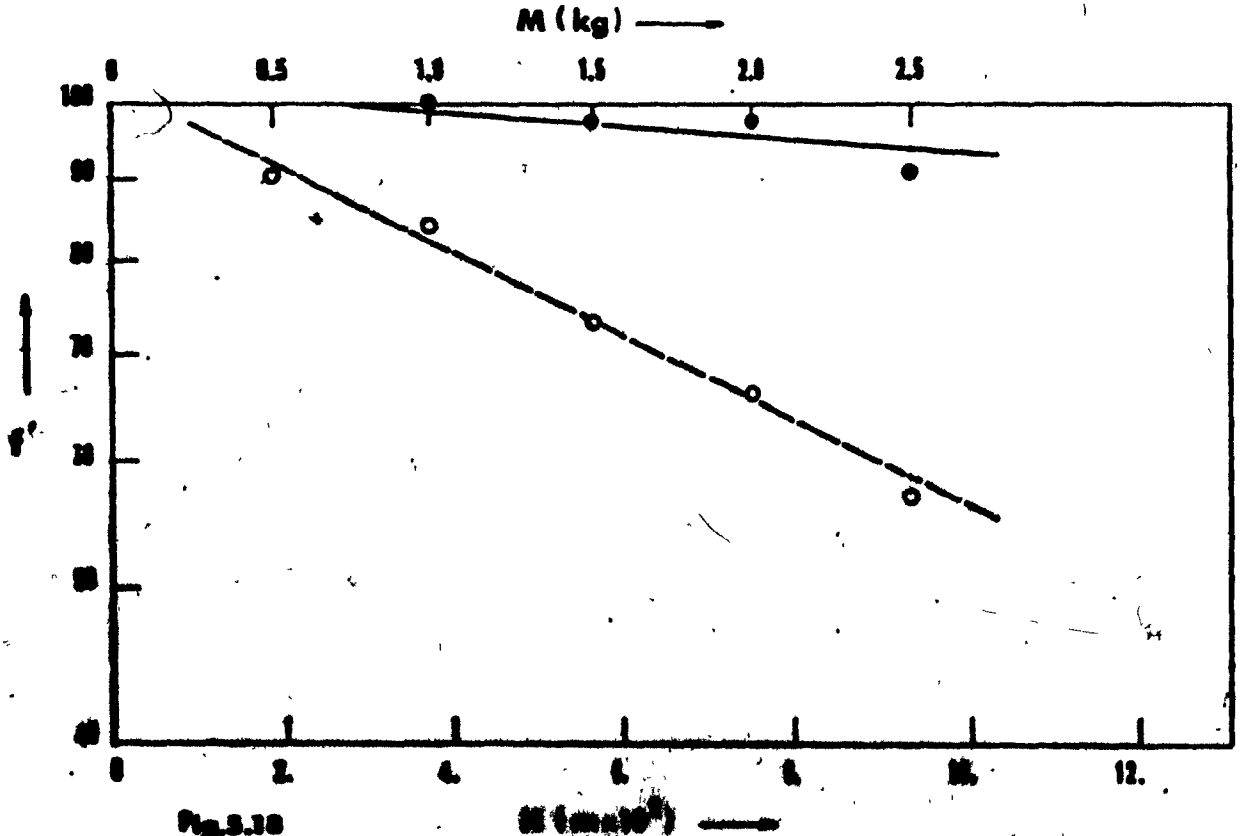

Fig.5.18

FIGURE 5.19 Fixed bed experiments - aerosol penetration vs bed depth

d_p = 600 μm
U^p = 0.0604 m/sec
open circles, d_A = 1.75 μm

FIGURE 5.20 Fixed bed experiments - aerosol penetration vs bed depth

d_p = 600 μm
U^p = 0.1237 m/sec
open circles, d_A = 1.75 μm
full circles, d_A = 1.35 μm

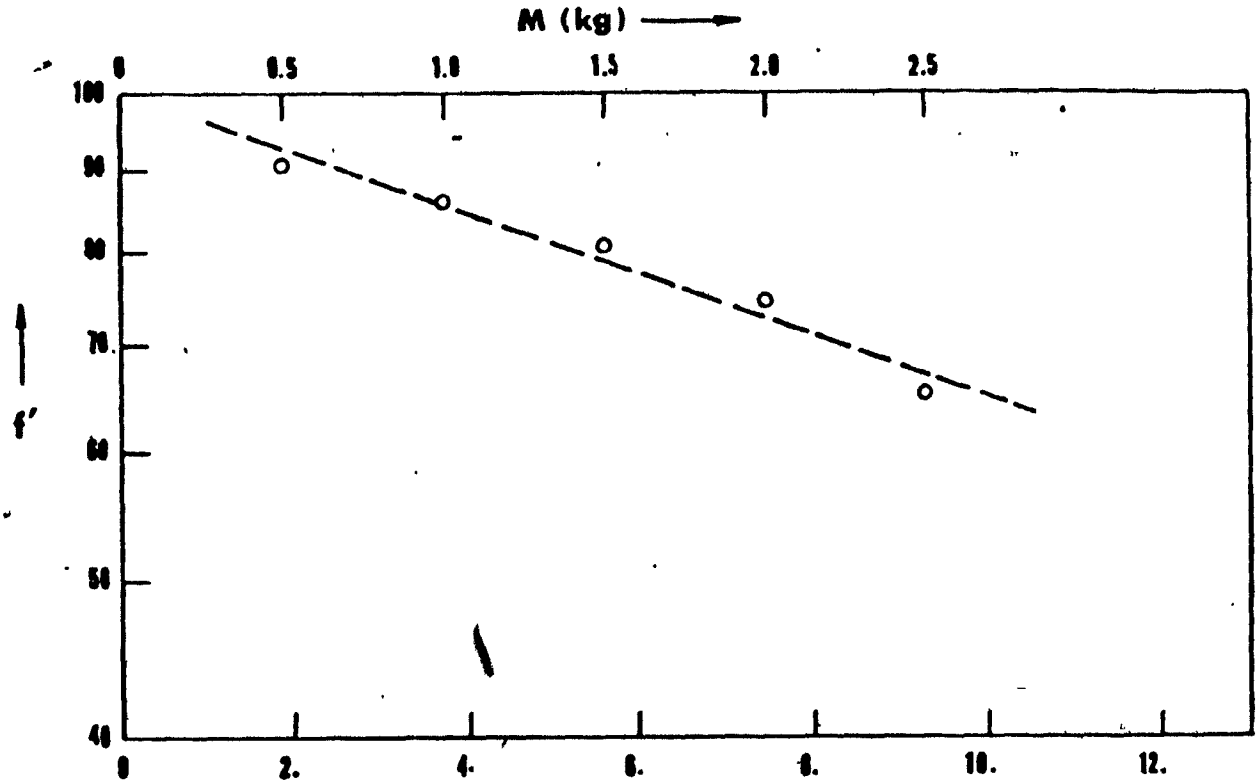
M (kg) ⟶
0
0.5
1.0
1.5
2.0
2.5
100
90
80
70
60
50
40
f'
0
2.
4.
6.
8.
10.
12.
H (m x 10²) ⟶

Fig.5.19

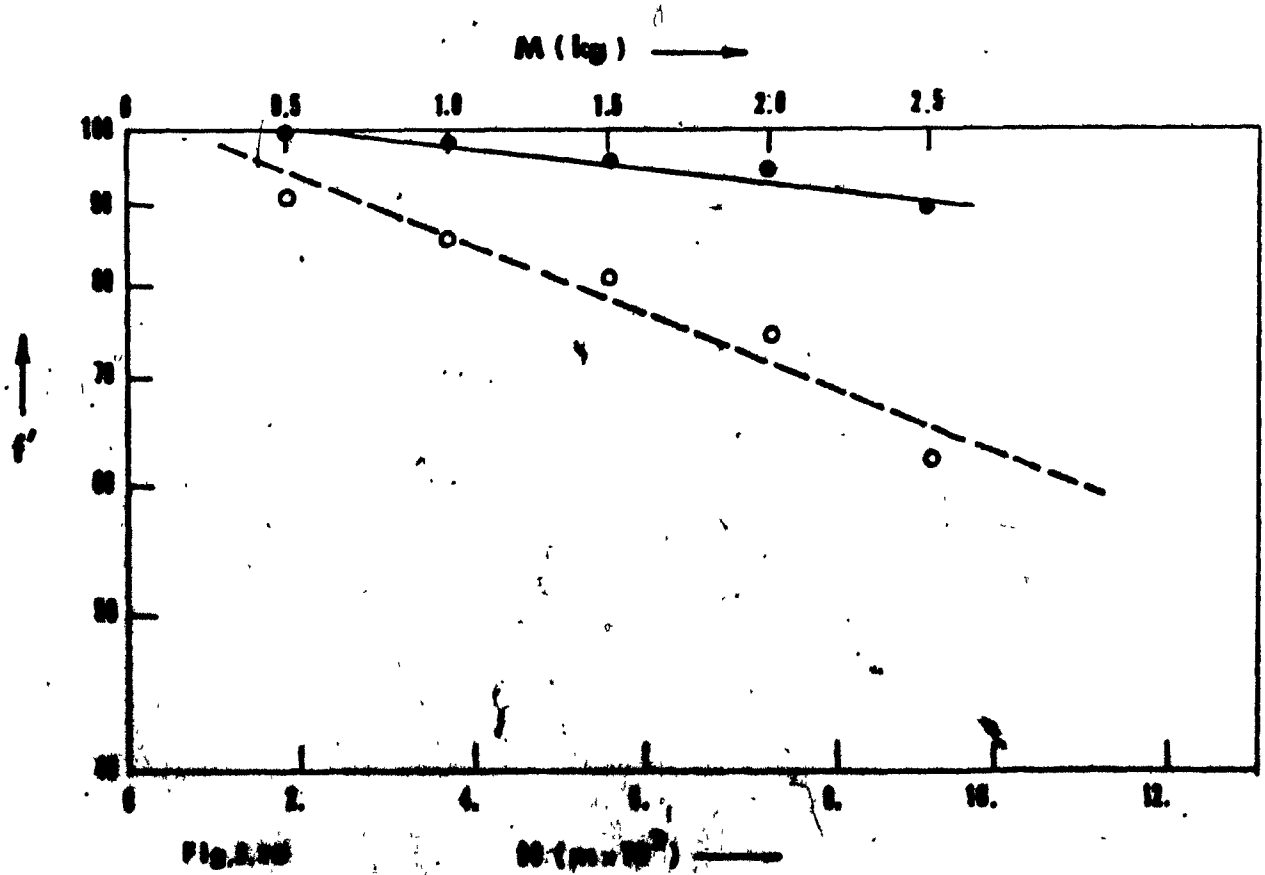
M (kg) ⟶
0
0.5
1.0
1.5
2.0
2.5
100
90
80
70
60
50
40
f'
0
2.
4.
6.
8.
10.
12.

FIGURE 5.21 Fixed bed experiments - aerosol penetration vs bed depth

d_p = 600 μm
U^p = 0.1951 m/sec
open circles, d_A = 1.75 μm
full circles, d_A = 1.35 μm

FIGURES 5.22 Fixed bed experiments - aerosol penetration vs bed depth

d_p = 600 μm
U^p = 0.3146 m/sec
open circles, d_A = 1.75 μm
full circles, d_A = 1.35 μm

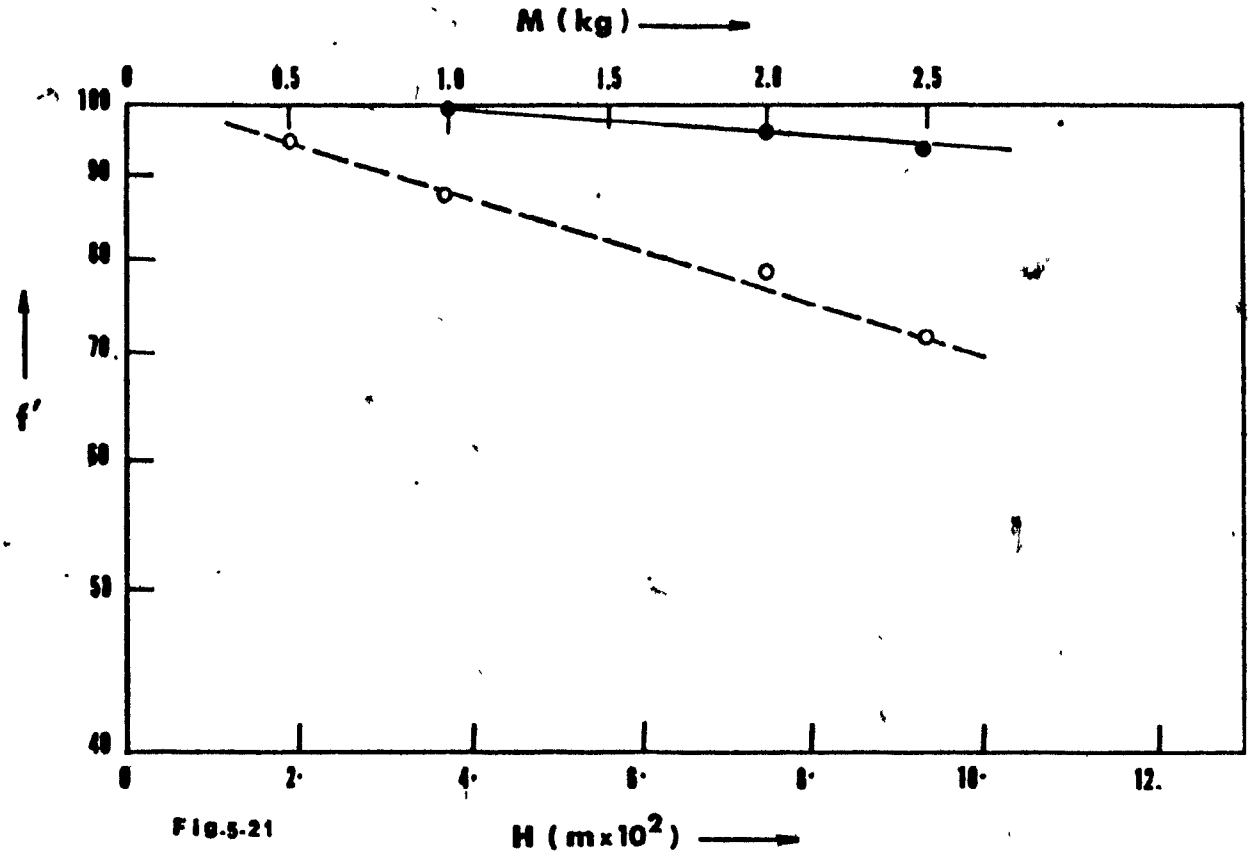

Fig.5-21

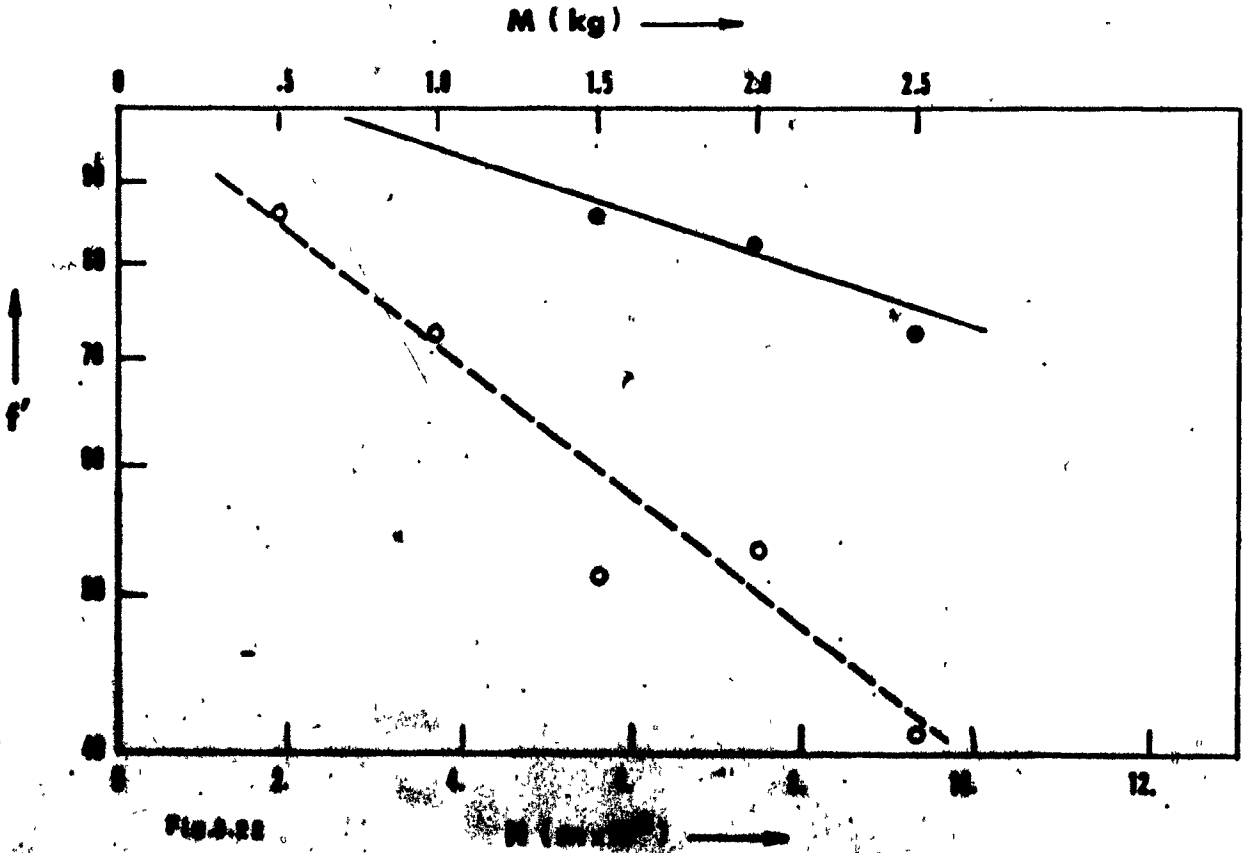

Fig.5-22

FIGURE 5.23 Fixed bed experiments - aerosol penetration vs bed depth

d_p = 600 μm
U^0 = 0.438 m/sec
open circles, d_A = 1.75 μm
full circles, d_A = 1.35 μm

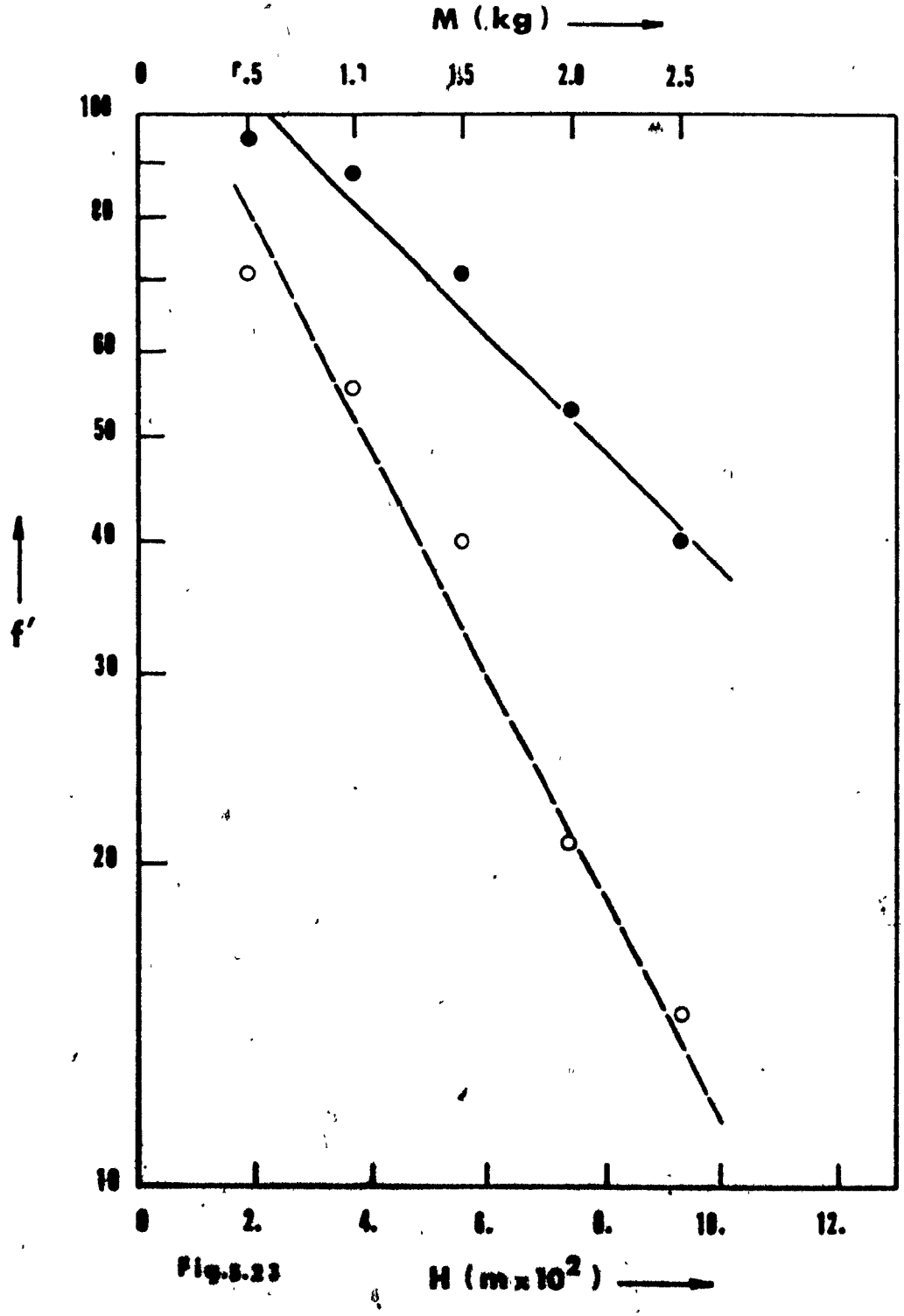

Fig.5.23

ln(f) vs M

the gradient over a straight section of the plot is, from Equation (5.13), equal to $(-K_M/A_B U)$. Thus the anomalous end effects of the bed can be eliminated and hence the collection coefficient of aerosol per unit mass and, using Equation (5.4), the total collection efficiency of a collector particle in a fixed bed can be calculated correctly.

5.4 Experimental Results

Fixed bed experiments with liquid dioctyl phthalate aerosols in the size ranges (1.0 - 1.2) μm, (1.2 - 1.5) μm, (1.5 - 2.0) μm were carried out at different superficial gas velocities and bed weights with glass collector particles of 109 μm and 599 μm surface to volume mean diameter. For convenience we refer to these particles as 110 μm collectors and 600 μm collectors, but all calculations were based on the surface to volume mean diameter which describes most realistically the surface area per unit volume of the bed.

Experimentally it was determined that total bed weights of 0.2 and 0.5 kg respectively were sufficient for the fixed bed end effects, discussed in the previous section, to be negligible in the 0.15 m diameter column used for this study. These weights correspond to bed heights approximately equal to 34 and 31 collector particle diameters respectively. Penetration of aerosol in the bed was measured at 4-6 bed heights at 0.1 kg weight increments for the 110 μm collectors for fixed aerosol diameters and superficial gas velocities. The penetration of aerosol through the 600 μm collector particles was measured at 5 different bed heights corresponding to 0.8 kg weight increments.

In order to eliminate bed loading effects each run was started with fresh collector particles regenerated by the method described in Section 4.3. Initial reproducibility problems were solved by the following method: after charging the collector particles to the column the bed was fluidized, with clean air, for a short period of time in order to obtain a "loose-packed" arrangement of the collector particles simulating the condition of the dense phase in a fluidized bed. The surface of the bed was subsequently smoothed by a piston-like device made of plexiglass. This procedure is illustrated in Figure 5.24 and proved to be effective in ensuring reproducibility between runs.

The results of fixed bed experiments are shown on Figures 5.5 to 5.23 where the per cent penetration of aerosol in the bed is plotted against the bed height H and bed mass M on semi-logarithmic axes. Straight lines were fitted through the experimental points by least-squares regression. The relatively low scatter in the data is evident.

Tables 5.1 to 5.4 present experiment collection efficiencies for the 110 μm and 600 μm diameter spherical collector particles in a fixed bed for 1.35 μm and 1.75 μm diameter DOP aerosol particles, calculated using Equations (5.13) and (5.4c). We believe that these are the most extensive and realistic data presented yet in the literature because of a number of precautions taken in this study. Firstly, liquid aerosols were used and the non-steady state behaviour of beds collecting solid aerosols, described in Section 5.2.2 was avoided. Secondly, the efficiencies were based on a number count and thus not biased to represent collection of the largest aerosol particles present. Thirdly, the extremely dilute test aerosol used (less than 10^8 particles/m^3) ensured

FIGURE 5.24 Device for ensuring reproducibility between runs in fixed bed experiments

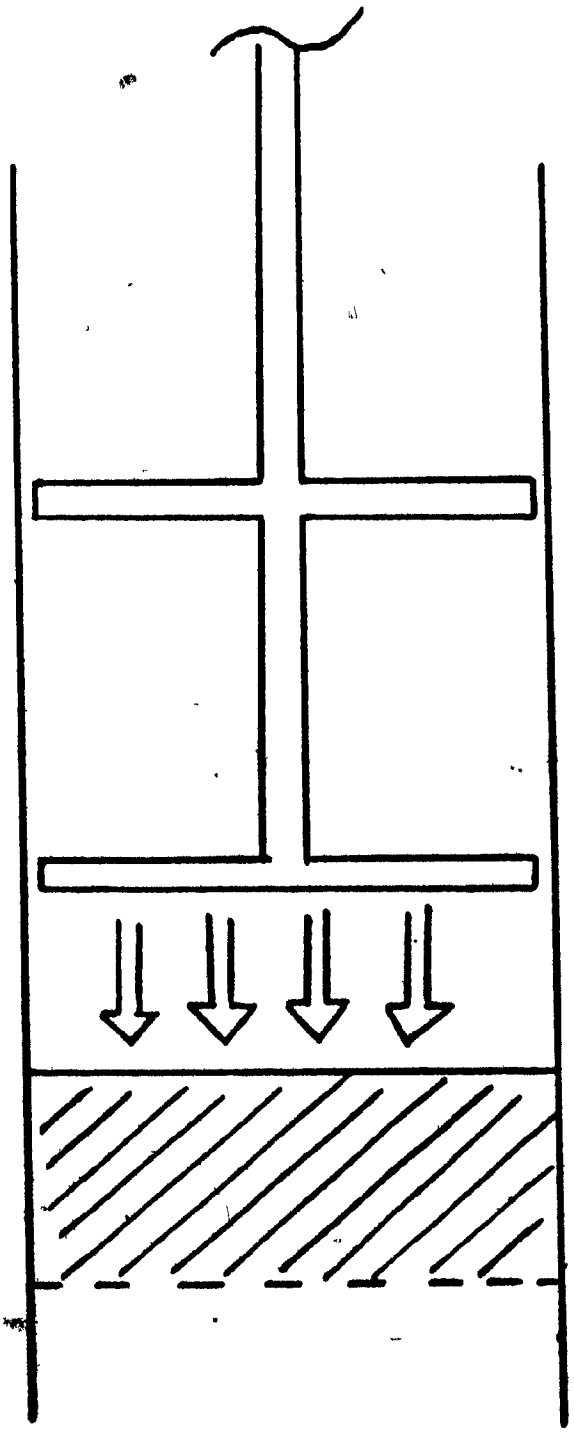

TABLE 5.1 Fixed Bed Experiments, d_A = 1.35 μm, d_p = 108.5 μm, D.O.P. Aerosol

$E_{BT} \times 10^2$	U m$\times 10^2$/s	$(Re)_p$	$N_R \times 10^2$	$N_R^2 \times 10^2$	$St \times 10^2$	$St^2 \times 10^4$	$U^{-2/3} D_A^{2/3} d_p^{-2/3} \times 10^2$	$U_{s/U} \times 10^2$
3.28	0.98	0.07	1.24	0.015	0.10	0.01	0.07	0.54
3.55	2.02	0.15	1.24	0.015	0.20	0.04	0.04	0.26
3.45	2.69	0.19	1.24	0.015	0.27	0.07	0.04	0.20
3.71	3.83	0.28	1.24	0.015	0.38	0.14	0.03	0.14
3.69	3.83	0.28	1.24	0.015	0.38	0.14	0.03	0.14
2.53	4.92	0.35	1.24	0.015	0.49	0.24	0.02	0.11
2.59	6.04	0.43	1.24	0.015	0.60	0.36	0.02	0.09
3.02	8.69	0.62	1.24	0.015	0.87	0.76	0.02	0.06
2.78	10.53	0.76	1.24	0.015	0.05	1.10	0.01	0.05
3.67	12.37	0.89	1.24	0.015	1.23	1.51	0.01	0.04
5.72	13.19	0.95	1.24	0.015	1.32	1.74	0.01	0.04
8.38	19.53	1.40	1.24	0.015	1.96	3.84	0.01	0.03

TABLE 5.2 Fixed Bed Experiments, $d_A = 1.75\,\mu m$, $d_p = 108.5\,\mu m$, D.O.P. Aerosol

$E_{BT} \times 10^2$	U $m \times 10^2/s$	$(Re)_p$	$N_R \times 10^2$	$N_R^2 \times 10^2$	$St \times 10^2$	$St^2 \times 10^4$	$U^{-2/3} D_A^{2/3} d_p^{-2/3} \times 10^2$	$U_s/U \times 10^2$
4.89	0.98	0.07	1.61	0.026	0.16	0.026	0.06	0.91
5.77	2.02	0.15	1.61	0.026	0.34	0.116	0.04	0.44
5.01	2.69	0.19	1.61	0.026	0.45	0.203	0.03	0.33
3.54	3.83	0.28	1.61	0.026	0.64	0.410	0.02	0.23
3.85	3.83	0.35	1.61	0.026	0.83	0.689	0.02	0.18
4.12	4.92	0.43	1.61	0.026	1.02	1.04	0.02	0.15
4.15	8.69	0.62	1.61	0.026	1.46	2.13	0.01	0.10
4.41	10.53	0.76	1.61	0.026	1.77	3.13	0.01	0.08
4.42	12.37	0.89	1.61	0.026	2.08	4.33	0.01	0.07
7.37	13.19	0.95	1.61	0.026	2.22	4.93	0.01	0.97
9.27	19.53	1.40	1.61	0.026	3.29	10.82	0.01	0.05

TABLE 5.3 Fixed Bed Experiments, d_A = 1.35 μm, d_p = 596 μm, D.O.P. Aerosol

$R_{ST}x10^5$	U $mx10^2/s$	$(Re)_p$	$N_a x10^3$	$N_R^2 x10^6$	$Stx10^3$	St^2x10^6	$U^{-2/3}D^{2/3}d_p^{-2/3}$ $x10^3$	$U_s/U x10^3$
1.24	2.86	1.13	2.25	5.06	0.52	0.27	0.11	1.86
0.72	3.83	1.52	2.25	5.06	0.69	0.48	0.09	1.39
0.10	12.57	4.90	2.25	5.06	2.24	5.02	0.04	0.43
0.06	19.51	7.74	2.25	5.06	3.54	12.53	0.03	0.27
2.05	31.46	12.47	2.25	5.06	5.70	32.50	0.02	0.17
0.11	43.80	17.36	2.25	5.06	7.94	63.04	0.02	0.12

TABLE 5.4 Fixed Bed Experiments, $d_A = 1.75 \mu m$, $d_p = 596 \mu m$, D.O.P. Aerosol

$E_{BT} \times 10^3$	U m$\times 10^2$/s	$(Re)_p$	$N_R \times 10^3$	$N_R^2 \times 10^6$	$St \times 10^3$	$St^2 \times 10^6$	$U^{-2/3} D_A^{2/3} d_p^{-2/3} \times 10^3$	$U_s/U \times 10^3$
5.15	2.86	1.13	2.92	8.53	0.87	0.76	0.09	3.12
4.17	3.83	1.52	2.92	8.53	1.17	1.37	0.08	2.33
2.97	6.04	2.39	2.92	8.53	1.84	3.39	0.06	1.48
3.32	12.37	4.90	2.92	8.53	3.77	14.21	0.04	0.72
2.40	19.51	7.74	2.92	8.53	5.94	35.28	0.03	0.46
6.32	31.46	12.47	2.92	8.53	9.58	91.78	0.02	0.28
15.11	43.80	17.36	2.92	8.53	10.33	106.7	0.01	0.20

that all secondary filtration mechanisms like the transient behaviour of bed as a result of loading, aerosol coagulation mechanisms and aerosol particle interference near the collector particle were eliminated. Finally, by performing experiments of penetration versus bed height and calculating the collector efficiency as described in Section 5.3, anomalous collection near the extremes of the fixed bed was eliminated. Thus, these efficiencies represent truly the collection mechanisms around a collector particle in a fixed bed.

Also shown in Tables 5.1 to 5.4 are the corresponding values of the following collection parameters: N_R, N_R^2, St, St^2, $U^{-2/3}D_A^{2/3}d_p^{-2/3}$, U_s/U, together with the superficial gas velocity through the bed and the collector particle Reynolds number based on superficial gas velocity. The theoretical collection parameters were calculated from equations presented in Chapter 3. In the following section, Tables 5.1 to 5.4 are analyzed to determine the dominant collection mechanisms in a fixed bed of spherical collector particles. The conclusions will be used in interpreting the fluidized bed results of Chapter 7.

5.5 Dominant Collection Mechanisms in a Fixed Bed

5.5.1 Introduction

In this section with the help of Tables 5.1 to 5.4, Figures 5.25 to 5.28 and the preliminary experiments described in Section 5.2.1 we will show that the diffusional and interception mechanisms are negligible in this study and that the dominant collection mechanisms are inertial deposition and gravitational settling. As it happens, these are exactly the opposite of the conclusions of McCarthy et al.[Mc1]

who, for almost identical operating conditions, claimed that the dominant collection mechanisms in a fixed or fluidized bed are interception and diffusion. The fundamental errors in their reasoning will be indicated in the course of the analysis.

5.5.2 Elimination of the interception collection parameter

One important aspect that needs clarifying is whether the interception mechanism, where the aerosol particle is intercepted as soon as it approaches the surface of the collector to a distance equal to its radius, is an important collection mechanism.

Interception is governed primarily by the parameter N_R, which is the ratio of aerosol to collector particle diameter (d_A/d_p). Inspection of Tables 5.1 and 5.2 shows that for 110 μm collector and aerosol particles of 1.35 μm and 1.75 μm diameter the experimental efficiency of the collector is of the order of N_R and could be expressed as N_R multiplied by a factor of 2 to 4. McCarthy et al. noted a similar effect, and claimed that interception must be an important collection mechanism for aerosol particles around 1 micron. Unfortunately, the situation is not as simple as this. Before any conclusions are reached we have to clarify whether the flow around the collector particles is in the creeping or potential flow regime. If creeping flow is assumed then the theoretical interception efficiency is given as

$$E_R \approx 3/2\ N_R^2 \qquad (3.18)$$

and is negligible. If potential flow is assumed then

$$E_R \simeq 3N_R \tag{3.20}$$

Thus in the potential flow régime interception increases by several orders of magnitude and may become an important collection mechanism.

Inspection of Tables 5.1 to 5.4 yields some useful information as to the relative importance of the various collection parameters in the ranges investigated in this study. As will be seen from these tables the ranges of experimental velocities covered correspond to ($0.07 < Re_p < 1.40$) for the 110 μm collector particles and ($1.1 < Re_p < 17.5$) for the 600 μm particles. As[B3] the creeping flow régime around spheres is approximated at $Re_p < 0.1$ and potential flow may be assumed only at high Re_p (theoretically $Re_p \to \infty$ for potential flow), we would expect, at the Reynolds numbers covered in this study, the flow around the collector particles to be more adequately approximated by the creeping flow equations. Paretsky[P1] ($6.5 < Re_p < 100$) assumed interception to be negligible. Meisen and Mathur[M3] also neglected interception but included a constant term in their correlation for E_{BT} as a function of St. Paretsky, in fact, based the equations of his theoretical cell model on the assumption of creeping flow. Both of the above studies presented successful empirical correlations which did not include interception for quite high Reynolds numbers. The above experimental evidence can be further supported by inspection of Tables 5.3 and 5.4 where it is seen that, for the 600 μm collectors, N_R is almost always larger than the measured experimental efficiency. If N_R is larger than E_{BT} for the

600 μm collectors then, for these particles the interception mechanism cannot be equal to multiples of N_R. Thus, we conclude that the flow around the 600 μm collectors is nearer to creeping than to potential régime; interception is proportional to N_R^2 and therefore negligible. If 600 μm particles are nearer to creeping flow than to potential flow ($1.1 < Re_p < 17.5$) then the 110 μm collectors must be even nearer to creeping flow ($0.07 \leq Re_p < 1.4$). Concurrently, if interception is represented by N_R^2 for 600 μm collectors then it must also be represented by N_R^2 for the 110 μm collectors which lie in a much lower Reynolds number range. We conclude then that interception is negligible for both collector particles of this study.

Inspection of Figures 5.25 and 5.26 where the experimental efficiencies of 110 μm collectors are plotted versus the superficial gas velocity shows that E_{BT} goes through a minimum at a velocity around 4 to 6×10^{-2} m/s. This minimum happens by chance to lie in a region where E_{BT} is of the order of N_R and McCarthy et al. were thus misled into concluding that, for $(0.15 < Re_p < 0.34)$, E_{BT} is proportional to N_R and thus to implicitly claim fully developed potential flow around the collectors for such low Reynolds numbers.

5.5.3 Elimination of the diffusional deposition parameter

Inspection of Tables 5.1 to 5.4 will show the diffusional collection parameter, $U^{-2/3} D_A^{2/3} d_p^{-2/3}$, to be at least one order of magnitude smaller than the gravitational parameter, U_s/U, at low velocities and much smaller than the Stokes number at higher velocities. There appears therefore to be no range of superficial gas velocity where

FIGURE 5.25 Individual collection efficiency of 110 μm collector versus superficial velocity (d_A = 1.35 μm)

——— = Model 2S
- - - - - - - - = Model 1S

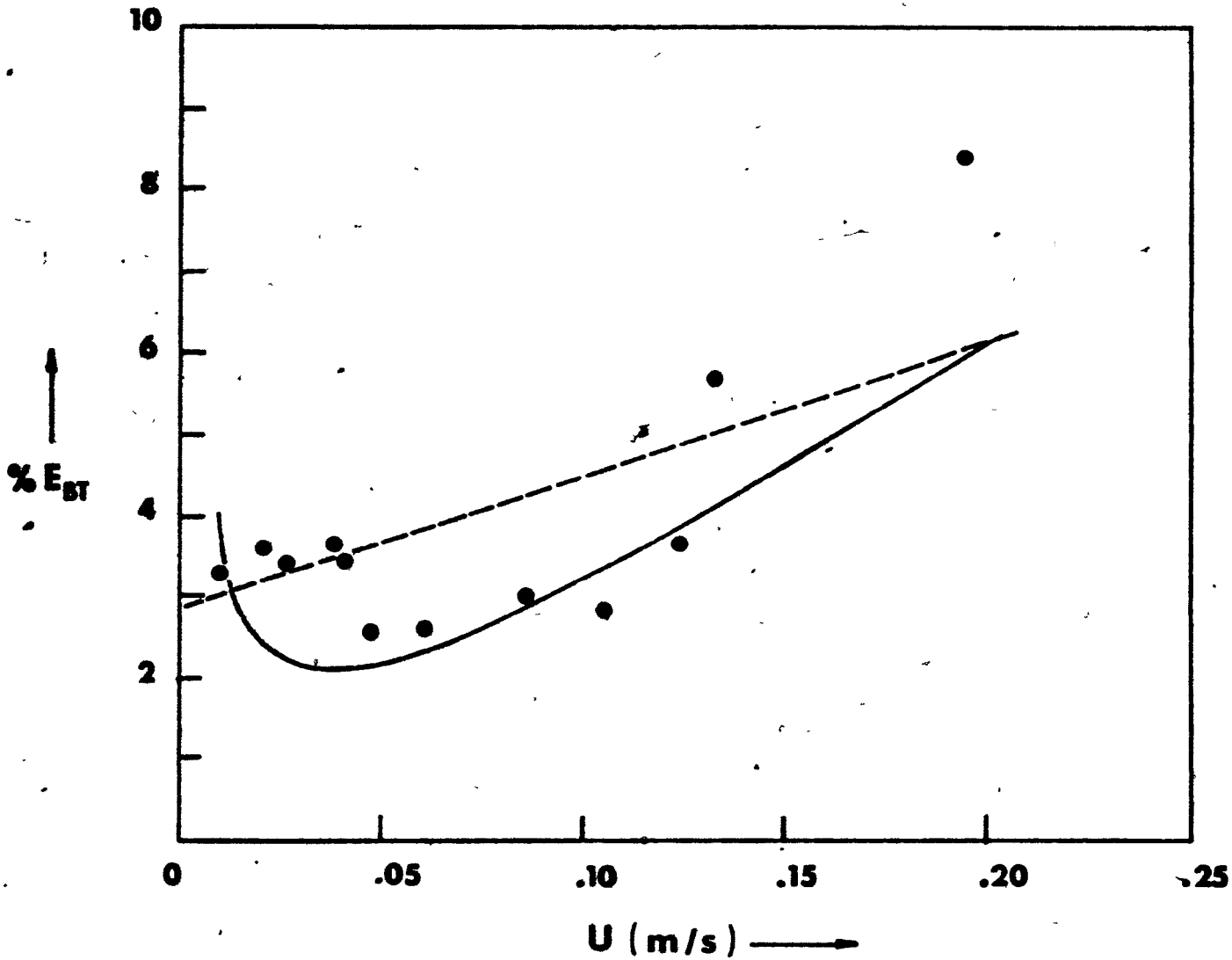
10
8
6
4
2
% E_{BT}
0
.05
.10
.15
.20
.25
U (m/s)

FIGURE 5.26 Individual collection efficiency of 110 μm collector versus superficial velocity (d_A = 1.75 μm)

_____ = Model 2S
- - - - - - - - = Model 1S

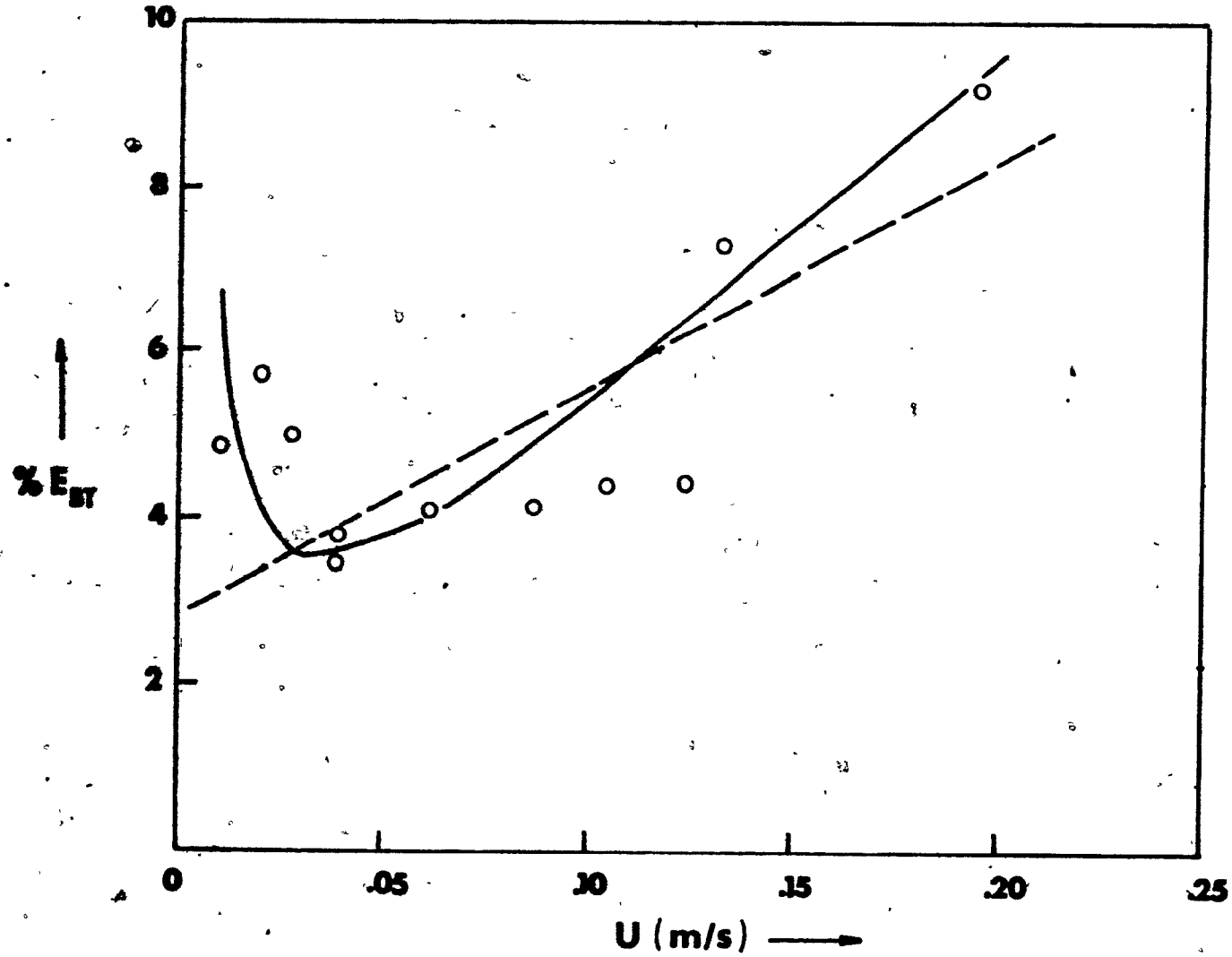
10
8
6
4
2
% E_{ST}
0
.05
.10
.15
.20
.25
U (m/s)

FIGURE 5.27 Individual collection efficiency of 600 μm collector versus superficial velocity (d_A = 1.35 μm)

_____ = Model 5B
- - - - - - - = Model 1B

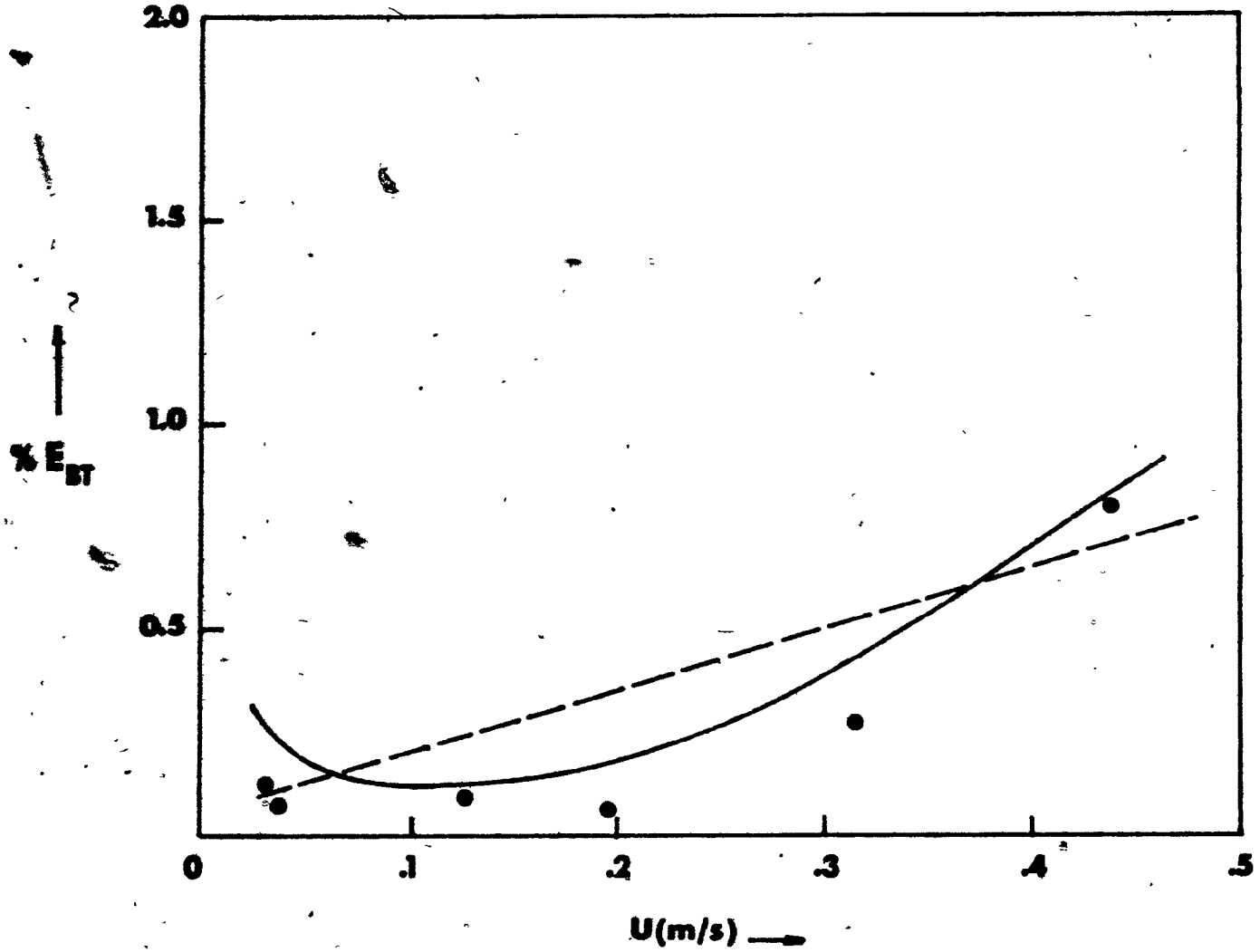
2.0
1.5
1.0
0.5
% E_{ET}
0
.1
.2
.3
.4
.5
U(m/s)

FIGURE 5.28 Individual collection efficiency of 600 μm collector versus superficial velocity (d_A = 1.75 μm)

_____ = Model 5B
--------- = Model 1B

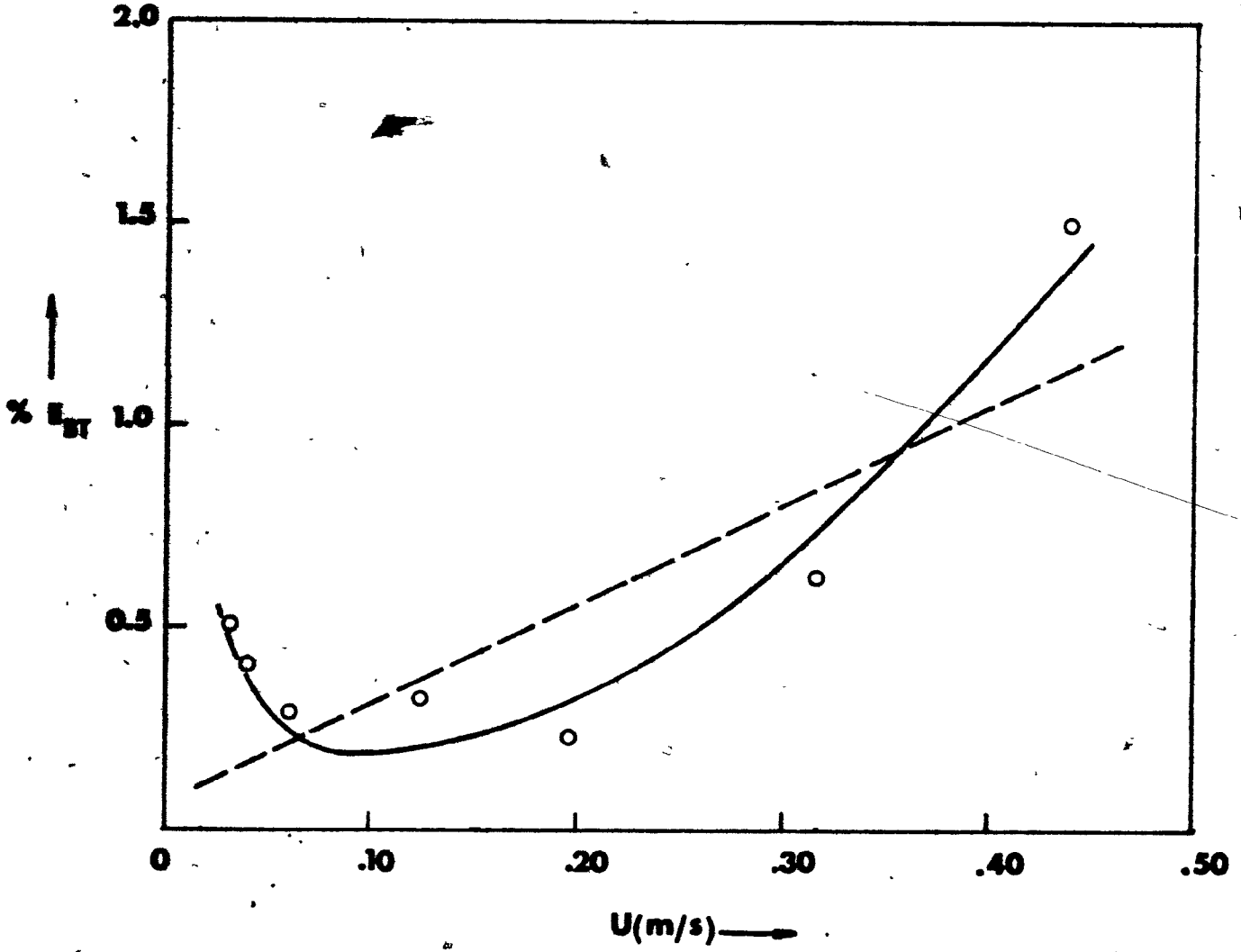
2.0
1.5
1.0
0.5
0
.10
.20
.30
.40
.50
% E_{ST}
U(m/s)

diffusional deposition could become important for aerosol particles around 1 μm in diameter. This confirms the qualitative conclusion indicated by the preliminary experiments of Section 5.2.1. The fact that gravitational and not diffusional deposition is dominant in the low velocity range is seen clearly from Tables 5.1 to 5.4 where the 1.75 μm aerosol has always a higher experimental collection efficiency than the 1.35 μm aerosol even in the range where inertial collection is negligible. This is a physical impossibility if diffusional deposition dominates over gravitational settling. Thus, by measuring E_{BT} as a function of d_A we are able to confirm experimentally the theoretical conclusion reached by inspection of the collection parameters of diffusion and gravitation. This, however, disagrees with the conclusions of at least two studies, McCarthy et al.[Mc1] and Knettig and Beeckmans[K4], who misinterpreted the effect of gravity as diffusion and claimed that diffusion was an important collection mechanism in fixed or fluidized beds operating at conditions similar to this study.

Knettig and Beeckmans drew their conclusion from experiments with fluidized beds and did not present any collection parameters so we can take their statement to reflect an erroneous interpretation of the process of fluidization.

McCarthy et al.[Mc1] however not only claimed that diffusion was important but also presented theoretical collection parameters of diffusion in order to support their theory. Their theoretical parameters for collection by diffusion for different aerosol diameters are presented in Table 5.6. In Section 5.5.2 we showed that the first column of this table, representing collection by interception, is based

TABLE 5.5 Erroneous Collection Parameters of McCarthy, Yankel, Patterson and Jackson ($d_p = 135 \mu m$, $U = 1.6 \times 10^{-2}$ m/s)

$d_A, \mu m$	$E_R \times 10^2$	$E_D \times 10^2$
1.4	3.12	0.88
1.0	2.22	1.07
0.67	1.56	1.34
0.37	0.81	1.94
0.28	0.63	2.34
0.13	0.30	4.12
0.06	0.12	7.95

on wrong assumptions. The numerical values of the second column, where theoretical efficiencies for diffusional deposition are presented, appeared at first sight to be extremely high. On investigating further, we found that McCarthy et al. used in their study an equation derived by Bosanquet[S7] from a very approximate analysis for an infinitely long isolated fibre in potential flow:

$$E_D - \sqrt{\frac{8}{Pe}} \qquad (5.13)$$

The applicability of this result to a spherical collector in a packed bed in creeping flow is, at best, questionable. Moreover, McCarthy et al. present no experimental data in support of their predictions.*

5.5.4 Conclusions

The elimination of interception and diffusion as possible contributing mechanisms in aerosol collection leaves inertial and gravitational deposition as dominant collection mechanisms. These two variables are investigated in the next section where different hypothetical models are tested by regression. It should perhaps be mentioned here that, as a check, interception and diffusion were initially included in the model. These two variables were always rejected as having very low significance levels, large standard errors and were sometimes assigned very large and/or negative coefficients (a physical impossibility) which

*The situation is further complicated by the facts that McCarthy et al. define D_A in the dimensions $L*T^{-1}$, and that it is impossible to back-calculate from their figures to obtain reasonable numerical values for D_A.

amounts to additional strong statistical evidence that diffusional and interception mechanisms may be safely neglected.

5.6 Analysis of Experimental Results

5.6.1 Introduction

The experimental results presented on fixed beds were analysed using multiple regression which is a statistical technique for analyzing a relationship between a dependent variable Y and a set of independent variables X_1, X_2.....X_m where m is the number of independent variables. The relationship is of the form.

$$Y = b_o + b_1X_1 + b_2X_2.....b_mX_m \qquad (5.14)$$

where the intercept of the regression equation, b_o, and the coefficients b_1, b_2.....b_m are estimated by the least squares method.

In our analysis the dependent variable is the experimental collection efficiency, E_{BT}, and the independent variables are the dimensionless collection parameters N_R, St, N_D and N_G. The assumption that the collection parameters are independent variables is tantamount to the assumption that individual collection efficiencies around the collector are independent of each other. In Section 3.2.5, it was noted that this assumption is not strictly true but is a reasonable approximation if individual collection efficiencies are all quite low and some are negligible. Furthermore, as the total collection efficiency, by definition, is the sum of the individual efficiencies then when all these efficiencies are zero the total collection efficiency must also

be zero. The intercept, b_o, from Equation 5.14 was therefore removed from the equation and the multiple regression line was forced to pass through the origin. Draper and Smith[D13] in "Statistical Analysis" comment: "The omission of b_o from a model implies that the response is zero when all the independent variables are zero. This is a very strong assumption which is usually unjustified." However, in the present case inclusion of b_o would lead to erroneous conclusions. As there is bound to be some experimental scatter in the data, the regression analysis will always manage to reduce the scatter by assigning a non-zero value to b_o which has no physical meaning; it mathematically represents the total collection efficiency when all contributing efficiencies are zero. In the present case, b_o would thus correspond to the contributions of diffusion and interception, which have already been shown to be negligible. In some of the models, as will be seen later, a constant term was included in the regression equation. This was done, however, in order to estimate coefficients for the type of equation suggested by Meisen and Mathur[M3] and Paretsky[P1] for inertial collection in fixed beds.

A summary of the basic theory of multiple regression analysis is presented in Appendix F and it is assumed here that the reader is familiar with the technique.

5.6.2 Statistical analysis of the aerosol collection models

The experimental collection efficiencies of the 110 μm and 600 μm collectors, presented in Tables 5.1 to 5.4 were tested by multiple regression analysis with five hypothetical collection models. The data

were divided into three sets. The first set contained only the data of 110 μm diameter collectors and is referred to as S (S for small collector particles). The second set contained only the data of 600 μm diameter collector particles and is referred to as B (B, big). The third set was simply the sum of the first two sets and is called Set SB.

Each set then was tested with five hypothetical models representing aerosol collection by a spherical collector in a fixed bed. So in all 15 cases were run and the five models tested were as follows:

Model 1 assumed that gravitational collection is negligible and may be removed from the equation describing the total efficiency of a collector particle in a fixed bed. This in fact has the form of the equation presented by Meisen and Mathur (Equation (3.12)) and is similar to the forms of the equations suggested by Paretsky for the velocity range where gravitational collection is negligible (Equations (3.9) and (3.10)).

$$E_{BT} = \alpha_I St + \alpha_o \tag{5.15}$$

However, Paretsky complicates his equation unnecessarily by raising the Stokes number to an empirical power which turns out to be very close to unity (9/8).

Model 2 is similar to the previous model but has, in addition, a gravitational settling term. Paretsky again complicated his model by including the gravitational collection parameter raised to an empirical power.

$$E_{BT} = \alpha_I St + \alpha_G N_G \tag{5.16}$$

Model 3 tested the hypothesis that the independent variable of inertial collection could be represented better by the Stokes number raised to the power of two and an intercept. This is a much simpler equation than the four parameter polynomial approximation fitted by Knettig and Beeckmans[K4] (Equation (3.13)).

$$E_{BT} = \alpha_I St^2 + \alpha_o \tag{5.17}$$

Model 4 is similar to Equation (5.16) with the modification of including the gravitational settling term in the collection equation, and removing the intercept.

$$E_{BT} = \alpha_I St^2 + \alpha_G N_G \tag{5.18}$$

Model 5 tested the hypothesis that the coefficient of the inertial parameter is not constant but a linear function of the collector particle Reynolds number based on superficial gas velocity. There is some indirect evidence for this in Paretsky's correlations for inertial collection (Equations (3.9) and (3.10)), where the coefficient of the inertial term increases with collector diameter, from 0.78 for 780 μm collectors to 2.5 for 1,700 μm collectors. The gravitational term was included in this model

$$E_{BT} = (\alpha_I Re_p) St + \alpha_G N_G \tag{5.19}$$

Table 5.6 presents the coefficients of the dominant collection parameters (inertial and gravitational), fitted by multiple regression, the square of the adjusted multiple correlation coefficient, R^2_{AD}, and the adjusted standard residual, S_{AD} (see Appendix F) for each of the fifteen cases described earlier. We now have fifteen different sets of coefficients and we refer to them with a number, specifying the number of model used and a letter specifying the data used by the regression. For example, Model 3B means the coefficients for Model 3 (Equation (5.17)) were estimated using Set B which contains the data for 600 μm collector particles.

Inspection of Table 5.6 and comparisons with previous attempts to correlate E_{BT} as a function of Stokes number yield some interesting conclusions. We make two comparisons:

First, we compare the coefficient of inertial collection of Model 1B (d_p = 600 μm) which, from Table 5.6, is given by the equation

$$E_{BT} = 0.81\ St + 5.7 \times 10^{-4} \qquad (5.20)$$

as 0.81 with Equation (3.10) which is suggested by Paretsky[P1] for aerosol removal in fixed beds of 775 μm collector.

$$E_I = 0.78\ St^{0.98} \qquad (3.10)$$

As seen above the two coefficients are almost identical.

TABLE 5.6 Summary of Multiple Regression Analysis of Fixed Bed Experiments

d_p	Model	Fitted Regression Coefficients				Statistical Analysis	
		St	St^2	N_G	$\alpha_o x10^2$	R^2_{AD}	$S_{AD} x10^2$
	1S	1.48	-	-	3.29	0.31	1.6
	2S	2.89	-	6.89	-	0.94	1.3
110 μm	3S	-	51.3	-	3.95	0.35	1.6
	4S	-	111.0	9.02	-	0.85	2.0
	5S	2.53 Re	-	9.27	-	0.90	1.7
	1B	0.81	-	-	$5.7x10^{-2}$	0.62	0.25
	2B	0.834	-	0.97	-	0.86	0.25
600 μm	3B	-	69.4	-	0.18	0.79	0.18
	4B	-	82.7	1.42	-	0.94	0.14
	5B	.0583 Re	-	1.42	-	0.96	0.12
	1SB	2.26	-	-	1.52	0.36	2.1
110 μm	2SB	2.69	-	6.60	-	0.89	1.4
+	3SB	-	76.3	-	2.5	0.33	2.1
600 μm	4SB	-	112	8.49	-	0.84	1.7
	5SB	0.151 Re	-	9.80	-	0.50	3.0

Now if we compare Paretsky's correlation for $d_p = 1{,}700\ \mu m$ with Meisen and Mathur's [M3] correlation which is suggested for $d_p = 1{,}500\ \mu m$ we see that the two coefficients are again almost identical. In fact, Paretsky suggests

$$E_I = 2.5\ St^{1.13} \tag{3.9}$$

and Meisen and Mathur claim*

$$E_{BT} = 2.6\ St + 7.5 \times 10^{-4} \tag{3.12}$$

The above two comparisons show that linear approximations of this sort are quite reproducible for collector diameters of the same size range. This strongly suggests that the form of Equation (3.14), where an undefined function of Reynolds number is included in the inertial term, is realistic and the coefficient of inertial collection is not constant but varies with Re_p. Model 5B, for 600 μm collectors indicates the same conclusion

$$E_{BT} = 5.83 \times 10^{-2} Re_p St + 1.42\ N_G \tag{5.21}$$

This correlation has the highest R^2_{AD} (0.96) and the lowest adjusted standard residual ($S_{AD} \times 10^2 = 0.12$) of its group. This is not the case for 110 μm collectors and Model 2S gives the best equation for aerosol

---

*Corrected as noted in Chapter 3.

removal in that collector size range as

$$E_{BT} = 2.89\ St + 6.89\ N_G \qquad (5.22)$$

which has the highest R^2_{AD} and lowest S_{AD} in its group explaining 94% of the variation in experimental data.

A substantial improvement is therefore noted in the value of R^2_{AD} and S_{AD} for the experiments with 600 μm collectors when it is assumed, as in Model 5B, that the coefficient of the inertial term is not constant but increases linearly with the collector particle Reynolds number. This agrees, in principle, with the conclusions of most previous studies on inertial collection by isolated spheres (for example Davies[D5] Chen[C3], Blasewitz and Judson[B5]) who claim that the inertial collection parameter should be a function of Reynolds number as well as Stokes number especially at intermediate Reynolds number. In the range of Re_p of these particles ($1.1 < Re_p < 17.4$) the flow field is in the intermediate régime for which reliable theoretical velocity distributions are not yet available. An increase in velocity, which of course reflects an increase in Re_p, affects the velocity distribution of the gas flowing around the collector. The perturbing effect of the collector particle is reduced to a smaller region close to the collector and this more abrupt spreading of the streamlines at a higher Reynolds number enhances the influence of particle inertia and therefore causes a higher collection efficiency. The 110 μm collector particles lie in a range of Re_p much closer to the creeping flow régime where theoretically the velocity field is governed entirely by viscous forces and thus collection efficiency is

insensitive to variations in the velocity of the fluid passing around the collector. By the same reasoning at high Reynolds number the velocity profile in the vicinity of each particle will be much less sensitive to Re_p, and the collection efficiency will be again insensitive to Reynolds number.

Another interesting point to note is that including the inertial term as St^2 in the equation does not lead to any improvement in the predictions of the model and, in fact, leads to a much poorer performance for the 110 μm collectors (Model 4S). A useful conclusion drawn from this is that in most of the range of previous work on aerosol removal in fluidized beds (100 μm < d_p < 600 μm) inertial collection can be approximated successfully by assuming a linear dependence of collector efficiency on Stokes number. Figures 5.25 to 5.28 show the experimental particle collection efficiencies of 1.35 μm and 1.75 μm aerosols by 110 μm and 600 μm diameter collectors as functions of superficial gas velocity. As observed from these figures E_{BT} goes through a minimum at approximately 5×10^{-2} m/s for 110 μm collectors and 10^{-1} m/s for 600 μm collectors. Model 1 will not predict this minimum and will therefore have a low R^2_{AD} value. Therefore inclusion of the gravity term markedly improves the fit of the efficiency equation, especially at low superficial gas velocities. This of course is reflected by a marked increase in R^2_{AD} and a corresponding reduction in the value of the adjusted standard residual, S_{AD}. Equations (5.21) and (5.22) which are the best fits for the 110 μm and 600 μm collector particle efficiencies

respectively are plotted in Figures 5.26 to 5.29 and compared with the Meisen and Mathur type correlation. As can be seen from these figures the correlations of this study are far superior predicting quite accurately in each set of experiments the minimum in E_{BT} where the effect of inertial and gravitational collection is weakest.

5.7 Summary

In this chapter we reported preliminary experiments on the transient behaviour of a fixed bed collecting solid aerosol particles and on the general collection behaviour of a fixed bed. We also presented the results of extensive experiments performed on the collection of 1.1 μm, 1.35 μm, 1.75 μm and 2.5 μm liquid DOP aerosol particles by fixed beds of 110 μm and 600 μm diameter collector particles. End effects on the bed-air and bed-support plate interface were analysed and we determined experimental collection efficiencies by performing experiments at different bed heights and thus eliminating these end effects. The dominant collection mechanisms in this study were shown to be inertial deposition and gravitational settling. Interception efficiency was eliminated because of the low range of Re_p and diffusional deposition was shown to be negligible when compared to the gravitational settling parameter. Experimental results justified the elimination of these two mechanisms. The experimental collection efficiencies were analysed by multiple regression and five hypothetical models were tested.

It was found that aerosol collection by the two sizes of particles could not be correlated by one equation as they lay in different flow regimes. The 110 μm collectors ($0.07 < Re_p < 1.4$) were in the creeping

flow regime and collection was insensitive to Reynolds number. Aerosol collection by the 110 μm collectors was best represented by the following equation

$$E_{BT} = 2.89\ St + 6.89\ N_G \qquad (5.22)$$

which accounted for 94% of the variations in the experiments.

Collection by the 600 μm collectors which lay in a higher Re_p range was found to be affected by the particle Reynolds number. The efficiency of these particles was best described by the following equation

$$E_{BT} = 5.83 \times 10^{-2} Re_p St + 1.42\ N_G \qquad (5.21)$$

which explained 97% of the variation in experimental data. It is thus seen that Equations (5.22) and (5.21) describe almost perfectly collection of aerosols by 110 μm and 600 μm collector and are therefore suggested as useful design equations.

CHAPTER 6. FLUIDIZED BED EXPERIMENTS

6.1 Introduction

This chapter presents experimental results for aerosol removal in a 0.15 m diameter fluidized bed composed of spherical collector particles. The equipment used for the generation and monitoring of the aerosols, a typical experimental run, and other experimental details are described in Chapter 4. The experiments presented here analysed the effect of superficial gas velocity through the bed, bed height at minimum fluidization, distributor effects, bed loading, diameter and physical state of aerosols, collector particle diameter and density, and removal of aerosols at high superficial gas velocities. The results are discussed qualitatively and compared with the conclusions of the most recent previous studies. This was found to be necessary in order to dispell the misleading belief which seems to have grown up that aerosol penetration in a fluidized bed increases with increasing gas velocity[Mc1,J2], and that the bed is a homogeneous contactor in plug flow.[K3] Chapter 7 presents a mathematical analysis of the process and calculates collection coefficients which are based on the experimental results of this study and on the two phase theory of fluidization. To the best of our knowledge the experiments described in this chapter are the most accurate presented yet in the literature, for the following reasons:

(i). The efficiencies were based on a number count and thus not biased to represent collection of the largest particles present.

(ii) The extremely dilute test aerosol used (less than 10^8 particles/m^3) ensured that all secondary filtration mechanisms, like aerosol coagulation and aerosol particle interference near the collector particles, were eliminated.

(iii) The distributors used were designed to ensure a good distribution of the incoming gas. Adequate distribution of the gas was confirmed by visual observation of the bubbles and the pressure drop across the distributor was measured, as a design precaution, as a function of superficial gas velocity (Figure 4.7). The distributor orifices were drilled as a regular array on triangular pitch, and were designed for minimal collection.

(iv) Blank tests at experimental velocities without the bed in place eliminated any errors due to collection by the distributor plate, fluidized bed column and sampling system, and any minor distortions introduced in the sample (Figure 4.13) as a result of non-isokinetic sampling.

(v) The experiments were performed with closely sized collector, the diameter of which was accurately determined by measuring 300 particles of each of the three batches used under an optical microscope. The almost clinical treatment of the collectors (Section 4.3) before each run and blank tests with aerosol-free filtered air ensured that the "background" concentration of the bed due to sterilism and contamination of the collectors by extraneous dust was negligible.

The experiments presented in this chapter encompass a far wider spectrum of gas velocity than previous studies, reaching a superficial gas velocity of 2.85 m/s in the extreme case.

6.2 Experiments on Basic Parameters of Aerosol Removal

6.2.1 Effect of superficial gas velocity

6.2.1.1 Penetration close to minimum fluidization

Perhaps the most misunderstood parameter of aerosol collection in a fluidized bed has been the superficial gas velocity. Discarding experiments with 5×10^{-2} m diameter beds which were probably operating in a slugging régime, previous studies have barely gone beyond 3-4 times the minimum fluidization velocity.

As an example of how the effect of superficial gas velocity on penetration has been misinterpreted in the past, the results of a recent publication (November 1974) by McCarthy et al.[Mc1] are presented in Figure 6.1. Their study, described in more detail in Chapter 2, investigated the removal of dioctyl phthalate aerosols (DOP) in a 0.15 m fluidized bed of 135 μm diameter alumina granules. On Figure 6.1 the per cent penetration of the challenging aerosol, f', is plotted versus the superficial gas velocity through the bed, U, divided by the minimum fluidization velocity, U_{mf}, for two aerosol sizes (d_A = 1.0 and 0.67 μm). They carried out experiments from 1.1 to 2.5 U/U_{mf}, which falls in a narrow velocity range of 1.7 to 3.9×10^{-2} m/s, and concluded that aerosol penetration increased considerably with increasing superficial gas velocity. McCarthy et al. then extrapolated from their experimental results and argued that the trend of increasing penetration will continue,

FIGURE 6.1 Aerosol penetration versus (U/U_{mf})

McCarthy et al.[M4]

open circle, $d_A = 1.0$ μm
open square, $d_A = 0.67$ μm
$d_p = 135$ μm
$H^p_{mf} = 2.5 \times 10^{-2}$
$U_{mf} = 1.56 \times 10^{-2}$ m/sec
alumina granules

this study

full circle, $d_A = 0.82$ μm
$d_p = 108.5$ μm
$H^p_{mf} = 2.8 \times 10^{-2}$
$U_{mf} = 2.0 \times 10^{-2}$ m/sec
glass microspheres

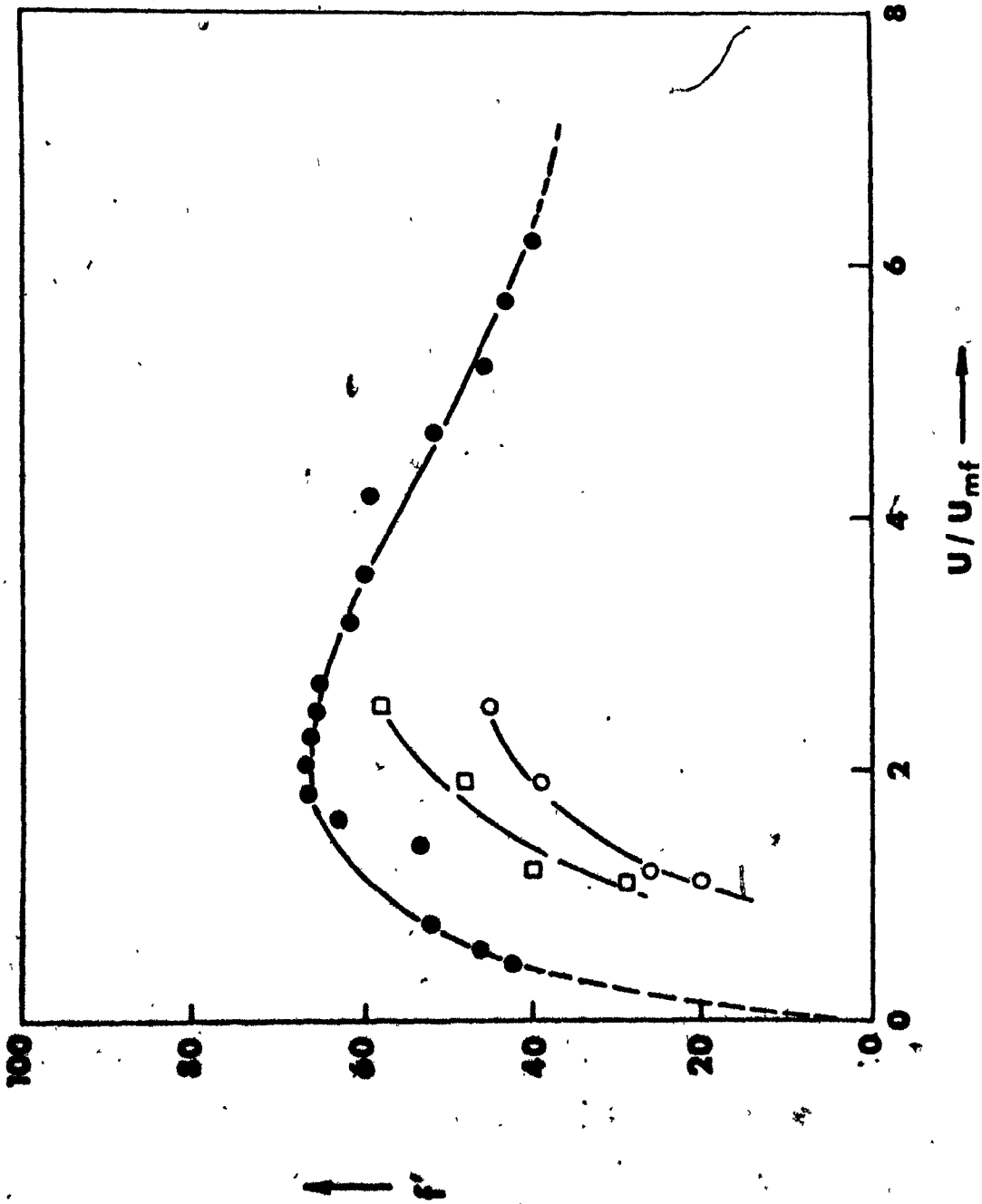
100
80
60
40
20
0
0
2
4
6
8
U/U_mf

approaching asymptotically a penetration of 100% as the gas velocity is increased. They conclude that the usefulness of the fluidized bed for aerosol collection is limited to low velocities and, as a solution to obtaining low collection efficiencies, they present a design incorporating four to five fluidized beds in series, each collecting a relatively small amount of the challenging aerosol. The final penetration through this rather complicated device, assuming complete mixing after each stage, is given by the following equation[Mc1,J2]

$$f'_{st} = f'^{n_{st}} \tag{6.1}$$

where n_{st} is the number of stages and H_{mf} is around 2 to 4×10^{-2} m. Equation (6.1) holds, of course, for an inlet aerosol which is monodisperse; otherwise collection mechanisms and target efficiencies will vary as collection proceeds from stage to stage depending on the particle size variation.

An attempt was made to duplicate McCarthy et al.'s fluidized bed experiments as closely as possible using a 0.8μm diameter DOP aerosol and the 110μm collector particles. The height of the bed at minimum fluidization was 2.8×10^{-2} m and the minimum fluidization velocity, 2.0×10^{-2} m/s, was sufficiently close to theirs (1.6×10^{-2} m/s), to enable comparisons to be made. The particle counter was prime calibrated before the experiments, as a precaution, in the manner described in Appendix C. In order to prevent the bed particles from falling through the orifices at these low velocities, the plate was covered with a wire mesh of 74 μm openings. One third of the holes in the distributor plate were blocked with silicone sealant; the reason for this will be disclosed when analyzing

the factors contributing to high penetrations at low gas velocities. Blank tests were performed in order to eliminate collection by the wire mesh. Aerosol collection by the wire mesh proved to be quite small and of the order of 1-3 per cent*.

Very closely spaced experiments were performed below and beyond the range investigated by McCarthy et al.; the results are plotted in Figure 6.1. As will be seen from the figure, for $U/U_{mf} < 2$ (i.e. gas velocity up to 4×10^{-2} m/s) penetration does increase with superficial gas velocity. However, penetration reaches a maximum at about $U/U_{mf} = 2.1$ and thereafter declines as the superficial gas velocity through the bed is increased. Interpreted in this manner, the same trend is noted in the results of McCarthy et al., but their curves have not quite reached their maxima. This observation is extremely important and to the best of our knowledge it has not been referred to or investigated previously in the literature. The penetration continues to decrease as the velocity through the bed is increased, with no indication of passing through a minimum. The lowest penetration in this set of experiments is at the highest velocity of .12 m/s and, as will be seen from Figure 6.1, at that point the bed is more efficient than the fixed bed portion of the curve. Thus, the data presented in this figure represent conclusive experimental evidence that the aerosol penetration in a fluidized bed does not increase continuously with increasing gas velocity but reaches a maximum and subsequently decreases. All subsequent experiments in this study, discussed below, fall into a velocity range where penetration

---

*It may be noted that this is the reason (see Section 2.3.1.1) why the author finds the results of Scott and Guthrie[82], who report a 15-20% collection of 0.57 μm aerosol particles by a screen of the same opening, highly improbable.

decreases with velocity. The reason for this surprising behaviour of the fluidized bed collecting aerosol particles at low velocities is, we believe, a combination of three contributing factors.

The first factor, and perhaps the most important of the three from an academic and practical point of view, is that aerosol removal in shallow fluidized beds operating at high velocities falls in the range where gas exchange between the bubble and the dense phase is very rapid and penetration is not controlled by this mechanism. The limiting step appears to be in the dense phase. This conclusion is justified by detailed analysis in Chapter 7, where it is shown that the fluidized bed may be modelled successfully on the assumption that the resistance to gas interchange between the phases is negligible. The reason for the rapid gas interchange between the phases, at high velocities, can be attributed to very fast bubble formation and coalescence occurring in the region close to the distributor plate. Clift[C5] and Clift et al.[C9] have shown that a large fraction of the gas forming the bubble clouds is transferred to the dense phase when coalescence occurs. The same authors have also shown that this contribution to mass transfer is important particularly in the region very close to the distributor. It appears, therefore, that the experimental results of this study agree, in principle, with their theory and coalescence contributes significantly to gas transfer between the phases.

The second factor contributing to aerosol collection, at high velocities, is that the motion of the bed particles is affected by the rising bubbles. This vigorous mixing of the collector particles especially in the clouds and in the wakes of the bubbles enhances inertial collection resulting, as will be seen in Chapter 7, in higher collection coefficients

for larger aerosol particles. At lower flow rates, where the influence of bubble-induced particle motion on inertial collection is much smaller, this effect is lost.

The third factor contributing to high penetrations at low gas velocities involves inefficient distributor design, and experimental difficulties, inherent in performing experiments with aerosols. The majority of previous studies, with the exception of the pioneering study of Meissner and Mickley[M4], used low superficial gas velocities*. The reason for this is simple: it is quite difficult to produce a monodisperse, spherical and electrically neutral aerosol at sufficiently large flow-rates and experimentally stable conditions. The problem was overcome in this study by the use of the spinning disk generator, modified in the manner described in Chapter 4, but the majority of the previous studies used quite crude and complicated devices for aerosol generation (see Chapter 2). For this reason, experiments with realistic bed sizes, around 0.15 m, have been avoided in the past. Unfortunately, major problems arise in achieving adequate distribution at low velocity of a gas containing an aerosol. Porous plates cannot be used because they collect most of the challenging aerosol, thereby clogging and showing unsteady filtration characteristics. An alternative is a perforated plate distributor, but the percentage free area required at low velocities is small. This is probably the reason why most previous studies have avoided commenting

---

*It may be noted that Meissner and Mickley, who were the only previous workers to use elevated gas velocities, are also the only workers to report decreasing penetration with increasing U.

extensively on gas distribution, and have chosen very simple distributor designs. Scott and Guthrie[S2] for example used a 75 μm opening wire mesh, while McCarthy et al. used a 0.07 m deep fixed bed of 10^{-2} m diameter ceramic spheres and a "retaining screen" with unspecified opening. The pressure drop across this "distributor bed" at the highest superficial gas velocity used by McCarthy et al. can be calculated approximately from the Ergun equation which is given for large spherical particles in fixed beds as[D2]

$$\frac{\Delta P}{H} = 150 \frac{(1-\epsilon)^2 \mu_f U}{\epsilon^3 d_p^2} + 1.75 \frac{(1-\epsilon)\rho_f U^2}{\epsilon^3 d_p} \qquad (6.2)$$

Taking $H = 0.07$ m, $\epsilon = 0.43$, $U = 3.9\times10^{-2}$ ms^{-1}, $\rho_f = 1.2\times10^{-6}$ kgm^{-3}, $d_p = 0.01$ m, $\mu_f = 1.84\times10^{-5}$ $kgm^{-1}s^{-1}$, we obtain $\Delta P = 1.32$ nm^{-2}; this can be considered to be a negligible pressure drop. Furthermore, any beneficial effect their ceramic spheres might have had in distributing the gas was destroyed by the inclusion of an empty section 0.2 m deep between the spheres and the retaining screen. This type of ineffective distributor results in the initial formation of large bubbles, few in number, and is partly the reason for increasing penetration with increasing velocity. The detrimental effect of an inefficient distributor on aerosol collection can be verified from the results of this study, plotted in Figure 6.1. where the partial blocking of the distributor orifices magnified the dependence of penetration on gas velocity at the low range and resulted in collection efficiencies even lower than observed by McCarthy et al.

6.2.1.2 Penetration at high velocities

Having clarified the effect of gas velocity and inefficient gas distribution we can examine further experimental results. All subsequent experiments were performed in the region where bubble formation and coalescence is rapid. Figure 6.2 shows the effect of gas superficial velocity, U, for three values of the bed height at minimum fluidization, H_{mf}, for 1.6 μm DOP in a bed of 110 μm collectors. Tables 6.1 to 6.4 present extensive experimental results for 0.72 μm, 0.9 μm, 1.1 μm and 1.6 μm DOP aerosol with 110 μm collector particles. Some of these results are plotted in Figures 6.2 to 6.5. With very shallow beds and large aerosol diameters (Figure 6.2) the bed is effectively "frozen" after a few minutes of operation (see Section 6.2.2.3), less than 80% of the aerosol is collected and there is little dependence on gas velocity. On increasing H_{mf} so that the bed is truly fluidized much higher collection is observed, and the penetration decreases with increasing velocity. At greater depths the aerosol penetration decreases substantially and is again effectively independent of U. As discussed earlier, the dependence of penetration on U at intermediate values of H_{mf} can be attributed to enhanced inertial collection due to bubble-induced particle movement. It may be noted that although the deepest bed is still very shallow in comparison with conventional fluidization operations, high collection efficiencies are obtained. From Tables 6.1 to 6.4 a 7×10^{-2} m deep bed operating at 0.36 m/s collects 98% of 1.6 μm aerosol and 80% of the 0.72 μm diameter aerosol, other aerosol diameters falling between these values. It is also interesting to note in Figure 6.2 to 6.5 that the dependence of penetration on velocity becomes weaker with increasing

FIGURE 6.2 The effect of gas superficial velocity on aerosol penetration for three values of the bed height at minimum fluidization

d_A = 1.6 μm
d_p = 110 μm

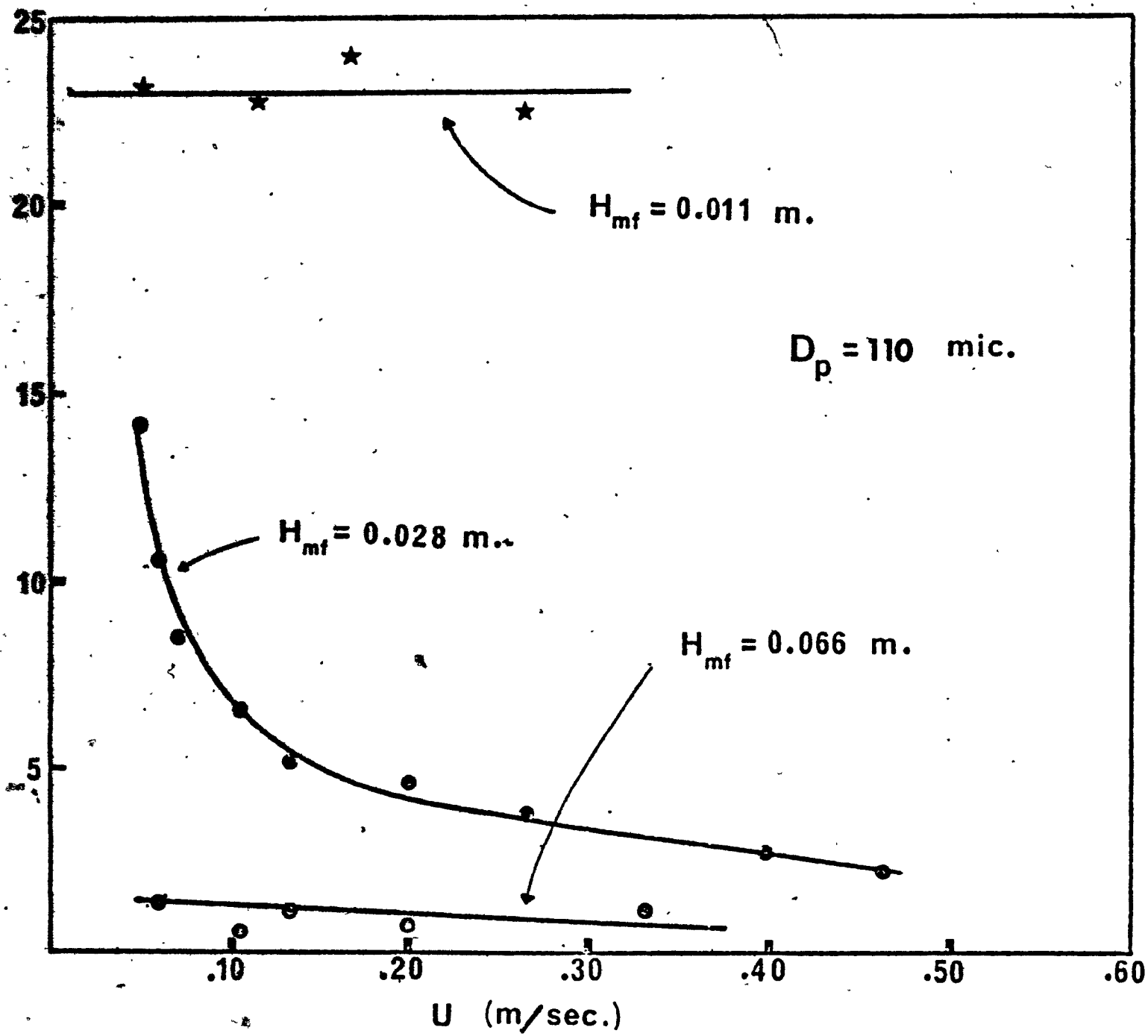
25
20
15
10
5
H_{mf} = 0.011 m.
D_p = 110 mic.
H_{mf} = 0.028 m.
H_{mf} = 0.066 m.
.10
.20
.30
.40
.50
.60
U (m/sec.)

FIGURE 6.3 Fluidized bed experiments - aerosol penetration versus U/U_{mf}

d_A = 0.72 μm
d_p = 110 μm
open square, $H_{mf} = 3.06 \times 10^{-2}$ m
circle with asterisk, $H_{mf} = 3.98 \times 10^{-2}$ m
open asterisk, $H_{mf} = 5.10 \times 10^{-2}$ m
full asterisk, $H_{mf} = 6.78 \times 10^{-2}$ m

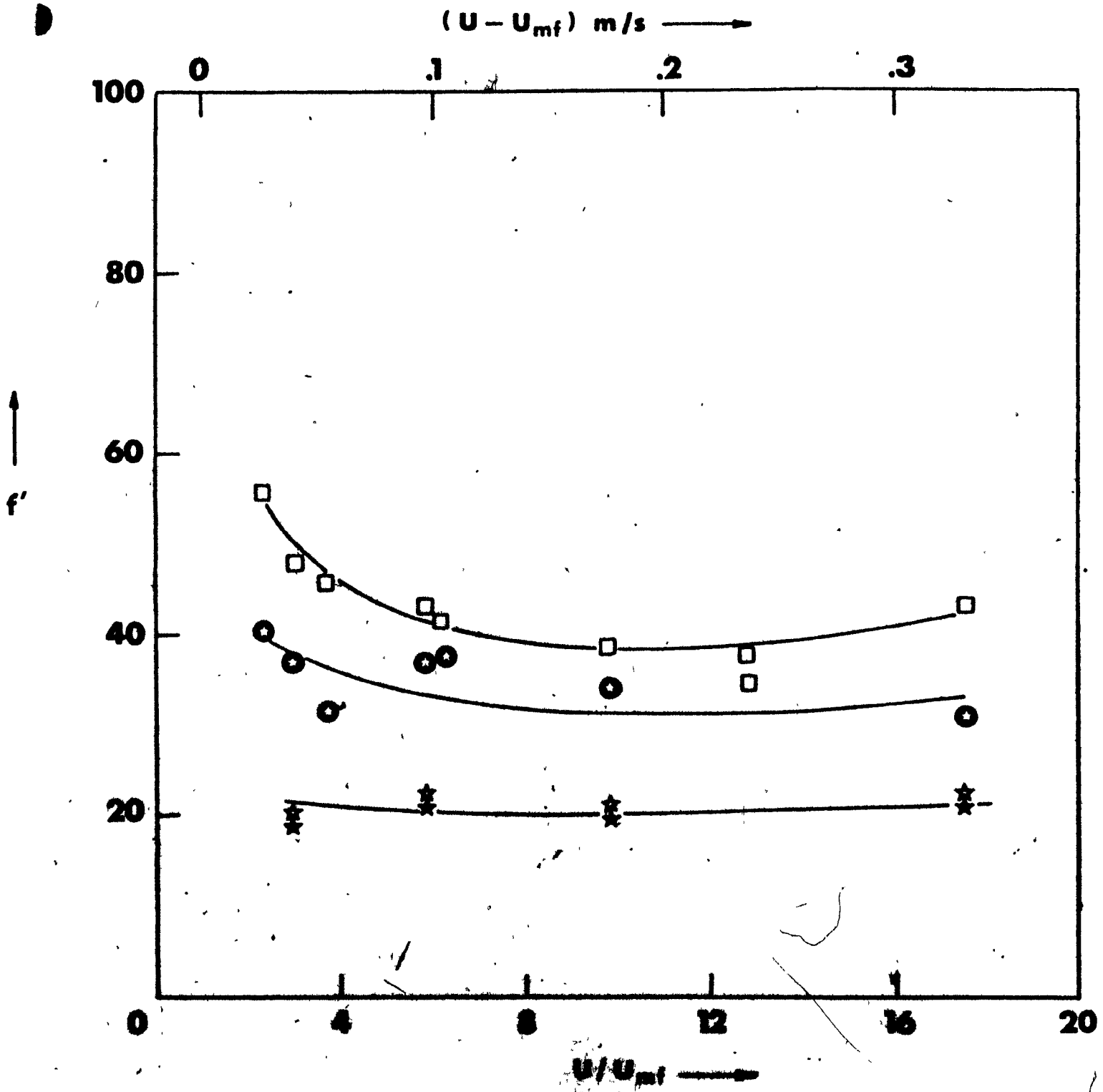
(U − Umf) m/s
0
.1
.2
.3
100
80
60
40
20
f'
0
4
8
12
16
20
U/Umf

FIGURE 6.4 Fluidized bed experiments - aerosol penetration versus U/U_{mf}

$d_A = 0.9$ μm
$d_p = 110$ μm
open circle, $H_{mf} = 1.22 \times 10^{-2}$ m
full circle, $H_{mf} = 1.86 \times 10^{-2}$ m
open square, $H_{mf} = 3.06 \times 10^{-2}$ m
circle with asterisk, $H_{mf} = 3.98 \times 10^{-2}$ m
open asterisk, $H_{mf} = 5.10 \times 10^{-2}$ m
full asterisk, $H_{mf} = 6.78 \times 10^{-2}$ m

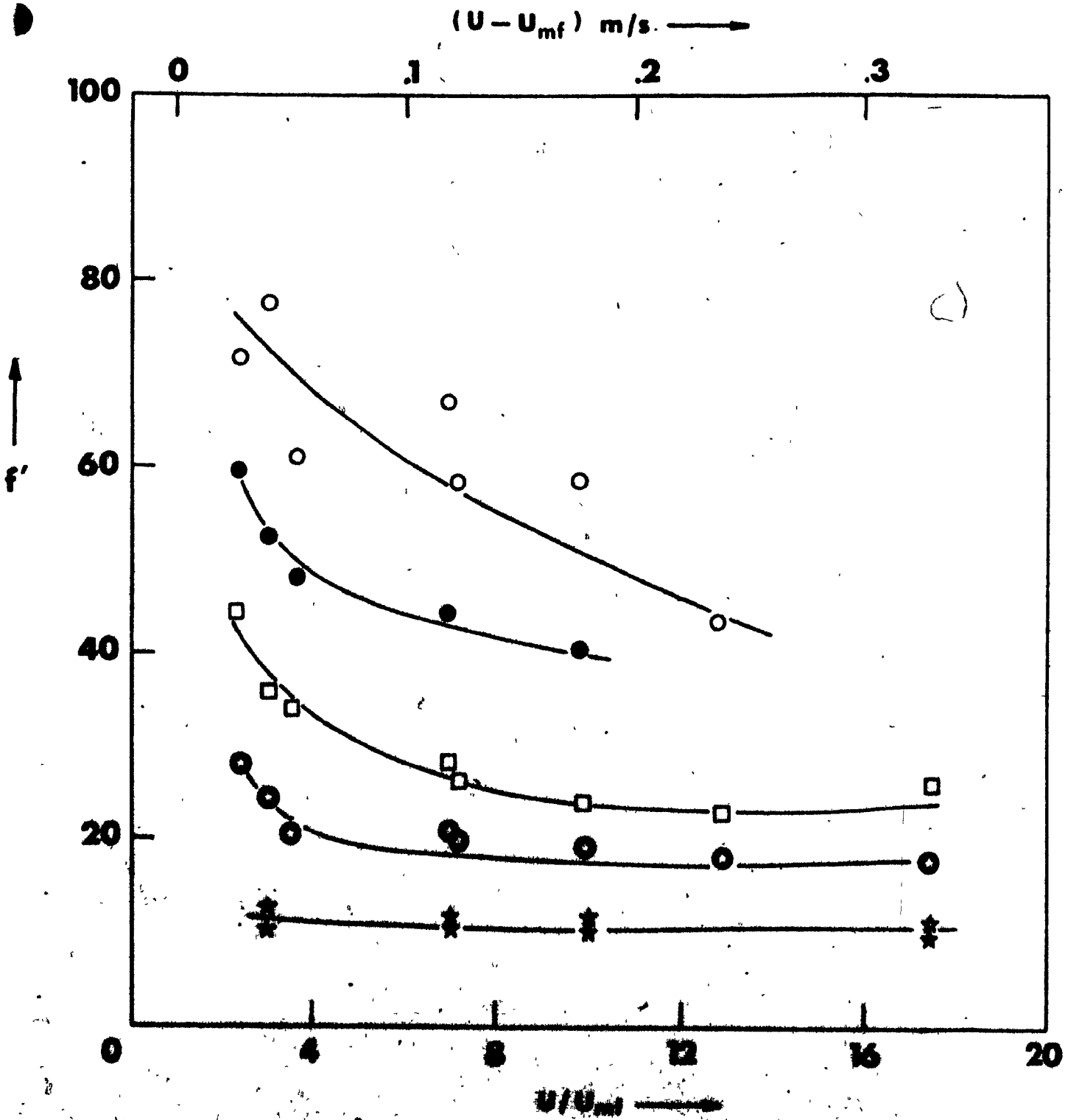
(U − U_mf) m/s.
0
.1
.2
.3
100
80
60
40
20
f'
0
4
8
12
16
20
U/U_mf

FIGURE 6.5 Fluidized bed experiments - aerosol penetration versus U/U_{mf}

$d_A = 1.1$ μm
$d_p = 110$ μm
open circle, $H_{mf} = 1.22 \times 10^{-2}$ m
full circle, $H_{mf} = 1.86 \times 10^{-2}$ m
open square, $H_{mf} = 3.06 \times 10^{-2}$ m
circle with asterisk, $H_{mf} = 3.98 \times 10^{-2}$ m
open asterisk, $H_{mf} = 5.10 \times 10^{-2}$ m
full asterisk, $H_{mf} = 6.78 \times 10^{-2}$ m

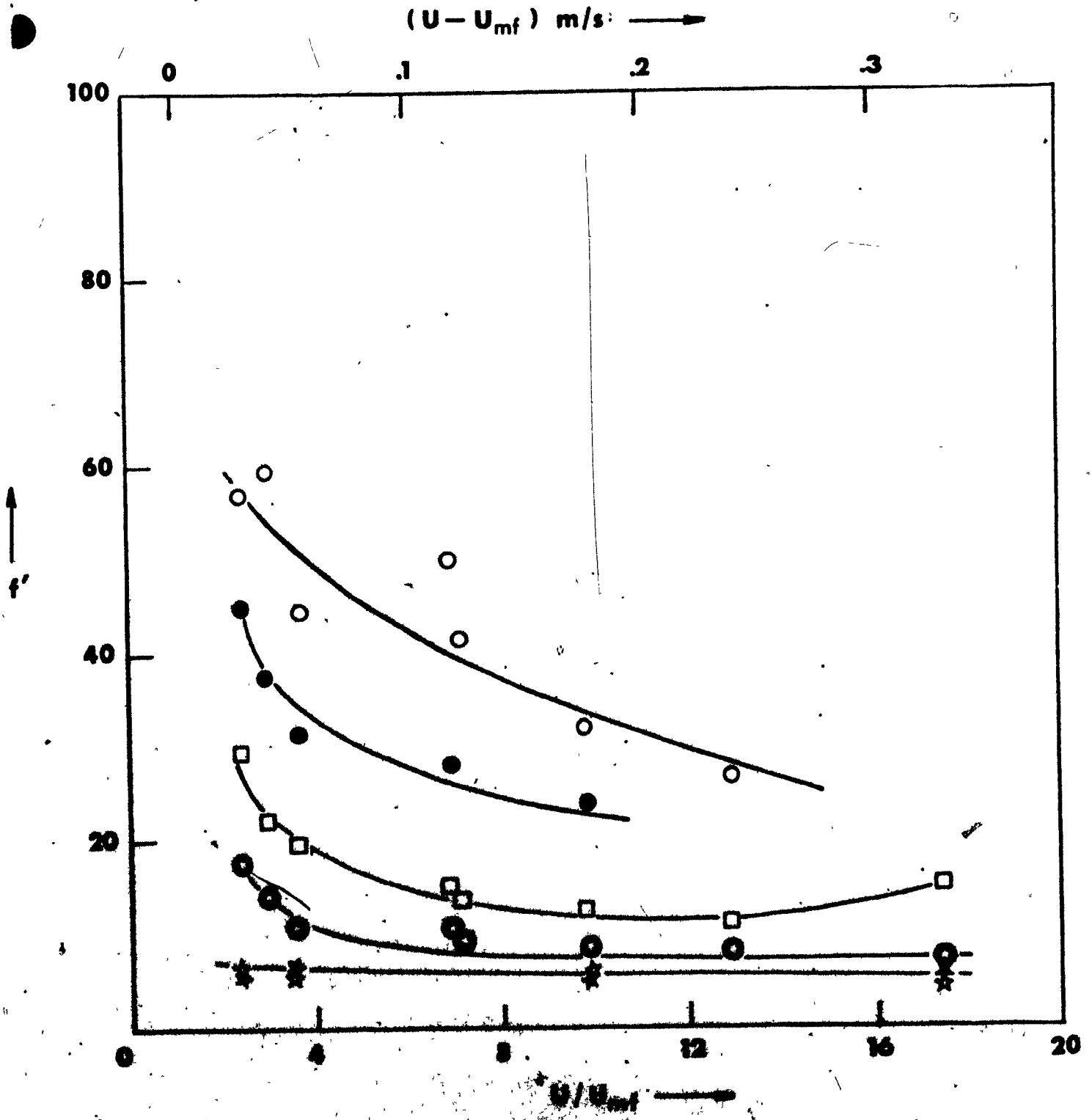
(U − Umf) m/s ⟶
0
.1
.2
.3
100
80
60
40
20
f'
0
4
8
12
16
20
U/Umf ⟶

TABLE 6.1 Penetration in Fluidized Bed Experiments, $d_A = 0.72$ μm, $d_p = 110$ μm

H_{mf}	Superficial Gas Velocity $U_m \times 10^2$/s							
$m \times 10^2$	4.92	6.03	7.24	12.88	13.06	19.53	25.61	34.93
0.372	-	99.4	-	96.6	-	-	-	-
0.744	-	96.3	-	94.3	-	96.6	-	-
1.22	79.7	91.4	76.0	81.6	73.4	87.6	70.1	-
1.86	69.1	66.9	62.9	61.0	-	56.0	-	-
3.06	56.2	48.2	46.1	43.8	41.9	39.3	38.5	43.2
3.98	40.3	37.1	32.3	37.0	37.5	34.3	35.2	31.6
5.10	-	20.4	-	22.8	-	21.6	-	23.0
6.78	-	19.8	-	20.8	-	20.4	-	21.9

TABLE 6.2 Penetration in Fluidized Bed Experiments, $d_A = 0.9$ μm, $d_p = 110$ μm

H_{mf}	Superficial Gas Velocity $mx10^2/s$							
$mx10^2$	4.92	6.03	7.24	12.88	13.06	19.53	25.61	34.93
0.372	-	90.9	-	87.0	-	-	-	-
0.744	-	88.6	-	80.7	-	83.1	-	-
1.22	72.3	78.0	61.7	66.9	58.5	58.7	43.6	-
1.86	59.8	52.8	48.3	44.6	-	40.2	-	-
3.06	44.6	36.8	34.3	28.6	26.6	24.6	23.5	26.8
3.98	28.1	24.5	20.4	21.4	20.8	19.7	18.7	17.1
5.10	-	13.2	-	11.8	-	11.1	-	11.1
6.78	-	11.3	-	10.8	-	10.3	-	10.8

TABLE 6.3 Penetration in Fluidized Bed Experiments, $d_A = 1.15$ μm, $d_p = 110$ μm

H_{mf}	Superficial Gas Velocity $mx10^{-2}/s$							
$mx10^2$	4.92	6.03	7.24	12.88	13.06	19.53	25.61	34.93
0.372	-	83.4	-	70.2	-	-	-	-
0.744	-	74.0	-	62.5	-	72.0	-	-
1.22	54.7	59.7	44.4	49.8	41.6	32.1	26.2	-
1.86	45.1	37.9	31.5	28.4	-	24.1	-	-
3.06	29.9	22.5	19.8	15.5	14.0	13.0	11.4	12.4
3.98	17.4	14.1	11.3	11.3	9.8	8.9	8.1	7.3
5.10	-	6.9	-	5.3	-	5.2	-	4.8
6.78	-	6.1	-	5.9	-	6.0	-	5.6

TABLE 6.4 Penetration in Fluidized Bed Experiments, $d_A = 1.6$ μm, $d_p = 110$ μm

U m/sx10^2	H_{mf} mx10^2	f'
7.1	1.23	23.1
12.1	1.23	22.7
13.6	1.23	24.0
26.1	1.23	22.4
4.9	3.04	14.1
6.0	3.04	10.6
7.1	3.04	8.5
11.0	3.04	6.6
13.0	3.04	5.2
19.5	3.04	4.6
26.1	3.04	3.7
38.1	3.04	2.7
43.8	3.04	2.2
6.0	6.73	1.4
11.0	6.73	0.6
13.0	6.73	1.1
19.5	6.73	0.7
31.5	6.73	1.1
12.4	0.37	95.7
12.4	0.74	92.9
12.4	2.04	19.7
12.4	3.96	3.0
12.4	5.07	1.5

velocity at intermediate bed heights. This is because the bubbles in the bed, although enhancing inertial collection, have a secondary effect of mixing the gas in the dense phase. As will be shown in Chapter 7 the bed goes through a transition from plug flow at low velocities to approach complete mixing at high velocities, and thus becomes less efficient with increasing gas velocity. This transitional behaviour of the fluidized bed is discussed in more detail in Chapter 7.

Tables 6.5 to 6.9 present experiments with DOP aerosols of 1.1 μm, 1.35 μm, 1.6 μm, 1.75 μm and 2.5 μm diameter with 600 μm diameter collector particles where penetration was measured as a function of velocity and bed height at minimum fluidization. Figure 6.6 shows experiments where the penetration of 1.1 μm diameter aerosol through a fluidized bed of 600 μm collector particles is measured as a function of U/U_{mf} and $(U-U_{mf})$ at four different bed heights. The figure shows clearly the effect of enhanced inertial collection at intermediate bed heights. At $H_{mf} = 1.9 \times 10^{-2}$ m, for example, the penetration of 1.1 μm particles falls from about 60% to 27% as U/U_{mf} is increased from 1.3 to 2.5. Over 90% of these aerosol particles which fall "in the range difficult to collect" are removed by a 8.8×10^{-2} m deep fluidized bed at a superficial gas velocity of 0.74 m/s.

6.2.2 Effect of bed depth at minimum fluidization and bed loading

6.2.2.1 Introduction

The effect of bed depth at minimum fluidization depends on superficial gas velocity and is described in more detail in Chapter 7, where a mathematical model for aerosol collection is derived from the

TABLE 6.5 Penetration in Fluidized Bed Experiments, $d_A = 1.1$ μm, $d_p = 600$ μm

H_{mf}	Superficial Gas Velocity, U $mx10^2/s$					
$mx10^2$	38.03	43.72	49.15	54.84	60.79	73.68
1.86	59.15	48.07	43.17	-	34.66	27.16
3.06	53.80	-	33.36	-	24.68	-
3.98	46.94	36.64	31.05	28.98	28.16	24.79
5.10	33.74	-	21.63	-	15.58	-
6.78	24.72	17.92	13.28	12.48	11.79	11.31
8.81	20.07	-	11.66	-	9.41	-

TABLE 6.6 Penetration in Fluidized Bed Experiments, $d_A = 1.35$ μm, $d_p = 600$ μm

H_{mf}	Superficial Gas Velocity, U $mx10^2$ s					
$mx10^2$	38.03	43.72	49.15	54.84	60.79	73.68
1.86	21.36	16.71	14.34	10.80	7.59	7.41
3.06	16.84	-	7.85	-	8.16	-
3.98	13.13	8.84	8.46	7.23	6.76	5.82
5.10	8.74	-	5.61	-	3.92	-
6.78	6.20	5.23	4.68	4.24	4.30	3.71
8.81	6.50	-	4.50	-	3.53	-

TABLE 6.7 Penetration in Fluidized Bed Experiments, d_A = 1.6 μm, d_p = 600 μm

U_o m/sx10^2	H_{mf} mx10^2	f'
34.5	1.11	7.9
34.5	1.44	6.9
34.5	2.04	6.7
34.5	2.63	5.5
34.5	3.37	5.8
34.5	4.33	4.7
49.1	1.11	7.7
49.1	1.44	6.0
49.1	2.04	5.0
49.1	2.63	4.2
49.1	3.37	3.1
49.1	4.33	2.1
49.1	5.55	1.4
49.1	7.14	0.6
49.1	9.25	0.3
34.5	4.33	3.3
43.8	4.33	3.9
47.6	4.33	2.1
51.0	4.33	2.2
60.3	4.33	1.9

TABLE 6.8 Penetration in Fluidized Bed Experiments, $d_A = 1.75$ μm, $d_p = 600$ μm

H_{mf}	Superficial Gas Velocity, U $mx10^2/s$					
$mx10^2$	38.03	43.72	49.15	54.84	60.79	73.68
1.86	5.89	3.81	2.80	2.67	1.73	1.65
3.06	5.12	-	1.67	-	1.08	-
3.98	3.38	2.16	1.81	1.96	1.59	1.42
5.10	1.87	-	0.922	-	-	1.18
6.78	1.27	-	0.56	-	-	0.39
8.81	0.89	-	0.47	-	-	0.32

TABLE 6.9 Penetration in Fluidized Bed Experiments, $d_A = 2.5$ μm, $d_p = 600$ μm

H_{mf}	U	f'
$mx10^2$	$mx10^2/s$	(-)
1.86	60.79	0.26
3.06	38.03	0.90
3.06	60.79	0.12
5.10	43.72	0.55
5.10	54.84	0.57
5.10	73.68	0.18

FIGURE 6.6 Fluidized bed experiments - aerosol penetration versus U/U_{mf}

d_A = 1.1 μm
d_p = 600 μm
full circle, $H_{mf} = 1.86 \times 10^{-2}$ m
open square, $H_{mf} = 3.98 \times 10^{-2}$ m
full asterisk, $H_{mf} = 6.78 \times 10^{-2}$ m
open circle, $H_{mf} = 8.81 \times 10^{-2}$ m

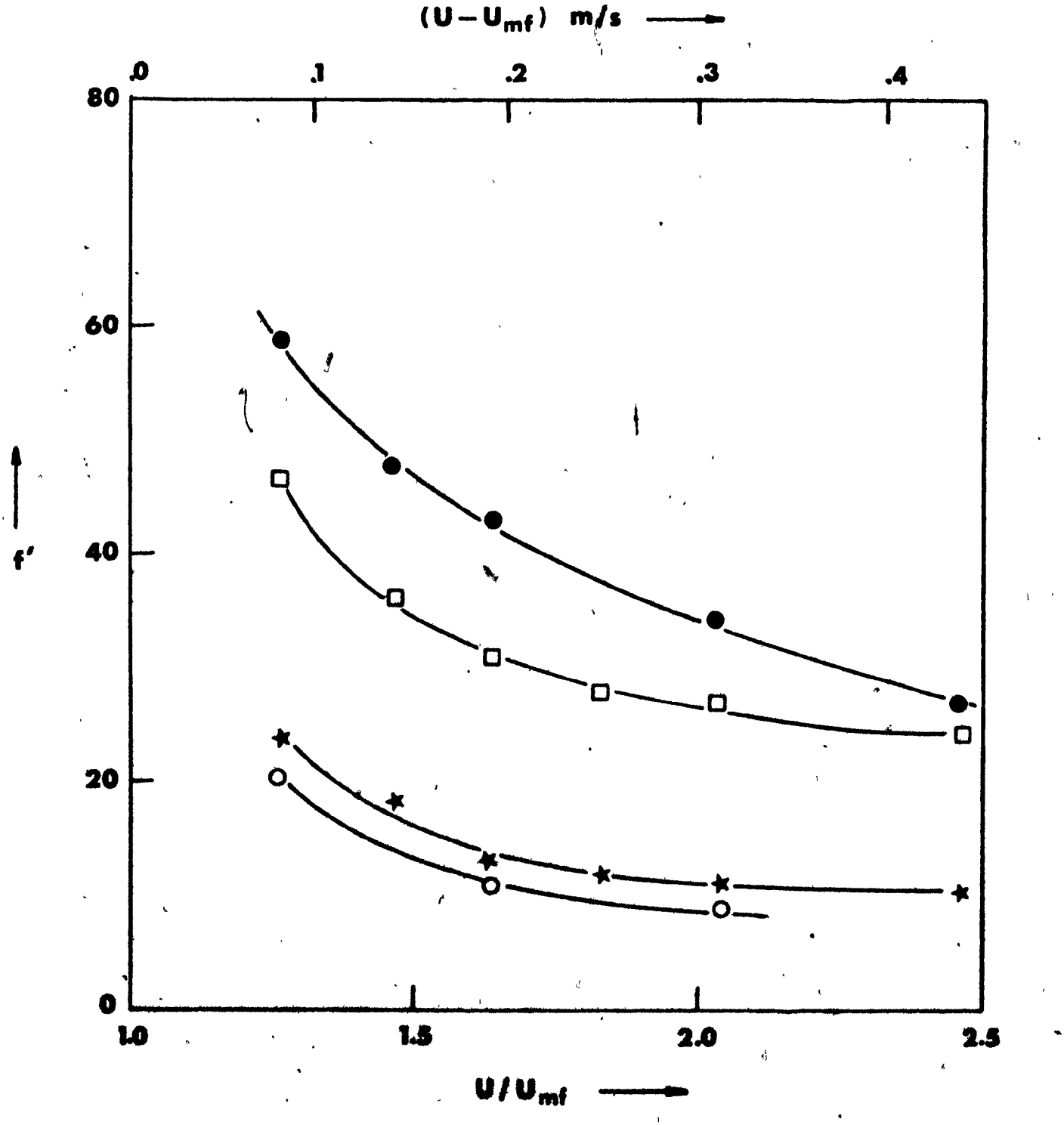
(U − U_mf) m/s
.0
.1
.2
.3
.4
80
60
40
20
0
f'
1.0
1.5
2.0
2.5
U/U_mf

FIGURE 6.7 Comparison of fixed and fluidized beds collecting dioctyl phthalate aerosol particles

d_A = 1.35 μm
d_p = 600 μm
open circle, fixed bed (H = 9×10^{-2} m)
full circle, fluidized bed (H_{mf} = 1.9×10^{-2} m)
circle with asterisk, fluidized bed (H_{mf} = 8.8×10^{-2} m)

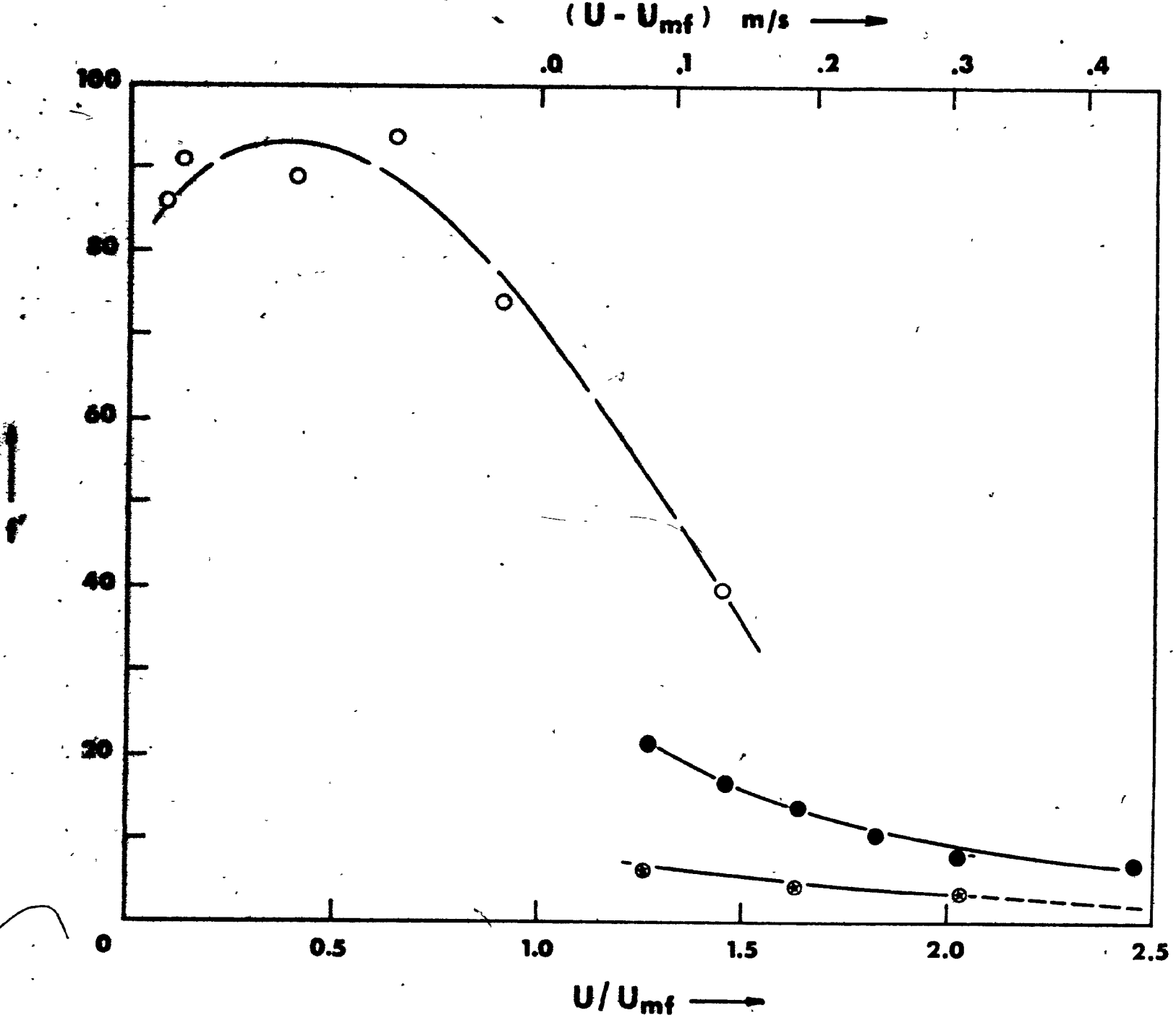
(U - Umf) m/s
.0
.1
.2
.3
.4
100
80
60
40
20
0
0.5
1.0
1.5
2.0
2.5
U / Umf

FIGURE 6.8 Comparison of fixed and fluidized beds collecting dioctyl phthalate aerosol particles

d_A = 1.75 μm
d_p = 600 nm
open circle, fixed bed
full circle, fluidized bed (1.86×10^{-2} m)
circle with asterisk, fluidized bed (8.81×10^{-2} m)

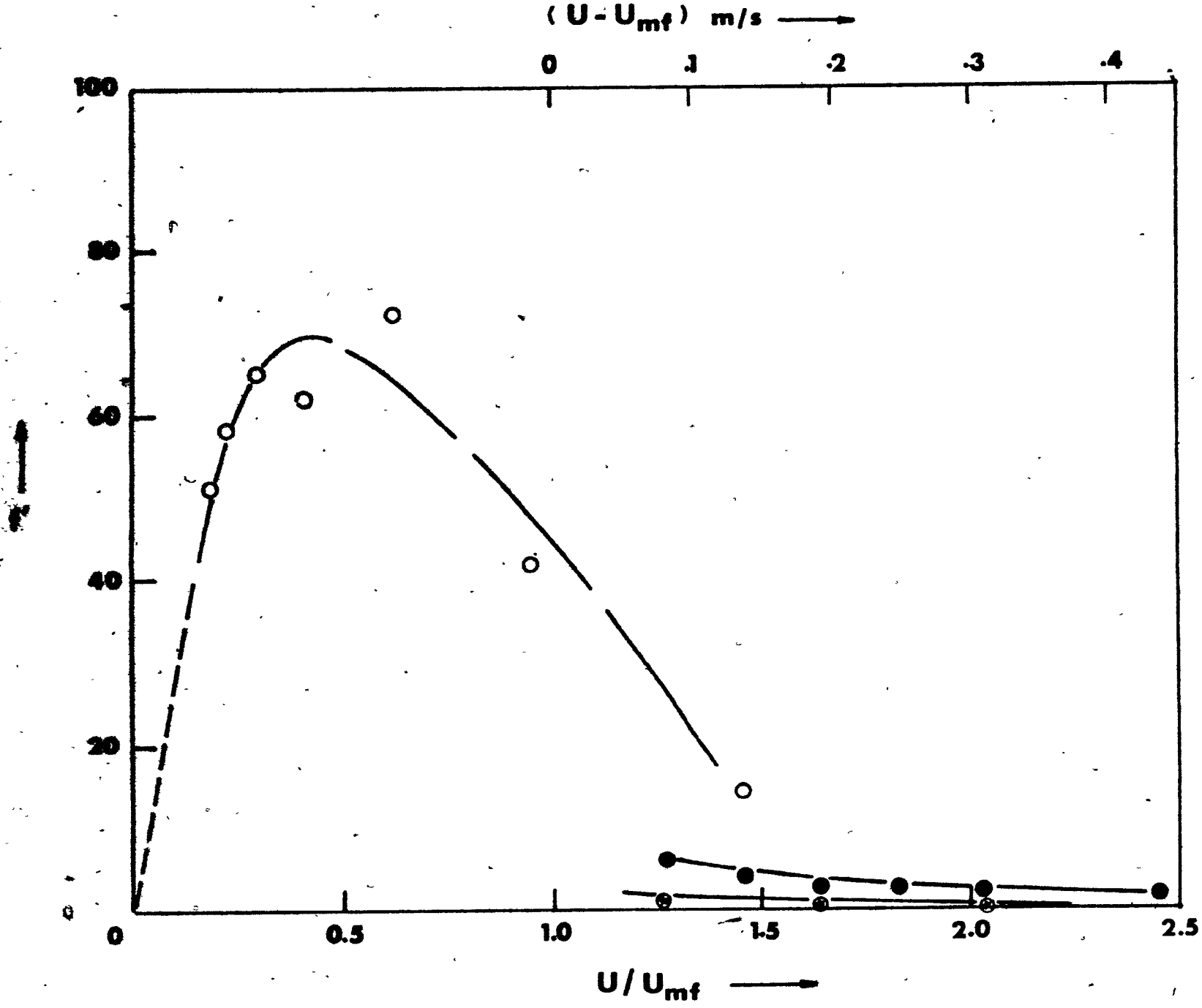
(U - Umf) m/s
0
.1
.2
.3
.4
100
80
60
40
20
0
0.5
1.0
1.5
2.0
2.5
U / Umf

modified two phase theory of fluidization. Therefore, only some qualitative observations on the effect of bed height on aerosol penetration are presented here. Further observations are discussed in Section 6.2.3.

6.2.2.2 Effect of bed depth

Figure 6.9 shows the penetration of 1.6 μm DOP aerosol as a function of bed depth. The bed was composed of 110 μm collector particles and was operated at a superficial gas velocity of 0.13 m/s which corresponds to 6.5 times the minimum fluidization velocity. At very low bed depths, $H_{mf} = 3.7 \times 10^{-3}$ m, the aerosol penetration is high (about 96%). The bed is not truly fluidized but consists of local spouts over the holes of the distributor. Increasing the bed depth to 7.4×10^{-3} m simply increases the height of the spouts and a small reduction in aerosol penetration is observed. When the bed height is increased to about 1.2×10^{-2} m a very sharp increase in efficiency is observed and penetration of the challenging aerosol falls from 93% to 20%. At this point visual observation of the bed showed that it had undergone a transition from local spouting to fluidization. This transition is shown with a broken line in Figure 6.9 and took place in the region $7.4 \times 10^{-3} < H_{mf} < 1.1 \times 10^{-2}$ m.

On Figure 6.10, plotted on semi-logarithmic axes, we see experiments with 110 μm collector particles where the penetration of 0.72 μm, 0.9 μm and 1.1 μm aerosol particles was measured as a function of bed height at a superficial gas velocity of 0.13 m/s.

Visual observation from the side and top of the bed confirmed that the gas was adequately distributed and that bubble formation and

FIGURE 6.9 Fluidized bed experiments - aerosol penetration versus bed depth

d_p = 110 μm
U^p = 0.13 m/sec

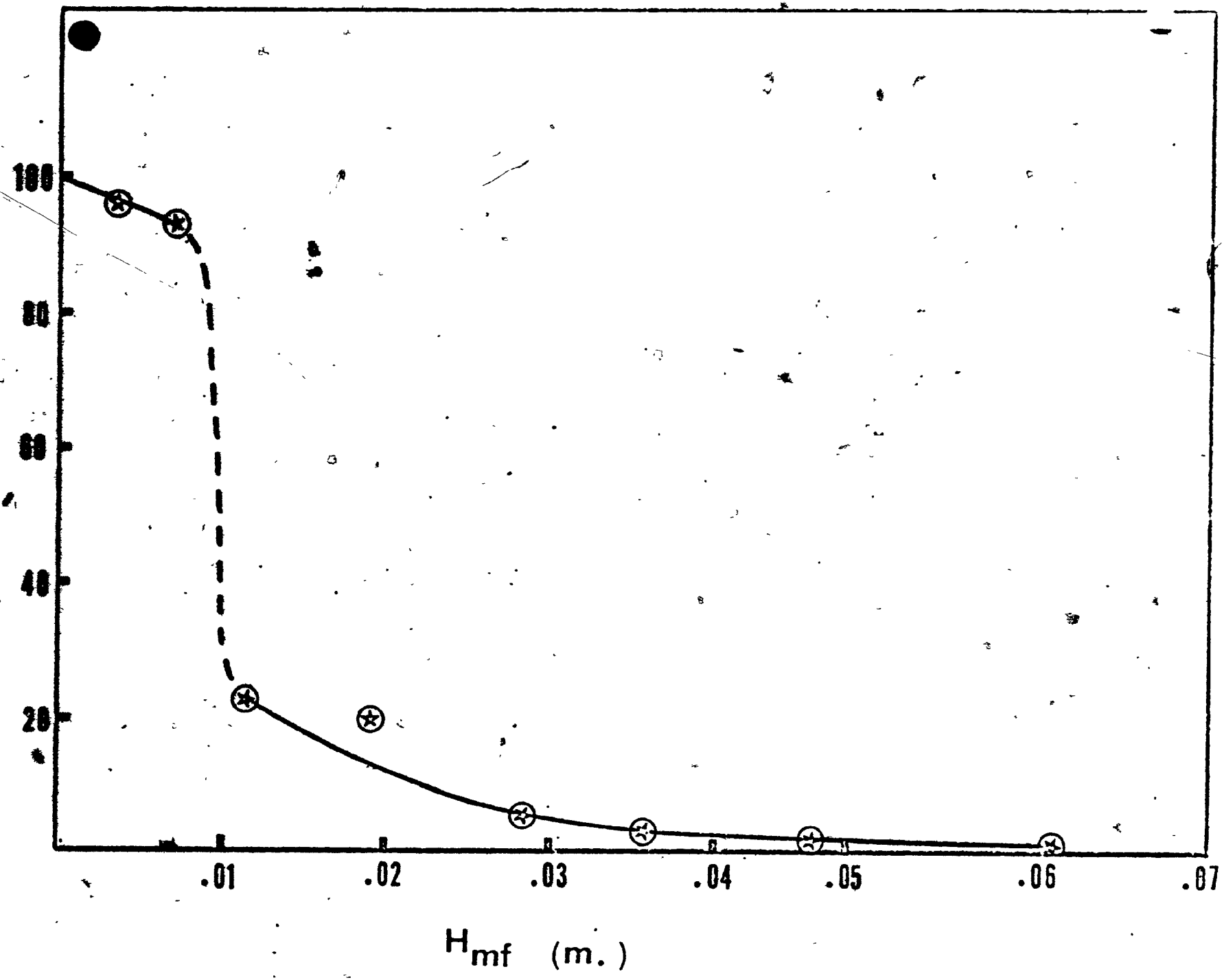
100
80
60
40
20
.01
.02
.03
.04
.05
.06
.07
H_{mf} (m.)

FIGURE 6.10 Fluidized bed experiments - aerosol penetration versus bed depth at minimum fluidization

d_c = 110 μm
U^p = 0.13 m/sec
full circle, d_A = 0.72 μm
open circle, d_A = 0.9 μm
open square, d_A = 1.1 μm

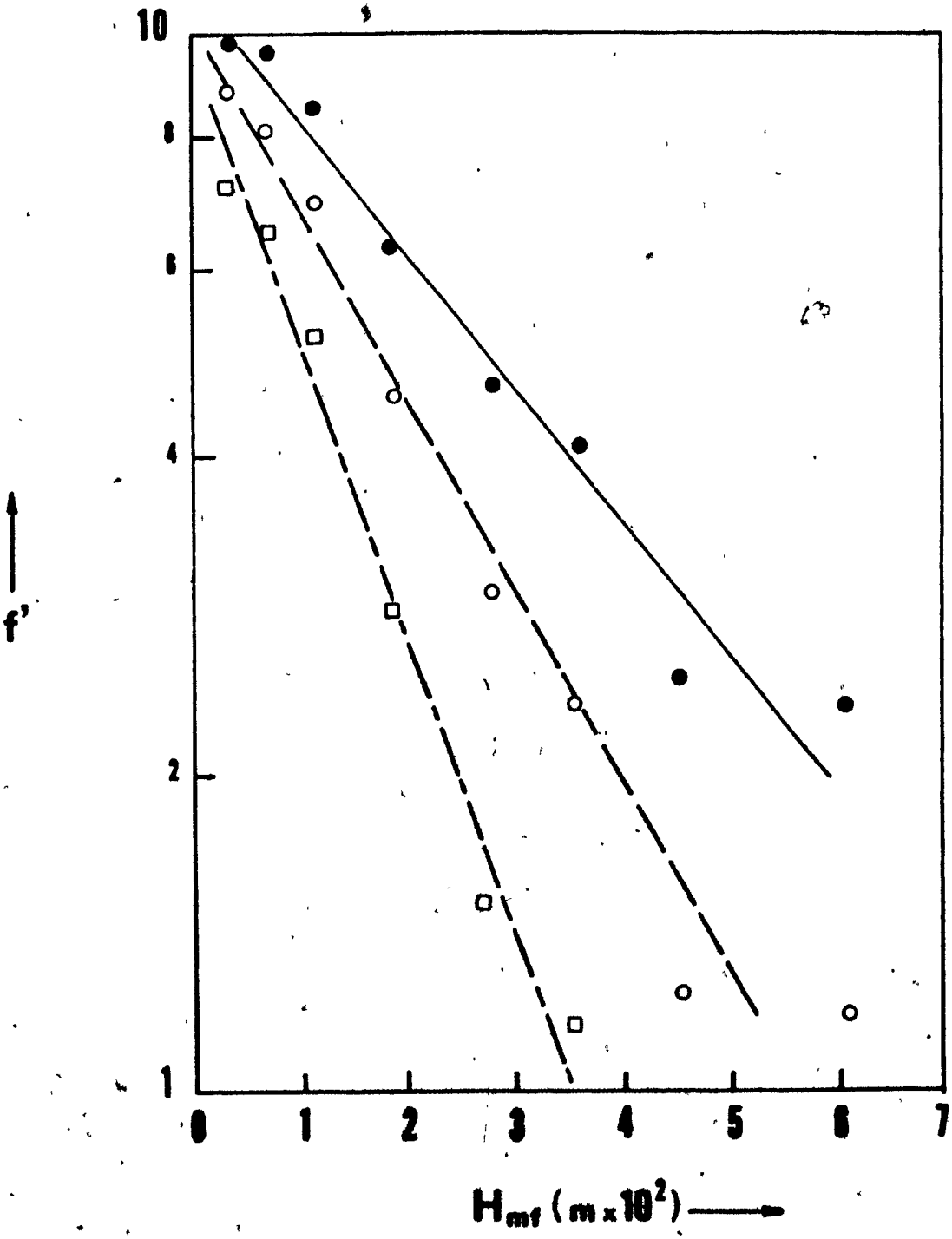
10
8
6
4
2
1
f'
0
1
2
3
4
5
6
7
H_{mf} ($m \times 10^2$)

coalescence were very rapid. Coalescence of the bubbles took place mainly in the region between 1 to $3x10^{-2}$ m. At a superficial velocity of 0.13 m/s the bubbles reaching the surface of the $3x10^{-2}$ m deep bed had coalesced to a mean diameter of approximately 10^{-2} m. As observation of Figures 6.9 and 6.10 shows, a substantial amount of the challenging aerosol is collected in a region close to the distributor. For example a $3x10^{-2}$ m deep bed collected 56% of the 0.72 μm diameter, 71% of the 0.9 μm aerosol and 84% of the 1.15 μm diameter aerosol. Inspection of Figure 6.10 shows that penetration decreases exponentially with bed height implying that the gas is in plug flow (see, however, Section 6.3.4). As will be seen in Chapter 7, at higher superficial gas velocities the backmixing of the gas by the rising bubbles is so marked that the gas is essentially completely mixed.

6.2.2.3 Effect of bed loading

Throughout the experiments reported in this study bed loading did not seem to affect aerosol penetration as long as the bed fluidized properly. This agrees with the conclusions of all previous studies, which report no dependence of penetration on bed loading. Meissner and Mickley[M4], for example, report that silica gel particles absorbed up to 7% of their weight without any appreciable change in aerosol penetration. For low H_{mf}, typically less than 0.02 m, the bed eventually reached a state where it would, in a matter of minutes, undergo a transition from fluidization to local channelling with little or no particle motion. This state of the bed was termed "freezing" and was accompanied by a substantial increase in aerosol penetration. The time required for

the initiation of "freezing" depended on the aerosol diameter and gas velocity and appears to correspond to saturation of the bed with DOP. Typically a shallow bed, $H_{mf} = 2.0 \times 10^{-2}$ m, of 110 μm collectors operating at 0.13 m/s and collecting 1.6 μm DOP particles froze after about 2 hours of operation. This loading is of the order of 10^{-5} times the bed weight and deeper beds could be operated with relatively higher bed loadings. A "frozen" shallow bed could be fluidized if fresh collector particles were added.

This phenomenon reflects the physical state of DOP and is probably a function of both liquid aerosol viscosity and, as 600 μm collectors could be operated with relatively higher bed loadings, particle to particle contact angle. Industrially, the collector particles would be porous, e.g. silica gel or alumina granules. These particles, as has been mentioned above, can collect a substantially larger amount of aerosol before collector saturation and deterioration of fluidization occurs.

6.3 Experiments with a Solid Aerosol

6.3.1 Introduction and description of experiments

This section describes a series of experiments which yielded information both on the removal of solid aerosols and on the effect of aerosol particle density on penetration. It also provided additional information on the effect of bed depth and, simultaneously, tested the performance of the particle counter (described in Section 4.2.2). Figure 6.11 shows the penetration of solid methylene blue aerosol as a function of bed depth at minimum fluidization. The superficial gas velocity through the bed was 0.13 m/s and the 110 μm particles were

FIGURE 6.11 Fluidized bed experiments - aerosol penetration versus bed depth at minimum fluidization

d_p = 110 μm
U^p = 0.13 m/sec
open circles, 1.0 - 1.3 μm DOP
full circles, methylene blue, with arithmetic mean diameter 1.1 - 1.3 μm

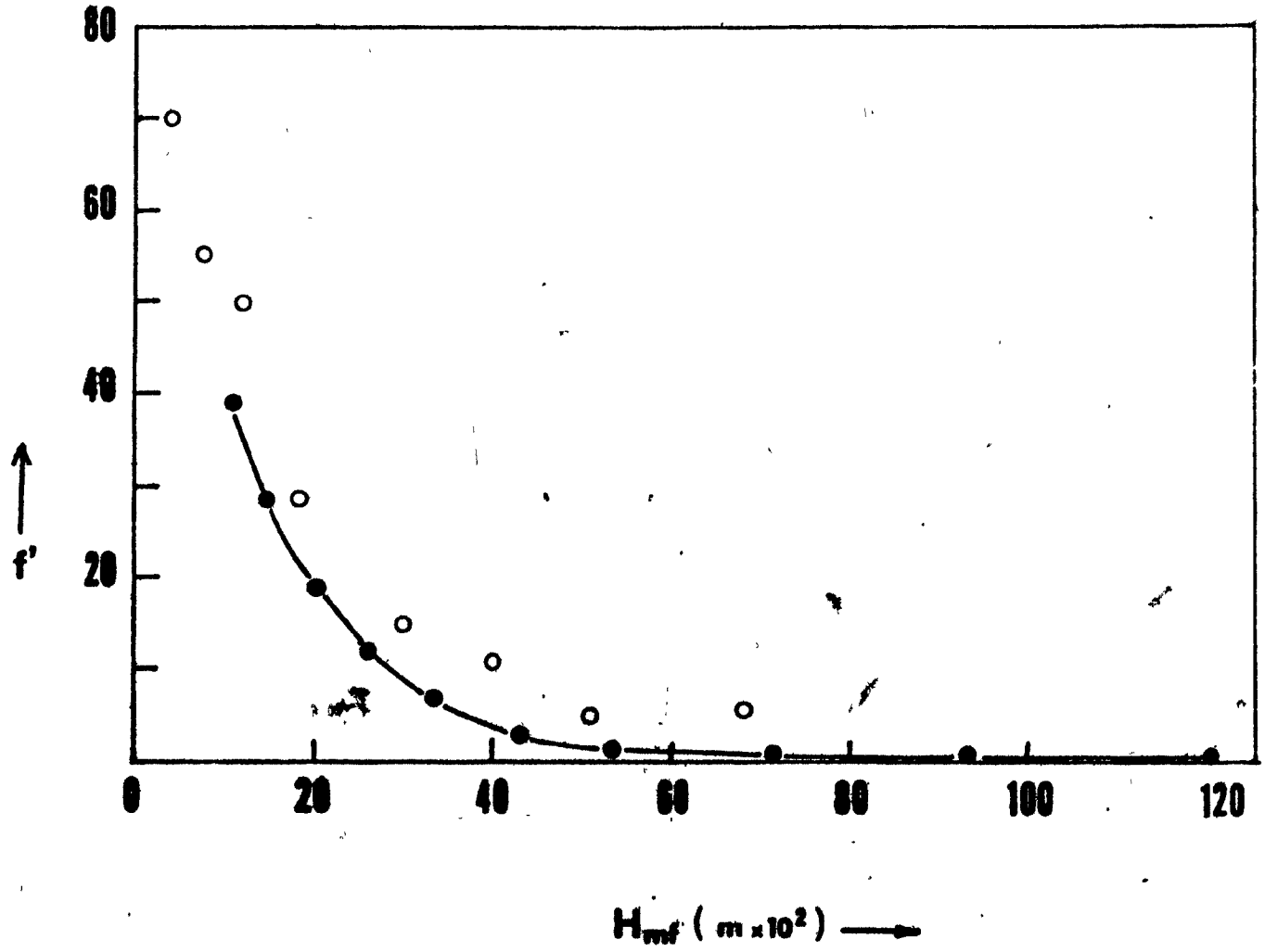
80
60
40
20
f'
0
20
40
60
80
100
120
H_{mf} (m x 10^2)

used as collectors. The bed depth was varied from 1 to 12×10^{-2} m and the surface of the collector particles was, prior to the experiment, covered with a thin layer of DOP which was introduced to the bed as an aerosol. The amount of added DOP was not sufficient to freeze the fluidized bed. Subsequently, a solid methylene blue aerosol, generated by dissolving methylene blue in a mixture of 80% methyl alcohol and 20% distilled di-ionized water, was introduced to the bed. The aerosol size distribution fell in three channels of the particle counter ((.8-1.)μm, (1.-1.3)μm, and (1.3-1.6)μm) . As, however, this set of experiments was designed primarily to determine whether solid aerosols could be removed in a fluidized bed, the aerosol diameter was of secondary importance and the three channels were summed to give a single penetration for the whole size range. This was achieved by operating the counter in TOTAL mode as described in Section 4.2.2. From the percentage distribution of aerosol in each channel it was estimated that the arithmetic mean diameter was approximately 1.1 to 1.3 μm.

Figure 6.11 also shows the penetration of (1.0-1.3) μm DOP aerosol at the same gas velocity, range of bed depths, and collector particle size. In this second set of experiments, however, the particle counter was operating in SINGLE mode, distinguishing between aerosol particles of different sizes (Section 4.2.2), and a time period of at least four months elapsed between the two sets of experiments. The measured penetration of methylene blue versus bed height are plotted again in Figure 6.12 on semi-logarithmic axes. We will refer to these figures later in the text.

FIGURE 6.12 Fluidized bed experiments - aerosol penetration versus bed depth at minimum fluidization

d_p = 110 μm
U^p = 0.13 m/s
open circles, 1.0 - 1.3 μm DOP
full circles, methylene blue, with arithmetic mean diameter 1.1 - 1.3 μm

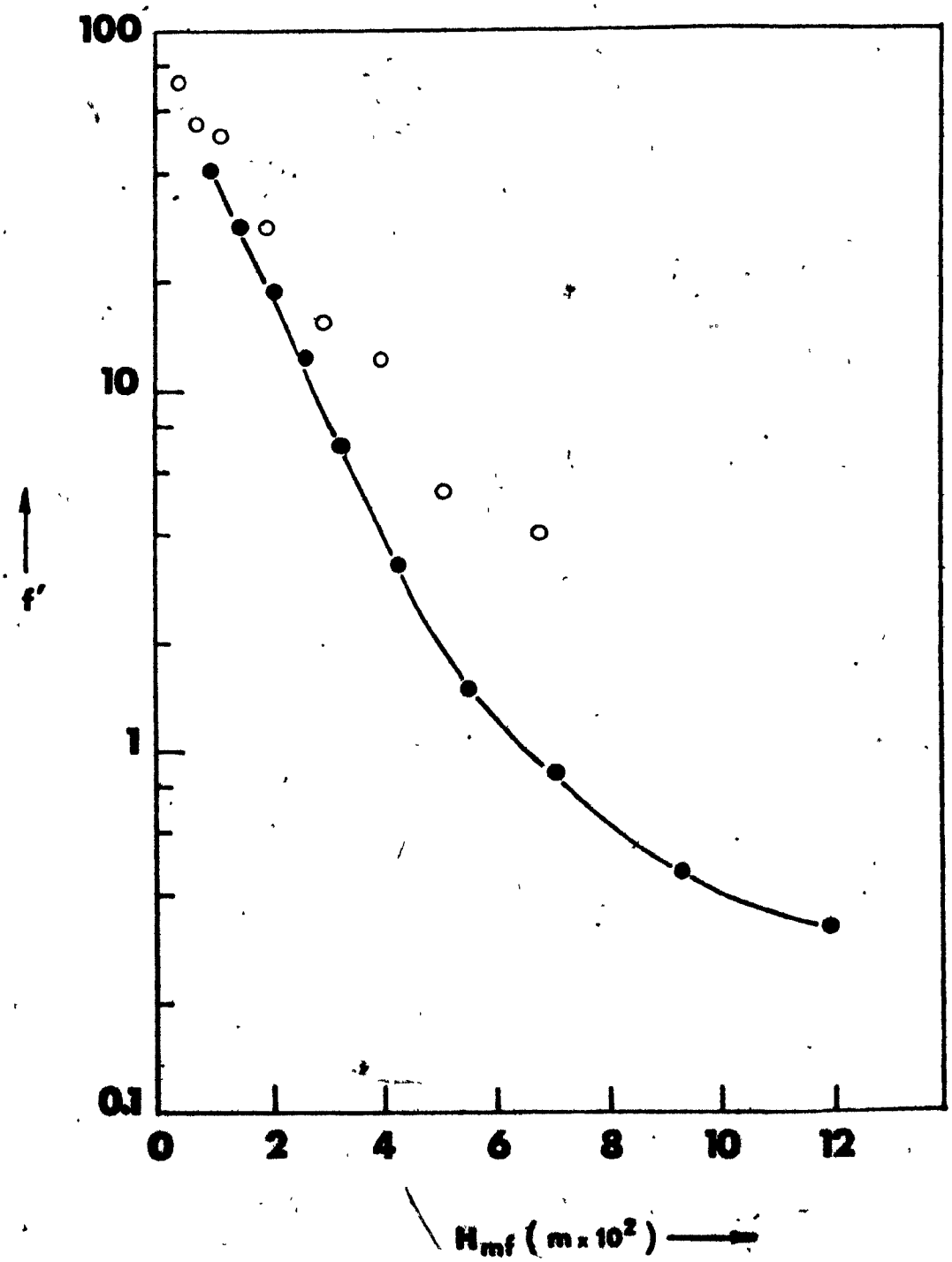
100
10
1
0.1
f'
0
2
4
6
8
10
12
H_{mf} (m x 10^2)

6.3.2 Removal of methylene blue aerosol

Inspection of Figure 6.11 shows that solid aerosol particles can be removed, very efficiently, by a bed of fluidized spherical collectors provided that the surface of the collector is previously covered with a thin layer of non-volatile liquid. It is entirely possible that a solid aerosol may be removed without covering the surface of the collector. However, such experiments will yield no useful general information, as the nature and magnitude of the cohesive forces between solid surfaces are a function of the surface materials, and will be different for each aerosol and collector substance. Corn[D6] gives a review of the subject and shows that the adhesion of solid particles to solid surfaces is dependent on the physical and chemical properties of the particles and the collector. Particle size, shape and microscopic surface texture, the microscopic surface texture of the collector and the presence of electrostatic charges all contribute to variations in observed forces of particle adhesion. Thus such an experiment is necessarily specific to the physical and chemical composition of the collector and aerosol*. The present experiments specifically refer to penetration of solid aerosols through a fluidized bed with no re-entrainment. They may therefore be used as a baseline for interpretation of data on collection of solid aerosols on dry collector surfaces. Any consistent deviation from these results can be attributed to re-entrainment of the captured aerosol particles in the fluidized bed. Inspection of Figure 6.11

*It may be noted in passing that this fact casts some doubt on the extrapolation of Paretsky's[P1] experiments on collection of latex particles by a fixed bed of fly ash to collection of fly ash on fly ash.

and Table 6.10, where penetration is given in tabular form, shows that the aerosol penetration is below 1% for a bed height of over 0.1 m. This is additional confirmation that, provided an adequate distribution of the gas is ensured, very high collection efficiencies of aerosols may be achieved in a fluidized bed. Therefore, high penetrations reported in previous studies must be partially attributed to ineffective distributors, resulting in formation of large bubbles giving significant by-passing. The third conclusion is that the penetration of methylene blue is consistently lower than the penetration of DOP. Again, this indicates negligible re-entrainment. It may be noted that methylene blue has a density of $1.2 \times 10^3 kg/m^3$, compared to $9.72 \times 10^2 kg/m^3$ for DOP. Combined with the results for DOP in earlier sections, we can now conclude that collection efficiency increases with both ρ_A and d_A. This gives further support to the conclusion, indicated previously, that the dominant collection mechanisms of micron-sized aerosols in fluidized beds of 110 μm collector are inertial and gravitational.

6.3.3 Testing the performance of the particle counter

Inspection of Figure 6.12, where the results of Figure 6.11 are shown on semi-logarithmic axes, shows that the scatter about the experiments with liquid DOP, where the particle counter was operating in SINGLE mode is, evidently, more than the scatter in the methylene blue experiments where the counter was operating on TOTAL mode. Thus the major error in the equipment appears to be in the particle counter and is at the cut-off point between size ranges. This section of the counter is called "the discriminator" by the manufacturers. According

TABLE 6.10 Penetration in Fluidized Bed Experiments, Methylene Blue Aerosol, d_A — 1.2 μm, d_p — 110 μm, U — 0.13 m/s

H_{mf}	f'
1.11	39.2 %
1.44	28.2 %
2.04	18.7 %
2.63	12.2 %
3.37	6.96 %
4.33	3.33 %
5.55	1.47 %
7.14	.88 %
9.25	.47 %
12.00	.33 %

to the manufacturers the error results from unavoidable electrical "noise" in the apparatus and changes in voltages of the order of fractions of a millivolt cause a small fraction of the particles to be counted in an upper or lower channel. From Figure 6.12, from the manufacturers[R5] and from our experimental experience this error is of the order of a few per cent, normally distributed and can be reduced when averaged over a few readings as was done in this study. Thus operation in SINGLE mode sacrifices the almost absolute number count accuracy for greater accuracy in determining the size of the particles.

6.3.4 Behaviour of a deep fluidized bed

Inspection of Figure 6.12 provides further information on the collection behaviour of the fluidized bed as a function of bed depth. This observation may be made visually from Figure 6.12 because of the very high accuracy of this set of experiments, achieved by summing three channels of the particle counter. As seen from the figure the semi-logarithmic plot of penetration versus bed height is almost exactly linear up to a bed depth of 6×10^{-2} m. This provides conclusive evidence that the gas in that section of the bed is in plug flow, and that interchange between the bubble and dense phase is not the limiting step of the process. For beds deeper than about $6 - 7 \times 10^{-2}$ m this is not true, and penetration is much less sensitive to subsequent increases in bed depth. Thus, at these bed depths, the bubbles in the bed have coalesced to a size sufficiently large for interchange between the bubble and dense phases to be relatively less rapid and thus influence the overall collection. Therefore, all other experiments of this study were performed with

beds shallower than 7×10^{-2} m, where the assumption of negligible resistance between the bubble and dense phase has been confirmed. It may be noted that the efficiency of a 7×10^{-2} m bed is in any case quite high and can be increased to over 95% for 1.35 μm particles if the superficial gas velocity through the bed is increased sufficiently; this is discussed in Section 6.5. For greater bed depths, devices such as baffles to reduce bubble size would be necessary to take advantage of the extra depth.

6.4 Comparison with Collection in a Fixed Bed

6.4.1 Introduction

In this study, analysis of experimental results indicated the existence of a velocity range for the 600 μm collector particles where a fluidized bed, collecting aerosol particles, was much more efficient than a fixed bed of the same depth and operating at the same velocity. The existence of such a velocity range effectively proves that the dense phase of a fluidized bed cannot be considered to be similar to a fixed bed for aerosol collection and that the fluctuating movement of the collector particles by the bubbles greatly enhances aerosol collection. Comparison with previous work showed that in at least one other study experimental results supporting this conclusion were obtained[K3]. Unfortunately, as will be seen below, the authors interpreted their results in a manner which did not reveal their importance.

6.4.2 Comparison of a fixed and a fluidized bed collecting aerosol

Table 6.6 shows experiments with a 1.55 μm DOP aerosol, and penetration is measured as a function of gas velocity at different bed

heights. The lowest ($H_{mf} = 1.9 \times 10^{-2}$ m) and the deepest bed heights ($H_{mf} = 8.8 \times 10^{-2}$ m) are plotted on Figure 6.7; penetrations at intermediate bed heights fall between these two limits. On the same figure the penetration of 1.35 μm diameter DOP aerosol through a 0.09 m fixed bed of 600 μm collector particles is plotted for comparison. In Chapter 4 it was noted that these particles fluidize at a superficial gas velocity of 0.3 m/s. From the fixed bed results in Figure 6.7, it is seen that at this superficial gas velocity penetration decreases sharply with increasing velocity. The primary collection mechanism in the fixed bed is then inertial deposition (see Chapter 5). If it is assumed, from the two phase theory of fluidization, that the gas in the dense phase travels with velocity of order U_{mf}, then the primary collection mechanism in the fluidized bed must also be inertial. Having now clarified these points we can observe, from Figure 6.7, that at a superficial gas velocity between 0.38 and 0.5 m/s the fluidized bed is much more efficient than a fixed bed of the same depth in removing particulates of the micron size range. As the pressure drop across the fixed bed is higher than the pressure drop across a fluidized bed at $U > U_{mf}$, this additional collection by the fluidized bed is achieved at significant saving in pressure drop.

This is a very important result, both from an academic and industrial point of view. It disagrees with the conclusions of all previous workers, and also could not have been foreseen from the two phase theory of fluidization. However, at least one previous study, by Knettig and Beeckmans[K4] (see Chapter 2) who used an adequate distributor design, gave experimental results which support this conclusion.

Unfortunately, these authors interpreted their results on the basis of an arbitrarily defined "grid region of a fluidized bed", and neglected experimental points in this region. This led them to conclude, erroneously, that "capture efficiency in the body of the fixed bed is larger than in the case of the fluidized bed". Diffusion was quoted, quite wrongly, as a possible collection mechanism (see Table 5.6) and results were expressed in the form[K4]

$$NTU = \text{constant} + k'H \tag{6.3}$$

where

$$NTU = -\ln(f) \tag{6.4}$$

where k' is the collection coefficient per unit bed height and H is the bed height of a fixed bed or the bed height at minimum fluidization of a fluidized bed. Knettig and Beeckmans, however, based all their conclusions on the value of k' neglecting the constant in both fixed and fluidized bed results. The author agrees entirely with neglect of the constant in Equation (6.3) for fixed beds because, as discussed in Section 5.2, this results from small end effects. However, there is no theoretical justification for neglecting the most important region of a fluidized bed, which is situated above the distributor. It will be interesting to note at this point that the bed depth neglected by Knettig and Beeckmans (2.5×10^{-2} m) is almost equal to the total bed height of the fluidized bed used by McCarthy *et al.*[Mc1] (2.54×10^{-2} m). The experimental results of Knettig and Beeckmans were recalculated from their data, using Equations (6.3) and (6.4), and are presented in

Table (6.11) assuming a bed height of 0.1 m in each case; for aerosol removal, this is a relatively deep bed.

The values in parentheses are calculated penetrations for the fixed bed without excluding the constant in Equation (6.3) and are given here only for completeness as they include end effects. As inspection of Table 6.11 will show, in the experiments by Knettig and Beeckmans a 0.1 m high fluidized bed at a superficial gas velocity of 0.14 m/s is far more efficient than a fixed bed of the same height and operating at the same velocity in removing aerosol particles 0.8 μm and 1.6 μm diameter. For 2.9 μm aerosol particles the two beds are effectively equal in efficiency. We are therefore faced with the important qualitative observation that a shallow fluidized bed is far more efficient than a fixed bed at certain operating conditions. This analysis strengthens even further our hypotheses that bubble to dense phase transfer is relatively rapid (presumably due to bubble coalescence) especially near the distributor plate, and collection is enhanced by bubble-induced particle motion.

Tables 6.8 and 6.9 present additional experiments on 1.75 μm and 2.5 μm diameter aerosols. As seen from these tables, there is very little penetration of these aerosol sizes. Over 99% of 1.75 μm aerosol is collected by a 8.8×10^{-2} m deep bed operating at 0.74 m/s and virtually all of the challenging 2.5 μm aerosol is collected by a bed approximately 5×10^{-2} m deep at the same gas velocity. Comparison of Tables 6.8 and 6.9 with the results of Knettig and Beeckmans (Table 6.11) shows the bed used in this study to be more efficient, probably as a result of better gas distribution at the higher velocities used here.

TABLE 6.11 Results of Knettig and Beeckmans, Assuming a Bed Height of 0.1 m

	U m/s	d_A (μm)	f'
Fixed bed, screen supported	0.112	0.8 1.6 2.9	58% (57%) 45% (38%) 5% (3%)
Fluidized bed, orifice plate distributor	0.138	0.8 1.6 2.9	31% 14% 5%

The higher U_{mf} of the 600 μm collectors must also have contributed to an increased inertial collection in the dense phase.

Some of the results on penetration of 1.75 μm DOP aerosol (Table 6.8) are shown in Figure 6.8 and compared, in the same way, to a similar set of fixed bed experiments. An identical picture emerges and inspection of Figure 6.8 suggests that the efficiency of the fixed bed will overtake the fluidized bed efficiency at a gas velocity around 0.5 m/s. Between 0.3 and 0.5 m/s, however, the fluidized bed is more efficient than a fixed bed as noted above. Two final observations are made from Figures 6.3 to 6.8. The first is that aerosol penetration decreases with increasing aerosol diameter. This gives additional strength to the theory of enhanced inertial collection and is discussed in more detail in Section 6.6. The second is that extrapolated lines of fixed bed experiments in Figures 6.7 and 6.8 meet the fluidized bed penetration curves at a point nearer to $U/U_{mf} = 1.0$, for larger d_A, suggesting that the advantage of increased inertial collection in a fluidized bed over a fixed bed decreases with increasing aerosol diameter. This is also seen in the results of Knettig and Beeckmans where the two beds perform almost equally in removing 2.9 μm aerosol particles.

6.5 High Velocity Experiments ($0.8 < U < 3.0$ m/s)

6.5.1 Introduction and description of experiments

In the experimental results presented previously in this chapter a definite trend of decreasing penetration with increasing superficial gas velocity was noted. In order, therefore, to perform experiments at higher superficial gas velocities a second experimental

apparatus was designed and built. All experiments reported here were performed in the velocity range from 0.8 to 2.9 m/s and it should be noted that this is at least one order of magnitude higher than previous experimental studies reported in the literature. Experiments were performed with the 600 μm collectors described previously, and with high density 550 μm collector particles (4.5×10^3 kg/m^3) which fluidized at a superficial gas velocity of 0.44 m/s. Penetration of 1.35 μm and 1.75 μm DOP aerosol particles was measured as a function of bed height at minimum fluidization and superficial gas velocity through the bed. The conical orifice distributor used in this set of experiments is described in Section 4.3 (see also Figure 4.6b) and had, approximately, a 7% free area on the top surface of the plate.

6.5.2 Effect of gas velocity; comparison of two distributors

Figures 6.14 and 6.15 show the penetration of 1.35 μm and 1.75 μm diameter DOP aerosol particles as a function of superficial gas velocity, expressed as a multiple of minimum fluidization velocity (U/U_{mf}) for different bed heights. Also shown on these figures are penetrations of 600 μm collector particles obtained at similar conditions but with distributor A, (see Figure 4.6a) used for experiments at lower gas velocities (data presented in Tables 6.6 and 6.7). Inspection of Figures 6.14 and 6.15 shows that the trend of increasing efficiency with increasing gas velocity extends to a higher velocity range, as expected. Very low penetrations are obtained with relatively low bed heights and, from the figures, a 0.046 m deep bed operating at 2.1 m/s collects about 94% and 98% of the 1.35 μm and 1.75 μm aerosol particles, respectively. There

FIGURE 6.13 Fluidized bed experiments - DOP aerosol penetration versus aerosol diameter

$d_p = 110\ \mu m$
$H_{mf} = 3.06 \times 10^{-2}$ m
upper line, $U = 4.9 \times 10^{-2}$ m/sec
lower line, $U = 2.6 \times 10^{-1}$ m/sec

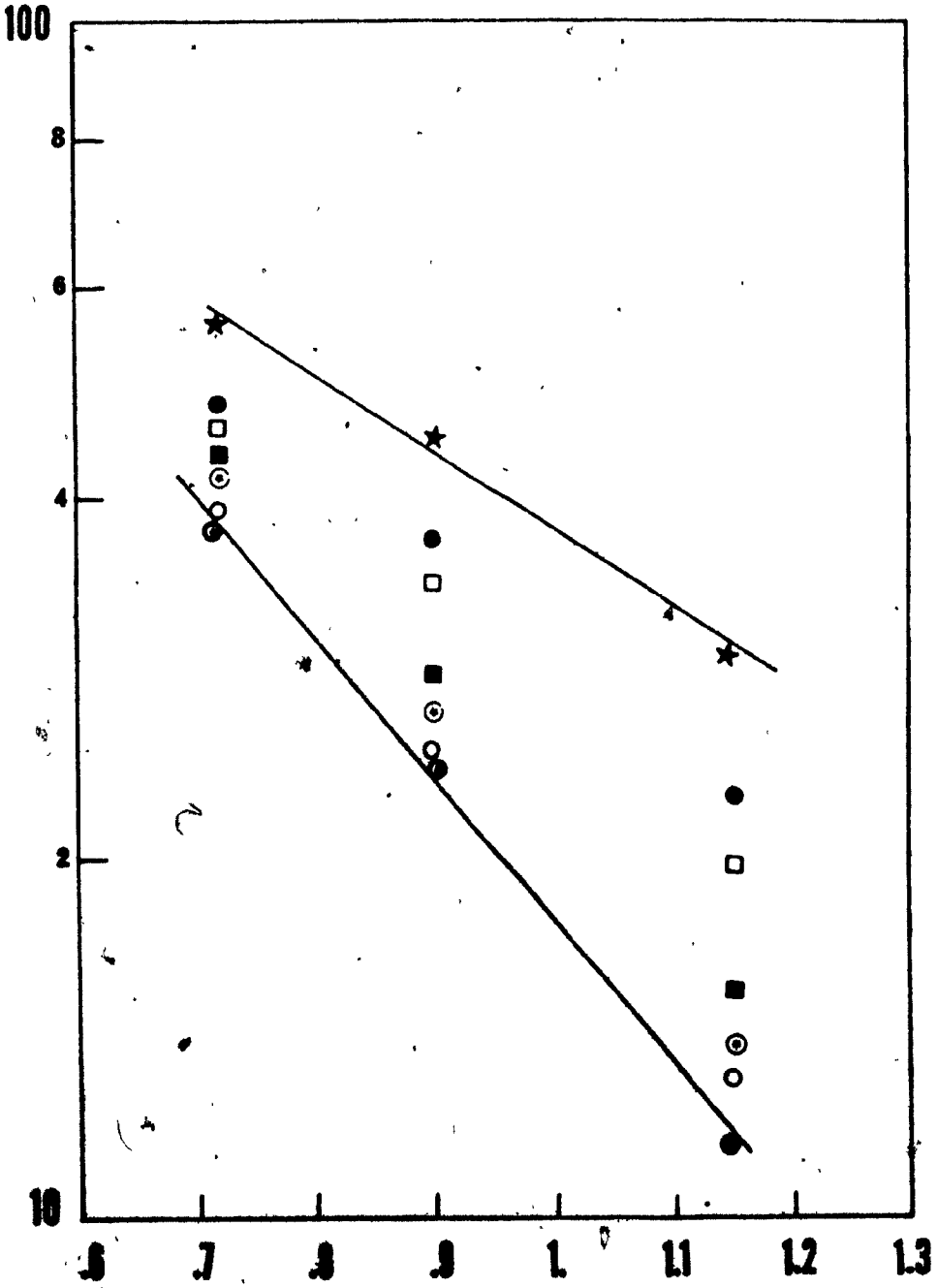
100
8
6
4
2
10
f'
.6
.7
.8
.9
1.
1.1
1.2
1.3
d_A , μm.

FIGURE 6.14 Fluidized bed experiments - DOP aerosol penetrator versus U/U_{mf}

$d_A = 1.35$ μm
$d_p = 600$ μm
open square, $H_{mf} = 0.74 \times 10^{-2}$ m
full circle, $H_{mf} = 1.85 \times 10^{-2}$ m
open circle, $H_{mf} = 4.63 \times 10^{-2}$ m
full circle with border, $H_{mf} = 1.86 \times 10^{-2}$ m (old distributor)
open circle with asterisk, $H_{mf} = 3.98 \times 10^{-2}$ m
circle with border and asterisk, $H_{mf} = 6.78 \times 10^{-2}$ m

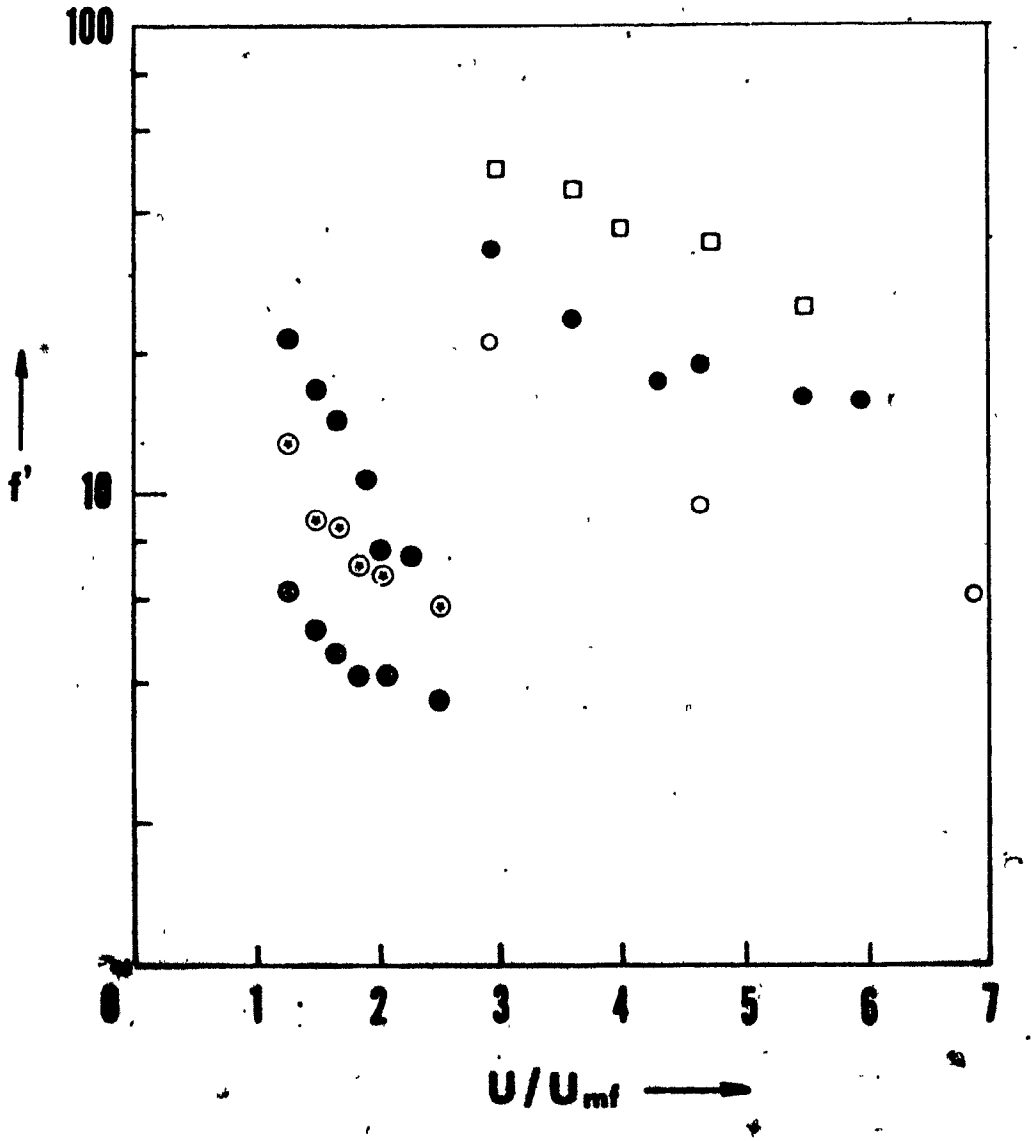
100
f'
10
0
1
2
3
4
5
6
7
U/U_mf

FIGURE 6.15 Fluidized bed experiments - penetration of DOP aerosol particles versus U/U_{mf}

$d_A = 1.75$ µm
$d_p = 600$ µm
open square, $H_{mf} = 0.74 \times 10^{-2}$ m, distributor B
full circle, $H_{mf} = 1.85 \times 10^{-2}$ m, distributor B
open circle, $H_{mf} = 4.63 \times 10^{-2}$ m, distributor B
full circle with border, $H_{mf} = 1.86 \times 10^{-2}$ m, distributor A
open circle with asterisk, $H_{mf} = 3.98 \times 10^{-2}$ m, distributor A
circle with border and asterisk, $H_{mf} = 6.78 \times 10^{-2}$ m, distributor A

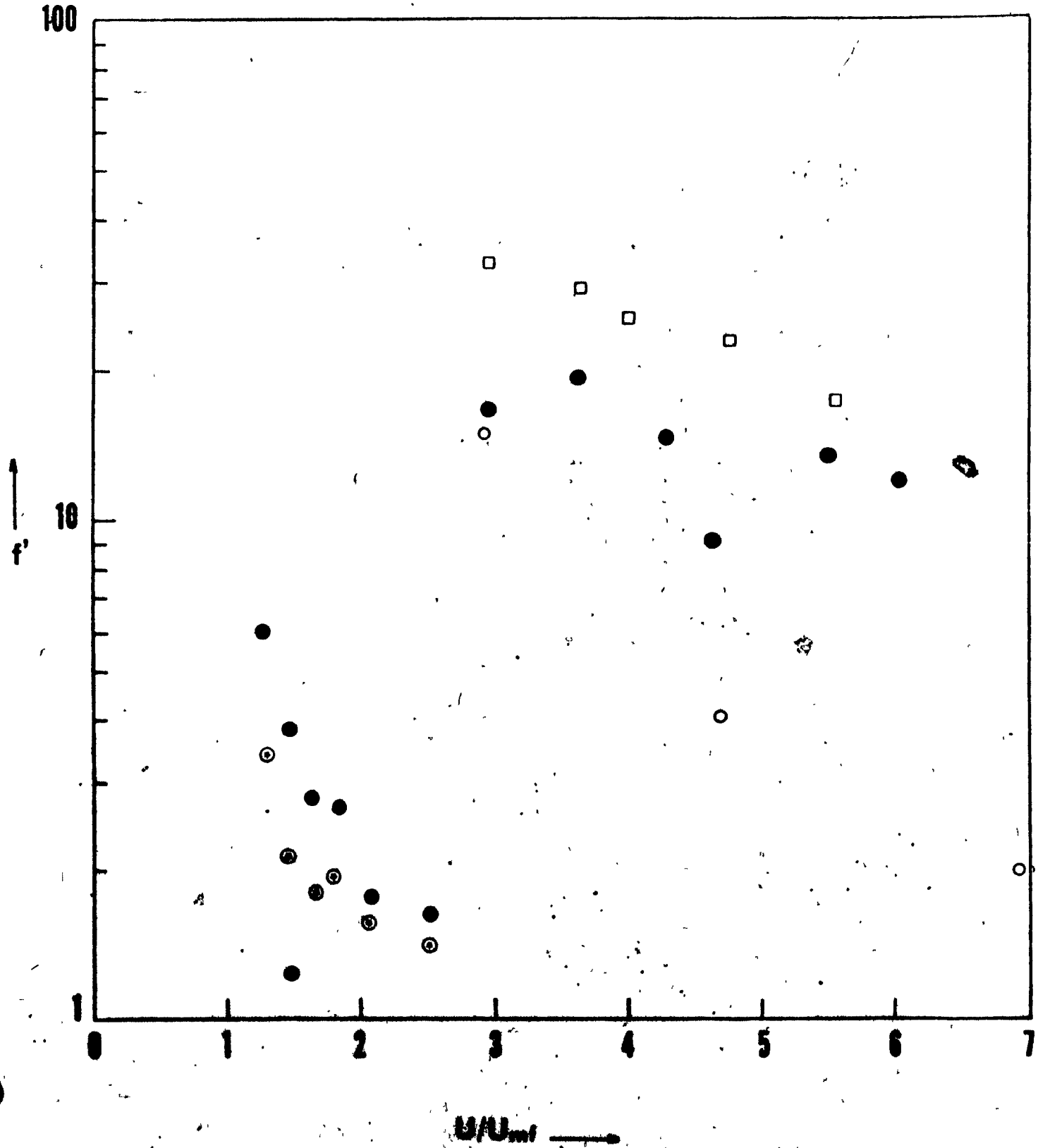
100
10
1
f'
0
1
2
3
4
5
6
7
U/U∞

is a substantial decrease in penetration with velocity and the bed operates most efficiently at higher velocities. These penetrations are substantially lower than those predicted by previous studies from extrapolation of their experiments performed at low superficial gas velocities. Visual observation of the bed during operation showed that at such high gas velocities the collector particles were agitated very rapidly and the bed depth increased by about 0.1 m. Individual bubbles comparable to the diameter of the bed were formed and the bed was approaching the slug flow régime although it was too shallow for the formation of stable slugs. Inspection of Figures 6.14 and 6.15 shows a substantial effect of distributor design on the amount of aerosol penetrating the bed. As distributor B (Figure 4.6b) had a much larger free surface area, this resulted in a lower pressure drop across the plate giving poorer distribution of the incoming gas. The two sets of experiments lie in different portions of the penetration versus velocity plot, and even an approximate correlation of the two sets would be grossly inaccurate. This inspection of the superior performance of a more efficient distributor facilitates interpretation of the disheartening conclusions reached by previous studies. Thus, the effect of the most important section of a fluidized bed has been demonstrated experimentally for the second time in this study, the first time being in Section 6.2.1, and it is concluded that adequate distribution of the gas in aerosol studies in fluidized beds is of prime importance.

6.5.3 Experiments with high density collectors; further conclusions on dominant collection mechanisms

Table 6.13 presents experiments performed on high density collector particles ($\rho_p = 4.49 \times 10^3$ kg/m^3) where penetration of 1.35 μm and 1.75 μm aerosols was measured as a function of superficial gas velocity and bed height at minimum fluidization. Results from Table 6.13 are shown in Figures 6.16 and 6.17 where the penetration of the challenging aerosol is plotted as a function of superficial gas velocity. Comparison of these results with experiments performed on 600 μm collectors shows the high density particles to be more efficient. If the characteristic velocity of the beds is taken as the superficial gas velocity then the denser particles, with a higher U_{mf} and a lower diameter have a significantly higher Stokes number. The observed increase in efficiency is therefore consistent with an inertial collection mechanism, but cannot be explained by gravitational or diffusional collection. Interception is also unlikely to explain the improved performance, since the interception parameter (N_R) is only very slightly larger for the dense particles. Moreover, as discussed in Section 6.6, it is unrealistic to distinguish between interception and inertial collection when the dense phase is rapidly agitated as under the conditions of these experiments.

6.5.4 Industrial implications of high velocity experiments

Although discussed more extensively in Chapter 8, the industrial implications of these experiments will be mentioned here. As observed from the experimental results (Tables 6.12 and 6.13) aerosol collection by a fluidized bed is substantial even when the bed is operated at very high velocities. In fact, measured collection efficiencies are at least

TABLE 6.12 Penetration in Fluidized Bed High Velocity Experiments, d_p = 600 μm

DISTRIBUTOR B

U, m/s	H_{mf}, mx10^2	f'	
		1.35 μm	1.75 μm
0.88	0.74	49.8	32.9
1.09	0.74	42.3	28.9
1.19	0.74	37.0	25.2
1.42	0.74	34.4	23.2
1.66	0.74	24.6	17.0
0.88	1.85	33.5	16.3
1.09	1.85	23.4	19.4
1.30	1.85	17.1	14.7
1.40	1.85	18.9	8.8
1.66	1.85	16.2	13.7
1.81	1.85	15.9	12.1
0.88	4.63	21.6	15.1
1.40	4.63	9.7	4.1
2.07	4.63	6.2	2.0
1.42	0.63	41.6	27.1
1.42	1.07	28.6	16.2
1.42	1.85	21.5	10.1
1.42	3.15	15.7	6.6
1.42	5.18	7.8	6.5
1.42	7.96	4.0	3.8

TABLE 6.13 Penetration in Fluidized Bed High Velocity Experiments, $d_p = 550$ μm

DISTRIBUTOR B

U, m/s	H_{mf}, mx10^2	f'	
		1.35 μm	1.75 μm
1.42	0.74	19.4	8.7
1.42	1.52	7.6	4.3
1.42	2.22	5.7	2.6
1.66	0.74	17.2	7.7
1.66	1.52	7.2	4.7
1.66	2.22	3.9	1.5
1.89	0.74	15.9	10.0
1.89	1.52	6.4	5.3
1.89	2.22	3.7	1.4
2.07	1.52	6.2	4.9
2.07	2.22	3.7	2.2
2.41	1.52	5.6	4.5
2.41	2.22	2.6	1.7
2.85	1.52	4.9	3.9

FIGURE 6.16 Aerosol penetration versus superficial gas velocity for high velocity experiments

d_p = 550 μm (high density particles)
d_A^p = 1.35 μm
open circle, H_{mf} = 0.74 mx10^2
full circle, H_{mf} = 1.52 mx10^2
open square, H_{mf} = 2.22 mx10^2

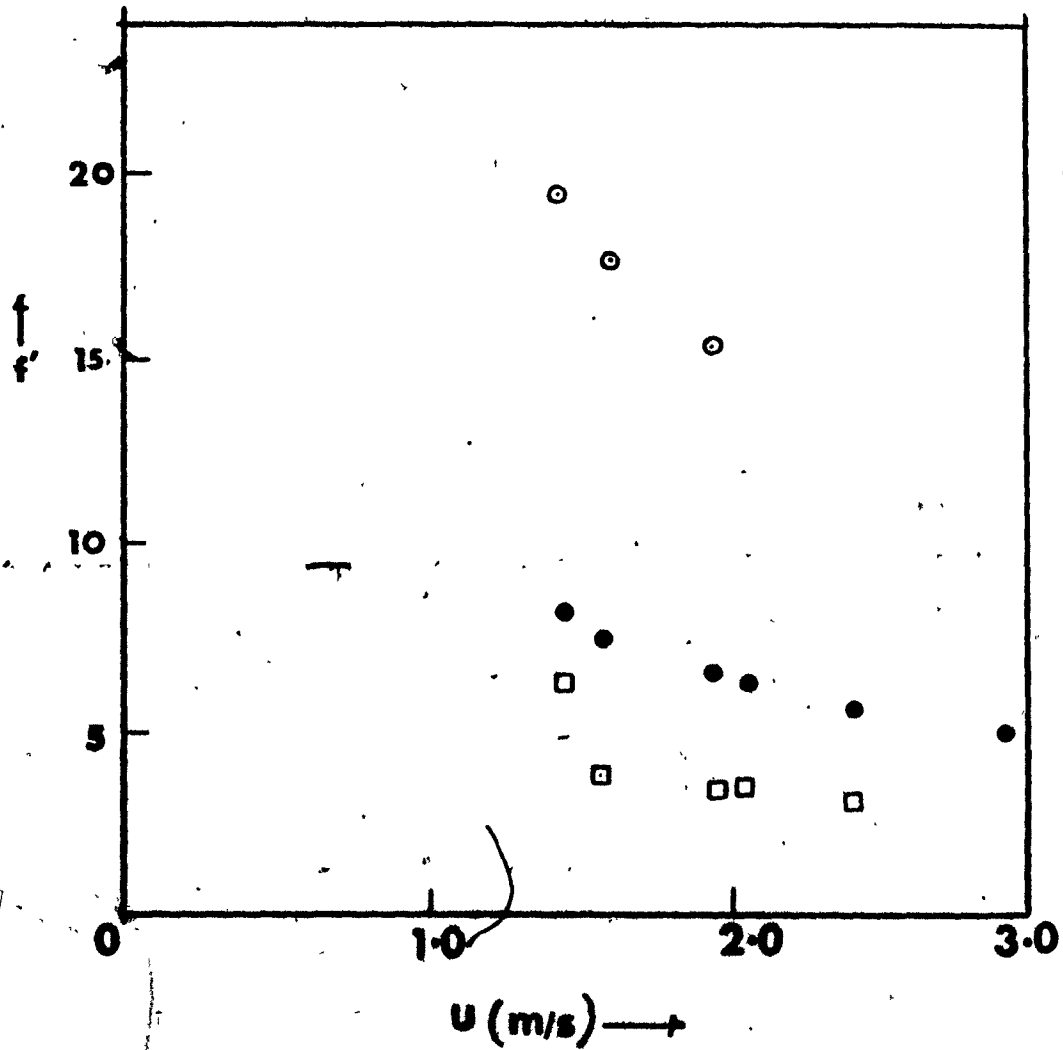
20
15
10
5
0
f
f'
1·0
2·0
3·0
U (m/s)

FIGURE 6.17 Aerosol penetration versus superficial gas velocity for high velocity experiments

d_p = 550 μm (high density particles)
d_A^p = 1.75 μm
open circle, H_{mf} = 0.74 mx10^2
full circle, H_{mf} = 1.52 mx10^2
open square, H_{mf} = 2.22 mx10^2

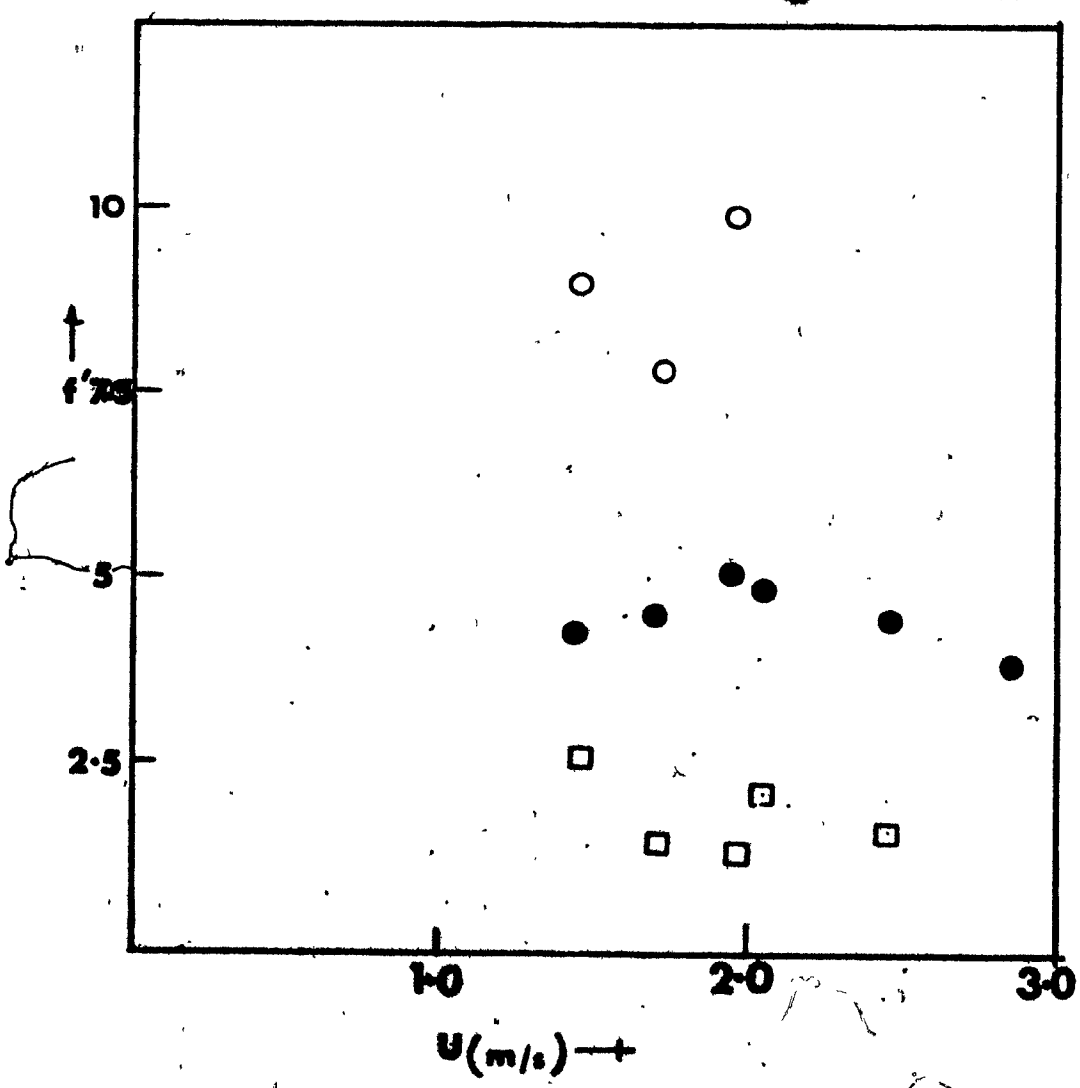
10
5
2·5
1·0
2·0
3·0
U(m/s)

an order of magnitude higher than the values suggested by extrapolation of experimental results obtained at low superficial gas velocities in previous studies. As the operable range of superficial gas velocity through the bed is increased (as was done here by at least an order of magnitude) the physical dimensions of such a filtering device are correspondingly reduced, together with the capital and maintenance cost of the process. Therefore, the practical significance of the experiments presented in this section is that they have increased the potential capacity of a fluidized bed collecting aerosol particles by at least one order of magnitude. It may be noted that these results give no indication of an upper velocity limit, beyond the requirement that the collector particles must not be entrained out of the bed.

6.6 Identification of Dominant Collection Mechanisms

The functional dependence of penetration on aerosol diameter is determined by the dominant collection mechanism. In Chapter 5 it was shown that the dominant collection mechanism, for micron range aerosol particles, in the fixed bed experiments of this study was inertial deposition. Gravitational settling was found to be the second most important mechanism, affecting the collector particle efficiency at low superficial gas velocities. These conclusions were in general agreement with most previous studies. However, the situation is quite different for aerosol removal in fluidized beds. Most previous studies have claimed that diffusion and interception were the dominant collection mechanisms. These conclusions resulted primarily from inspection of experimental results where penetration was measured as a function of superficial gas velocity.

These authors seem to have regarded the fluidized bed as a homogeneous contactor. The inference that diffusion is the dominant collection mechanism was therefore drawn from observations of increasing penetration with increasing gas velocity. In previous sections it was shown that this kind of behaviour actually results from operating the bed at low superficial gas velocity, and is aggravated by poor distributor design which results in a large portion of the gas bypassing the bed in the form of large bubbles. We have also argued that the dominant collection mechanisms in fixed and fluidized beds should be the same, assuming that the characteristic velocity in a fluidized bed can be taken as U_{mf}. However, there is at least one study[K3] where the authors claim that for an exactly similar set of operating conditions (i.e. for similar bed collector diameter, aerosol diameter and superficial gas velocity) inertial collection is the dominant collection mechanism in fixed beds while diffusion and interception are dominant in fluidized beds. It is therefore useful at this stage to consider the dependence of penetration on aerosol diameter.

Figure 6.13 shows the per cent penetration of three sizes of aerosol particles (0.72 μm, 0.9 μm and 1.15 μm) through a 3.1×10^{-2} m deep bed of 110 μm collectors. On the figure the penetrations of the three aerosol sizes, measured at seven different superficial gas velocities, are plotted on semi-logarithmic axes as a function of aerosol diameter, μm. The velocity through the fluidized bed ranged from 4.9×10^{-2} m/s ($U/U_{mf} = 2.5$) to 0.26 m/s ($U/U_{mf} = 13$).

As the per cent penetration decreases with increasing aerosol diameter, it is evident that the dominant collection mechanism cannot

be diffusion. If it were, then penetration would increase with increasing aerosol diameter. As inspection of Figure 6.13 will show, the dependence of penetration on aerosol size becomes stronger as the superficial gas velocity through the bed is increased. At higher velocities the mean residence time of an aerosol particle in the bed is lower, giving relatively less gravitational settling. Electrostatic collection, discussed in Chapter 3 is another possible contribution. However, the aerosol particles in this study were electrically neutral (see Section 4.2.1). Moreover, the experiments were performed with a wide range of relative humidity in the fluidizing air, from very low values (winter) to values in excess of 90% (high summer). It is known that[B7] electrostatic charge dissipation in fluidized beds is strongly dependent on relative humidity, especially above 70%. No difference could be detected between penetration measurements using dry and very humid air. Hence it may be concluded that electrostatic effects were not significant in this study.

The possible mechanisms remaining are interception and inertia. It was shown in Chapter 5 that interception is not a significant mechanism in fixed beds under the conditions of the experiments performed. Moreover, it is unrealistic to make a clear distinction between inertial and interception collection when the collector particles are agitated, as in the dense phase of a fluidized bed. The combined mechanism will therefore be termed "inertial collection", this term being suggested by the increase of collection with increasing ρ_A, d_A and decreasing d_p noted earlier.

6.7 Summary

This chapter described experiments performed on collection of 0.7 - 1.7 μm diameter liquid and solid aerosol particles by fluidized beds. Solid aerosol particles could be collected provided the surface of the collector was covered with a non-volatile liquid. High collection efficiencies were observed and penetration decreased exponentially with bed height till the bypassing of aerosol in the form of large bubbles became dominant at H_{mf} greater than 0.06 m. Penetration increased with increasing velocity close to minimum fluidization, but subsequently reached a peak and decreased steadily. The increased efficiency of a fluidized bed operating at high velocities is the result of a more effective distribution of gas, enhancement of the bubble to dense phase transfer mechanism by rapid bubble coalescence near the distributor plate, and enhanced inertial collection due to the rapid agitation of the collector particles by the rising bubbles. Diffusion and gravitation are minor collection mechanisms while inertial deposition is dominant; this is verified by observing that efficiency increases with increasing U_{mf}, ρ_A, d_A and decreasing d_p. Over a narrow velocity range a fluidized bed is more efficient than a fixed bed; there is at least one previous study with similar experimental results supporting this conclusion. The distributor of the bed is an important design variable as it influences the initial bubble size in the bed and thus the amount of aerosol penetration. Fluidized bed experiments at superficial gas velocities approaching 3 m/s are presented and the industrial implications of these experiments are mentioned.

CHAPTER 7. MATHEMATICAL ASPECTS OF AEROSOL REMOVAL IN A FLUIDIZED BED OF COLLECTOR PARTICLES

7.1 Introduction

The previous chapter presented experimental data on aerosol collection in fluidized beds of spherical collector particles. Qualitative analysis of the data indicated dominance of the inertial collection mechanism in fluidized beds collecting micron range aerosol particles. In the first part of this chapter the collection coefficients obtained from fixed bed experiments are used to estimate aerosol collection in the immediate vicinity of an isolated bubble. A Davidson bubble, surrounded by a concentric spherical cloud, is considered and numerical estimates of the percentage of uncollected aerosol are obtained as a function of bubble diameter, aerosol particle diameter and bed height at minimum fluidization. In view of the simplifying assumptions made and described below, no great accuracy may be attached to the numerical estimates of the model. However, when its predictions are compared with the experimental results of this study, they suggest strongly that the lean phase of a shallow fluidized bed collecting aerosol particles may not be visualized as consisting of isolated bubbles rising to the surface without interaction with their neighbours. Overall collection in the dense phase is then treated in Section 7.3. Estimates for the collection coefficients, and more conclusive evidence for the dominant collection mechanism are obtained.

7.2 Aerosol Collection Around Isolated Bubbles

7.2.1 Introduction

The experimental data presented in Chapter 6 indicated the enhancement of aerosol collection in a fluidized bed operating at high superficial gas velocities. It is possible that this increased collection could be due to the higher relative velocities occurring between the fluid and particles in the "cloud" surrounding the bubble (see Section 7.2.2). However, this has not been analyzed previously. The purpose of this section is to estimate the amount of aerosol collected in the dense phase around an isolated bubble, and to determine the significance of increased collection resulting from the higher relative velocity between the collector particles and the fluid.

7.2.2 Definition of the bubble

The analysis is based on the theory developed by Davidson and Harrison[D1] and their bubble model is shown schematically in Figure 7.1. A fluidized bed bubble is considered to be a spherical void and, if it is isolated and remote from the boundaries, there are known stream functions to describe the associated gas and particle motion. The fluid within a rising bubble is assumed to stay with the bubble but to make regular excursions into the surrounding particulate phase without, however, travelling beyond the surface of a sphere concentric with the bubble. This sphere, surrounding the bubble, is called "the bubble cloud". The Davidson bubble is not as accurate in predicting the cloud shape and the streamlines around the bubble as later models developed by Jackson[J1] and Murray[M3]. However, as only approximate estimates of the aerosol

FIGURE 7.1 Gas streamlines and particle trajectories around a spherical Davidson bubble

full lines, particle trajectories
broken lines, fluid streamlines

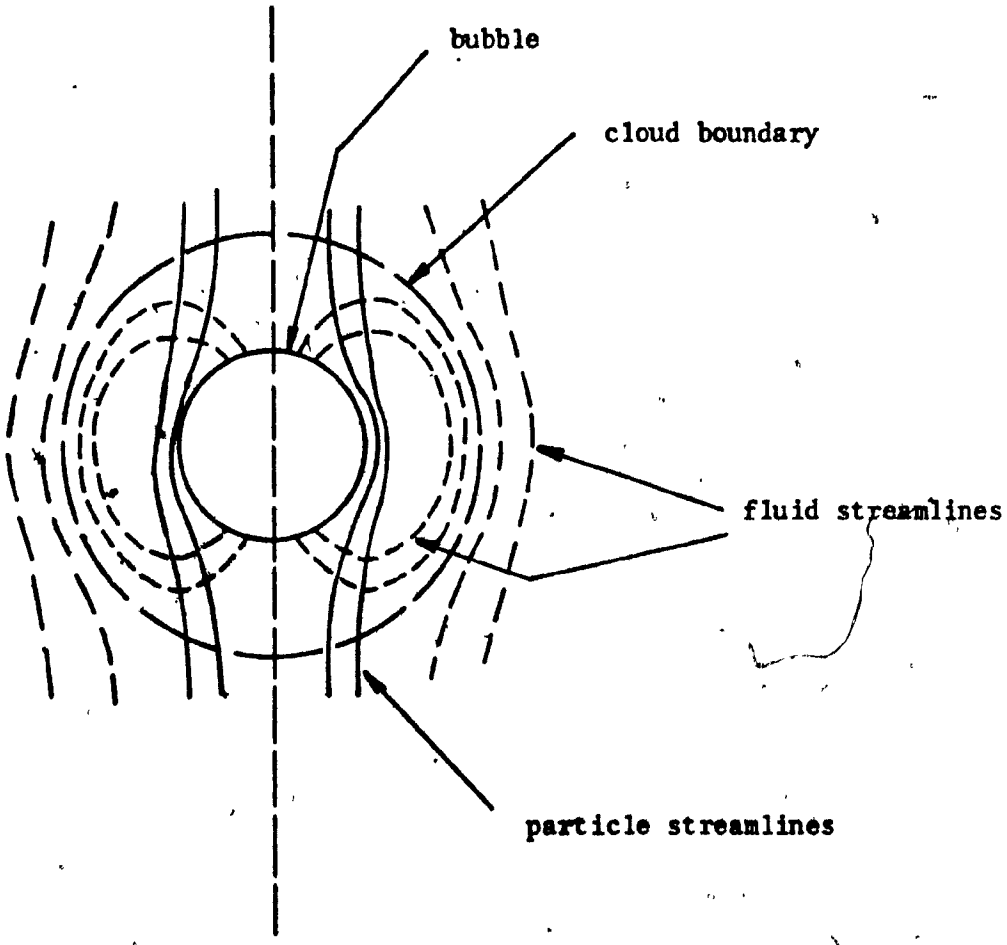
bubble
cloud boundary
fluid streamlines
particle streamlines

collected around bubbles were required it was prefered for its simplicity.

Davidson and Harrison propose that the motion of the solids is simply superimposed on what would otherwise be the motion of the gas. The local velocity is, then, the vector sum of the gas velocity amongst stationary particles and the particle velocity. The particle and the fluid streamlines are shown schematically in Figure 7.1.

It should perhaps be mentioned that a "fast" bubble, i.e. a bubble travelling faster than the fluid in the particulate phase is described here. In the case of "slow" bubbles, i.e. bubbles with a rise velocity lower than the interstitial velocity of the fluid in the particulate phase, the bubble cloud does not exist and the fluid uses the spherical void termed "bubble" as a short cut when rising to the surface. Fluidized beds where the fluid in the particulate phase rises faster than the bubbles are called "teeter beds", using Squires'[S5] terminology, and experiments in this study performed with 600 μm and 550 μm collector particles belong to this type of fluidization.

7.2.3 Bubble velocity and bubble diameter

There is an analogy between liquids and fluidized beds applied to bubble rise velocity. Davies and Taylor[D10] derived the rise velocity of a spherical cap bubble in a liquid as

$$U_b = \frac{2}{3}\sqrt{gr_b} \qquad (7.1)$$

where r_b is the radius of curvature of the bubble at its nose. Although r_b is not the same as the radius of the circumscribing sphere it will be

considered, as an approximation, to be so. Collins[C10] has shown that for three-dimensional bubbles in liquids the error in making this assumption is of the order of a few per cent only.

Extending the analogy between a liquid and a fluidized bed, an estimate of the size of bubble formed at a multiorifice type distributor may be obtained. In gas liquid systems Davidson and Schüler[D3] calculated the volume of an individual bubble in a stream produced at an orifice to be

$$V_b = 1.138 \frac{G^{1.2}}{g^{0.6}} \tag{7.2}$$

where G is the volumetric gas flow rate through the orifice. Harrison and Leung[H2] made analogous experiments on bubble formation from an injector tube placed in a bed at minimum fluidization and confirmed Equation (7.2) for fluidized beds. For a fluidized bed G is defined as the volumetric gas flow rate through an orifice in excess of minimum fluidization. Leung[L13] suggests Equation (7.2) for the design of distributors in gas fluidized beds. For the spherical bubble model used in this study, Equation (7.2) may be re-arranged to give the bubble diameter

$$d_b = 0.324 * \frac{G^{0.4}}{g^{0.2}} \tag{7.3}$$

Thus, using Equation (7.3), and a superficial gas velocity range of $0.03 < U < 0.3$ m/s for the 110 μm collectors and $0.35 < U < 0.7$ m/s for the 600 μm collecters, estimates for the initial bubble size ranges

formed at the multiorifice distributor of this study (Distributor A, Figure 4.4a) may be obtained. These are presented in Table 7.1, together with estimated bubble velocities, calculated from Equation 7.1 and bubble residence times assuming a bed depth of 0.1 m. These approximate values serve in providing an insight into the physical dimensions of the quantities involved in this study.

7.2.4 Exchange of aerosol between the bubble and the particulate phase

The fluid in a rising bubble is exchanged continuously with the fluid in its vicinity. This transfer is the result of two contributing mechanisms, namely transfer by throughflow and transfer by diffusion. Approximate estimates of these transfer rates may be obtained from the analysis presented by Davidson and Harrison for the percolation of gas through a spherical void in a particulate bed. Assuming the motion of the particles around the bubble to be similar to the motion of an inviscid liquid around a spherical object, a constant pressure inside the bubble, a pressure gradient in the bed governed by D'Arcy's Law, and a constant voidage around the bubble equal to the voidage of the particulate phase they derived the transfer rate due to throughflow to be

$$q = 3U_{mf}\pi r_b^2 \qquad (7.4)$$

According to Davidson and Harrison the diffusional contribution to interphase transfer can be estimated separately from penetration theory, assuming that resistance to diffusion resides in a gas film inside the bubble. Following their derivation, the diffusional interphase mass

transfer coefficient of aerosol particles, based on unit area of bubble surface is

$$k_A = 0.975\, D_A^{\frac{1}{2}} d_b^{-\frac{1}{4}} g^{\frac{1}{4}} \qquad (7.5)$$

Equations (7.4) and (7.5) may be expressed per unit bubble volume. Their relative contribution to interphase transfer of aerosol particles may thus be estimated. Then

$$k_b = \frac{q}{4/3\pi r_b^3} = \frac{9U_{mf}}{2d_b} \qquad (7.6a)$$

$$k_{Ab} = \frac{6k_A * \pi d_b^2}{\pi d_b^3} = \frac{6k_A}{d_b} \qquad (7.6b)$$

where k_b and k_{Ab} are the interphase mass transfer coefficients of aerosol particles, based on unit bubble volume, representing transfer of aerosol due to the mechanisms of throughflow and diffusion respectively. Hence, the ratio of diffusional to throughflow transfer is

$$\frac{k_{Ab}}{k_b} = \frac{1.3 * D_A^{\frac{1}{2}} d_b^{-\frac{1}{4}} g^{\frac{1}{4}}}{U_{mf}} \qquad (7.7)$$

Taking U_{mf} = 0.02 m/s (110 μm collector particles), $D_A = 3.6\times10^{-11}$ m^2/s (diffusivity of 0.8 μm aerosol particles in air at 30°C) and $d_b = 4\times10^{-4}$ m the ratio of diffusional transfer to transfer by throughflow is of the order of 5×10^{-3}. The important conclusion is therefore drawn that, as diffusional transfer in a typical bubble of this study (see Table 7.1) is negligible, interphase transfer is determined by through-

TABLE 7.1 Estimates for Bubble Diameters Forming at Distributor A, Bubble Velocities and Residence Times, $H_{mf} = 0.1$ m

	110 μm collectors		600 μm collectors	
U m/s	0.03	0.30	0.35	0.70
d_f, mx10 ^{2}	7.1×10^{-2}	2.7×10^{-1}	1.4×10^{-1}	3.1×10^{-1}
U_f, mx10 ^{2}/s	5.9	1.2×10^{1}	8.3	1.2×10^{1}
t_f, s	1.7	8.3×10^{-1}	1.2	8.3×10^{-1}

flow and hence is independent of aerosol particle diameter. Thus, Equation (7.4) was used in the spherical bubble model to estimate gas interchange between the phases.

This conclusion has a further important implication. A popular approach to analysis of gas/solid processes in fluidized beds is based on a model originally proposed by Orcutt et al.[03], which distinguishes between the gas in the bubbles and the dense phase. Innumerable subsequent developments of this model have been proposed[G7]. All predict that, in the case of a fast gas/solid process (normally chemical reaction, although the process could be aerosol collection) "bypassing" depends on the mass transfer rate between the bubbles and the dense phase. It has been demonstrated that this transfer rate is independent of aerosol size, although the results in Chapter 6 show that penetration depends strongly on d_A. Hence, penetration in these experiments cannot depend primarily on bubble bypassing, and must be dominated by processes occurring in the dense phase. These processes are examined in detail in the remainder of this chapter.

7.2.5 Equations describing aerosol collection around a spherical bubble

7.2.5.1 Motion of particles and fluid around the bubble

The equations governing the motion of the particles and fluid around a spherical bubble were derived by Davidson and Harrison based on the assumptions presented in Section 7.2.4. No purpose will be served in their re-derivation and the reader is referred to the original publication[D1]. Figure 7.2 shows schematically a three dimensional Davidson bubble. The cloud radius, r_c, bubble radius, r_b, and two typical stream-

FIGURE 7.2 Description of aerosol collection in the cloud of a Davidson bubble

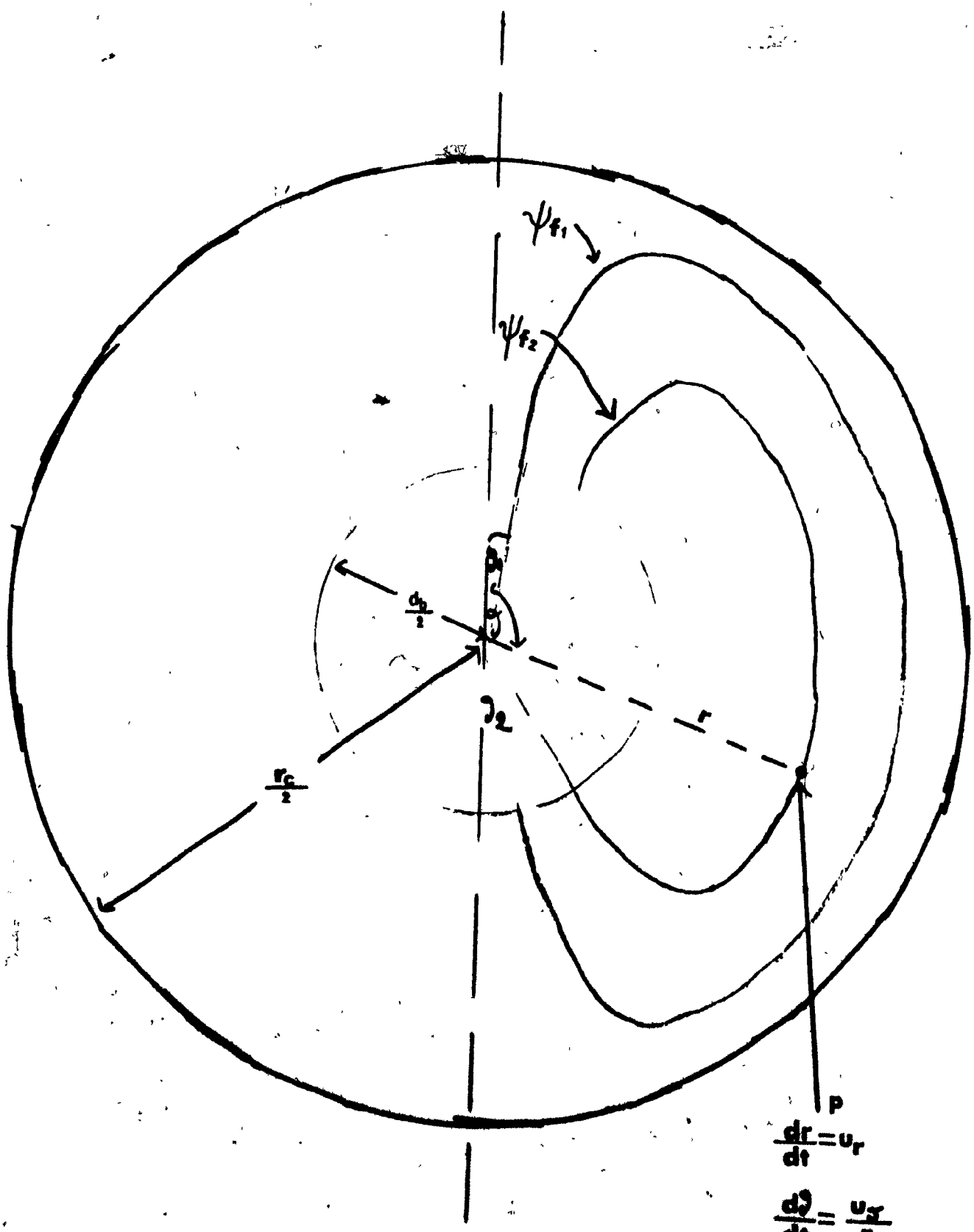

$$\frac{dr}{dt} = u_r$$

$$\frac{d\vartheta}{dt} = \frac{u_\vartheta}{r}$$

$$\frac{dn}{dt} = -N$$

lines ψ_{f_1}, and ψ_{f_2} are shown in the figure. The fluid streamlines, starting from the surface of the bubble at angle θ from the vertical and joining the bubble at angle $(\pi-\theta)$, are defined by the stream function

$$\psi_f = (U_b - u_{mf})(1 - \frac{r_c^3}{r^3}) \frac{r^2 \sin^2\theta}{2} \tag{7.8}$$

where r, θ are polar co-ordinates. The interstitial minimum fluidization velocity is

$$u_{mf} = \frac{U_{mf}}{\epsilon_{mf}} \tag{7.9}$$

where U_{mf} and ϵ_{mf} are the voidage and superifical gas velocity at minimum fluidization. The cloud radius is determined from

$$r_c = r_b \sqrt[3]{\frac{U_b + 2u_{mf}}{U_b - u_{mf}}} \tag{7.10}$$

At a point P on Figure 7.2, defined by distance r from the centre of the bubble and angle θ with the direction of bubble motion, the velocities of the collector particles in the cloud relative to the bubble are

$$v_r = -\cos\theta(U_b + \frac{r_b^3}{r^3})$$
$$v_\theta = \sin\theta(U_b - \frac{r_b^3}{2r^3}) \tag{7.11}$$

where v_r and v_θ are the components of particle velocity relative to the bubble. Similarly, the components of the fluid velocity relative to the bubble are

$$u_r = -\left[\frac{r_b^3}{r^3}(U_b + 2u_{mf}) - (U_b - u_{mf})\right]\cos\theta$$

$$u_\theta = -\left[\frac{r_b^3}{r^3}\left(\frac{U_b}{2} + u_{mf}\right) + (U_b - u_{mf})\right]\sin\theta \qquad (7.12)$$

The components of the relative velocity between the collector particles and the aerosol stream are obtained from subtracting Equations (7.11) from Equations (7.12)

$$(u_r)_{rel} = u_r - v_r = u_{mf}\left(1 + \frac{2r_b^3}{r^3}\right)\cos\theta$$

$$(u_\theta)_{rel} = u_\theta - v_\theta = -u_{mf}\left(1 - \frac{r_b^3}{r^3}\right)\sin\theta \qquad (7.13)$$

The magnitude of the relative velocity between collector particles and aerosol stream is determined from Equation (7.13)

$$U_{rel} = \sqrt{(U_r)_{rel}^2 + (U_\theta)_{rel}^2} \qquad (7.14)$$

The equations given above are simplified if expressed in dimensionless form, as follows:

$$r^+ = \frac{r}{r_b}$$

$$u_\theta^+ = \frac{u_\theta}{u_{mf}}$$

$$u_r^+ = \frac{u_r}{u_{mf}}$$

$$(u_r^+)_{rel} = \frac{(u_r)_R}{u_{mf}} \tag{7.15}$$

$$(u_\theta^+)_{rel} = \frac{(u_\theta)_R}{u_{mf}}$$

$$\psi_f^+ = \frac{\psi_f}{u_{mf} r_b^2}$$

$$U_b^+ = \frac{U_b}{u_{mf}}$$

Making the above substitutions, the relative velocity between the collector particles and the fluidizing fluid and its components are

$$(u_r^+)_{rel} = (1 + \frac{2}{r^{+3}})\cos\theta$$

$$(u_\theta^+)_{rel} = (1 - \frac{1}{r^{+3}})\sin\theta \tag{7.16a}$$

$$(u^+)_{rel} = \sqrt{(u^+_r)^2_{rel} + (u^+_\theta)^2_{rel}}$$

The dimensionless components of the fluid velocity relative to the bubbles are

$$u^+_r = \left[\frac{1}{r^{+3}}(U_b^+ + 2) - (U_b^+ - 1)\right]\cos\theta$$

$$u^+_\theta = \left[\frac{1}{r^{+3}}(\frac{U_b^+}{2} + 1) + (U_b^+ - 1)\right]\sin\theta \tag{7.16b}$$

Similarly, the dimensionless stream function simplifies at the surface of the bubble, where $r^+ = 1$, to

$$\psi_{f_b} = -3/2 \sin\theta \qquad (7.17)$$

Equations (7.15) to (7.17) will be used in the next section describing the collection of aerosol in the bubble cloud.

7.2.5.2 Rate of aerosol collection in the vicinity of the bubble

The rate of aerosol collection along a streamline (Figure 7.2) is determined by the components of the fluid velocity relative to the bubble, u_r, u_θ, and by the collection rate constant K_V. This was defined in Chapter 5 as the aerosol collection parameter based on unit dense phase volume

$$K_V = \frac{3(1-\epsilon_{mf})E_{FT}U}{2d_p} \qquad (5.3b)$$

The above equation may be used for calculating collection efficiencies in the bubble cloud assuming the voidage in the cloud to be equal to the voidage of a fixed bed.* The relative superficial gas velocity between collector particles and aerosol is determined from

$$U = (u)_{rel} * \epsilon_{mf} \qquad (7.18)$$

where $(u)_{rel}$ is given in Equation (7.14). The individual collection efficiency of a collector particle in a fluidized bed may be represented

---

*There is evidence in the literature[D2] that ϵ may change as much as 10% in the bubble cloud; therefore this equation is only an approximation.

by the correlation determined in Chapter 5 for the individual collector efficiency of a particle in a fixed bed

$$E_{FT} = 2.89\ St + 6.89\ N_G \tag{5.22}$$

where the inertial and gravitational collection parameters are based on the superficial gas velocity between collector particles and aerosol (Equation 7.18). Equation (5.22) was determined for a fixed bed where the direction of the challenging aerosol was "downflow". As collection due to gravitational deposition is not necessarily independent of orientation to the vertical, this equation is an approximation. It is, however, the best correlation available and, furthermore, collection due to gravitational deposition is secondary in importance.

Thus, aerosol collection at a point (r,θ) on a streamline may be expressed in the form of three ordinary differential equations

$$\frac{dr}{dt} = u_r$$

$$\frac{d\theta}{dt} = \frac{u_\theta}{r} \tag{7.19}$$

$$\frac{dC}{dt} = - K_V C$$

where C is the local concentration of aerosol, u_r and u_θ are defined in Equation (7.12) and K_V may be determined in the manner described above.

The number of unknown variables may be reduced to two by making certain simplifying assumptions. The bubble with its cloud is considered

to form instantly at the distributor orifice and thus zero collection during formation is assumed. An instant acceleration to constant velocity U_b and no neighbouring interference are postulated. Under these "quasi steady state" assumptions the time variables may be eliminated from Equations (7.19) and the determination of the aerosol concentration at a point (r,θ) is achieved by the simultaneous solution of two differential equations

$$\frac{dr}{d\theta} = \frac{u_r r}{u\theta}$$
$$\frac{dC}{d\theta} = \frac{-K_V C r}{u_\theta} \qquad (7.20)$$

Defining the following dimensionless variables

$$f_b = \frac{C}{(C_b)_t}$$
$$K_V^+ = \frac{r_b K_V}{u_{mf}} \qquad (7.21)$$

where $(C_b)_t$ is the average aerosol concentration in the bubble at time t. Equations (7.20) become, in dimensionless form

$$\frac{dr^+}{d\theta} = \frac{u_r^+ r^+}{u_\theta^+}$$
$$\frac{df_b}{d\theta} = -\left(\frac{K_V^+ r^+}{u_\theta^+}\right) f_b \qquad (7.22)$$

The solution of these equations is discussed in the following section.

7.2.6 Numerical integration of equations

Equations (7.22) describing the rate of aerosol collection near a bubble were integrated along the bubble streamlines by the following computational procedure:

(i) A minimum and a maximum angle of 4^{o} and 86^{o} from the vertical were chosen, for computational convenience (see Figure 7.2). The minimum and maximum value of the velocity potential on the surface of the bubble, ψ_f, was determined from Equation (7.17) and an odd number of computational points were chosen.

(ii) The two dimensionless differential equations, describing the rate of aerosol collection, were integrated along each streamline by the fourth order Runge-Kutta-Merson process[L4]. Thus the aerosol concentration entering the bubble was determined along each computational streamline.

(iii) The average concentration entering the bubble is expressed as

$$(f_b)_{AV} = \frac{\int_{\psi_1}^{\psi_2} f_b \psi_f^+ \, d\psi^+}{\psi_2^+ - \psi_1^+} \qquad (7.23)$$

where

$$\psi_1^+ = \psi_f \, (\theta = 0)$$

$$\psi_2^+ = \psi_f \, (\theta = \pi/2)$$

The integral in Equation (7.23) was evaluated by Simpson's rule. It was determined, experimentally, that integrating over 21 streamlines was adequate for $(f_b)_{AV}$ to be sufficiently close to the true prediction of the model.

The rate of depletion of aerosol in the bubble with respect to time, assuming the gas in the bubble to be well mixed, can be described by a first order differential equation of the form

$$\frac{d}{dt}(C_b) = -\frac{\left[1 - (f_b)_{AV}\right] * q}{V_b} * C_b \qquad (7.30)$$

where V_b is the volume of the bubble and q is determined from Equation (7.4). As the gas re-entering the bubble covers a range of residence times, i.e. different starting concentrations in the streamlines, the model implicitly assumes that the aerosol in the bubble is depleted at a relatively slow rate. In view of the approximations already made, this assumption represents no serious limitation provided that the aerosol concentration in the bubble does not change very rapidly. The average concentration of the aerosol returning to the bubble, $(f_b)_{AV}$ was determined for 10 bubble diameters, from $d_b = 10^{-3}$ m to $d_b = 0.25$ m, and 6 different aerosol sizes, from $d_A = 0.7$ μm to $d_A = 1.8$ μm. The results of these calculations and the conclusions that may be drawn from them are presented in the next section.

7.2.7 Discussion and conclusions

The numerical predictions of the simplified model used to simulate aerosol collection in the bubble phase of a fluidized bed may be used to draw some useful qualitative conclusions. Although quanti-

tative precision may not be expected, it is unlikely that more realistic models, predicting more accurately the shape of the bubble cloud and the fluid streamlines, will give qualitatively different results.

The predicted average concentration of aerosol returning to the bubble, $(f_b)_{AV}$, is shown as a function of bubble diameter in Figure 7.3. For the range of bubble sizes of interest ($5x10^{-3} < d_b < 5x10^{-2}$ m), significant aerosol collection in the cloud is predicted. Because the predominant collection mechanism is inertial, this collection is more pronounced for the larger aerosol sizes. Collection in the cloud is predicted to increase slightly with increasing bubble diameter. However, this effect is more than offset by the higher velocities and hence shorter residence times of larger bubbles. This is shown by Figure 7.4, which shows the ratio of final to initial concentration in the bubble for a constant bed depth of $4x10^{-2}$ m. Moreover, it is interesting to note that, for d_b larger than about 10^{-2} m, the concentration in the bubble as it reaches the bed surface is relatively insensitive to bubble diameter, with most of the aerosol bypassing the collector particles. Figure 7.5 shows the predicted amount of uncollected aerosol as a function of bed depth for a single bubble diameter of $4x10^{-3}$ m. Hardly any collection is predicted for a 0.72 μm aerosol, while a significant amount of the 1.75 μm aerosol is collected in the cloud.

These predictions lead to further important conclusions on the mechanism of aerosol collection. It does appear that the dependence of penetration on aerosol diameter can be explained by processes occurring in the dense-phase (Figure 7.5). However, the decrease of penetration with U clearly cannot be explained by a model based on single non-interacting

FIGURE 7.3 Predicted average concentration of aerosol returning to the bubble as a function of bubble diameter (d_p = 110 μm)

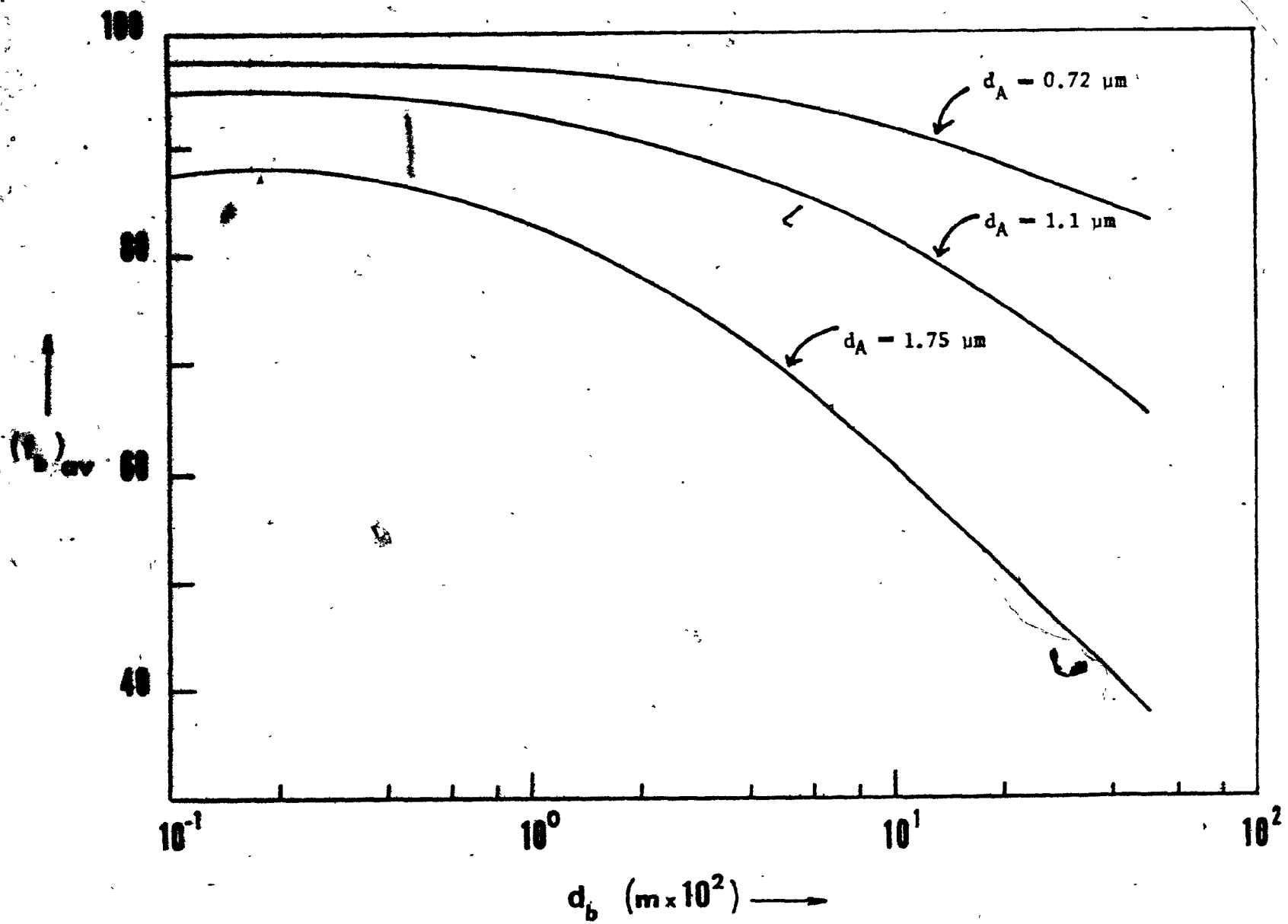
100
80
60
40
$(\eta_b)_{av}$
d_A = 0.72 μm
d_A = 1.1 μm
d_A = 1.75 μm
10^{-1}
10^0
10^1
10^2
d_b $(m \times 10^2)$ ⟶

FIGURE 7.4 Predicted fraction of aerosol uncollected as a function of bubble diameter (H_{mf} = 0.05 m)

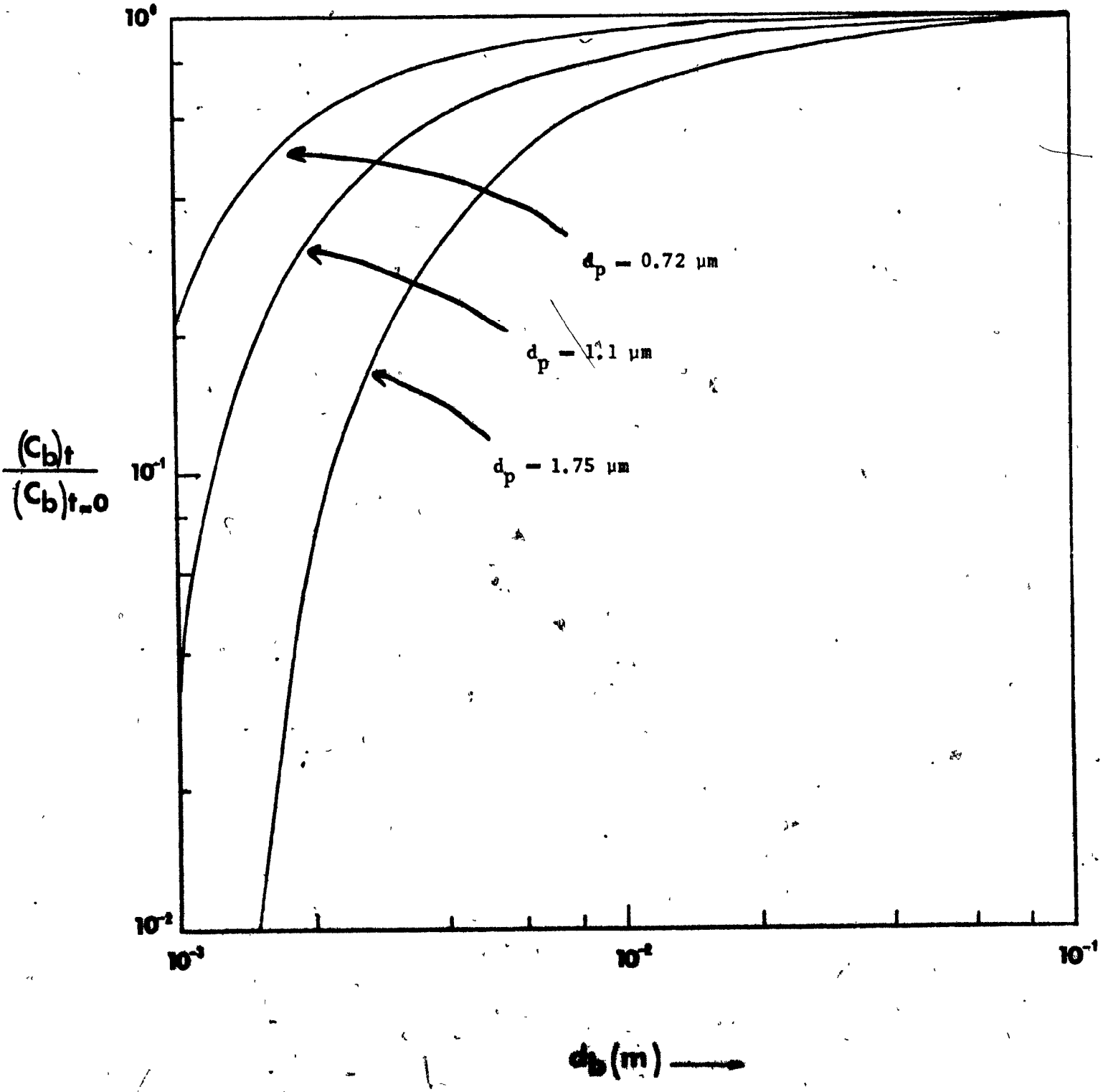
10^0
10^{-1}
10^{-2}
10^{-3}
10^{-2}
10^{-1}
d_p – 0.72 μm
d_p – 1.1 μm
d_p – 1.75 μm
$\frac{(C_b)_t}{(C_b)_{t=0}}$
d_b (m) ⟶

FIGURE 7.5 Predicted fraction of aerosol uncollected as a function of bed height ($d_b = 4 \times 10^{-2}$ m)

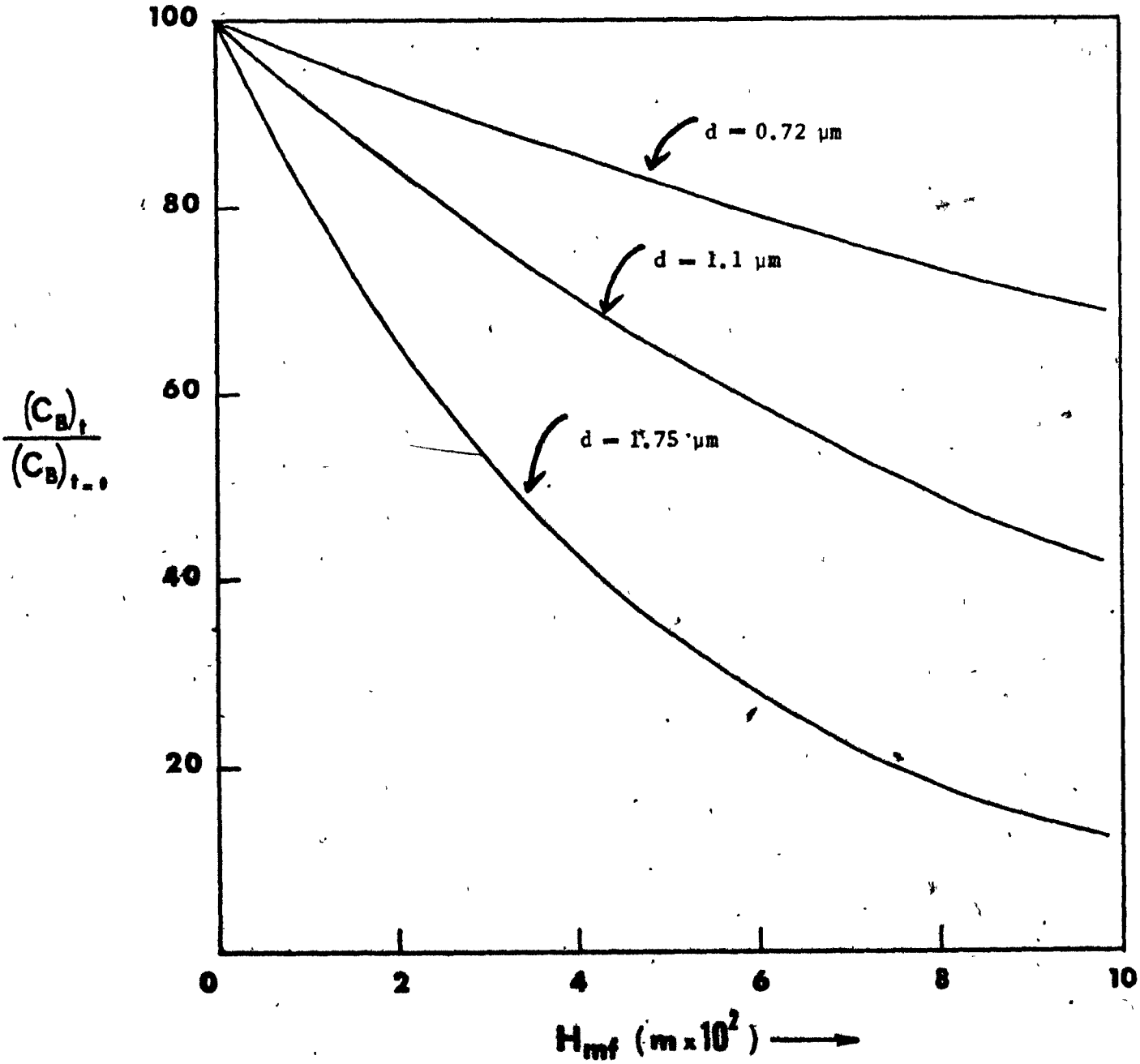
100
80
60
40
20
0
2
4
6
8
10
d = 0.72 μm
d = 1.1 μm
d = 1.75 μm
$\frac{(C_B)_t}{(C_B)_{t=0}}$
H_{mf} ($m \times 10^2$) ⟶

bubbles. From Figure 7.4, this observation would have to be attributed to substantial decrease in mean bubble size with increasing velocity, whereas in reality the reverse occurs. It is also notable that the predicted penetration in single rising bubbles is an order of magnitude larger than the measured values. It must therefore be concluded that, in the present study, the bubbles formed at the distributor were so small and coalesced so frequently that exchange between bubbles and dense phase was very much more rapid than can be predicted by a model based on single rising bubbles. The implications of this conclusion are developed in the following section.

It may also be noted that this conclusion highlights the importance of operating with shallow beds and distributors designed for small initial bubble size. If the distributor gives large bubbles, collection will be limited by transfer between the bubble and dense phases. Higher penetrations will then be observed, even in deep beds, and the penetration can be expected to increase with increasing gas velocity. Exactly this effect was noted in the results of McCarthy et al.[Mc1], and in the set of experiments with DOP aerosol described in Section 6.2.1.1.

7.3 Aerosol Collection in a Fluidized Bed

7.3.1 Introduction

This section presents a theoretical treatment of aerosol collection in a fluidized bed assuming the behaviour of the bed to be consistent with the modified two phase theory of fluidization. There are only two previous attempts, both unsuccessful, to describe the phenomenon of aerosol removal in fluidized beds:

The first was by Tardos, Gutfinger and Abuaf[T1] who claimed to have simulated mathematically the behaviour of a fluidized bed "at minimum fluidization". Their treatment is based on the "cell model" concept, which attempts to calculate the steady flow pattern and resultant collection around one collector particle. Because they implicitly assume that all the gas passes through the dense phase and flow is steady, their model is essentially a simulation of a fixed bed rather than a fluidized bed. Moreover, they assume that diffusional collection is dominant for 2-3 μm particles (see Section 2.3.1.1). Thus, their model bears little relationship to reality, and as a result they predict that bed depths of the order of metres are required for effective aerosol removal.

The second attempt was by McCarthy et al.[Mc1] and Jackson[J2] who, by going to the other extreme, attempted a qualitative explanation claiming that the efficiency of a fluidized bed collecting aerosol is low at high superficial gas velocities because of gas bypassing in the bubble phase. It was shown in Section 7.2.7 that this may be the case if the gas velocity is low and/or the distributor is poorly designed, but that this mechanism cannot explain the results of the present work. Therefore, it is concluded that the qualitative explanation given by McCarthy et al.[Mc1] and Jackson[J2] is not realistic for a well-designed shallow collector bed.

Thus, up to the present time, there does not appear to be an adequate theoretical treatment of aerosol removal in fluidized beds. The following section offers the first such attempt, and shows that aerosol collection may be adequately described in terms of the two-phase theory of fluidization.

7.3.2 Development of a model

7.3.2.1 The modified two phase theory of fluidization

In general, two phase fluidization theory assumes the bed to be composed of two distinct phases, namely a dense or particulate phase, consisting of particles and interstitial gas, and a lean or bubble phase, composed of rising voids termed "bubbles" and essentially free from particles. Effectively, all of the conversion in a reactor or collection in a fluidized filter takes place in the particulate phase.

The classical two phase theory of fluidization was originally postulated by Toomey and Johnstone[T4] and developed further by the experimental results and theoretical treatments of Orcutt[02], Orcutt et al.[03] and Davidson and Harrison[D2]. It assumes that all the gas in excess of minimum fluidization travels in the bed in the form of bubbles giving a superficial bubble velocity

$$\frac{G}{A_B} = U - U_{mf} \tag{7.31}$$

where G is the flow rate of the gas in excess of minimum fluidization and A_B is the cross sectional area of the bed. Subsequent experimental results by a number of workers (e.g. G-7, C-7, G-8) suggested that the superficial bubble velocity through the bed is more adequately described by an equation of the form

$$\frac{G}{A_B} = U - KU_{mf} \tag{7.32}$$

where K is an empirical parameter.

This led to what is now established as the modified or n-type two phase theory of fluidization which postulates[G9]

$$\frac{G}{A_B} = U - U_{mf}(1 + n\bar{\epsilon}_b) \tag{7.33}$$

where n is a constant and $\bar{\epsilon}_b$ is the average volume fraction of the lean phase*. Although the n-type theory agrees with the classical two phase theory in assuming that the dense phase has voidage ϵ_{mf} and mean interstitial gas velocity U_{mf}/ϵ_{mf} it postulates an additional mean throughflow velocity inside a bubble equal to $(n + 1)U_{mf}$. If the mean bubble velocity is U_b, then

$$\bar{\epsilon}_b U_b = \frac{G}{A_B} \tag{7.34}$$

so that

$$\bar{\epsilon}_b = \frac{U - U_{mf}}{U_b + nU_{mf}} \tag{7.35}$$

Thus the differences between the original two phase theory and the n-type theory may be summarized in terms of superficial velocities, as follows:

---

*In its more general form the modified two phase theory of fluidization assumes that the volume fraction of the bubble phase is a function of bed height.

Original two phase theory

Gas velocity = bubble velocity + dense phase velocity (7.36a)

$$U = (U - U_{mf}) + U_{mf} \qquad (7.36b)$$

n-type two phase theory

Gas velocity = bubble velocity + bubble throughflow velocity + dense phase velocity .....(7.37a)

$$U = U - U_{mf}(1 + n\bar{\varepsilon}_b) + U_{mf}(1 + n)\bar{\varepsilon}_b + U_{mf}(1 - \bar{\varepsilon}_b) \qquad .....(7.37b)$$

The conventional two phase theory then becomes a special case of the n-type two phase theory obtained by putting $n = 0$; parameter K thus becomes 1. The subject was reviewed extensively by Grace and Clift[G8] who summarized previous literature and showed that the n-type theory, which is an improvement over the original two phase model is an over-simplification itself and that n and K are not constant, as was originally hoped, but vary with experiments in the range $-1.2 < n < 140$ and $0.7 < K < 27$. As the n-type theory is conceptually a more accurate formulation of the process of fluidization and is more general, it will be preferred in deriving the equations describing aerosol removal in fluidized beds.

7.3.2.2 Dense phase in plug flow

Figure 7.6 shows schematically the n-type two phase model of a fluidized bed. The bubble phase is assumed to be completely void of particles, and travelling in plug flow with a superficial velocity $\varepsilon_b U_b$,

FIGURE 7.6 Schematic representation of the modified two phase model of a fluidized bed

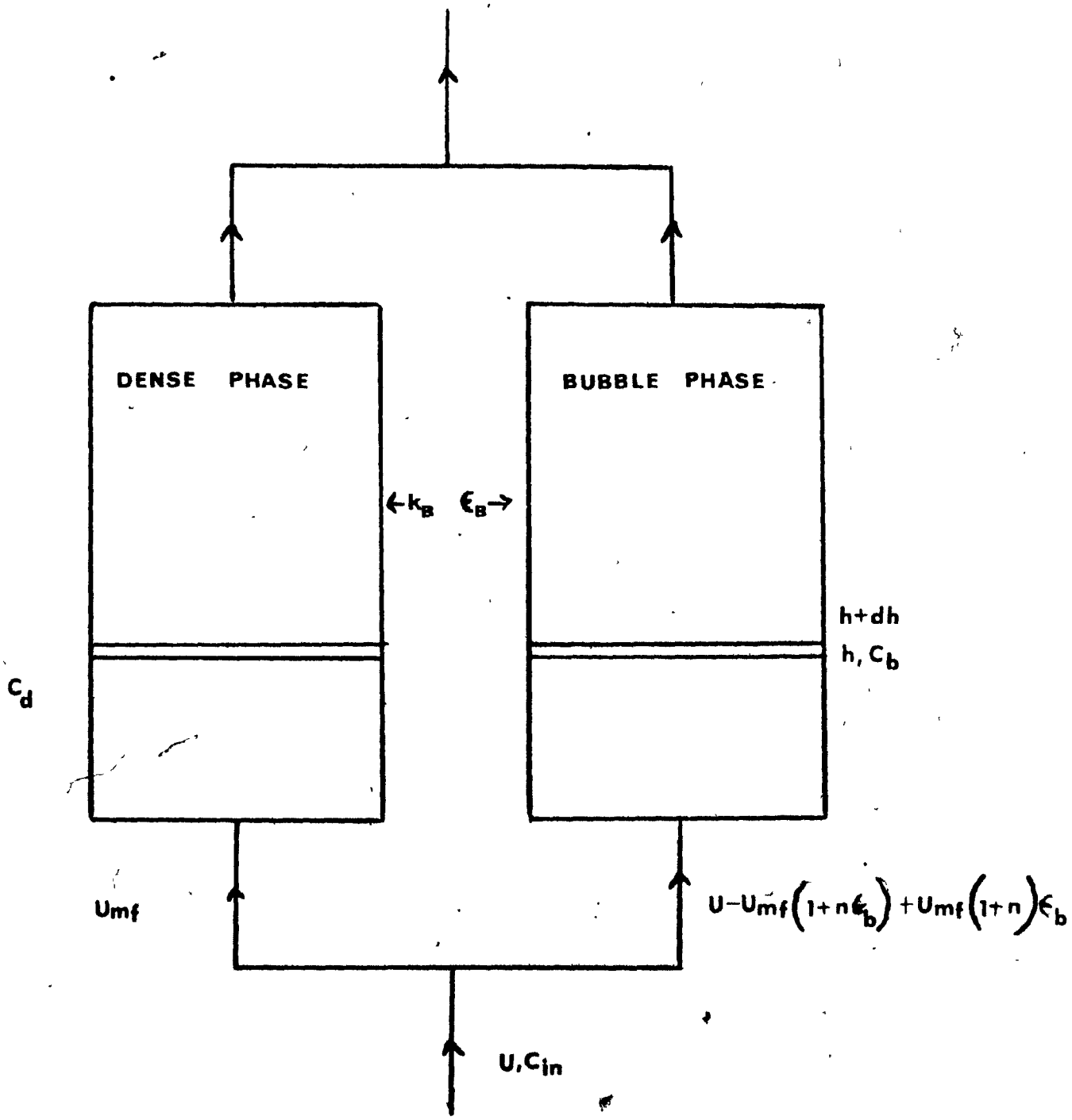
DENSE PHASE
BUBBLE PHASE
$\leftarrow k_B \quad \epsilon_B \rightarrow$
$h+dh$
h, C_b
C_d
U_{mf}
$U-U_{mf}\left(1+n\epsilon_b\right)+U_{mf}\left(1+n\right)\epsilon_b$
U, C_{in}

given by Equation (7.33), and a throughflow superficial velocity $\varepsilon_b(n+1)U_{mf}$. The dense phase contains all the collector particles, is (in this case) in plug flow, and travels with a superficial velocity $U_{mf}(1-\bar{\varepsilon}_b)$. It is postulated that all aerosol collection occurs in the particulate phase.

At height h above the inlet of the bed, where the bubble and dense phase concentrations are C_b and C_d, respectively, the flux of aerosol per unit bed area is

$$(1 - \bar{\varepsilon}_b)U_{mf}C_d + (U - (1 - \bar{\varepsilon}_b)U_{mf})C_b$$

Thus, considering a differential element between h and (h + dh) in Figure 7.6 and taking a mass balance on the aerosol particles gives for the dense phase

$$\begin{pmatrix}\text{Rate of particles}\\ \text{in}\end{pmatrix} - \begin{pmatrix}\text{Rate of particles}\\ \text{out}\end{pmatrix} + \begin{pmatrix}\text{Rate of}\\ \text{particle collection}\end{pmatrix} + \begin{pmatrix}\text{Rate of particle}\\ \text{transfer to bubble phase}\end{pmatrix} \qquad \text{.....(7.38a)}$$

so that,

$$(1 - \bar{\varepsilon}_b)U_{mf}C_d - (1 - \bar{\varepsilon}_b)U_{mf}(C_d + dC_d) - k_b\,\bar{\varepsilon}_b\,dh(C_b - C_d) + K_v(1 - \bar{\varepsilon}_b)C_d dh \qquad \text{.....(7.38b)}$$

where k_b is the interphase mass transfer coefficient of aerosol particles based on unit bubble volume and K_V is the aerosol collection parameter based on unit dense phase volume (Equation (5.3b)). It should be noted that K_V was defined, in Chapter 5, in terms of the relative superficial velocity between aerosol and collector particles, which, according to the two phase theory, is U_{mf} in a fluidized bed irrespective of superficial gas velocity. Re-arranging Equation (7.38b)

$$(1 - \bar{\varepsilon}_b)U_{mf}\frac{dC_d}{dh} = k_b\bar{\varepsilon}_b(C_b - C_d) - K_V(1 - \bar{\varepsilon}_b)C_d \qquad (7.39)$$

Similarly, a mass balance on the aerosol particles over the differential element dh gives for the bubble phase

$$\begin{pmatrix}\text{Rate of}\\ \text{particles in}\end{pmatrix} = \begin{pmatrix}\text{Rate of}\\ \text{particles out}\end{pmatrix} + \begin{pmatrix}\text{Rate of particle}\\ \text{transfer to dense}\\ \text{phase}\end{pmatrix} \qquad (7.40a)$$

so that,

$$(U - (1 - \bar{\varepsilon}_b)U_{mf})C_b = (U - (1 - \bar{\varepsilon}_b)U_{mf}) * (C_b + dC_d)$$

$$- k_b\,\bar{\varepsilon}_b(C_b - C_d)dh \qquad .....(7.40b)$$

Re-arranging,

$$(U - (1 - \bar{\varepsilon}_b)U_{mf})\frac{dC_b}{dh} = - k_b\,\bar{\varepsilon}_b(C_b - C_d) \qquad (7.41)$$

Adding Equations (7.39) and (7.41) to obtain a total mass balance over a differential height dh of the bed

$$(1 - \bar{\varepsilon}_b)U_{mf} \frac{dC_d}{dh} + (U - (1 - \bar{\varepsilon}_b)U_{mf}) \frac{dC_b}{dh} + K_V(1 - \bar{\varepsilon}_b)C_d = 0 \quad \text{.....(7.42)}$$

The equations presented above are simplified if expressed in the form of dimensionless groups. Denoting the fraction of the gas passing in the bubble phase as β

$$\beta = \frac{\text{superficial bubble velocity}}{\text{superficial velocity}} \quad (7.43a)$$

$$= \frac{U - (1 - \bar{\varepsilon}_b)U_{mf}}{U} \quad (7.43b)$$

Then, Equation (7.41) and (7.42) simplify to

$$\frac{dC_b}{dh} + \frac{k_b\bar{\varepsilon}_b}{U\beta}(C_b - C_d) = 0 \quad (7.44a)$$

$$(1 - \beta)\frac{dC_d}{dh} + \beta\frac{dC_b}{dh} + \frac{K_V(1 - \bar{\varepsilon}_b)}{U} * (C_b - C_d) = 0 \quad (7.44b)$$

Defining the following dimensionless variables

$$K'_V = \frac{K_V H(1 - \bar{\varepsilon}_b)}{U} \quad (7.45)$$

$$X = \frac{k_b\bar{\varepsilon}_b H}{U\beta} = \frac{k_b\bar{\varepsilon}_b H}{U - (1 - \bar{\varepsilon}_b)U_{mf}} \quad (7.46)$$

Equations (7.44) simplfy further,

$$\frac{dC_b}{dh} + \frac{X}{H}(C_b - C_d) = 0 \qquad (7.47a)$$

$$(1 - \beta)\frac{dC_d}{dh} + \beta\frac{dC_b}{dh} + \frac{K'_V}{H} C_d = 0 \qquad (7.47b)$$

K'_V, the dimensionless collection rate constant, expressed in this form, is the number of collection units (NCU) that would have been present in a uniformly fluidized bed, and is the parameter which Knettig and Beeckmans[K3] termed NTU. The number of interphase transfer units, X, is the number of times the bubble gas is interchanged with gas in the dense phase on passage through the bed. A high K'_V value implies high aerosol collection efficiencies and a high X value implies low resistance to interphase transfer. These dimensionless groups are similar to corresponding dimensionless groups defined in the classical two phase theory of fluidization[D2]. In the general case β, X, K'_V vary with bed height. Making the simplifying assumption that they are constant the solution of Equations (7.47) is of the general form

$$C_b = C_1 e^{-m_1 h} + C_2 e^{-m_2 h} \qquad (7.48)$$

where

$$m_1 = \frac{(X + K'_V) + \left[(X + K'_V)^2 - 4K'_V X(1 - \beta)\right]^{0.5}}{2H(1 - \beta)} \qquad (7.49a)$$

$$m_2 = \frac{(X + K'_V) - \left[(X + K'_V)^2 - 4K'_V X(1 - \beta)\right]^{0.5}}{2H(1 - \beta)} \qquad (7.49b)$$

Differentiating Equation (7.48) with respect to bed height

$$\frac{dC_b}{dh} = -m_1C_1e^{-m_1h} - m_2C_2e^{-m_2h} \tag{7.50}$$

Assuming that the rate of removal of aerosol particles during bubble formation is zero at the distributor plate and expressing aerosol concentrations as fractions of the inlet value (i.e. $C_{IN} = 1$) the boundary conditions are at $h = 0$, $C_b = 1$, $\frac{dC_b}{dh} = 0$.

Substituting these boundary conditions in Equations (7.48) and (7.50)

$$C_1 = \frac{m_2}{m_2-m_1} \tag{7.51a}$$

$$C_2 = \frac{m_1}{m_2-m_1} \tag{7.51b}$$

Therefore,

$$C_b = \frac{1}{(m_2-m_1)} * (m_2e^{-m_1h} - m_1e^{-m_2h}) \tag{7.52}$$

$$\frac{dC_b}{dh} = \frac{-m_1m_2}{m_2-m_1}(e^{-m_1h} - e^{-m_2h}) \tag{7.53}$$

Substituting Equations (7.52) and (7.53) in Equation (7.47a) and rearranging, one obtains the concentration of the aerosol particles in the dense phase at bed depth h:

$$C_d = \frac{1}{(m_2-m_1)} * \left[m_2 e^{-m_1 h}\left(1 - \frac{Hm_1}{X}\right) - m_1 e^{-m_2 h}\left(1 - \frac{Hm_2}{X}\right)\right] \quad (7.54)$$

The average exit concentration of aerosol particles is

$$\frac{C_{out}}{C_{in}} = \begin{pmatrix}\text{fraction of}\\ \text{gas passing}\\ \text{as bubbles}\end{pmatrix} * \begin{pmatrix}\text{bubble phase}\\ \text{aerosol con-}\\ \text{centration}\\ \text{at exit}\end{pmatrix} + \begin{pmatrix}\text{fraction of}\\ \text{gas passing}\\ \text{in dense}\\ \text{phase}\end{pmatrix} * \begin{pmatrix}\text{dense phase}\\ \text{aerosol}\\ \text{concentration}\\ \text{at exit}\end{pmatrix}$$

.....(7.55a)

$$= \beta(C_b)_H + (1-\beta)(C_d)_H \quad (7.55b)$$

Then the fractional penetration of the aerosol particles, defined as the fraction of the particles not collected by the bed C_{out}/C_{in} is

$$f = \frac{1}{(m_2-m_1)}\left[m_2 e^{-m_1 H}\left(1 - \frac{H(1-\beta)m_1}{X}\right) - m_1 e^{-m_2 H}\left(1 - \frac{H(1-\beta)m_2}{X}\right)\right]$$

.....(7.56)

where m_1 and m_2 are given by Equation (7.49), H is the height of the bed which, assuming constant $\bar{\epsilon}_b$ is

$$H = \frac{H_{mf}}{(1-\bar{\epsilon}_b)} \quad (7.57)$$

and X is the number of interphase transfer units, defined in Equation (7.46).

This then is the general expression for the fractional aerosol penetration when the bed is in plug flow. Equation (7.56) is similar to equations describing conversion of a gas by a first-order chemical reaction in a fluidized bed model based on the conventional two phase theory

of fluidization. Its novel features, however, are that it is derived based on the n-type theory of fluidization and that it treats aerosol removal as a pseudo-first order reaction. Thus, it is the first equation presented in the literature to describe aerosol removal in a fluidized bed using fluidization theory.

7.3.2.3 Dense phase well mixed

In the case when the dense phase is assumed to be well mixed the aerosol concentration in the dense phase is constant and independent of bed height. Thus, re-arranging Equation (7.47a)

$$\frac{d}{dh}(C_b - C_d) + \frac{X}{H}(C_b - C_d) = 0 \qquad (7.58)$$

and solving,

$$(C_b - C_d) = (1 - C_d) * EXP\left[-Xh/H\right] \qquad (7.59)$$

Since the particulate phase is assumed to be perfectly mixed, its material balance can be written by considering the total height H. Thus,

$$\begin{pmatrix}\text{Rate of}\\ \text{particles in}\end{pmatrix} - \begin{pmatrix}\text{Rate of}\\ \text{particles out}\end{pmatrix} + \begin{pmatrix}\text{Rate of}\\ \text{particle}\\ \text{collection}\end{pmatrix} + \begin{pmatrix}\text{Rate of}\\ \text{particle}\\ \text{transfer}\end{pmatrix}$$

.....(7.60a)

$$(1 - \bar{\epsilon}_b)U_{mf}C_{in} = (1 - \bar{\epsilon}_b)U_{mf}C_d + K_v(1 - \bar{\epsilon}_b)C_d H$$

$$- k_{mc}\bar{\epsilon}_b \int_0^H (C_b - C_d)dh \qquad .....(7.60b)$$

The last term may be evaluated from Equation (7.59). Then, using Equation (7.55b), substituting the dimensionless group β (Equation 7.43b) and re-arranging

$$f = \beta e^{-X} + \frac{(1 - \beta e^{-X})^2}{1 + K'_V - \beta e^{-X}} \qquad (7.61)$$

gives the fractional aerosol penetration when the particulate phase of the fluidized bed is considered to be well mixed. Like Equation (7.56), which was derived for plug flow, this is the first equation presented in the literature describing aerosol removal when the particulate phase of the fluidized bed is considered to be well mixed.

7.3.3 Effect of bubble coalescence and simplification of equations

The assumption that the lean phase of a fluidized bed consists of isolated bubbles rising to the surface without interference from neighbouring bubbles may be a reasonable approximation when the lean phase has coalesced into large bubbles, few in number. This assumption, however, does not take into consideration bubble interaction and its possible effects on interphase mass transfer.

Clift et al.[C9], Clift[C5], Clift and Grace[C7,C8,C6], and Grace and Venta[G10] have made an extensive investigation on bubble coalescence and bubble splitting in fluidized beds. Their studies have found that during bubble coalescence the volume of the final bubble is more than the sum of the volumes of the original bubbles. However, as Clift[C5] has first shown, when two bubbles are in the process of coalescing a substantial amount of the gas forming the bubbles is inter-

changed with gas from the dense phase. Thus coalescence contributes significantly to interphase transfer.

A second mechanism enhancing interphase transfer occurs as a result of bubble interaction. As, Clift[C5] has shown, when two bubbles are in certain orientations they might not coalesce but, as a result of cloud overlapping, gas may leak from one bubble to the next. This leaking gas is transferred through the particulate phase and brings the essentially untreated bubble gas into contact with particles thus improving interphase transfer.

It appears then that bubble interaction results in the enhancement of the interphase transfer mechanism. As bubble formation and coalescense and bubble interaction is extremely rapid near the distributor this suggests that the interphase transfer is very high in this region of the bed. This is consistent with Grace's observation[G7] that the hydrodynamic behaviour of the bed is relatively unimportant near the distributor for fast reactions. As the experimental results of this study have shown, aerosol removal may be regarded as a fast reaction essentially requiring relatively shallow bed heights. There is, therefore, ample theoretical and experimental information in the literature to justify a postulate which assumes negligible interphase resistance near the distributor plate for aerosol collection.

The equations for aerosol penetration developed in the previous section may therefore be simplified by taking the limit $X \to \infty$. Equation (7.56), for plug flow in the dense phase, becomes:

$$f = e^{-K'V} \qquad (7.62)$$

while Equation (7.61) for well mixed dense phase becomes:

$$f = \frac{1}{1+K'_V} \tag{7.63}$$

Comparison between these equations and the results of the present study is examined in the next section.

7.4 Comparison with Experimental Results

7.4.1 Introduction

The previous section developed the equations describing aerosol removal in a fluidized bed. With the assumption that interphase resistance between the bubble and dense phase is negligible Equations (7.62) and (7.63) describe the aerosol penetration when the dense phase gas is in plug flow or well mixed. The form of these simplified equations was justified by the effect of rapid bubble formation and coalescence near the distributor plate, resulting in increased transfer between the two phases. This section proves, experimentally, the validity of these assumptions and simultaneously determines statistically whether the gas in the dense phase is well mixed or in plug flow.

7.4.2 Estimation of collection rate constants

The data were analysed in the form of a collection coefficient defined as

$$k' = \frac{K_V}{U} \tag{7.64}$$

where K_V is the collection rate constant of aerosol in the particulate phase, defined in Equation (5.3b) and described further in Section 7.2.5.2. From Equation (7.57) and from the definition of K'_V (Equation 7.45) Equations (7.62) and (7.63) become, for dense phase in plug flow

$$f = e^{-k'_{pl}H_{mf}} \tag{7.65}$$

and for dense phase well mixed

$$f = \frac{1}{1 + k'_w H_{mf}} \tag{7.66}$$

Thus, if the dense phase of the fluidized bed is approximated by plug flow a plot of

$$(-\ln f) \text{ vs } (H_{mf})$$

will be linear, the gradient of the line being numerically equal to k'_{pl}. Similarly, if the particulate phase is well mixed, then a plot of

$$\frac{(1-f)}{f} \text{ vs } H_{mf}$$

will be linear and yield the value of k'_w. The data on aerosol penetration in fluidized beds composed of 110 μm and 600 μm collector particles, presented in Tables 6.1 to 6.3, 6.5, 6.6 and 6.8 were chosen for analysis; the high velocity experiments were excluded firstly because they were performed with a different distributor plate and secondly because these

experiments have an inherent lower accuracy due to the design difficulties described in Chapter 4. Values of k' were estimated from experiments at different bed heights assuming that $f = 1.0$ at $H_{mf} = 0.0$. Thus for plug flow the regression equation, forced through zero intercept, reduces to

$$k'_{pl} = \frac{\sum_{i=1}^{n} (-\ln f_i) * (H_{mf})_i}{\sum_{i=1}^{n} (H_{mf})^2_i} \tag{7.67}$$

where n is the number of experimental bed depths. For the case when the dense phase is well mixed the analogous equation is

$$k'_w = \frac{\sum_{i=1}^{n} (H_{mf})_i * (1-f_i)/f_i)}{\sum_{i=1}^{n} (H_{mf})^2_i} \tag{7.68}$$

However, as both $(H_{mf})_i$ and $(1-f_i)/f_i$ will increase with decreasing penetration the above equation is biased to give most significance to experimental points with the lowest f_i. By simple re-arrangement an unbiased regression equation may be obtained, this is

$$k'_w = \frac{\sum_{i=1}^{n} (1-f_i) * f_i (H_{mf})_i}{\sum_{i=1}^{n} \left[f_i * (H_{mf})^2_i \right]^2} \tag{7.69}$$

which gives equal weight to all experimental points.

Thus two k' values, one for dense phase in plug flow and one for dense phase well mixed, were estimated from experiments at different bed heights and constant U and d_A. Then the original experimental points of each set were predicted using the estimated k' values. The residual deviation from the regression lines is given by

$$(\text{Deviation})_{pl} = \sqrt{\frac{\sum_{i=1}^{n}\left[f_i - e^{-k'_{pl}(H_{mf})_i}\right]^2}{n}} \qquad (7.70a)$$

$$(\text{Deviation})_{w} = \sqrt{\frac{\sum_{i=1}^{n}\left[f_i - \frac{1}{1 + k'_{w}(H_{mf})_i}\right]^2}{n}} \qquad (7.70b)$$

where $(\text{Deviation})_{pl}$ and $(\text{Deviation})_{w}$ are the square root of the sum of squares of the difference between experimental and estimated aerosol penetration divided by the number of experimental points, n, subscript pl refers to dense phase in plug flow and subscript w refers to dense phase well mixed. By comparing the relative magnitudes of $(\text{Deviation})_{pl}$ and $(\text{Deviation})_{w}$, it was determined whether the dense phase was near to being well mixed or could be assumed to be in plug flow. Table 7.2 and Table 7.3 show the results of these calculations in condensed form, together with the estimated values of k'_{pl} and k'_{w} for each set of experiments with the 110 μm and 600 μm collectors. The values of $(\text{Deviation})_{pl}$ and the ratio of $(\text{Deviation})_{w}$ to $(\text{Deviation})_{pl}$ are also given. The next section determines, from these results, the hydrodynamic behaviour of the bed.

7.4.3 Behaviour of the fluidized bed

Inspection of Table 7.2 shows that the particulate phase in almost all sets of experiments with 110 μm collectors was nearer to plug flow. Thus in almost all velocities, except perhaps the highest (U = 0.35 m/s), Equation (7.65) may be used more accurately to describe aerosol collection in the bed. Inspection of the table confirms that resistance to interphase transfer is negligible since k'_{pl} increases slightly with increasing superficial velocity. If the reverse was true then k'_{pl} would

TABLE 7.2 Analysis of 110 μm Collector Particles

d_A, μm	U, $mx10^2/s$	$k'_{pl} x10^4$ (m^{-1})	$k'_w x10^4$ (m^{-1})	$(Deviation)_{pl}$ $x10^2$	$\frac{(Deviation)_w}{(Deviation)_{pl}}$
0.72	4.9	.212	.285	1.3	1.8
0.72	6.0	.256	.389	3.2	1.4
0.72	7.2	.269	.392	1.3	2.2
0.72	12.9	.253	.431	2.0	1.8
0.72	13.1	.262	.412	1.3	1.9
0.72	19.5	.264	.460	3.3	1.5
0.72	25.6	.283	.465	1.6	1.5
0.72	34.9	.258	.535	1.9	0.8
0.90	4.9	.296	.441	1.5	2.1
0.90	6.0	.347	.617	2.2	1.9
0.90	7.2	.385	.669	0.9	2.8
0.90	12.9	.373	.804	1.2	2.8
0.90	13.1	.413	.839	1.0	3.2
0.90	19.5	.391	.926	2.0	1.9
0.90	25.6	.456	1.07	4.6	0.4
0.90	34.9	.387	1.17	1.8	0.8
1.15	4.9	.429	.805	1.3	1.7
1.15	6.0	.457	1.06	0.9	4.0
1.15	7.2	.559	1.32	1.9	1.1
1.15	12.9	.511	1.51	2.5	1.1
1.15	13.1	.615	1.71	2.0	1.7
1.15	19.5	.532	1.78	3.7	1.1
1.15	25.6	.689	2.57	5.7	0.2
1.15	34.9	.537	2.78	2.3	0.3

TABLE 7.3 Analysis of 600 μm Collector Particles

d_A, μm	U, $mx10^2/s$	$k'_{pl}x10^4$ (m^{-1})	$k'_w x10^4$ (m^{-1})	$(Deviation)_{pl}$ $x10^2$	$\frac{(Deviation)_w}{(Deviation)_{pl}}$
1.10	38.0	.197	.371	1.8	1.0
1.10	43.7	.262	.545	4.5	0.5
1.10	49.2	.281	.725	3.2	0.4
1.10	54.8	.310	.766	0.2	0.2
1.10	60.8	.316	.939	4.3	0.3
1.10	73.7	.351	.991	8.3	0.4
1.35	38.0	.404	1.81	5.0	0.1
1.35	43.7	.509	2.66	7.6	0.0
1.35	49.2	.473	2.94	5.5	-0.01
1.35	54.8	.555	3.52	8.5	0.1
1.35	60.8	.509	3.68	5.8	0.1
1.35	73.7	.593	4.35	8.8	0.2
1.75	38.0	.672	8.30	4.1	0.1
1.75	43.7	1.11	12.3	4.5	0.1
1.75	49.2	.796	18.8	3.5	0.1
1.75	54.8	1.16	14.6	4.5	0.0
1.75	60.8	1.33	20.7	2.3	0.1

decrease with increasing velocity as more of the gas would travel in the bubble phase. The fact that interphase transfer is not limiting can also be seen from the fact that k'_{pl} increases with increasing aerosol diameter. As was shown in Section 7.2, bypassing in the bubble phase is not a function of aerosol diameter. This confirms the theoretical conclusions reached in Section 7.3.3. Figure 7.7 shows the per cent penetration of DOP aerosol through a fluidized bed composed of 110 μm collectors at $U = 6.0 \times 10^{-2}$ m/s, with the predicted penetration curves assuming the dense phase is in plug flow. As seen from the figure this assumption is in very good agreement with experimental results; each point on the figure is hardly a few per cent away from its predicted value. It is also interesting to note from Figure 7.7 that at bed depths approximately below 1.5×10^{-2} m penetrations are higher than predicted due to local spouting and jet penetration in the bed.

Figure 7.8 shows per cent penetration of 1.1 μm aerosol as a function of bed depth for U = 0.13 m/sec, as a further example. Plotted on the figure are the predictions calculated from assuming (i) dense phase is in plug flow; (ii) dense phase is well mixed. It is demonstrated clearly that the dense phase is much closer to plug flow.

Inspection of Table 7.3 shows that the particulate phase in almost all sets of experiments with 600 μm collectors was well mixed. This is shown clearly in Figure 7.9 where measured penetration of particles is plotted as a function of bed depth for U = 0.4915 m/s compared with the two fitted curves. This clear difference from the behaviour of the 110 μm particles may be ascribed to two effects:

FIGURE 7.7 Aerosol penetration versus bed depth

$U = 6.02 \times 10^{-2}$ m/s
$d_p = 110$ μm
full circle, $d_A = 0.72$ μm
open circle, $d_A = 0.90$ μm
full square, $d_A = 1.15$ μm
lines, estimated penetrations assuming dense phase is in plug flow

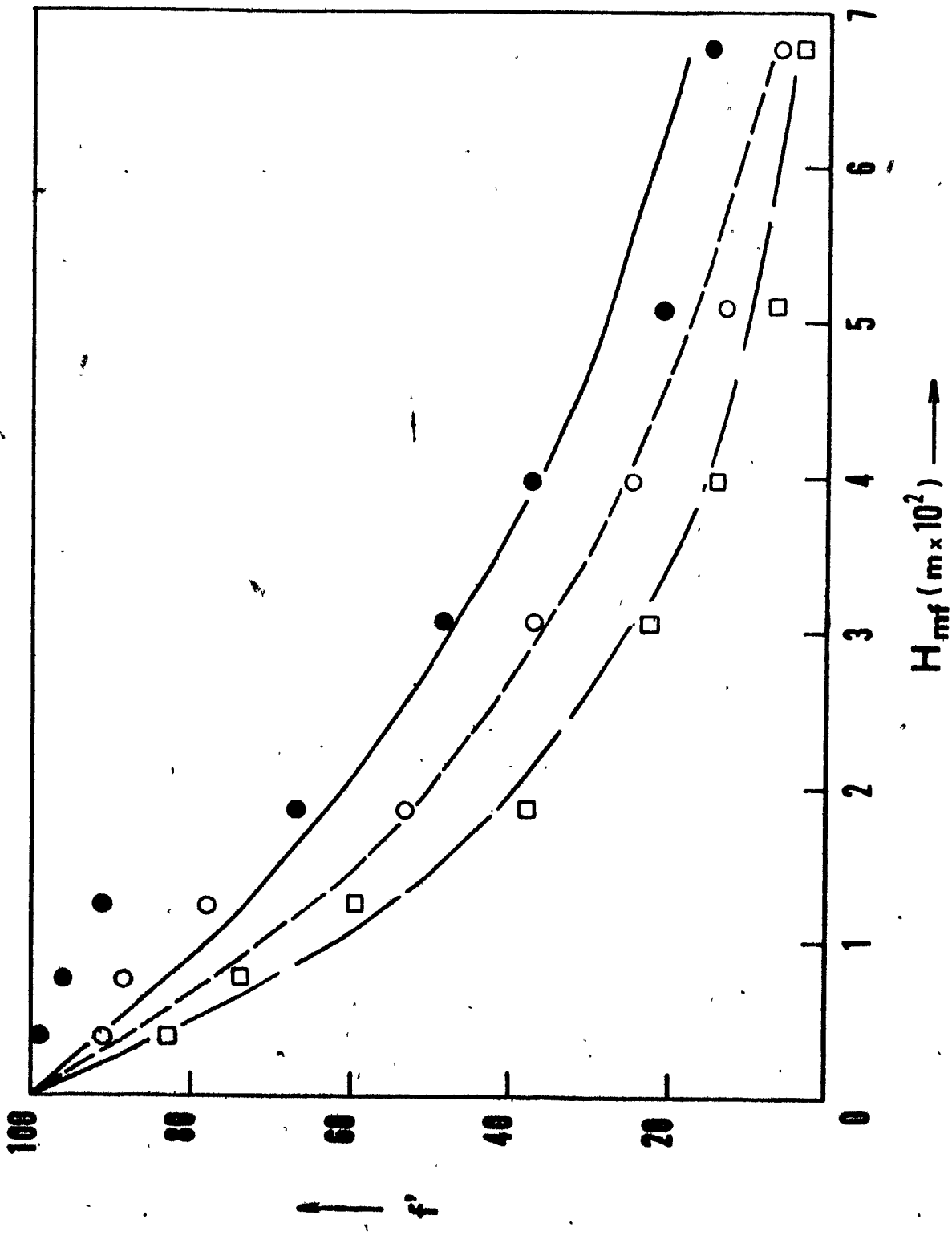
100
80
60
40
20
0
f'
1
2
3
4
5
6
7
H_{mf} (m x 10^2)

FIGURE 7.8 Aerosol penetration versus bed depth

$U = 0.13$ m/s
$d_p = 110$ μm
full circle, $d_A = 1.1$ μm
solid line, dense phase in plug flow
broken line, dense phase in well mixed

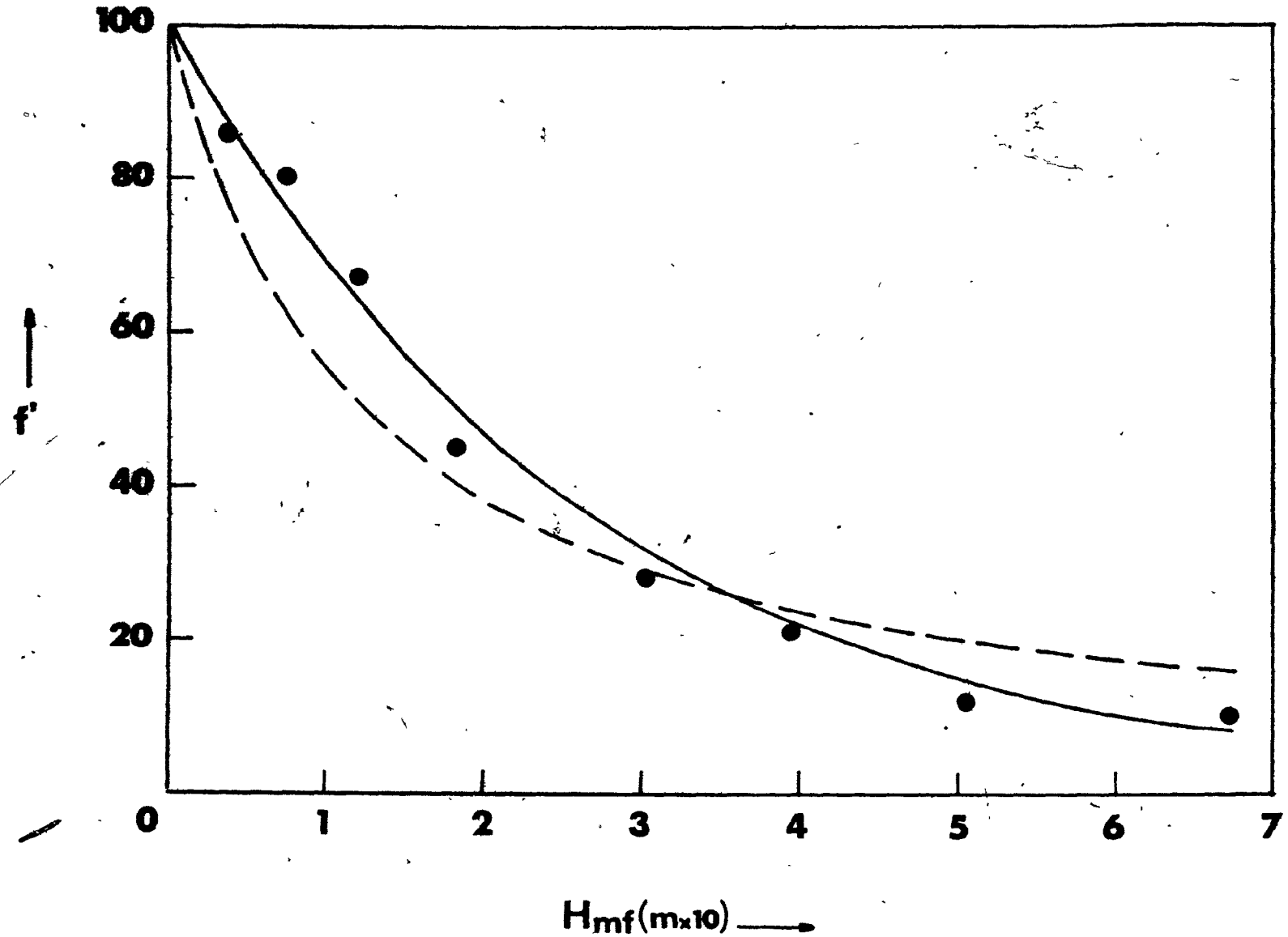
100
80
60
40
20
0
1
2
3
4
5
6
7
f'
Hmf(mx10)

FIGURE 7.9 Aerosol penetration versus bed depth

d_p = 600 μm
U^p = 0.4915 m/sec
full circle, d_A = 1.75 μ
broken line, plug flow model
solid line, well mixed model

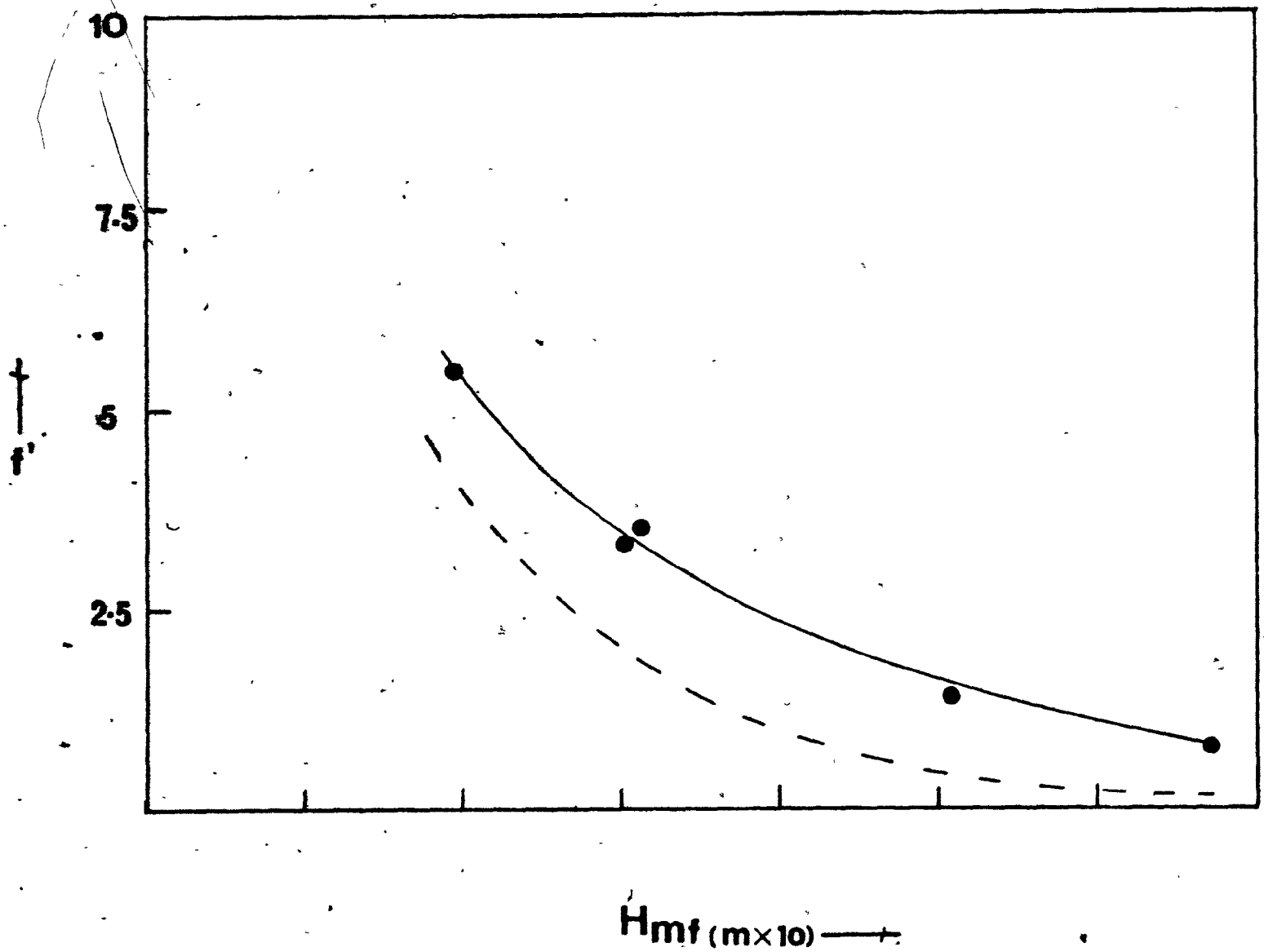
10
7·5
5
2·5
f'
Hmf (m×10)

1. Larger bubbles, due to the higher values of $(U-U_{mf})$ used with the 600 μm particles (see Table 7.1) and to the lower probability of bubble break-up in beds of larger particles.[D1]
2. Higher particle mobility, resulting from lower apparent viscosity in beds of large particles.[D2]

It may also be noted that k'_w increases both with U and d_A, once more confirming that collection cannot be limited by interphase transfer.

In summary, it has been shown in this section that, in the bed of 110 μm collector, the dense phase gas was close to plug flow, whereas in the 600 μm particles the gas is in a condition close to complete mixing. With both collector sizes, resistance to interphase transfer was negligible and aerosol penetration could be adequately described either by Equation (7.65) for dense phase in plug flow, or by Equation (7.66) for dense phase well mixed.

7.5 Interpretation of Collection Rate Constants and Comparison with Fixed Beds

7.5.1 Efficiency of a collecter particle in a fluidized bed

7.5.1.1 Introduction

It could be argued that the concept of an individual collector particle efficiency in a fluidized bed has no precise meaning. In a fixed bed the superficial velocity between collector particles and fluid is equal to the superficial velocity through the bed. In a fluidized bed however this is not so; assuming the two phase theory of fluidization is correct, then the superficial velocity between collector particles and fluid is the minimum fluidization velocity, U_{mf}. The situation might

appear further complicated when the particulate phase is well mixed. In this section, therefore, it will be shown that the collection efficiency of an individual particle in a fluidized bed may be derived from the general definition of the efficiency of a spherical collector incorporating, simultaneously, the conditions imposed by the two phase theory of fluidization. It will also be shown that the relationship between E_{FT} and k' is similar, irrespective of whether the particulate phase is in plug flow or well mixed. As these equations have not been presented previously in the literature, a detailed derivation will be given.

7.5.1.2 Dense phase in plug flow

The number of collector particles per unit volume in a fixed bed was given as

$$N_p = \frac{6(1-\epsilon)}{\pi d_p^3} \tag{5.2}$$

Assuming the void fraction in the dense phase of a fluidized bed is constant at the value corresponding to minimum fluidization, ϵ_{mf}, then the number of collector particles in a differential bed depth dh is equal to

$$N_p = dh A_B N_p = \frac{6(1-\epsilon_{mf})dh A_B}{\pi d_p^3} \tag{7.71}$$

Let the concentration of the aerosol change in that differential bed depth from C to (C + dC). Then rate of aerosol collection by differential bed depth is

$$R_B = U * A_B * dC \tag{7.72}$$

The collection efficiency of an individual spherical collector was defined in general terms as

$$E_{FT} = \frac{\text{particles of aerosol collected}}{\text{particles in approach volume}} \tag{3.1}$$

Thus the number of aerosol particles collected by one spherical collector, diameter d_p, per unit time is

$$R_T = E_{FT} * \frac{\pi d_p^2}{4} * U_{mf} * C \tag{7.73}$$

where C is the number concentration of aerosol particles in the approach volume. Now since

$$R_B = N_p * R_T * dh * A_B \tag{7.74}$$

Then from Equations (7.71) and (7.73)

$$UA_B dC = \frac{6(1-\epsilon_{mf})dhA_B}{\pi d_p^3} * E_{FT} * \frac{\pi d_p^2 U_{mf} C}{4} \tag{7.75}$$

which simplifies to

$$E_{FT} = \frac{2d_p U}{3U_{mf}(1-\epsilon_{mf})} * \frac{1}{U} * \frac{dC}{dh} \tag{7.76}$$

A mass balance on aerosol particles over a differential bed depth dh gives:

$$\begin{matrix}\text{Rate of} \\ \text{aerosol in}\end{matrix} = \begin{matrix}\text{Rate of} \\ \text{aerosol out}\end{matrix} + \begin{matrix}\text{Rate of} \\ \text{aerosol removal}\end{matrix} \qquad (7.77a)$$

$$UC = U(C + dC) + k'_{p1}CdhU \qquad (7.77b)$$

therefore

$$\frac{1}{C}\frac{dC}{dh} = k'_{p1} \qquad (7.78)$$

Substituting in Equation (7.76), the individual collection efficiency of a spherical collector, assuming the dense phase is in plug flow, is

$$(E_{FT})_{p1} = \left(\frac{U}{U_{mf}}\right) * \left(\frac{2}{3}\right) * \frac{k'_{p1}d_p}{(1-\varepsilon_{mf})} \qquad (7.79a)$$

or alternatively from Equation (7.64)

$$(E_{FT})_{p1} = \frac{2K_V d_p}{3U_{mf}(1-\varepsilon_{mf})} \qquad (7.79b)$$

This is equivalent to Equation (5.3b) obtained for packed beds.

7.5.1.3 Dense phase well mixed

When the particulate phase is assumed to be well mixed the aerosol concentration in the bed is constant. Using Equation (5.2) the total number of aerosol particles in the bed is

$$H_{mf}A_B N_p = \frac{6(1-\epsilon_{mf})H_{mf}A_B}{d_p^3} \tag{7.80}$$

The rate of aerosol collection in the bed is

$$R_B = A_B U(C_{in} - C_{out}) \tag{7.81}$$

where C_{in} and C_{out} refer to the number concentration of aerosol entering and leaving the bed respectively. The rate of aerosol collection per particle is

$$R_T = E_{FT} * \frac{\pi d_p^2}{4} * U_{mf} * C_{out} \tag{7.82}$$

where C_{out} in this context is equivalent to the concentration of aerosol in the particle approach volume, and is used because the dense phase is well mixed and resistance to interphase transfer is negligible. However, from Equation (7.74)

$$R_B = N_p * R_T * H_{mf} * A_B \tag{7.74}$$

Substituting from Equations (7.80), (7.81) and (7.82) and simplifying

$$(E_{FT})_w = \frac{(C_{in} - C_{out})/C_{out}}{H_{mf}} * \frac{U}{U_{mf}} * \frac{2d_p}{3U_{mf}(1-\epsilon_{mf})} \tag{7.83}$$

since for a well mixed dense phase

$$k'_w = \frac{(1-f)/f}{H_{mf}} = \frac{(C_{in} - C_{out})/C_{out}}{H_{mf}} \tag{7.6}$$

then

$$(E_{FT})_w = \left(\frac{U}{U_{mf}}\right) * \left(\frac{2}{3}\right) * \frac{k'_w d_p}{(1-\epsilon_{mf})} \qquad (7.84)$$

Thus Equations (7.79a) and (7.84) are identical and the relationship between E_{FT} and k' does not depend on whether the dense phase is well mixed or in plug flow. The above conclusion is extremely useful as it allows a direct comparison between the efficiency of a collector in a fixed and in a fluidized bed. Corresponding experimental values for E_{FT} are given for the two sizes of collector in Tables 7.4 and 7.5, and the comparison with efficiency in a fixed bed is investigated in Section 7.5.2.

7.5.2 Statistical analysis of fluidized bed data and comparison with fixed beds

7.5.2.1 Introduction

The experimental efficiencies of the 110 μm and 600 μm collector particles, calculated as described in the previous section, were analysed by multiple regression, with a procedure similar to that described in Chapter 5. The 110 μm collectors were analysed first and the conclusions drawn were used to narrow the search for an efficiency equation for 600 μm collectors. In Section 6.6 it was determined that the dominant collection mechanism in a fluidized bed is inertial deposition. This can be confirmed qualitatively by inspection of Tables 7.4 and 7.5. As seen from these tables, particle efficiency goes up quite sharply with increasing aerosol diameter, proportional to a power of aerosol diameter greater than unity. Thus the analysis concentrated on determining the form of the relationship

TABLE 7.4 Experimental Collection Efficiency of 110 μm Collectors in a Fluidized Bed

	$E_{FT} \times 10^2$		
U, $mx10^2/s$	(0.64 - 0.8) μm	(0.8 - 1.0) μm	(1.0 - 1.3) μm
4.9	0.66	0.92	1.34
6.0	1.00	1.33	1.79
7.2	1.24	1.77	2.57
12.9	2.07	3.05	4.17
13.1	2.17	3.43	5.10
19.5	3.27	4.84	6.60
25.6	4.60	7.41	11.2
34.9	5.73	8.57	11.9

TABLE 7.5 Experimental Collection Efficiency of 600 μm Collectors in a Fluidized Bed

	$E_{FT} \times 10^2$		
U, $m \times 10^2/s$	(1.0 - 1.20) μm	(1.2 - 1.5) μm	(1.5 - 2.0) μm
38.0	3.29	16.1	73.8
43.7	5.56	27.2	126
49.2	8.32	33.9	216
54.8	9.81	45.1	187
60.8	13.3	52.4	295
73.7	17.0	74.9	-----

between individual particle collection efficiency and the inertial collection parameter, St.

7.5.2.2 Analysis of 110 μm collectors

The 110 μm collector particles were analyzed by testing two hypothetical models. A notation similar to the approach of Chapter 5 is used, the model tested being identified by a letter (S for 110 μm, B for 600 μm) and a number. The two models tested were as follows:

Model 1S assumed, in accordance with the two phase theory of fluidization, that the relative velocity between collector and fluid is the minimum fluidization velocity, irrespective of U. Thus,

$$E_{FT} = \alpha_I St_{mf} \tag{7.85}$$

This model disagrees with all previous studies, which claimed that inertial deposition for micron range particles in a fluidized bed is negligible.

Model 2S is an extension of the first hypothesis. It incorporates an additional term which allows for the enhancement of inertial collection caused by the motion of collector particles induced by rising bubbles.

$$E_{FT} = (\alpha_I)_1 St_{mf} \left[1.0 + (\alpha_I)_2 \left(\frac{U-U_{mf}}{U_{mf}}\right)\right] \tag{7.86}$$

It is thus assumed that the enhancement of inertial collection is a linear function of the ratio of bubble to dense phase gas flow.* The coefficients of these two models were determined by multiple regression and their

*It is implicitly assumed here that the bubble phase flow is $(U-U_{mf})$ as predicted by the simple two phase theory. Since the value of n in Equation (7.33) is essentially unknown, there is little point in including it in an empirical correlating equation.

values are given in Table 7.6, together with the square of the adjusted multiple correlation coefficient, R^2_{AD}, and the adjusted standard residual, S_{AD} (see Appendix F). Inspection of the table shows that Model 2S, which incorporates the dimensionless velocity collection parameter $(\frac{U-U_{mf}}{U})$ and yields the following efficiency equation

$$E_{FT} = 3.70\ St_{mf}\left[1.0 + 1.56\left(\frac{U-U_{mf}}{U_{mf}}\right)\right] \qquad (7.87)$$

is far superior. With $R^2_{AD} = 0.989$ and $S_{AD} = 5.5\times10^{-3}$ Model 2S explains over 98% of the variation in experimental data and is an almost perfect simulation of the process of aerosol removal in the bed. This is shown more clearly on Figures 7.10 to 7.12.where the experimental efficiencies of the three aerosol sizes are compared with the predictions of the two models. The fact that the dominant collection is inertial deposition, enhanced by the fluctuating movement of collectors induced by the bubble phase, is undisputable even for 0.72 μm diameter aerosol particles. Perhaps an illustrative comparison with fixed bed experiments should be made at this point. The second term of Equation (7.87) tends to zero as $U \to U_{mf}$. Thus the efficiency of the fluidized bed collector particles extrapolates to the Stokes number at minimum fluidization multiplied by a factor of 3.7. Comparison of this with the best equation presented in Chapter 5 for collection in fixed beds of 110 μm collectors

$$E_{BT} = 2.9\ St + 6.9\ N_G \qquad (5.22)$$

shows a 22% agreement in the value of the two coefficients. The coefficient of Equation (7.87) is slightly higher, compensating for the neglected effect

FIGURE 7.10 Measured and predicted collector efficiencies in fluidized bed as a function of superficial gas velocity

d_p — 110 μm
full circle, d_A — 0.72 μm
broken line, model 1S
solid line, model 2S

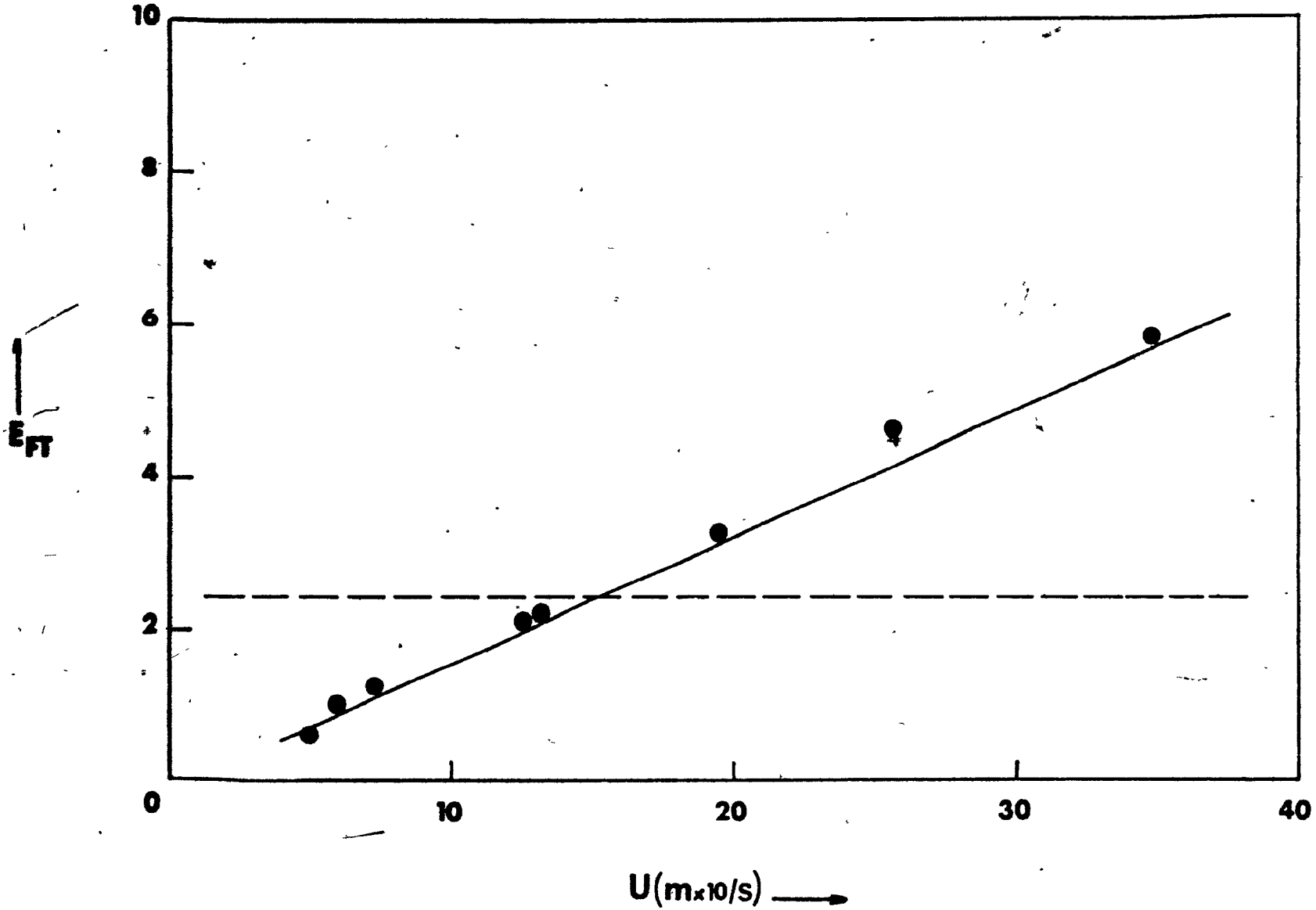
10
8
6
4
2
0
10
20
30
40
E_{FT}
U(m×10/s)

FIGURE 7.11 Measured and predicted collector efficiencies in fluidized bed experiments as a function of superficial gas velocity

d_p = 110 μm
full circle, d_A = 0.90 μm
broken line = model 1S
solid line = model 2S

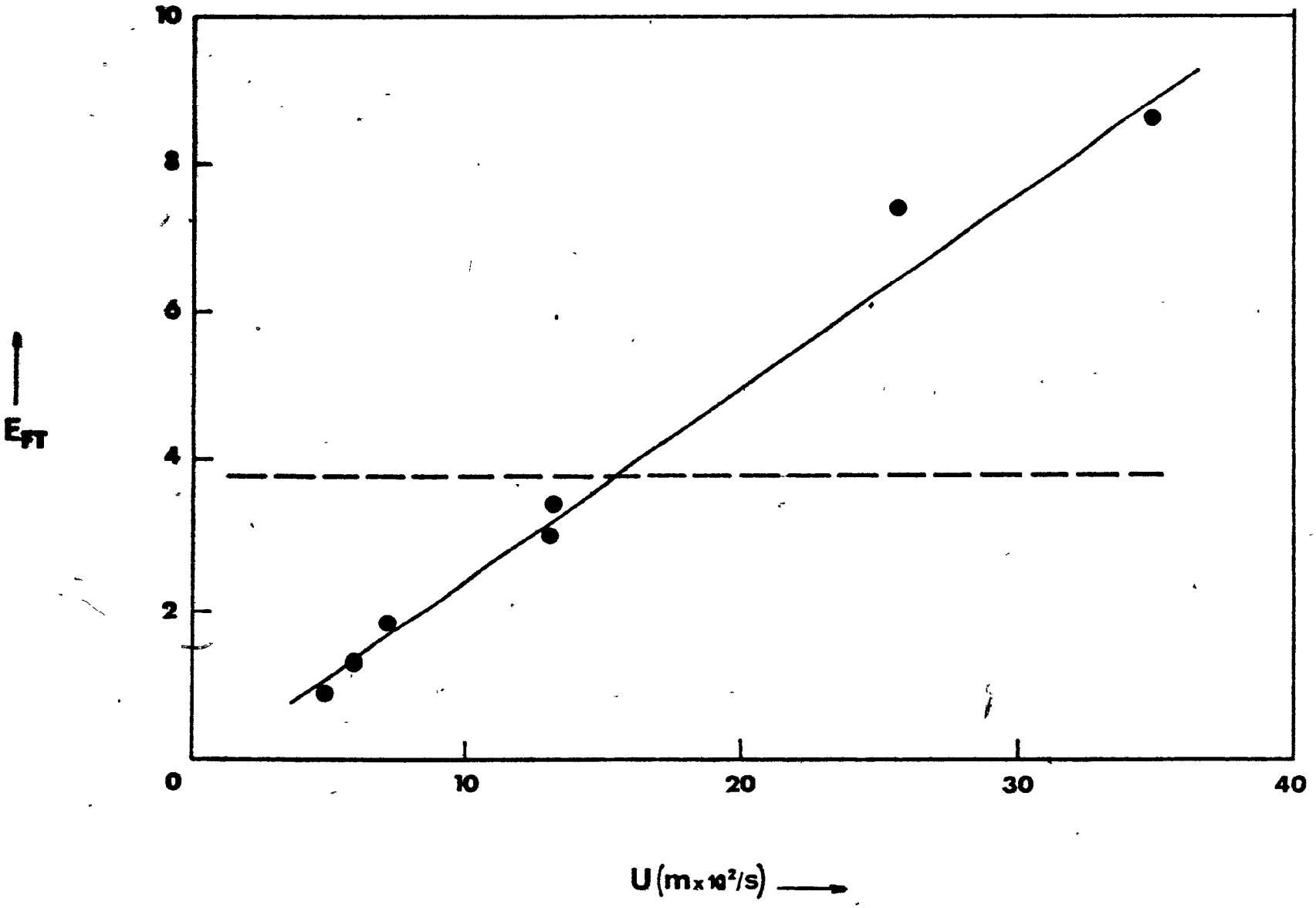
10
8
6
4
2
0
10
20
30
40
E_{FT}
U (m x 10²/s)

FIGURE 7.12. Measured and predicted collector efficiencies in fluidized bed experiments as a function of superficial gas velocity

d_D = 110 μm
full circle, d_A = 1.15 μm
broken line = model 1S
solid line = model 2S

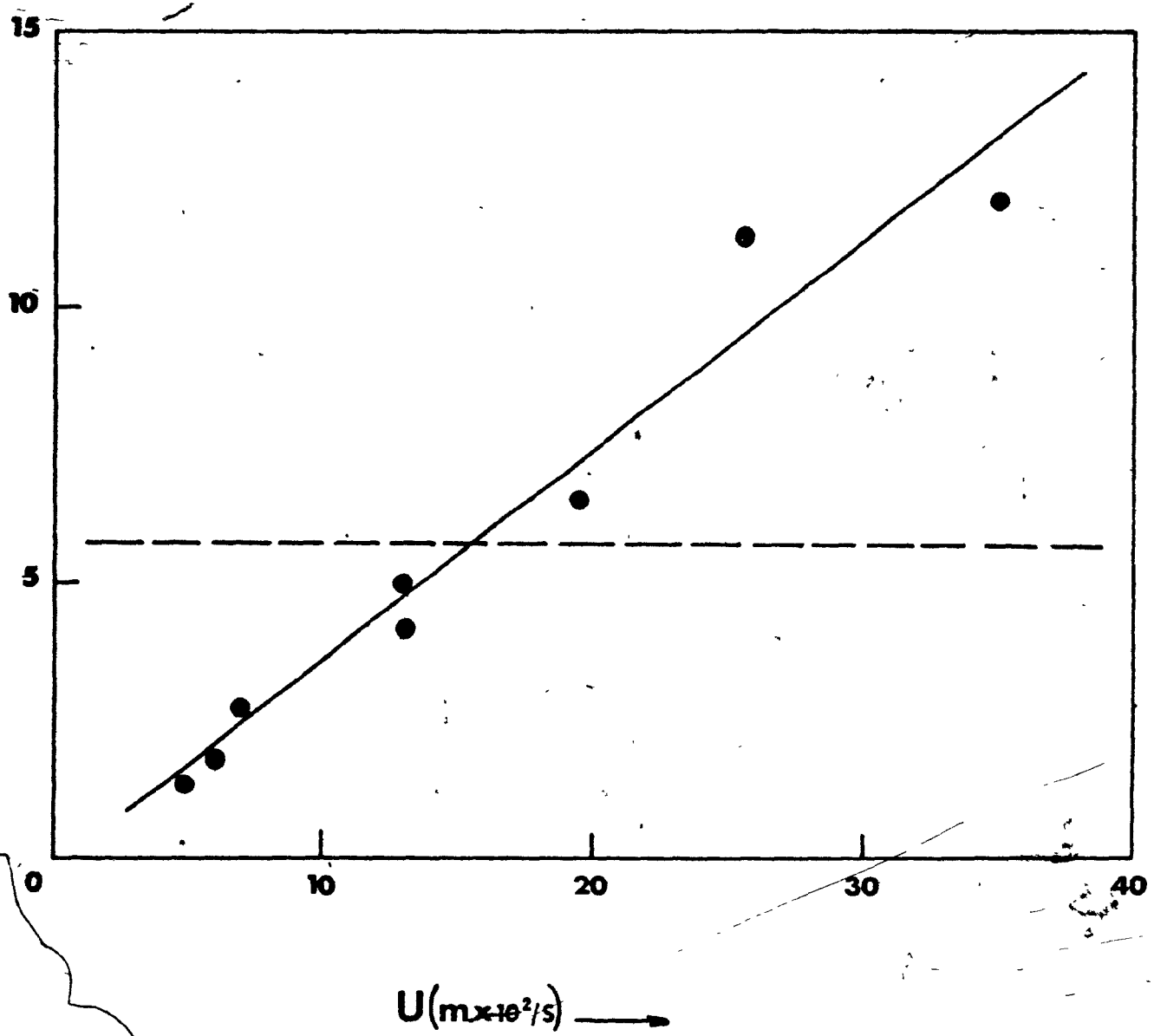
15
10
5
0
10
20
30
40
U(m.x10²/s)

of gravitational settling. This term could not be determined separately in the fluidized bed since, like St_{mf}, it is proportional to d^2_A, and U_{mf} could not be varied in the same way as U in the fixed bed experiments. Thus, this remarkable agreement between two completely different types of experiments, performed with different aerosol sizes, reflects the predictive accuracy of the collection equations presented in this study.

7.5.2.3 Analysis of 600 μm collector

The analysis of 110 μm collectors established the form of Equation (7.86) for aerosol collection in the bed. A preliminary analysis of the data efficiency data presented in Table 7.5 showed that, for the 600 μm collector particles, the dependence of inertial collection in the fluidized bed on the Stokes number was of the form

$$E_{FT} = (\alpha_I)_1 \, St^c \left[(1.0 + (\alpha_I)_2 \left(\frac{U-U_{mf}}{U_{mf}} \right) \right] \qquad (7.88)$$

where c is a constant. The analysis of 600 μm collector particles, thus, concentrated on the determination of this constant and Models 1B to 5B tested the hypotheses that this constant was c = 1.0, 2.0, 3.0, 3.5 and 4.0, respectively. The results of these computations are presented in Table 7.6 together with corresponding R^2_{AD} and S_{AD} values. Inspection of the table will show that $3.0 < c < 4.0$. As the efficiencies of (1.0 - 1.2) μm aerosol were far lower than the other size ranges (Tables 7.5), they played a weak role in determining the coefficients of Models 1B to 5B. Thus the predicted efficiencies of this size range are essentially an extrapolation of the correlated coefficients determined by the largest two size ranges.

TABLE 7.6 Summary of Multiple Regression Analysis of Fluidized Bed Experiments

d_p	Model	Fitted Regression Equation	Statistical Analysis	
			R^2_{AD}	$S_{AD} \times 10^2$
110 μm	1S	$42.9\ St_{mf}$	0.685	2.9
110 μm	2S	$3.70\ St_{mf}\ [1.0 + 1.56(U-U_{mf})/U_{mf}]$	0.989	0.55
600 μm	1B	$61.5\ St_{mf}\ [1.0 + 1.95(U-U_{mf})/U_{mf}]$	0.749	0.58
600 μm	2B	$3.69 \times 10^3 St^2_{mf}\ [1.0 + 6.72(U-U_{mf})/U_{mf}]$	0.934	0.30
600 μm	3B	$1.40 \times 10^5 St^3_{mf}\ [1.0 + 24.3(U-U_{mf})/U_{mf}]$	0.983	0.15
600 μm	4B	$8.59 \times 10^5 St^{3.5}_{mf}\ [1.0 + 43.1(U-U_{mf})/U_{mf}]$	0.983	0.15
600 μm	5B	$6.11 \times 10^6 St^{4.0}_{mf}\ [1.0 + 64.3(U-U_{mf})/U_{mf}]$	0.976	0.18

FIGURE 7.13 Measured and predicted collector efficiencies in fluidized bed experiments as a function of superficial gas velocity

d_p = 600 μm
full circle, d_A = 1.1 μm
irregular broken line = model 3B
broken line = model 4B
solid line = model 5B

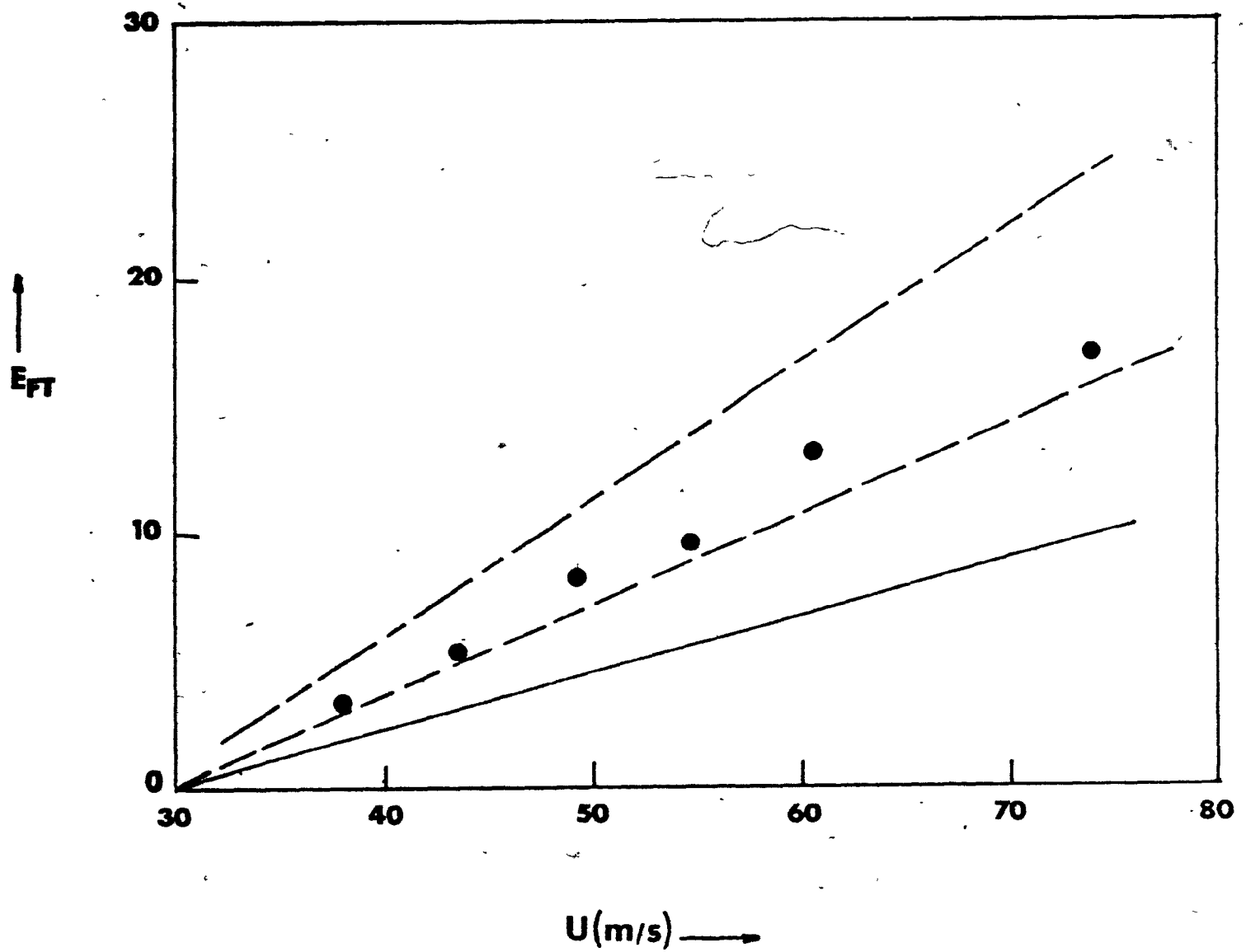
30
20
10
0
E_{FT}
30
40
50
60
70
80
U(m/s)

Therefore, Models 3B to 5B were tested graphically by comparing the predictions of these Models for the (1.0 - 1.2) μm with the experimental points. This is shown in Figure 7.13. Inspection of the figure shows that Model 4B, which assumes that $c = 3.5$ is superior to the other two. Assumption of $c = 3$, (Model 3B), overpredicts the experimental efficiencies of 1.1 μm aerosol and assumption of $c = 4$, Model 5B, underpredicts them. Thus it may be concluded that Model 4B is superior in describing the aerosol collection efficiencies of 600 μm collectors in a fluidized bed. This yields the following efficiency equation.

$$E_{FT} = 8.59 \times 10^{5}\ St_{mf}^{3.5} \left[1.0 + 43.1\left(\frac{U-U_{mf}}{U_{mf}}\right)\right] \qquad (7.89)$$

which simplifies to

$$E_{FT} = 3.70 \times 10^{7}\ St_{mf}^{3.5} \left(\frac{U-U_{mf}}{U_{mf}}\right) \qquad (7.90)$$

without much loss of accuracy as a comparison of the two contributing terms in Equation (7.89) will show.

The experimental collection efficiencies of 600 μm collector particles are plotted with their predicted values, calculated from Equation (7.90), in Figure 7.14 and compared with the corresponding collection efficiencies of 1.75 μm aerosol in a fixed bed. The enhancement of inertial collection is most obvious in this figure where it is observed that the 600 μm collector particles collecting 1.75 μm aerosol become at least one order of magnitude more efficient when fluidized by the challenging aerosol. This increase more than offsets the effect of dense phase mixing,

FIGURE 7.14 Collection efficiencies of 600 μm collector particles in a fluidized bed

full square, d_A = 1.75 μm
open circle, d_A = 1.35 μm
full circle, d_A = 1.1 μm

FOR FIXED BED COMPARISON

circle with asterisk, d_A = 1.75 μm

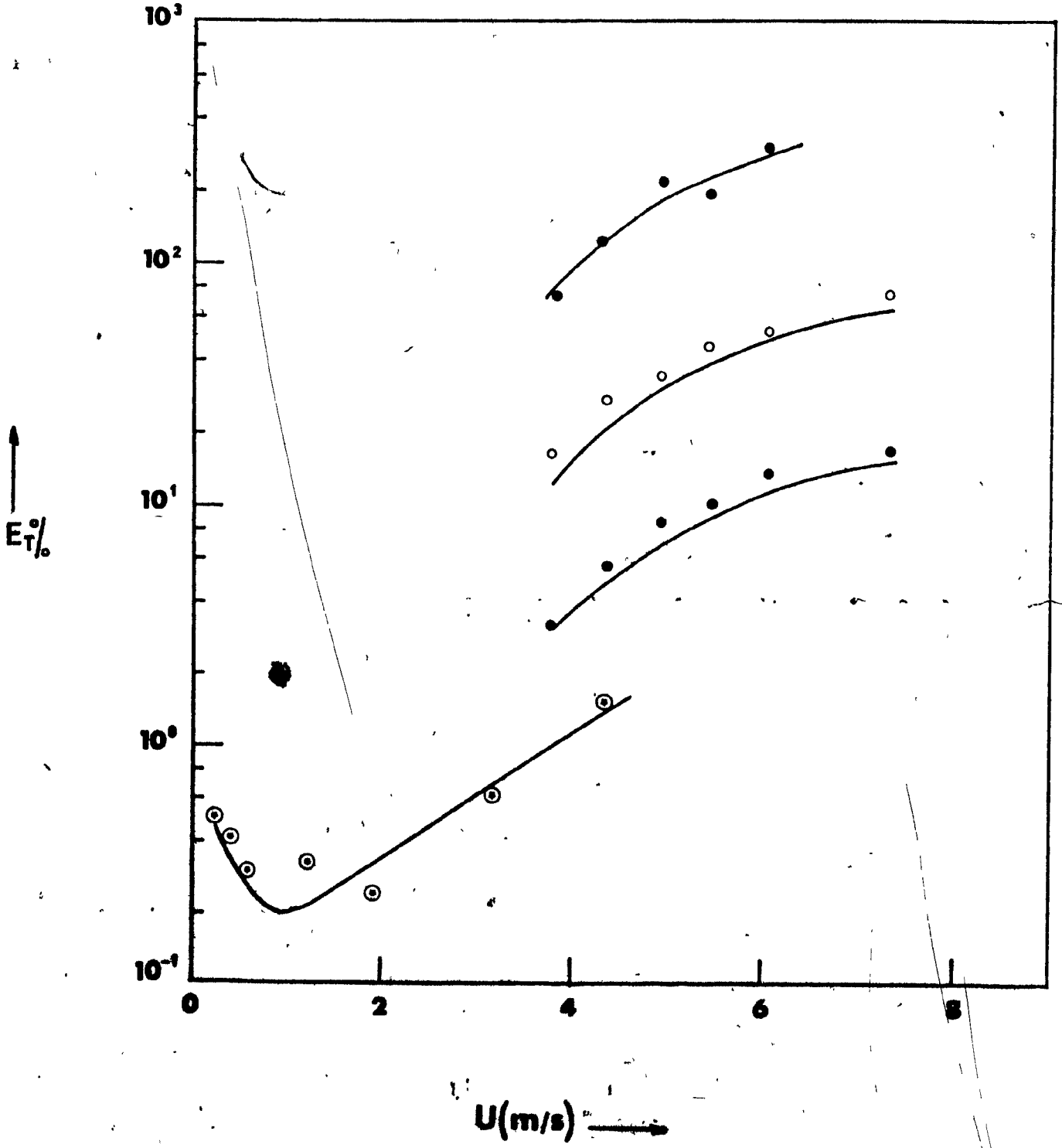
10^3
10^2
10^1
10^0
10^{-1}
E_T%
0
2
4
6
8
U(m/s)

so that, as noted earlier, a well mixed fluidized bed can give lower penetration than a packed bed with plug flow.

The high power of St_{mf} in Equations (7.89) and (7.90) compared to (7.87) merits some comment. In part, the stronger dependence of E on St_{mf} may result from the larger values of Re_{mf} and St_{mf} for the 600 μm collector, as predicted by various workers for isolated collectors and also found in packed beds in Chapter 5. However, the magnitude of the dependence suggests that collection is not as simple as in a steady flow situation, and this is also reflected by the fact that individual particle collection efficiency in a fluidized bed can be greater than unity. Presumably the fluctuating motion of the particles in the dense phase causes them to sweep a gas volume greater than the particle approach volume.

7.6 Summary

This chapter analyzed the experimental results on aerosol collection presented in Chapter 6.

A preliminary analysis, which simulated aerosol collection around an isolated spherical Davidson bubble, showed that collection in a fluidized bed may not be described by visualizing the lean phase as consisting of isolated bubbles rising to the surface of the bed without interference from neighbouring bubbles. This is due to the fact that, in a very shallow bed, bubble coalescence is frequent. Subsequently, a theory describing aerosol removal in fluidized beds was developed, based on the modified two phase theory of fluidization. It was shown that bubble coalescence causes transfer between the bubble and particulate phases to be so rapid in the shallow beds used here that simplified equations can be used for the two cases where the dense phase is in plug flow or well mixed.

A preliminary analysis of aerosol transfer coefficients showed that the particulate phase of beds fluidized with 110 μm collectors was nearer to plug flow, while for the 600 μm collectors the dense phase was nearer to being well mixed. Subsequently the individual collection efficiency of a spherical collector in a fluidized bed was derived from first principles. The resulting experimental efficiencies were correlated by multiple linear regression. It was shown that the dominant collection mechanism of micron range aerosol particles in fluidized beds is inertial collection enhanced by the fluctuating movement of collector particles induced by the bubble phase. For aerosol collection in the beds of 110 μm collectors the best equation for aerosol removal is

$$E_{FT} = 3.70\ St_{mf} \left[1.0 + 1.56\left(\frac{U-U_{mf}}{U_{mf}}\right)\right] \qquad (7.87)$$

which explains 98.9% of the variation in experimental data. The corresponding equation of collection by 600 μm diameter particles is

$$E_{FT} = 3.70\times10^{7}\ St_{mf}^{3.5}\left(\frac{U-U_{mf}}{U_{mf}}\right) \qquad (7.90)$$

which explains 98.2% of the variation in experimental data. Thus the accuracy of the above correlations is demonstrated and they are suggested as useful design equations.

CHAPTER 8. INDUSTRIAL IMPLICATIONS OF THE WORK AND RECOMMENDATIONS FOR FUTURE STUDIES

As has been demonstrated in this study, the fluidized bed offers itself as a candidate for the development of efficient filtering devices in industry. The prime advantages of a fluidized bed filter together with their industrial implications and recommended extensions of the work are presented below:

The most important advantage of a fluidized bed is its continuous operation mode. Aerosol particles may be collected continuously while "spent" collectors are removed and fresh collectors added while the bed is in operation. Thus the need for expensive batch or semi-batch operation is eliminated. The economic advantages of such a device are then partially determined by the cost of regenerating or replacing the spent collector particles. Although this study did not concentrate on bed loading effects there is sufficient evidence in the literature[M4] that porous collectors (alumina granules, silica gel) can pick up to 7% of their weight in aerosol before becoming too sticky to fluidize. As this process is also a function of the diffusion rate of liquid aerosol in a porous collector, further investigation on specific applications would be desirable. However, if collection is achieved at high temperature and the aerosol particles are destroyed by burning in the bed this additional cost is eliminated.

As was shown in this study, very high collection efficiencies may be obtained with a fluidized bed provided an adequate distribution of gas is achieved. Thus the distributor plate should be given prime consideration in designing such a unit. As adequate distribution of gas is invariably accompanied by a pressure loss across the plate, pilot

scale experiments will determine the minimum operating pressure drop and density of orifice holes necessary to ensure initial formation of small bubbles and thus rapid transfer between the lean and dense phases. As a rough guideline, the results of this thesis suggest that an orifice hole density of 3×10^4 holes/m^2 and a pressure drop of the order of 100 n/m^2 provide adequate distribution of gas for aerosol collection.

There does not appear to be an upper limit to the superficial gas velocity through the bed at which high collection efficiencies are obtained, apart from the requirement that the collector particles are not carried over from the bed. As the results of this study have shown, collection of micron range particles in the bed is by inertial deposition. Since,

$$U_{mf} \propto d_p^{1.98} \rho_p$$

then $$St_{mf} \propto \frac{U_{mf}}{d_p} \propto d^{0.98} \rho_p$$

It has been shown in this work that E_{FT} is proportional to St_{mf} to a power equal to or greater than unity. Hence the efficiency through the bed may, potentially, be increased by increasing the collector diameter or density. This has been demonstrated in this study for superficial gas velocities up to 3 m/s but potentially much higher velocities could be used. Large, dense collector particles are also recommended because their higher terminal velocity raises the upper limit on superficial gas velocity.

For solid aerosols, it is quite likely that the aerosol particles will agglomerate in the bed, possibly with the help of small amounts of

a liquid phase, and re-entrain in the form of large particles. These would be more easily collectable in a cyclone device situated downstream from the bed. Thus regeneration of the bed collecters would be completely eliminated and the bed would behave as an agglomerating device, increasing the aerosol diameter to a size easily removed. Similarly, it is possible to use the agglomerated particles as collectors, thus eliminating the need to regenerate and return the collector.[D4]

Another important advantage of the fluidized bed is that it can operate at high temperatures and pressures. Thus it is not limited by these physical factors, as fibrous collectors are. It should be pointed out however that little or nothing is known about the collection mechanisms around spherical collectors in a fluidized bed at high temperatures and/or pressures. All the results of this study were performed at ambient temperature (20 - 30°C) and pressure. Also, there is evidence[D6] that forces holding solid particles to solid surfaces weaken with increasing temperature and this should be kept in mind when studies with dry collectors and solid aerosols are performed. It will not, in general, be possible to extrapolate directly from studies on spherical, laboratory aerosols at ambient conditions to collection of irregularly-shaped industrial particulates at high temperatures.

CHAPTER 9. SUMMARY

An experimental facility has been developed to enable rapid collection of aerosols in the size range around 1 μm in fixed and fluidized beds of collector particles. Solid and liquid aerosols were formed using a commercial spinning-disk generator, modified to give an aerosol whose size and number concentration remained stable over long periods of time. Light-scattering counters were used to measure the number concentration of aerosol in narrow size ranges. It was shown that, over the range of these experiments, precisely isokinetic sampling of the aerosol was not required. Penetrations in the collector beds were determined by difference from the sample concentration without the bed in place, corrected for small long-term variations in generator output by periodic sampling upstream from the bed. The bed diameter was .15 m in all experiments.

For fixed beds, experiments were performed with 1.35 and 1.75 μm aerosols in beds of 110 and 600 μm diameter spherical collector. The gas flow was vertically downwards, with velocity from 2×10^{-2} to .45 m/sec. For solid aerosols, it was found that bed loading effects caused the penetration to decrease with time. The majority of the experiments were therefore performed with a dilute liquid aerosol (dioctyl phthalate). The experimental results served to resolve previous uncertainty about the mechanism of filtration under these conditions. It was shown that the predominant collection mechanisms are gravitational settling (for U < 0.08 m/sec) and inertial deposition (for U > 0.08 m/sec), with all other mechanisms at least an order of magnitude less important. The following correlations were developed for the collection efficiency of a single collector particle.

$$E_{BT} = 2.89\ St + 6.89\ N_G \qquad (0.07 < Re_p < 1.4) \quad (5.22)$$

$$E_{BT} = 5.83 \times 10^{-2}\ Re_p\ St + 1.42\ N_G \qquad (1.1 < Re_p < 17.4) \quad (5.21)$$

For fluidized beds, two distinct experimental arrangements were developed, the first for superficial gas velocities up to 0.7 m/sec and the second for operation up to 3 m/sec. Spherical collector particles of diameter 110 and 600 μm with density 2.49×10^3 Kg/m^3, and 550 μm with density 4.5×10^3 Kg/m^3 were used. A special multi-orifice distributor was developed, to give good gas distribution with low aerosol collection. It was shown that, in the range just above minimum fluidization, aerosol penetration increases with gas velocity, especially if the distributor is ineffective. At higher velocities with adequate gas distribution, penetration decreases steadily with increasing gas velocity, right up to the point at which the collector particles are conveyed out of the bed. Shallow beds, with depths of typically .03 to 0.08 m, were found to collect more than 95% of the challenging aerosol. Liquid aerosols were collected stably until the concentration on the collector reached such a level that the bed "froze". For solid aerosols, the collector was first coated with a layer of a non-volatile liquid; collection then occurred at the same rate as for a liquid aerosol, with no evidence of re-entrainment or other unsteady characteristics. Collection rates increased with aerosol particle size. For the 600 μm particles, a range of gas superficial velocity was found in which the penetration in the fluidized bed was lower than in a fixed bed operated under the same conditions.

The fluidized bed results were analyzed in terms of established theories of the mechanics of fluidization. It was shown that aerosol is transferred from the bubbles to the dense phase primarily by bulk gas flow, with negligible contribution from Brownian diffusion. By calculating aerosol collection in the cloud region around a Davidson bubble, it was shown that the results cannot be interpreted in terms of a model based on non-interacting gas bubbles rising through the collector bed. The model for fluidized bed reactors proposed by Orcutt et al. was extended, to incorporate modifications to the simple two-phase theory of fluidization and to describe aerosol collection. It was shown that, as a result of frequent bubble coalescence, aerosol transfer between the bubble and dense phases was very rapid in these experiments, so that collection was determined entirely by processes occurring in the particulate phase. The dependence of aerosol penetration on bed depth predicted by this model was found to agree closely with the experiments, with the dense phase gas in plug flow in the 110 μm particles and fully mixed in the 600 μm particles. New expressions for the collection efficiency of a particle in a fluidized bed were developed from first principles, based on the modified two-phase theory of fluidization:

$$E_{PT} = 3.70\ St_{mf}\left[1 + 1.56\left(\frac{U-U_{mf}}{U_{mf}}\right)\right] \quad (d_p = 110\ \mu m) \qquad (7.87)$$

$$E_{PT} = 8.59\times10^{5}\ St_{mf}^{3.5}\left[1 + 43.1\left(\frac{U-U_{mf}}{U_{mf}}\right)\right] \quad (d_p = 600\ \mu m) \qquad (7.89)$$

The second term in each of these equations is dominant, and describes the enhancement of inertial deposition by the fluctuating particle motion induced by bubbles.

CLAIMS TO ORIGINALITY

1. Development of experimental systems to enable rapid determination of aerosol penetration in fixed beds, and in fluidized beds at intermediate and high gas velocities, with penetration based on number concentration for narrow size ranges.
2. Design of a distributor to give good gas distribution with negligible aerosol collection.
3. Development of an experimental technique to determine collection efficiencies in a fixed bed, without bed loading or end effects.
4. Unambiguous identification of the dominant collection mechanisms of micron-range aerosols in fixed and fluidized beds.
5. Presentation of useful design equations for the collection efficiency of an individual particle in a fixed bed.
6. Comprehensive experimental data for aerosol penetration in a fluidized bed of realistic size operated at industrially viable gas velocities.
7. Analysis of aerosol collection in fluidized beds, based on the modified two-phase theory of fluidization, and of collection in the cloud region of a Davidson bubble.
8. Derivation, from first principles, of a meaningful definition of individual particle collection efficiency in a fluidized bed, and development of useful design correlations.
9. Demonstration of negligible resistance to transfer between bubble and particulate phases in a shallow fluidized bed collecting aerosol.

10. Demonstration that the particulate phase of a fluidized bed does not behave in the same manner as a fixed bed for aerosol collection, so that bubble induced particle motion causes higher individual particle collection efficiencies.

11. Demonstration that aerosol penetration in a shallow fluidized bed operated sufficiently above minimum fluidization decreases monotonically with increasing gas velocity.

NOTATION

A	collecting surface area of electrostatic precipitator (1.0), m^2
A_B	cross sectional area of bed (5.5a), m^2
$b_{i-o,m}$	coefficients of regression equation (5.14), dimensionless
b_o	intercept of regression equation (5.14), dimensionless
C	concentration of aerosol particles, part/m^3
c, c_1-c_4	free constants, defined in equations used
c_{ij}	coefficient matrix
D	effective diffusivity (3.25), m^2/s
d	diameter (1.2), m
E	deposition efficiency of collector particle (3.1), dimensionless
E_{BT}	total collection efficiency of a collector particle in a fixed bed (5.1), dimensionless
E_{FT}	total collection efficiency of a collector particle in a fluidized bed (7.73), dimensionless
F	Stokes-Cunningham slip correction factor (3.30), dimensionless
F_E	electric field intensity (.12), volts/m
$F( )$	function of variable in brackets
f	fraction of aerosol not collected (1.1), dimensionless
f'	per cent of aerosol not collected (2.1), dimensionless
$f(u)$	function of variable in brackets
G	volumetric gas flow rate (7.2), m^3/s
g	acceleration due to gravity (2.6), m/s^2
H	depth of filter (2.10), m

h	distance from inlet surface of bed, m
K	empirical parameter of modified two phase theory (7.32), dimensionless
K_M	collection parameter based on unit dense phase mass (5.4a), m^3/Kgs
K_V	collection parameter based on unit dense phase volume (5.3b), s^{-1}
k_A	mass transfer coefficient of aerosol particles (3.23), m/s
k_B	Boltzmann's constant (3.29), joule/^oK
k_b	interphase mass transfer coefficient due to throughflow based on unit bubble volume (7.6a), s^{-1}
k_{Ab}	interphase mass transfer coefficient due to diffusion based on unit bubble volume (7.6b), s^{-1}
k'	collection coefficient per unit bed height (6.3), m^{-1}
M	mass of collector bed (5.5a), kg
M_A	mass of collector particles per unit bed area (5.5a), kg/m^2
m	mass of collector bed at height h (5.5b), kg
m_A	mass per unit cross sectional area of bed at height h (5.5b), kg/m^2
m_1, m_2	solutions of Equation (7.47), m^{-1}
N	collection parameter (3.17), dimensionless
N_{E1}-N_{E5}	electrostatic collection parameters defined in Equations (3.41 - 3.45), dimensionless
N'_p	number of spherical collector particles per unit dense phase volume (5.2), particles/m^3
NTU	number of transfer units (6.3), dimensionless
n	empirical parameter of modified two phase theory; Chapter 7 (7.33), dimensionless
q	transfer rate due to throughflow (7.4), m^3/s

q'	electrostatic charge on particle, coulombs
R	rate of deposition of aerosol particles on a collector (3.23), particles/s
R^2	multiple correlation ceofficient (F.16)
r	polar co-ordinate, m
r_b	radius (7.4), m
S^2	residual mean square (F.9)
SSAM	sum of squares about the mean (F.14)
SSAR	sum of squares about regression (F.14)
SSDR	sum of squares due to regression (F.14)
T	absolute temperature (3.29), ^oK
U	superficial gas velocity (2.1), m/s
U_M	migration velocity of aerosol particles (1.2), m/s
U_p	superficial velocity of maximum aerosol penetration (2.3), m/s
U_S	settling velocity of aerosol particle (3.39a), m/s
u	interstitial fluid velocity in a fixed bed (5.6), m/s
V	volume (7.2), m^3
v	collector particle velocity relative to bubble (7.11), m/s
$X_{i-1,m}$	set of dependent variables in regression analysis (5.14), dimensionless
Y	independent variable in regression analysis (5.14), dimensionless
y	distance from x-axes perpendicular to direction of flow (3.2), m

SUBSCRIPTS

A	aerosol particle
AD	adjusted
AV	average

atm	atmospheric
b	bubble
c	bubble cloud
CR	critical
D	diffusional
d	dense phase
E	electrostatic
F	fluidized bed collector
f	fluid
H	depth
I	inertial
in	inlet
m	number of independent variables in regression equation
mf	minimum fluidization
n	number of experimental points
n_{st}	number of stages
out	out-let
P	collector particle
pl	plug
R	interception
RP	rotameter pressure
r	polar co-ordinate
rel	relative between collector and fluid
T	total
t	time
W	dense phase

GREEK LETTERS

α	collection constant (2.1), dimensionless
β'	fraction of the gas passing in the bubble phase (7.43a), dimensionless
β_D	diffusional collection constant (3.33), dimensionless
$\beta_{i-o,m}$	parameters of regression equation (F.1)
γ	coincidence loss factor (D.1), dimensionless
ΔP	pressure difference across length H of filter (6.2), kg/ms^2
δ_1	effect of fixed bed-support plate interface on aerosol collection (5.11), dimensionless
δ_o	effect of fixed bed air interface on aerosol collection (5.9), dimensionless
ϵ	dielectric constant of aerosol particle (3.42), dimensionless
ϵ'	dielectric constant of aerosol particle (3.42), dimensionless
ϵ'_o	permittivity of free space (3.41), $coulombs^2 s^2/kgm^3$
θ	polar co-ordinate, radians
μ	viscosity (1.2), kg/ms
π	ratio of circumference to diameter of a circle (3.23), dimensionless
ρ	density (2.6), kg/m^3
σ	surface tension of liquid (4.1), n/m
σ'^2	variance of regression line
τ	dimensionless time (3.5)
Ψ	fluid streamline, m^3/s
ω	angular speed (4.1), radians/s

DIMENSIONLESS GROUPS

Pe	Peclet number (3.25)
Re	Reynolds number (3.3)
Sc	Schmidt number (3.26)
Sh	Sherwood number (3.27)
St	Stokes number (3.4)

REFERENCES

A1 Aksel'rud, G.
Zh. Fiz. Khim. 27, 1445 (1953).

A2 Albrecht, F.
Phys. Z. 32, 48 (1931).

A3 Anderson, D.M. and Silverman, L.
"Fifth Atomic Energy Commission Air Cleaning Conference", USAEC TID 7551, p.140 (1957).

A4 Avedesian, M.
(private communication), Noranda Research Institue, Montreal.

B1 Behie, S.W., Beeckmans, J.M., Knettig, P. and Bulani, W.
The Can. J. of Chem. Eng. 50, 241 (1972).

B2 Bennett, C.A. and Franklin, N.L.
"Statistical Analysis in Chemistry and the Chemical Industry", John Wiley & Sons Inc. (1954).

B3 Bird, R.B., Stewart, W.E. and Lightfoot, E.N.
"Transport Phenomena", John Wiley & Sons Inc. (1966).

B4 Black, C.H. and Boubel, R.W.
Ind. & Eng. Chem. Process Design and Development 8, No.4, 573 (1969).

B5 Blasewitz, A.G. and Judson, B.F.
Chem. Eng. Progress, p.6-J (1955).

B6 Boehme, G., Krupp, H., Rabenhorst, H. and Sandstede, G.
Trans. Instn. Chem. Engrs. 40, 252 (1962).

B7 Boland, D. and Geldart, D.
Powder Technology 5, 289 (1971-72).

B8 Boubel, R.W. and Junge, D.C.
AIChE Symp. Ser. No.128, 69, 138 (1971).

C1 Carnahan, B., Luther, H.A. and Wilkes, J.O.
"Applied Numerical Methods"; John Wiley & Sons Inc. (1969).

C2 Chavarie, C.
Ph.D. Thesis, McGill Univ. (1973).

C3 Chen, C.Y.
Chemical Reviews 55, 595 (1955).

C4 Ciborowski, I. and Wlodarski, A.
Chem. Eng. Sci. 17, 23 (1962).

C5 Clift, R.
Ph.D. Thesis, McGill Univ. (1970).

C6 Clift, R. and Grace, J.R.
CEPSS 66 No.105, 14 (1970).

C7 Clift, R. and Grace, J.R.
AIChE J. 17 No.1, 252 (1971).

C8 Clift, R. and Grace, J.R.
AIChE Symp. Ser. No. 116, 67, 23 (1971).

C9 Clift, R., Grace, J.R., Cheung, L. and Do, T.H.
J. Fluid Mech. 51, 187 (1972).

C10 Collins, R.
Chem. Eng. Sc. 24, 1291 (1969).

C11 Cook, C.C., Swany, G.R. and Colpitts, J.W.
J. Air Poll. C. Ass. 21 479 (1971).

D1 Davidson, J.F. and Harrison, D.
"Fluidized Particles", Cambridge Univ. Press (1963).

D2 Davidson, J.F. and Harrison, D.
"Fluidization", Academic Press (1971).

D3 Davidson, J.F. and Schüler, B.O.G.
Trans. Instn. Chem. Engrs. 38, 335 (1960).

D4 Davies, C.N.
Proc. Phys. Soc. 57, 259 (1945).

D5 Davies, C.N.
Proc. Instn. of Airborne Dust and Particles B. 1, 185 (1952).

D6 Davies, C.N.
"Aerosol Science", Academic Press (1966).

D7 Davies, C.N., Aylward, M. and Leacey, D.
Arch. Ind. Hyg. 4, 354 (1951).

D8 Davies, C.N. and Peetz, C.V.
Proc. R. Soc. A. 234, 269 (1956).

D9 Davies, G. and Robinson, D.S.
Can. J. Chem. Eng. 38, 175 (1960).

D10 Davies, R.M. and Taylor, G.
Proc. Royal Soc. A. 200, 375 (1950).

D11 Doganoglu, Y.
Design Project, Heriot-Watt Univ., Edinburgh (1971).

D12 Dorman, R.C.
"Aerodynamic Capture of Particles", E.G. Richardson, Pergamon Press, London (1960).

D13 Draper, N.R. and Smith, H.
"Applied Regression Analysis", John Wiley & Sons Inc. (1967).

E1 Engelbrecht, H.L.
J. Air Poll. C. Ass., 15, 43 (1965).

E2 Environment
"Scrubber Handbook", 1, PB-213-016 (1972).

E3 Environmental Research Corp.
"Operating Manual for the Spinning Disk Aerosol Generator Model 8330", Report 12M, Minnesota (1970).

E4 Ergun, S.
Chem. Eng. Progress 48, 89 (1952).

F1 Fairs, G.L. and Godfrey, E.
in Dust in Industry, Soc. of Chem. Ind., London (1948).

F2 Freundlich, H.
"Colloid and Capillary Chemistry", Methuen, London (1926).

F3 Friedlander, S.K.
AIChE J. 3, No.1, 43 (1957).

F4 Frössling, N.
Gerlands Beitr. 52, 170 (1938).

F5 Fuchs, N.A.
"The Mechanics of Aerosols", Pergamon Press (1964).

F6 Furmidge, L.G.C.
J. Colloid Sc. 17, 309 (1962).

G1 Gallily, I. and LaMer, V.K.
J. Phys. Chem. 62, 1295 (1958).

G2 Garner, F. and Keey, R.
Chem. Eng. Sc. 9, 119 (1958).

G3 Geldart, D.
Powder Tech. 1, 355 (1968).

G4 Gillespie, T.
J. Colloid Sc. 10, 299 (1955).

G5 Gillespie, T. and Rideal, E.
J. Colloid Sc. 10, 281 (1955).

G6 Grace, J.R.
"Fluidization Course", Dept. of Chem. Eng., McGill Univ. (1972).

G7 Grace, J.R.
AIChE J. Symp. Ser. No.141, 70, 21 (1974).

G8 Grace, J.R. and Clift, R.
Chem. Eng. Sc. 29, 327 (1974).

G9 Grace, J.R. and Harrison, D.
Chem. Eng. Sci. 24, 497 (1969).

G10 Grace, J.R. and Venta, J.
Can. J. Chem. Eng. 51 No.1, 110 (1973).

H1 Happel, J.
AIChE J. 4, 197 (1958).

H2 Harrison, D. and Leung, L.S.
Trans. Instn. Chem. Engrs. 39, 409 (1961).

H3 Harrop, J.A. and Stenhouse, J.I.T.
Chem. Eng. Sc. 25, 1475 (1969).

H4 Harstad, J.B., Filler, M.E., Hushen, W.T. and Decker, H.M.
Appl. Microb. 20 No.1, 94 (1970).

H5 Hazlett, R.N.
I. and E.C. Fund. 8 No.4,625 (1969).

H6 Hazlett, R.N.
I. and E.C. Fund. 8 No.4,633 (1969).

H7 Herling, B.
(private communication), Env. Res. Corp., Minnesota (1973).

H8 Herne, H.
"Aerodynamic Capture of Particles", Pergamon Press (1960).

J1 Jackson, R.
Trans. Instn. Chem. Engrs. 41, 22 (1963).

J2 Jackson, M.
AIChE Symp. Ser. No.141, 70, 82 (1974).

J3 Johnstone, H.F., Field, R. and Tassles, H.
Ind. Eng. Chem. 46, 1601 (1954).

J4 Jugel, W., Reher, E.O., Grobler, R. and Tittmann, A.
Chem. Techn. 22 No.7, 403 (1970).

K1 Kalen, B. and Zenz, F.A.
Report, The Ducon Comp. Inc., New York (1974).

K2 Kisel' nikov, V.N., Vyalkov, V.V. and Filatov, V.M.
Int. Chem. Eng. 7, 428 (1967).

K3 Knettig, P. and Beeckmans, J.M.
Can. J. of Chem. Eng. 52, 703 (1974).

K4 Knettig, P. and Beeckmans, J.M.
Aerosol Science 5, 225 (1974).

K5 Kraemer, H.F. and Johnstone, H.F.
I. and E.C., 47 No.12, 2426 (1955).

K6 Kunii, D. and Levenspiel, O.
"Fluidization Engineering", John Wiley & Sons Inc. (1969).

L1 LaMer, V.K.
A.E.C. Rep. NYO-512, Tech. Inf. Serv. (1951).

L2 LaMer, V.K. and Drozin, V.G.
Proc. of the 2nd. Int. Congr. on Surface Activity III,
Butterworth Sci. Pub., p.600 (1957).

L3 LaMer, V.K., Gendron, P.R. and Gruen, R.S.
Nucl. Sci. Abs. 5, No.755 (1951).

L4 Lance, G.N.
"Numerical Methods for High Speed Computers", Cliffe
and Sons Ltd. (1960).

L5 Landahl, H. and Herrmann, K.
J. Colloid Sci. 4, 103 (1949).

L6 Langmuir, I.
Sci. Res. and Dev. Report #OSRD-865 (1942).

L7 Langmuir, I.
J. Meteor., 5, 175 (1948).

L8 Langmuir, I. and Blodgett, K.B.
Gen. Elec. Res. Lab. Report #RL-225, Schenectady (1944-45).

L9 Langmuir, I. and Blodgett, K.B.
Army Air Force Tech. Rep. No.5418 (1946).

L10 Larsen, R.J.
Am. Ind. Hyg. Ass. 19, 265 (1958).

L11 LeClair, B.P. and Hamielec, A.E.
Can. J. of Chem. Eng. 49, 713 (1971).

L12 Leers, R.
Staub, 50, 402 (1957).

L13 Leung, L.S.
Powder Tech. 6, 189 (1972).

L14 Leva, M.
"Symp. on Interaction between Fluids and Particles", Inst. Chem. Engrs., p.143, London (1962).

L15 Levich, V.
"Physico-Chemical Hydrodynamics", Ac. Sci., Moscow, USSR (1952).

L16 Lewis, W.K., Gilliland, E.R. and Bauer, W.C.
Ind. Eng. Chem. 41, 1104 (1949).

L17 Lockett, M.J. and Harrison, D.
"Proc. of the Int. Symp. on Fluid.", p.257, Netherlands Univ. Press (1967).

M1 Malnar, J.
(private communication), Royco Inst. Inc., California

M2 May, K.R.
J. of Appl. Phy. 20, 932 (1949).

M3 Meisen, A. and Mathur, K.B.
"Symp. on Multi-Phase Flow System", Instn. Chem. Engrs. Symp. Ser. No.38 (1974).

M4 Meissner, H.P. and Mickley, H.S.
Ind. Eng. Chem. 41, 1238 (1949).

M5 Murray, J.D.
J. Fluid Mech. 22, 57 (1965).

Mc1 McCarthy, D., Yankel, A.J., Patterson, R.G. and Jackson, M.L.
Ann. Meet. Air Poll. Contr. Ass. paper 74-AP-24 (1974).

O1 Oglesby, S.
Nat. Tech. Inf. Ser. PB-196-380 (1970).

O2 Orcutt, J.C.
Ph.D. Thesis, Univ. of Delaware (1960).

O3 Orcutt, J.C., Davidson, J.F. and Pigford, R.L.
Chem. Eng. Prog. Symp. Ser. 38, 1 (1962).

P1 Paretsky, L.C.
Ph.D. Thesis, The City Univ. of New York (1972).

P2 Parker, H.W. and Stevens, W.F.
AIChE J. 5, 314 (1959).

P3 Perry, J.H.
"Chemical Engineers' Handbook", Ed. 4th, McGraw-Hill (1963).

P4 Pilney, J.P. and Erickson, E.E.
J. Air. Poll. Cont. Ass. 18, 684 (1968).

R1 Radushkevich, L.V.
Kolloid Zh. 26, 235 (1964).

R2 Ramskill, E.A. and Anderson, W.L.
J. of Colloid Sci. 6, 416 (1951).

R3 Ranz, W.E. and Wong, J.B.
Ind. & Eng. Chem. 44 No.6, 1371 (1952).

R4 Robinson, A.
Com. Pure Appl. Math. 9, 69 (1956).

R5 Royco Inst. Inc., California, (1963).
"Operating Man. for Royco Particle Counter Model 200/202."

R6 Rubin, Y.U.M. and Margolin, Y.U.A.
Coke & Chem. USSR, No.3, 15 (1974).

S1 Schurr, G.A., Zippler, D.B. and Guyton, D.C.
E.I. du Pont de Nemours and Co., South Carolina (1972).

S2 Scott, D.S. and Guthrie, D.A.
Can. J. Chem. Eng. 37, 200 (1959).

S3 Sell, W.
Ver. dtsch. Ing. Forschungsheft, 347, 1 (1931).

S4 Shannon, L.J.
"Control Technology for Particulate Emissions", Env. Prot. Agency Report PB-236-646 (1974).

S5 Squires, A.M.
Chem. Eng. Progr. Symp. Ser. 58, 57 (1962).

S6 Squires, A.M.
"Method and Apparatus for Treating Fluids and Non-Fluid Materials", U.S. Patent 3,296,775 (1967).

S7 Stairmand, C.J.
Trans. Instn. Chem. Eng. 28, 130 (1950).

S8 Stechina, I.B. and Fuchs, N.A.
Ann. Occup. Hyg. 11, 299 (1968).

S9 Stern, S., Zeller, H. and Schekman, A.
J. Colloid Sci. 15, 546 (1960).

T1 Tardos, G., Gutfinger, C. and Abuaf, N.
Israel J. of Tech. 12, 184 (1974).

T2 Thomas, J.W. and Yoder, R.E.
AMA Arch. Ind. Health, 13, 545 (1956).

T3 Thomas, J.W. and Yoder, R.E.
AMA Arch. Ind. Health, 13, 550 (1956).

T4 Toomey, R.D. and Johnstone, H.F.
Chem. Eng. Prog. 48, 220 (1952).

W1 Willeke, K., Lo, C.S.K. and Whitby, K.T.
Aerosol Science, 5, 449 (1974).

W2 Willhelm, R.H. and Kwauk, M.
Chem. Eng. Progr. 44 No.3, 201 (1948).

APPENDIX A

DERIVATION OF EQUATIONS 3.5 AND 3.6

Consider the motion of a spherical aerosol particle of diameter d_A and density ρ_A, carried by a gas stream approaching a spherical collector of diameter d_p at velocity U remote from the collector. Taking Cartesian coordinates, the components of the equation of motion for the aerosol particle are:

$$\frac{\pi}{6} d^3_A \rho_A \frac{d}{dt} (U_A)_x = F_x \tag{A1}$$

$$\frac{\pi}{6} d^3_A \rho_A \frac{d}{dt} (U_A)_y = F_y \tag{A2}$$

where the velocity components of the aerosol particle are $((U_A)_x, (U_A)_y)$ at time t, (F_x, F_y) are the components of the drag of the gas on the particle, and it is assumed that gravitational effects are negligible. If, as is the case in the present work, the Reynolds number of the aerosol particle is small, then the drag componenets are given by Stokes' Law as:

$$F_x = 3\pi d_A \mu \left[(U_{rel})_x - (U_A)_x\right] \tag{A3}$$

$$F_y = 3\pi d_A \mu \left[(U_{rel})_y - (U_A)_y\right] \tag{A4}$$

where $(U_{rel})_x$, $(U_{rel})_y$ are the components of the gas velocity relative to the collector particle at (x,y), and μ is the gas viscosity. It is implicitly assumed, in Equations (A3) and (A4), that the aerosol particle

is so much smaller than the collector that it has negligible effect on the gas flow, and that the ratio of ρ_A to the gas density is so large that drag components due to history and virtual mass can be neglected. Substituting Equations (A3) and (A4) into (A1) and (A2) and simplifying yields

$$\frac{d}{dt}(U_A)_x = \frac{18\mu}{d^2_A \rho_A}\left[(U_{rel})_x - (U_A)_x\right] \tag{A5}$$

$$\frac{d}{dt}(U_A)_y = \frac{18\mu}{d^2_A \rho_A}\left[(U_{rel})_y - (U_A)_y\right] \tag{A6}$$

It is convenient to render these equations dimensionless in terms of:

$$(U_A)'_x = (U_A)_x/U \,,\; (U_A)'_y = (U_A)_y/U \tag{A7}$$

$$(U_{rel})'_x = (U_{rel})_x/U \;;\; (U_{rel})'_y = (U_{rel})_y/U \tag{A8}$$

$$St = d^2_A \rho_A U/9\mu d_p \tag{A9}$$

$$\tau = 2tU/d_p \tag{A10}$$

Equations (A5) and (A6) then yield the dimensionless equations of motion discussed in Chapter 3:

$$St \cdot \frac{d(U_A)'_x}{d\tau} = \left[(U_{rel})'_x - (U_A)'_x\right] \tag{3.5}$$

$$St \cdot \frac{d(U_A)'_y}{d\tau} = \left[(U_{rel})'_y - (U_A)'_y\right] \tag{3.6}$$

APPENDIX B

DERIVATION OF INTERCEPTION PARAMETERS FOR IDEALIZED CASES

B.1 $St \to \infty$

Interception may be regarded as the increased collection resulting from the finite size of the aerosol particle. In the limit $St \to \infty$, the particle's inertia is so high that it follows a rectilinear trajectory. Hence all particles in an approach cylinder of diameter $(d_p + d_A)$ are collected, whereas for vanishingly small aerosol the corresponding diameter is d_p. Thus the additional collection due to interception is described by the efficiency

$$E_R = \frac{\pi(d_p + d_A)^2/4 - \pi d_p^2/4}{\pi d_p^2/4} = \frac{(d_p + d_A)^2 - d_p^2}{d_p^2} \qquad (3.16a)$$

For small d_A, E_R can be approximated as

$$E_R = \frac{2d_A d_p + d_A^2}{d_p^2} \approx 2d_A/d_p = 2N_R + 0[N_R^2] \qquad (3.16b)$$

B.2 $St \to 0$

In this case, the particle inertia is so low that it follows the gas streamlines. Collection due to interception is therefore determined by calculating the gas-flow through the annulus of width $(d_A/2)$

around the equator of the collector. Two limiting cases can be considered, corresponding to creeping flow ($Re_p \to 0$) and potential flow ($Re_p \to \infty$). The corresponding collection efficiency is most conveniently obtained from the value of the stream function at the outer boundary of the annulus; clearly this is equivalent to integrating the gas velocity through the annulus.

B.2.1 Creeping flow

From the standard result for the stream function, ψ, in Stokes flow around a sphere, the interception efficiency is

$$E_R = \frac{\psi(r = (d_A + d_p)/2 \ , \ \theta = \pi/2)}{U d_p^2/4}$$

$$= (1 + \frac{d_A}{d_p})^2 - \frac{3}{2}(1 + \frac{d_A}{d_p}) + \frac{1}{2(1 + d_A/d_p)}$$

$$= (1 + N_R)^2 - \frac{3}{2}(1 + N_R) + \frac{1}{2(1 + N_R)} \qquad (3.17)$$

For small N_R, this result simplifies as:

$$E_R = 1 + 2N_R + N_R^2 - \frac{3}{2}(1 + N_R) + \frac{1}{2}(1 - N_R + N_R^2 \cdots\cdots)$$

$$= \frac{3}{2}N_R^2 + O[N_R^3] \qquad (3.18)$$

B.2.2 Potential flow

In exactly analogous fashion, the interception collection efficiency follows as:

$$E_R = \left(1 + \frac{d_A}{d_p}\right)^2 - \frac{1}{1 + d_A/d_p}$$

$$= (1 + N_R)^2 - \frac{1}{1 + N_R} \qquad (3.19)$$

Again, for small N_R, this is approximated as:

$$E_R = 1 + 2N_R + N^2_R - (1 - N_R + N^2_R \ldots\ldots)$$

$$= 3N_R + 0\left[N^3_R\right] \qquad (3.20)$$

APPENDIX C

PRIME CALIBRATION OF THE PARTICLE COUNTER

C.1 Introduction

The Royco Model 200/202 particle counter must be calibrated at periodic intervals, usually 2 to 6 months, to compensate for the deterioration of its various degradable components with time. Prime calibration is carried out by passing aerosol particles of a known size through the counter, comparing the indicated size distribution with the known distribution, and making any necessary calibration adjustments. Thus, the accuracy of the procedure is a function of the monodispersity of the test aerosol and of the individual performing the calibration. Usually, as the particle size distribution of the test aerosol is not precisely known, some judgement on the part of the individual is required. This results in small differences in calibration of the instrument depending on who performs the task. It is strongly recommended that latex particles manufactured by Dow Chemical Company, Midland, Michigan, be used for a test aerosol. These particles are available in a spectrum of dierete sizes of exceptionally low standard deviation (see Table C.1). They are spherical and with known physical constants (index of refraction — 1.595, density — 1.06×10^3 kg/m^3).

As a test, the latex particles used in this study for prime calibration were analysed under a scanning electron microscope. Figures C.1a and C.1b show electron micrographs of these particles, taken by Dr. D. Atack, Pulp and Paper Research Institute of Canada. His analysis (d_A — 0.74) agreed to within 1.3% of the size stated by Dow Chemical Company (d_A — 0.75 ± 0.0026 μm). It is thus seen that these latex particles provide a dependable test aerosol for calibrating the particle counter.

TABLE C.1 Latex Particle Hydrosols Manufactured by Dow Chemical Company, Bio-Products Department, Midland, Michigan

Particle Size in Microns	Accuracy
0.750	± 0.0026
1.171	± 0.013
1.190	± 0.0126
2.68	± 0.0149

FIGURE C.1 Scanning electron microscope photographs of Dow latex sphere:

a) Magnification x 6800
b) Magnification x 27180

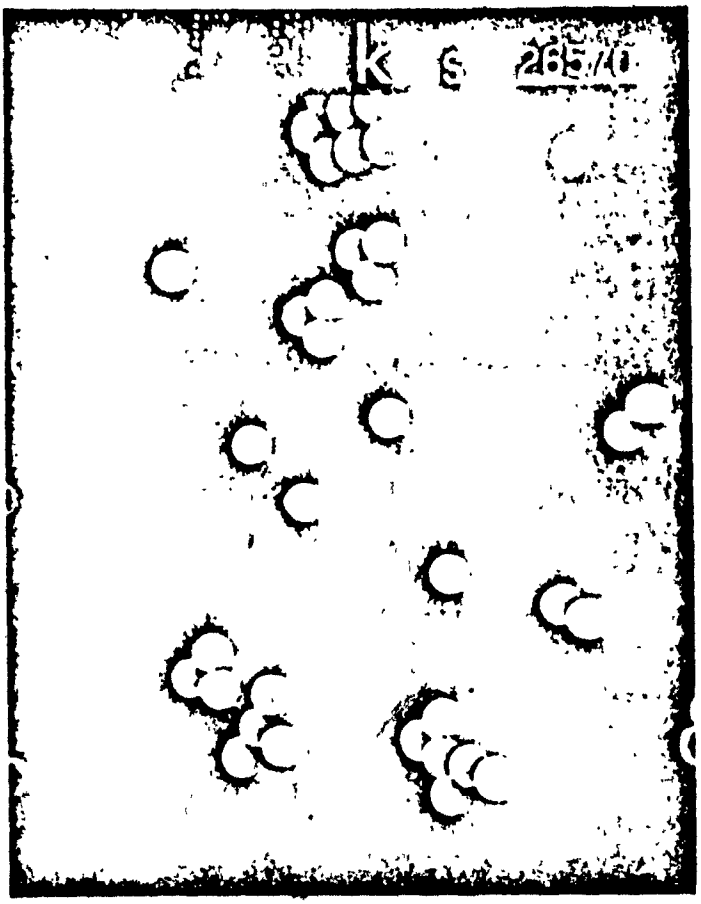
k s 2656

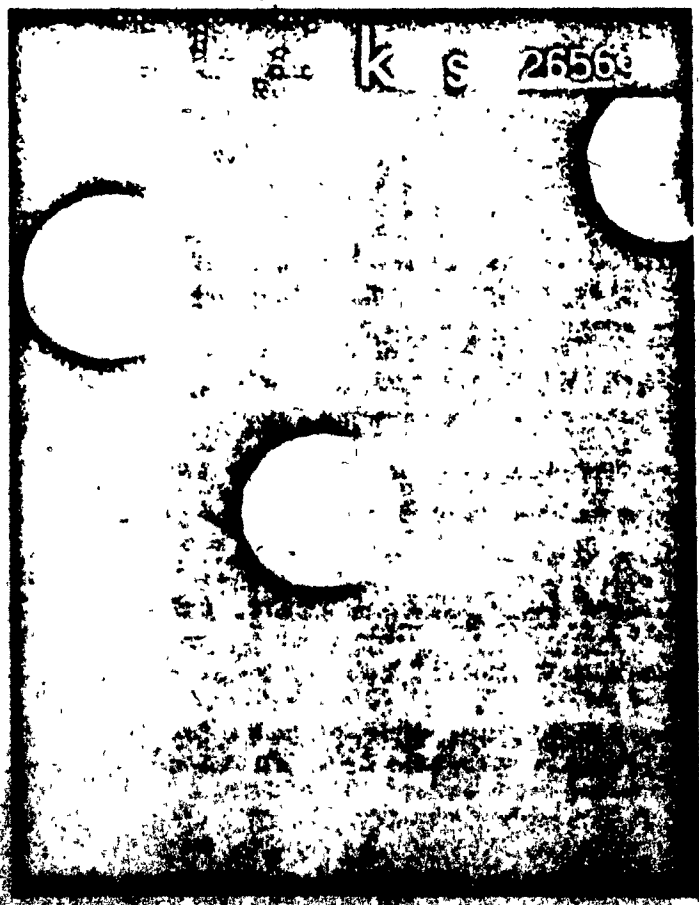
k s 2656

C.2 Description of Generator

Royco Instruments Inc. manufactures an aerosol generator (Model AGS 256) which is recommended when prime calibrating the particle counter. The generator is shown schematically in Figure C.3. Compressed air is used as a source of air for the atomizer and drier. The input air line pressure is regulated at around 2.0×10^5 n/m^2. The drier air valve controls the total volume of air that passes through the drier to the aerosol mixer-tube. The drier air flow should be set to at least 1.6×10^{-4} m^3/s to provide an ample supply of dry air. The drier is filled with anhydrous calcium sulphate the colour of which changes from pink to blue when saturated with moisture. From the drier the air passes through a 0.3 μm filter to the aerosol mixer-tube where it is used to dilute and dry the moist aerosol from the atomizer. The atomizer is a small nebulizer or jet pump. The input air causes a partial reduction in pressure over the jet that protrudes into the water, so that the water is drawn out of the jet to be dispersed as a fine spray. The stream of partially evaporated water and latex particles flows out of the atomizer, through the funnel and into the aerosol mixer tube. The air from the drier passes into the aerosol mixer tube at two points in a direction that causes the air from the drier to flow into a helix around the air from the atomizer. Remaining water is thus evaporated. At the end of the aerosol mixer-tube, the output air is drawn off axially, while the exhaust air exits around the periphery of the center stream.

C.3 Procedure for Prime Calibration

The method described below is the result of the procedure recommended by the manufacturers, the experience of the author and several private communications with the manufacturers.

(i) Purge the optical cell (Figure 4.3) for half an hour with clean air prior to prime calibration.

(ii) Clean the atomizer with acetone, distilled water and soap and rinse at least half a dozen times..

(iii) Mix a very small portion of latex material (in standard concentrations supplied by Dow Chemicals Company) with about 10^{-5} m^3 of distilled water in a clean container. Place the mixture in an ultrasonic cleaning bath for at least 20 minutes to break any agglomerates formed.*

(iv) Pour the particle mixture into the nebulizer and turn on the air flow until a faint mist appears on the walls of the nebulizer bowl.

(v) Turn on the drier air.

(vi) Connect the drier output (Figure C.3) to the particle counter inlet.

(vii) Operate the particle counter at a flow rate of 5×10^{-6} m^3/s after having allowed a one-and-a-half hour warm-up period.

(viii) Monitor three size ranges centered around the known size peak.

---

* See comments on the experimental procedure of Paretsky (Section 2.2.1.2).

(ix) Make the necessary adjustments to the particle counter until the monitored aerosol "peaks" in the correct size range. These adjustments are described in detail in the manufacturers' service manual[R5].

C.4 Operating Hints

The following are useful operating hints:

(i) Possible fracture of latex particles by excessive air pressure in the nebulizer should be avoided.

(ii) Agglomeration of particles must be avoided by placing the solution in an ultrasonic cleaning bath as described in the previous section.

(iii) Insufficient drying air may result in the formation of water droplets in the test aerosol (see Paretsky, Section 2.2.1.2).

(iv) Inefficient filters will cause atmospheric dust to pollute the test aerosol.

(v) Excessive concentration of test aerosol will cause coincidence loss (see Appendix D).

(vi) Impure water will contaminate the test aerosol (see Paretsky, Section 2.2.1.2). To check for this condition make a test run with nothing except the distilled water in the nebulizer.

APPENDIX D

CORRECTION OF COINCIDENCE LOSS IN PARTICLE COUNTER

D.1 Introduction

Coincidence loss in the Model 200/202 Royco particle counter results from the simultaneous appearance of two particles within the sensitive volume where measurement takes place (see Figure 4.3). The aerosol particles appear randomly during the measurement interval, with an average rate proportional to the concentration. As the concentration increases there is greater probability that two particles appear at the same time, causing coincidence loss. The operation is such that if the particles are not of the same size, the larger particle masks the smaller one, effectively hiding the smaller one while the larger is counted; two particles of the same size produce an additive effect which simulates a single particle. Coincidence loss, therefore, is not the same in all channels, but instead is a function of the count in a particular size range related to the total count in that size range plus all larger particles. Also, the response of the instrument is such that particles which pass through the sensitive volume less than 5×10^{-4}s apart produce coincidence loss. This 5×10^{-4}s separation time covers effects which include optical coincidence and optical and electronic "dead time". Electronic "dead time" may be roughly described as the time period required for the instrument to be ready to count after a particle has been registered; if a second particle enters the sensitive volume during the "dead time" period it will not be counted at all.

D.2 Correction of Coincidence Loss

For experiments where great accuracy is not required, coincidence loss may be neglected without much loss of accuracy for concentrations up to approximately 10^8 particles/m^3. For situations however, as in this study, where high monitoring accuracy is desirable coincidence loss has to be considered. It can be corrected quite effectively from a graph supplied by the manufacturers. In general, therefore,

$$\text{Actual count}_T = \text{Measured count}_T \times (1 \quad \gamma) \tag{D.1}$$

where γ is termed, by the manufacturers[R5], the coincidence loss factor.

The experimental results of this study were corrected for coincidence loss by applying two methods. For concentrations greater than 6×10^7 particles/m^3 coincidence loss was corrected from a graph supplied by the manufacturers (Figure 4.4) which relates actual count per minute, when sampling at 5×10^{-6} m^3/s, to measured count. For concentrations less than 6×10^7 particles/m^3 the graph was inaccurate because of the limited accuracy with which points can be read from it. It was therefore assumed that γ, the coincidence loss factor, could be linearized below this concentration. The linearization of coincidence loss was expressed in terms of total particles counted in a channel and all larger channels per minute, sampling at a flow rate of 5×10^{-6} m^3/s. The average of two values of γ were taken from Figure (4.4) and extrapolated to zero. Thus, at a total count rate of 1.6×10^4 particles/minute

$$(1 \quad \gamma_1) = \frac{(R_A)_T}{(R_M)_T} = \frac{17,100}{16,000} = 1.06875 \tag{D.2}$$

where $(R_A)_T$ is actual count rate and $(R_M)_T$ is measured count rate, particles/min. and at a count rate of 1.8×10^4 particles/min.

$$(1 \quad \gamma_2) = \frac{19,400}{18,000} = 1.0778 \qquad (D.3)$$

Thus

$$\gamma_{AV} = \frac{\gamma_1 \quad \gamma_2}{(1.6 \quad 1.8) * 10^4} = 4.31 \times 10^{-6} \text{ min/particle} \qquad (D.4)$$

so for a count up to 18,000 particles/minutes while sampling at 5×10^{-6} m^3/s

$$R_A = R_M \times (1 \quad \gamma_{AV}) \qquad (D.5)$$

$$= R_M(1 \quad 4.31 \times 10^{-6} \times R_M) \qquad (D.5)$$

The above procedure was approved by the manufacturers (private communication).

C.3 Example of Correcting Coincidence Loss

Suppose that the particle counter is sampling at a flow rate of 5×10^{-6} m^3/s and three sizes of aerosol in the ranges of (1.0 - 1.2) μm, (1.2 - 1.5) μm and (1.5 - 2.0) μm are monitored. The measured count rates of the challenging and penetrating aerosol and the apparent penetrations, expressed as a percentage, are given in Table D1.where (2.0 μm) signifies the total number of particles equal to or larger than 2.0 μm. Now these results are expressed in the form of $(R_M)_T$ and $(R_A)_T$. $(R_M)_T$ of

	(1.0 - 1.2) μm	(1.2 - 1.5)μm	(1.5 - 2.0) μm	2.0 μm +
challenging aerosol	9939	8664	5723	2862
penetrating aerosol	4327	1334	319	150
apparent penetration	43.5%	15.4%	5.6%	—

TABLE D.1 Measured Concentrations of Challenging and Penetrating Aerosol

channel (1.0 - 1.2) μm is the total number of counted particles equal to or greater than 1.0 μm. $(R_A)_T$ of channel (1.0 - 1.2) μm is the actual number of particles equal or greater than 1.0 μm, corrected by one of the two ways described in Section D.2.

Thus, for the challenging aerosol we obtain the following table.

	(1.0 - 1.2) μm	(1.2 - 1.5) μm	(1.5 - 2.0) μm
$(R_M)_T$	27,188	17,249	8565
$(R_A)_T$	29,600	18,531	8902
R_A	11,070	9621	6005

TABLE D.2 Correction of Coincidence Loss for Challenging Aerosol

The equivalent table for the penetrating aerosol is

	(1.0 - 1.2) μm	(1.2 - 1.5) μm	(1.5 - 2.0) μm
$(R_M)_T$	6130	1803	469
$(R_A)_T$	6292	1817	470
R_A	4475	1347	319

TABLE D.3 Correction of Coincidence Loss for Penetrating Aerosol

Thus, the actual penetration of aerosol in the three size ranges of this example may be obtained by dividing the last row of Table D3 by the last row of Table D2. The resulting actual penetrations are given in Table D4 together with uncorrected penetrations for comparison.

	(1.0 - 1.2) μm	(1.2 - 1.5) μm	(1.5 - 2.0) μm
apparent penetration	43.5%	15.4%	5.6%
actual penetration	40.4%	14.3%	5.3%
per cent difference	3.1%	1.1%	0.3%

TABLE D.4 Comparison of Actual and Uncorrected Penetrations

As inspection of Table D4 will show the difference in the uncorrected penetrations is largest for the smallest size range and if coincidence loss was not corrected, this would result in an error of 3%. Thus, although correction of coincidence loss is a cumbersome process, the effort required is worth the extra increase of accuracy. All penetrations presented in this study were corrected for coincidence loss in the way described above.

APPENDIX E

OPTIMIZATION OF ROTAMETER SELECTION

The capacity of the large rotameter is fixed at 0.011 m^3/sec. The problem is to select a small rotameter, to minimize the error in flow determination over the whole range from 4.7×10^{-4} m^3/sec.up to the capacity of the large rotameter. Let the maximum capacity of the small rotameter be a m^3/sec. The accuracy of the large rotameter is ± 0.01 of full scale, while that of the small rotameter is ± 0.02 of full scale. Hence the relative error in any individual flow rate, x m^3/sec, is 0.02 a/x for $4.7 \times 10^{-4} < x < a$, and 0.01 x 0.011/x for $a < x < 0.011$. The integrated error over the whole range of the measurements is then

$$\int_{4.7\times10^{-4}}^{a} \frac{0.02a}{x} \cdot dx + \int_{a}^{0.011} \frac{1.1\times10^{-4}}{x} \cdot dx$$

$$= 0.02a \cdot \ln(2.13\times10^{3}a) + 1.1\times10^{-4} \cdot \ln(0.011/a)$$

The smaller rotameter was therefore selected as the catalog instrument which gave the smallest value for the above function.

APPENDIX F

MULTIPLE REGRESSION AND EXAMINING THE REGRESSION EQUATION

The multiple regression model in its general form is

$$Y = \beta_o + \beta_1 X_1 + \beta_2 X_2 \ldots\ldots \beta_m X_m \qquad (F.1)$$

where Y is the dependent variable, $X_1, X_2 \ldots X_m$ is the set of independent variables, m is the number of independent variables and β_o is the intercept of the regression equation. As a model it is assumed that X_i are known precisely but that Y is subject to normal error, being normally distributed about the regression line with constant variance σ^2. We wish to find estimates b_o, b_i of the parameters β_o, β_i. The procedure [C1] is to minimize the sum of squares

$$S = (Y - \beta_o - \beta_1 X_1 - \beta_2 X_2 \ldots\ldots \beta_m X_m)^2 \qquad (F.2)$$

by setting $\partial S/\partial \beta_o = 0$, $\partial S/\partial \beta_i = 0$ and replacing β_o, β_i by their estimates f_o, f_i. If we denote the number of observations by n, and, for convenience define unsubscripted summations over the number of observations then defining

$$C_{ij} = X_i X_j - \frac{X_i X_j}{n}$$

$$C_{iY} = X_i Y - \frac{X_i Y}{n}$$

$$C_{YY} = Y^2 - \frac{(Y)^2}{n}$$

leads to the m simultaneous linear equations

$$\begin{aligned} c_{11}b_1 \quad & c_{12}b_2 \quad \ldots \quad c_{1m}b_m = c_{1y} \\ c_{21}b_1 \quad & c_{22}b_2 \quad \ldots \quad c_{2m}b_m = c_{2y} \\ \cdot \quad & \cdot \quad \cdot \quad \cdot \\ \cdot \quad & \cdot \quad \cdot \quad \cdot \\ \cdot \quad & \cdot \quad \cdot \quad \cdot \\ c_{m1}b_1 \quad & c_{m2}b_2 \quad \ldots \quad c_{mm}b_m = c_{my} \end{aligned} \tag{F.6}$$

together with

$$b_o = \bar{y} - \sum_i b_i \bar{x}_i \tag{F.7}$$

The system described by (F.6) is conveniently solved by inverting the (mxm) coefficient matrix $C = (c_{ij})$ to give the matrix $C^{-1} = (c'_{ij})$. We then have

$$b_i = \sum_j c'_{ij} c_{jy} \tag{F.8}$$

Solutions of these equations gives estimates b_o and b_i for the parameters β_o, β_i. The quantity called the residual mean square, s^2, is given by the following equation

$$s^2 = \frac{c_{yy} - \sum_i b_i c_{iy}}{(n-m-1)} \tag{F.9}$$

and as will be seen later it can be used to evaluate the performance of a model. Once the estimates have been obtained it is necessary to examine the regression equation, and have some criteria to compare its dependability and performance with regression equations which may include different numbers of independent variables. It should be kept in mind that the equation describing the system should be as simple as possible without, however, undue sacrifice of generality and accuracy. The inclusion of more independent variables will increase the apparent accuracy of the model by reducing the residual degrees of freedom but this does not answer the question of whether the predictive accuracy of the model has been improved. There are several useful criteria which can be employed to answer this question and the two most important ones will be discussed here.

In an effort to tackle the question of what measure of precision to be attached to our estimates of the regression model, consider the following identity.

$$Y_j - \hat{Y}_j = (Y_j - \bar{Y}) - (\hat{Y}_j - \bar{Y}) \qquad \text{(F.10)}$$

where $\hat{Y}_j$ is the predicted value of the dependent variable Y_j and $\bar{Y}$ is the mean value of Y_j defined as

$$\bar{Y} = \frac{\sum_{i=1}^{n} Y_i}{n} \qquad \text{(F.11)}$$

Squaring both sides of Equation (F.10) and summing over all observations n we obtain

$$\sum_{j=1}^{n}(Y_j - \hat{Y}_j)^2 = \sum_{j=1}^{n}(Y_j - \bar{Y}) - (\hat{Y} - \bar{Y})^2 \qquad \text{(F.12)}$$

it can be shown that[D13] Equation (F.12) is equivalent to

$$\sum_{j=1}^{n}(Y_j - \bar{Y})^2 = \sum_{j=1}^{n}(Y_j - \hat{Y})^2 + \sum_{j=i}^{n}(\hat{Y}_j - \bar{Y})^2 \qquad \text{(F.13)}$$

Now, $(Y_j - \bar{Y})$ is the deviation of the jth observation from the overall mean so the left hand side of Equation (F.13)is the sum of squares of deviations of the observations from the mean; this is shortened to "SS about the mean" and is also the corrected sum of squares of the Y's. Since $(Y_j - \hat{Y}_j)$ is the deviation of the jth observation from its predicted or fitted value (the jth residual) and $(\hat{Y}_j - \bar{Y})$ is the deviation of the predicted value of the jth observation from the mean we can express Equation (F.13) in words as follows

$$\begin{pmatrix}\text{Sum of squares}\\ \text{about the mean}\end{pmatrix} = \begin{pmatrix}\text{Sum of squares}\\ \text{about regression}\end{pmatrix} + \begin{pmatrix}\text{Sum of squares}\\ \text{due to regression}\end{pmatrix} \qquad \text{(F.14a)}$$

or

$$\text{SSAM} = \text{SSAR} + \text{SSDR} \qquad \text{(F.14b)}$$

Thus, some of the variation can be ascribed to the regression line (SSDR) and some (SSAR) to the fact that the actual observations do not all lie on the regression line. From this procedure we see that a way of assessing how useful the regression line will be as a predictor is to see how much of the sum of squares about the mean is due to SSAR and how much due to SSDR; we would be pleased if SSDR is much larger than SSAR.

Defining the multiple correlation coefficient as

$$R = \sqrt{\frac{SSDR}{SSAM}} \qquad (F.15)$$

$$R^2 = \frac{SSDR}{SSAM} \qquad (F.16)$$

we are looking for a model that will bring the value of the square of the multiple correlation coefficient as close to unity as possible. In physical terms, R^2 measures the proportion of total variation about the mean explained by the regression; i.e. if $R^2 = 0.825$ then our regression model explains 82.5% of the total variation in the data.

The situation is slightly more complicated when models with different numbers of independent variables are compared because of the different degrees of freedom in each case. In fact, if the number of independent variables was made equal to the number of observations ($n=m$) then the degrees of freedom would be zero and the multiple correlation would be 1, our model "predicting" precisely every observation!

We therefore define an "adjusted multiple correlation coefficient", which eliminates the apparent increase in R due to the addition of more independent variables as follows[B2]

$$R_{AD} = \sqrt{1 - (1-R^2)\frac{(n-1)}{(n-m-1)}} \qquad (F.17)$$

and

$$R^2_{AD} = 1.0 - (1-R^2)\frac{(n-1)}{(n-m-1)} \qquad (F.18)$$

Another indicator for evaluating a regression model is the standard error of the estimate

$$S = \sqrt{\text{residual mean square}} \qquad \text{(F.19)}$$

where the residual mean square (SSDR/(n-m-1)) is given by Equation (F.9)

Adjusting the standard error of the estimate by

$$S_{AD} = S\cdot\frac{n-1}{n-m} \qquad \text{(F.20)}$$

we eliminate the effect of having different numbers of independent variables. Examination of this statistic indicates that the smaller it is the better, that is to say the more precise will be the predictions of our model.

Equations (F.18) and (F.20) are used to quantify the performance of a regression model. However, the final decision has to be made by the analyst who will decide whether R^2_{AD} is sufficiently close to 1 and S_{AD} is sufficiently small and determine whether inclusion of additional independent variables is justified by corresponding improvements in these quantities..